Technical Report Documentation Page

| 1. Report No. | 2. Government Accession No. | 3. Recipient's Catalog No. |
|---|---|---|
| FHWA/TX-09/0-4825-1 | | |

| 4. Title and Subtitle | 5. Report Date |
|---|---|
| CORROSION PERFORMANCE TESTS FOR REINFORCING STEEL IN CONCRETE: TECHNICAL REPORT | October 2008<br>Published: October 2009 |
| | 6. Performing Organization Code |
| 7. Author(s) | 8. Performing Organization Report No. |
| David Trejo, Ceki Halmen, and Kenneth Reinschmidt | Report 0-4825-1 |
| 9. Performing Organization Name and Address | 10. Work Unit No. (TRAIS) |
| Texas Transportation Institute<br>The Texas A&M University System<br>College Station, Texas 77843-3135 | 11. Contract or Grant No.<br>Project 0-4825 |
| 12. Sponsoring Agency Name and Address | 13. Type of Report and Period Covered |
| Texas Department of Transportation<br>Research and Technology Implementation Office<br>P. O. Box 5080<br>Austin, Texas 78763-5080 | Technical Report<br>September 2003 – August 2008 |
| | 14. Sponsoring Agency Code |

15. Supplementary Notes

Research performed in cooperation with the Texas Department of Transportation and the U.S. Department of Transportation, Federal Highway Administration.
Project Title: Corrosion Performance Tests for Reinforcing Steel in Concrete
URL: http://tti.tamu.edu/documents/0-4825-1.pdf

16. Abstract

The existing test method used to assess the corrosion performance of reinforcing steel embedded in concrete, mainly ASTM G 109, is labor intensive, time consuming, slow to provide comparative results, and can be expensive. However, with corrosion of reinforcement a major challenge to the durability of infrastructure systems, improvements in the corrosion performance of materials could add significant value. With limited resources, new procedures and test methods are needed to assess corrosion performance of potentially value-adding materials. This research evaluated four accelerated test procedures (rapid macrocell (a.k.a. mini-macrocell), ACT test, CCIA test, and a modified ASTM G109 test) and compared these tests with the standard ASTM G 109 tests. The reasonableness of the test results, test simplicity, test cost, and test duration were all assessed. Results indicate that the rapid macrocell, ACT, and CCIA tests can reduce the time required to perform the tests by approximately 90 percent compared to standard ASTM G 109 test. Not considering the one-time equipment cost, the rapid macrocell, ACT, and CCIA decrease the cost by approximately 75, 58, and 67 percent compared to the standard ASTM G 109 test, respectively. The rapid macrocell test was determined to be relatively simple while the CCIA and ACT tests were considered to be more complex to perform. Based on the research findings, it is proposed that TxDOT use the rapid macrocell test to evaluate the corrosion performance of most materials. To evaluate the performance of dielectric coatings on reinforcement, it is recommended that the MG 109 test be used to evaluate these system types. For specific testing needs, other tests may be appropriate.

| 17. Key Words | 18. Distribution Statement |
|---|---|
| Corrosion, Test, Accelerated Corrosion Test, Polarization Resistance, Half-Cell Potential, Corrosion Rate, Critical Chloride Threshold | No restrictions. This document is available to the public through NTIS:<br>National Technical Information Service<br>5285 Port Royal Road<br>Springfield, Virginia 22161 |

| 19. Security Classif.(of this report) | 20. Security Classif.(of this page) | 21. No. of Pages | 22. Price |
|---|---|---|---|
| Unclassified | Unclassified | 254 | |

Form DOT F 1700.7 (8-72) Reproduction of completed page authorized

# CORROSION PERFORMANCE TESTS FOR REINFORCING STEEL IN CONCRETE: TECHNICAL REPORT

by

David Trejo, Ph.D., P.E.
Associate Research Engineer
Texas Transportation Institute

Ceki Halmen
Assistant Professor
University of Missouri, Kansas City

and

Kenneth Reinschmidt
Research Associate
Texas Transportation Institute

Report 0-4825-1
Project 0-4825
Project Title: Corrosion Performance Tests for Reinforcing Steel in Concrete

Performed in cooperation with the
Texas Department of Transportation
and the
Federal Highway Administration

October 2008
Published: October 2009

TEXAS TRANSPORTATION INSTITUTE
The Texas A&M University System
College Station, Texas 77843-3135

# DISCLAIMER

Contents of this report reflect the views of the authors, who are responsible for the facts and the accuracy of the data presented herein. The contents do not necessarily reflect the official view or policies of the Federal Highway Administration (FHWA) or the Texas Department of Transportation (TxDOT). References to specific products are for information only and do not imply any claim of performance for that particular product. This report does not constitute a standard, specification, or regulation. The researcher in charge was David Trejo, P.E. #93490.

# ACKNOWLEDGMENTS

This project was conducted at Texas A&M University (TAMU) and was supported by the Texas Department of Transportation (TxDOT) and the Federal Highway Administration (FHWA) through the Texas Transportation Institute (TTI) as part of Project 0-4825, Corrosion Performance Tests for Reinforcing Steel in Concrete. The valuable input from R. Sarcinella (Research Project Director), L. Lukefar (Program Coordinator), R. Owens, T.J. Hollen, J. Farris, C. Russel, and Jamine Aparicio, project advisors from TxDOT was appreciated. The authors also wish to thank Erica Sanchez and Stephanie Streid.

# TABLE OF CONTENTS

# LIST OF FIGURES

# LIST OF TABLES

# CHAPTER I. INTRODUCTION

## 1.1 BACKGROUND

Reinforced concrete is one of the most widely used construction materials in the world. It is a versatile and economical material that generally performs its intended use well over its service life. The most important and costly deterioration mechanism affecting the reinforced concrete structures is the corrosion of steel reinforcement. In good quality concrete reinforcement steel is unlikely to corrode even if sufficient moisture and oxygen are available due to formation of a protective oxide film (passive film) in the highly alkaline environment (Elsener 2002). However, this passive film can be disrupted and corrosion initiated by carbonation, due to the penetration of carbon dioxide into the concrete, which lowers the alkalinity of the environment or by the presence of high concentrations of aggressive ions, mainly chlorides (Andrade and Alonso 2001).

A report published by the Federal Highway Administration (FHWA) in 2001 stated that the cost of corrosion for United States (US) industry and government agencies was $276 billion per year (CC-Technologies 2001). The average annual direct cost of corrosion for highway bridges is estimated to be $8.29 billion including the replacement of structurally deficient bridges, maintenance of substructure, superstructure, decks of bridges, and painting cost of steel bridges. Life cycle analysis studies estimate the indirect cost of corrosion for highway bridges due to traffic delays and lost productivity to be 10 times the direct cost of corrosion (Yunovich et al. 2002). Because of this enormous cost, many production and manufacturing companies, state and federal highway agencies, public utilities, and infrastructure developers are aggressively pursuing corrosion protection methods for reinforced concrete structures. Different corrosion protection methods include increased cover depths, lower permeability concrete (lower water-cement ratio and mineral admixtures), corrosion inhibitors, pre-treating sealers, and corrosion resistant reinforcement. Corrosion resistant reinforcements on the market include epoxy coated steel, stainless steel, stainless steel clad reinforcement, galvanized steel, microcomposite steel, steels with multiple coatings, and others. Different corrosion protection methods are also being used for existing structures, such as cathodic protection, re-alkalization, and electrochemical removal of chlorides (Smith and Tullman 1999).

Because of the limited resources available to state and federal highway agencies and the large number of requests by the industry to these agencies to evaluate new materials and new corrosion protection methods , there is a dire need to develop a standardized, unbiased, cost-effective procedure to evaluate the corrosion performance of new materials and methods. In addition to existing standard test methods, such as ASTM G 109 (*Standard Test Method for Determining Effects of Chemical Admixtures on Corrosion of Embedded Steel Reinforcement in Concrete Exposed to Chloride Environments*), southern exposure test, and cracked beam test, several newer test methods have been recently developed to evaluate the corrosion performance of steels in concrete. In general, the established test methods take several years to generate results, whereas the newer proposed test methods have attempted to significantly reduce the testing time periods (Castellote et al. 2002; Ha et al. 2007; Trejo and Pillai 2003). The challenges associated with the newer test methods are that limited results are available and the reliability and repeatability of these methods has not been established in the literature. Because federal and state highway agencies have limited resources to allocate for evaluating new materials and corrosion protection methods, the effectiveness, time requirements, complexity, and cost requirements of these newer test methods need to be evaluated.

## 1.2 OBJECTIVES

The objective of this research program was to evaluate the effectiveness of four new test methods reported in the literature for evaluating the corrosion performance of steel reinforcement embedded in cementitious materials and to evaluate the correlation of the results of these new methods with the results of the standard ASTM G 109 macrocell method. These four test methods are:

- accelerated chloride test method (ACT),
- rapid macrocell test method,
  chloride ion threshold test method (CCIA), and
- modified ASTM G 109 test method (MG 109).

Complexity, cost, and time requirements of these tests were also evaluated and reported in detail to provide TxDOT with all the necessary information to select and implement a screening and evaluation program for new materials and corrosion protection methods.

## 1.3 TASKS

To accomplish the stated objectives, the following tasks were completed.

1. Literature review: A comprehensive literature review was performed to document the state of the practice and state of the art on corrosion testing of metallic materials in cementitious materials. The literature search included applicability and limitations of test methods, laboratory testing procedures, anticipated costs, and time requirements for the different test methods.
2. Experimental design: The largest drawback to corrosion testing in cementitious materials is the lack of statistically valid research data. Because the objective of this research project was to recommend testing procedures for evaluating the corrosion performance of metallic materials embedded (partially or entirely) in cementitious materials, the research team attempted to perform statistically valid research for the testing. For each of the test methods explanatory variables to be evaluated and the range of their levels were carefully selected based on the current practice in the industry and the findings of the literature review. Response variables were determined based on the possible data to be collected from each test method. For most cases, the principles of full factorial design were used to establish the testing programs of each corrosion test method (Chapter III). Materials to be evaluated were randomly distributed among different corrosion test experiments.
3. Corrosion testing of steel embedded in cementitious materials: Two different types of conventional steel, ASTM A 706 (*Standard Specification for Low-Alloy Steel Deformed and Plain Bars for Concrete Reinforcement*) and A 615 (*Standard Specification for Deformed and Plain Carbon-Steel Bars for Concrete Reinforcement*), conventional epoxy coated reinforcement, stainless steel 304, and galvanized steel were evaluated for corrosion performance using four newer methods and the ASTM G 109 test method. The newer methods were the accelerated chloride threshold test developed at Texas A&M University, the rapid macrocell test developed by the University of Kansas, the rapid mortar chloride ion threshold determination test being developed by the ASTM committee G 01, and a modified version of the standard ASTM G 109 method (MG109). The

MG109 test followed the exact procedure of the ASTM G 109 test but samples were kept in a 100°F (38°C) environment during the ponding and drying cycles.

4. Corrosion testing in solutions: A limited number of corrosion tests were performed in solutions. However, the results varied significantly, and no correlation was observed with the other tests. Testing was terminated after the initial tests.
5. Testing for material characteristics: All the mortar and concrete mixtures (containing or not containing corrosion inhibitors) were evaluated for their diffusivity using the ASTM C 1202, *Electrical Indication of Concrete's Ability to Resist Chloride Ion Penetration*, and the ASTM C 1556, *Apparent Chloride Diffusion Coefficient of Cementitious Mixtures by Bulk Diffusion*. Tests were performed at different ages to evaluate the effect of aging on the results.
6. Compilation and analysis of data and performance of economic analysis: Results from different corrosion test methods were statistically analyzed to determine statistically significant variables (when appropriate). Correlation of corrosion rate data, total corrosion loss data, and when available, chloride threshold data between the four test methods and the ASTM G 109 test method were evaluated. Time and cost requirements of each test method for the total duration of each test method were determined.
7. Provide recommendations to TxDOT: Based on the results obtained from corrosion testing, material characterization, and economical analysis from the different test methods, recommendations are made for implementing a corrosion performance screening and evaluation program.

## 1.4 REPORT LAYOUT

This report is organized into six chapters. Chapter I provides the background and objectives of this research. Chapter II discusses the findings of the literature review. General information on the corrosion of reinforcement steel in concrete, corrosion monitoring methods used in the field and laboratory, different corrosion test methods, and information on the corrosion protection methods is provided. Chapter III provides detailed information on the corrosion and material characterization tests and their experimental design. The results and their statistical analysis for

each evaluated test procedure are given in Chapter IV. Chapter V compares the results of different test methods, evaluates the correlation of new test methods with the established ASTM G 109 method, and compares the corrosion test methods based on their cost, complexity, and time requirements. Conclusions and recommendations to TXDOT based on the results of this research program are provided in Chapter VI.

# CHAPTER II. LITERATURE REVIEW

## 2.1 CORROSION OF STEEL IN CONCRETE

Corrosion of reinforcing steel embedded in concrete is an electrochemical process that requires an anode, a cathode, an electrolyte, and an electrical connection between the anode and cathode for the transfer of electrons. Coupled anodic and cathodic reactions take place on the surface of the reinforcing steel. Concrete pore water acts as the electrolyte. and the body of reinforcement provides the electrical connection between the anode and cathode. Cathodes and anodes may be located on the same rebar (microcell) or on different bars (macrocell) that are electrically connected through metallic ties or chairs.

The oxidation and reduction reactions that take place at the anode and cathode are called half cell reactions. At the anode, iron is oxidized and goes into solution as ferrous ions releasing its electrons [Eq. (2.1)].

$$Fe \rightarrow Fe^{2+} + 2e^{-} \tag{2.1}$$

Depending on the availability of oxygen and the pH of the environment, different reduction reactions can take place at the cathode. In the highly alkaline concrete pore solution where oxygen is available, the most likely reaction is shown in Eq. (2.2) that produces hydroxyl ions.

$$2H_2O + O_2 + 4e^{-} \rightarrow 4OH^{-} \tag{2.2}$$

The iron ions in solution react further with hydroxyl ions to form ferrous hydroxide [Eq. (2.3)].

$$Fe^{2+} + 2OH^{-} \rightarrow Fe(OH)_2 \tag{2.3}$$

Ferrous hydroxide can be oxidized to hydrated ferric oxide (red brown rust) [Eq. (2.4)] and hydrated magnetite (green rust) [Eq. (2.5).]. Hydrated ferric oxide and hydrated magnetite can further dehydrate to produce red rust, ferric oxide, $Fe_2O_3$, and black magnetite, $Fe_3O_4$. In highly alkaline concrete pore solution environments, ferrous hydroxide can also oxidize to gamma ferric oxyhydroxide, which is more impermeable and strongly adherent to the steel surface [Eq. (2.6)].

$$4Fe(OH)_2 + O_2 \rightarrow 2Fe_2O_3 \cdot H_2O + 2H_2O \tag{2.4}$$

$$6Fe(OH)_2 + O_2 \rightarrow 2Fe_3O_4 \cdot H_2O + 4H_2O \quad (2.5)$$

$$2Fe(OH)_2 + \frac{1}{2}O_2 \rightarrow 2\gamma - FeOOH + H_2O \quad (2.6)$$

The products of these reactions in concrete combine together and build a stable film that passivates and protects the reinforcing steel from corrosion (Montemor et al. 2003). There are several studies on the nature of the passive film. The presence of $Fe_2O_3$ and $Fe_3O_4$ were thought to be the reason of passivation by some researchers (Hansson 1984), and other researchers attributed it to the presence of gamma ferric oxyhydroxide (Metha and Monteiro 1993). Other researchers suggested that the passivity was due to a $Ca(OH)_2$ rich layer, which adhered to the reinforcement steel (Page 1975; Page and Treadaway 1982). A study that investigated the structure of the passive film using X-ray photoelectron spectroscopy indicated the presence of an outer calcium rich layer and the presence of gamma ferric oxyhydroxide whose concentration decreased with depth (Montemor et al. 1998).

The passive film protecting the reinforcement steel can be disrupted by two mechanisms: carbonation and chloride induced corrosion. Disruption of passive film initiates corrosion of reinforcing steel, initiating corrosion. The volume of corrosion products may be more than six times larger than the volume of iron (Mansfeld 1981). This expansion causes tensile stress in the hardened cement paste that leads to cracking, spalling, eventual loss of concrete cover, and serious deterioration of structural concrete. Pfeifer (2000) estimated that a uniform corrosion of 1 mil (25 μm) of reinforcement would cause cracks to develop. Torres-Acosta and Sagues (2004) estimated a localized corrosion loss of 30 to 270 μm to crack concrete based on the anodic length and member dimensions (cover depth, etc.). In addition to cracking, the reduction of the steel cross section, possible loss of steel ductility, and reduced bond strength are all possible consequences of reinforcement corrosion that can lead to serviceability problems and structural failures (Andrade and Alonso 2001). Stray currents and bacterial action are other causes of corrosion identified in the literature besides carbonation and chloride induced corrosion. Stray currents from different sources such as building power systems or cathodic protection systems may cause electrolytic corrosion (Peabody 1967). Bacterial action may cause disintegration of cementitious materials that enables corrosion reactions in the absence of oxygen (Berkely and Pathmanaban 1990).

### 2.1.1 Carbonation

Atmospheric carbon dioxide diffuses into the concrete and dissolves in pore solution to form carbonic acid [Eq. (2.7)], which neutralizes the alkalis in the concrete pore solution and combines with calcium hydroxide to form calcium carbonate [Eq. (2.8)].

$$CO_2 + H_2O \rightarrow H_2CO_3 \tag{2.7}$$

$$Ca(OH)_2 + H_2CO_3 \rightarrow CaCO_3 + 2H_2O \tag{2.8}$$

Due to the neutralization of alkalis, carbonation and diffusion of other acidic gases, such as $SO_2$ and $NO_2$, cause a decrease in the pH of concrete pore solution, which is typically between 12.5 and 13.6. A reduction of pH to a lower level may cause loss of passivity and initiate corrosion of reinforcement. Different studies stated different limits of pH for the stability of passive film. Berkely and Pathmanaban (1990) stated that a pH level lower than 9.5 would commence corrosion of steel reinforcement as shown in Table II-1. Later Metha and Monteiro (1993) stated that the protective film tends to be stable in the absence of chloride ions as long as the pH of concrete pore solution stays above 11.5.

**Table II-1 State of Reinforcement Corrosion at Various pH Levels.**

| pH of Concrete | State of Reinforcement Corrosion |
|---|---|
| Below 9.5 | Commencement of steel corrosion |
| At ~ 8.0 | Passive film on the steel surface disappears |
| Below 7 | Corrosion occurs |

### 2.1.2 Chloride Induced Corrosion

In the presence of moisture and oxygen, chloride ions at the interface of steel and concrete can destroy the passive film locally and initiate local corrosion. Chloride ions in concrete can be bound by concrete leading to the formation of calcium chloroaluminate (Friedel's salt), a complex between the hydration products of cement and chloride. Suryavanshi et al. (1996) studied the formation of Friedel's salt and proposed two mechanisms, based on adsorption and anion-exchange mechanisms. If the chloride concentration exceeds the binding capacity of

concrete, chloride ions are free in concrete and become available to initiate corrosion. Based on this simple model, researchers defined a chloride threshold value, which is the chloride concentration at the steel concrete interface that causes a significant corrosion rate (Schiessl and Raupach 1990). Chloride threshold is affected by many factors including the pore solution chemistry and pH, water-cement ratio, cement type, mineral admixtures, pore and capillary structure, curing period, and environment (Montemor et al. 2003). Because of the high number of factors affecting the chloride threshold level, the values reported in the literature as percent by weight of cement ranged from 0.17 to 2.5, changing about 15 times (Glass and Buenfeld 1997). Another study also reported that bound chlorides play an important role in the corrosion process by affecting the chloride ingress rate, the threshold value, and the time to corrosion initiation. The same study also reported that bound chlorides may be released as free chlorides as if a fall in pH induces dissolution of complexing phases (Glass and Buenfeld 2000).

A large number of studies investigated the passive film breakdown by chloride ions, and three general models were proposed: 1) adsorption-displacement, 2) chemico-mechanical, and 3) migration-penetration. The strengths and weaknesses of each model is discussed in detail by Jovancicevic et al. (1986).

Chloride ions may be mixed into the concrete with contaminated ingredients and chemical admixtures or they may come from external sources such as deicing salt application, sea salt spray, and direct seawater spraying. Marine structures, especially substructures, are susceptible to severe corrosion due to chloride ingress (Sagues 1994). Concrete bridges and parking garages are also deteriorating at alarming rates due to chloride induced corrosion caused by the use of deicing salts since the 1960s (Berke et al. 1988). Chlorides typically enter the concrete bridge deck or slab of parking garages from the top, reach the top reinforcement layer and initiate localized corrosion, where the bottom reinforcement layer connected with chairs and ties acts as the cathode of a macro corrosion cell. Magnesium chloride, calcium chloride, and calcium magnesium acetate (CMA) are among the deicing chemicals that are available on the market. A study indicated that magnesium chloride is the most destructive deicing chemical followed by the calcium chloride (Cody et al. 1996). CMA is not as destructive as the other alternatives, however it needs to be applied at a much higher rate and can cost 10 times more than deicing salts (Roberge 2000). Also Ge et al. (2004) stated that CMA can cause severe concrete surface deterioration.

## 2.2 CORROSION MONITORING METHODS

Because of the large economical impact of deterioration of reinforced concrete structures due to corrosion, a number of different corrosion monitoring methods have been developed and evaluated. Rodriguez et al. (1994) performed a detailed review of available monitoring techniques and evaluated them for speed of individual measurements, speed of response to change, provided quantitative information, destructivity, disturbing of sample, and measurement parameters (Table II-2).

A more recent review of corrosion monitoring techniques included additional methods not shown in Table II-2: Surface potential (SP) measurements, Tafel extrapolation, galvanostatic pulse transient method, embeddable corrosion monitoring sensor, ultrasonic pulse velocity, X-ray/gamma radiography measurement, and infrared thermograph electrochemical methods (Song and Saraswathy 2007). Cella and Taylor (2000) also proposed measuring the change of resistance of reinforcement as an additional corrosion monitoring technique and stated that this method was more accurate than other more expensive electrochemical methods such as the linear polarization resistance measurements. Some of the corrosion test methods being discussed in this report will be discussed in more detail.

**Table II-2 Features of the Most Widely Used Methods of Corrosion Monitoring.**

| Characteristics | Potential Mapping | Concrete Resistivity | Linear Polarization Method | Guard Ring Method | Coulastic Method | Electro-chemical Noise | EIS | Harmonics | Gravimetric Test | Visual Observation |
|---|---|---|---|---|---|---|---|---|---|---|
| Speed for Measurement | ● | ● | ● | ● | ● | ♦ | ♦ | ♦ | ○ | ○ |
| Speed of Response to Changes | ● | ● | ● | ● | ● | ● | ● | ● | ○ | ○ |
| Quantitative Information | ○ | ♦ | ● | ● | ● | ♦ | ♦ | ● | ● | ● |
| Non-destructive | ● | ● | ● | ● | ● | ● | ● | ● | ○ | ○ |
| Non-disturbing | ● | ○ | ○ | ○ | ♦ | ● | ♦ | ○ | ○ | ○ |
| Measurement Parameter | Prob. Of corrosion | Prob. Of corrosion | $i_{corr}$ | $i_{corr}$ | $i_{corr}$ | $i_{corr}$ | $i_{corr}$ mechanism | $i_{corr}$ | Mean $i_{corr}$ | Geometric failure of attack |

● Method possesses the listed characteristic in an optimal degree.

♦ Method possesses the listed characteristic in a less than fully-satisfactory degree.

○ Method does not possess the listed characteristic.

### 2.2.1 Corrosion Potential (Half Cell Potential)

This method is described in American National Standards ASTM C 876 and because of its simplicity it is widely used. The half-cell potential (a.k.a. open-circuit potential, rest potential, corrosion potential) is measured as a potential difference against a reference electrode at different points on a structure and is used to determine the likelihood of reinforcement corrosion. This method does not provide information about the rate of corrosion, therefore it is usually used together with another monitoring method. Potential readings are interpreted following ASTM C 876, *Standard Test Method for Half-cell Potentials of Uncoated Reinforcing Steel in Concrete* (Table II-3).

**Table II-3 Corrosion Interpretations (ASTM C 876).**

| Half-Cell Potential Reading (V) | | Corrosion Activity |
|---|---|---|
| CSE[1] | SCE[2] | |
| >-0.200 | >-0.125 | Greater than 90% probability of no corrosion |
| -0.200 to -0.350 | -0.125 to -0.275 | An increasing probability of corrosion |
| <-0.350 | <-0.275 | Greater than 90% probability of corrosion |

[1]Copper-copper sulfate electrode, [2]Saturated calomel electrode

Half-cell potential readings can be affected by many factors, such as polarization phenomena due to limited oxygen diffusion. If oxygen diffusion is restricted, such as fully immersed samples deep in solution, reinforcement potential can fall to very negative values without any actual corrosion (Arup 1983; Elsener and Bohni 1992). Existence of high resistance layers in concrete, conductivity of formed corrosion products, the age of concrete, reference electrode position, cement type, and presence of cracks were reported as factors affecting the half-cell potential (Alonso et al. 1998; Browne et al. 1983; Elsener et al. 2003).

### 2.2.2 Macrocell Corrosion Rate

As stated earlier, reinforced concrete bridge decks and parking structures typically deteriorate due to chloride ion induced corrosion. They are exposed to chloride ions and high moisture contents that can decrease the resistivity of the concrete, making it possible for anodes and cathodes to be separated. Therefore, the type of corrosion observed is typically macrocell

corrosion where the top reinforcement mat is the anode and the bottom reinforcement acts as the cathode (Wipf et al. 2006). The potential difference between the anode and cathode causes current flow and corrosion. This corrosion mechanism was mimicked with properly designed samples containing two layers of reinforcement that were electrically connected through a resistor. The corrosion current flowing between the reinforcement layers can be measured by measuring the voltage drop over the resistor, and this information can further be used to calculate a corrosion rate using Faraday's Law. Some of the well-known laboratory tests that measure macrocell corrosion current to monitor corrosion activity are the ASTM G 109 method, the southern exposure method, and the cracked beam method.

### 2.2.3 Polarization Resistance

The polarization resistance technique is a non-destructive electrochemical test method that measures the instantaneous corrosion current density, $i_{corr}$, of steel reinforcement. The method involves increasing or decreasing the potential of reinforcement relative to its open circuit potential by a fixed amount, $\Delta E$, and monitoring of the current decay, $\Delta I$. In the vicinity of the open circuit potential (10 to 30 mV) the voltage-current density curve is linear, and the slope of this section is defined as the polarization resistance, $R_p$ [Eq. (2.9)] (Stern and Geary 1957).

$$R_p = \left( \frac{\Delta E}{\Delta i} \right)_{\Delta E \to 0} \tag{2.9}$$

Current density, $i$, is the measured current divided by the exposed steel surface area. The potential can be changed potentiostatically (potential is changed a fixed amount and current change is monitored) or galvanostatically (fixed amount of current is supplied and the change in potential is monitored). The instantaneous corrosion current density, $i_{corr}$, is calculated by dividing the Stern-Geary constant, *B*, by the $R_p$ value as shown in Eq. (2.10):

$$i_{corr} = \frac{B}{R_p} \tag{2.10}$$

where $R_p$ is in Ωcm$^2$, and $B$ is in Volts. The Stern-Geary constant, $B$, is a combination of anodic and cathodic Tafel coefficients, $\beta_a$ and $\beta_c$ as shown in Eq. (2.11):

$$B = \frac{(\beta_a \beta_c)}{2.3(\beta_a + \beta_c)} \tag{2.11}$$

The value $B$ has been documented to vary from 13 to 52 mV for a wide range of systems (Stern 1958). However, for reinforcing steel in concrete a study recommended the use of 26 mV for bare steel in the active state and for galvanized steel, and 52 mV for bare steel in the passive state (Andrade and Gonzales 1978). Although many studies in the literature used 26 mV as the $B$ value, a more recent study indicated that calculating this value from the measured $E_{corr}$ values can provide better estimates and better correlations with weight loss measurements (Baweja et al. 2003).

A three electrode system is typically used to measure polarization resistance of reinforcement steel that acts as the working electrode. A counter electrode of the same size of the reinforcing steel and a reference electrode are used to shift the potential 20 mV from the free corrosion potential in the anodic or cathodic direction. Measured polarization resistance includes the resistance of electrolyte (the concrete pore solution), which should be accounted for otherwise high resistivity will result in too low $i_{corr}$ values. Potential sweep rates for potentiodynamic measurements or waiting times for potentiostatic and galvanostatic measurements also affect the results. Recommended wait time is 15 (for actively corroding state) to 60 (passive state) seconds for potentiostatic measurements and between 30 and 100 seconds for galvanostatic measurements. A sweep rate of 2.5 to 10 mV/min is recommended for potentiodynamic measurements (Andrade and Alonso 2004).

Polarization resistance measurements are still being evaluated and developed. In a recent study Chang et al. (2007) discussed that performing the potential sweeps in the anodic and cathodic regions in two separate tests results in better potential current curves and that a sweep of ±120 mV will not affect the surface of the reinforcing steel. Videm (2001) and Andrade et al. (1995) also stated that the amount of corrosion products build-up may have an effect on the measured polarization resistance values by consuming current in addition to that directly linked to corrosive reactions.

An important issue with the application of polarization resistance to on-site structures arises from the size mismatch of the small counter electrode and the large working electrode (reinforcement in the structure). Unlike the laboratory samples with similar sized counter and working electrodes, electrical signals are not uniformly distributed over the entire metallic system. This tends to decrease with increasing distance from the counter electrode. Two

methods were developed to solve this issue. The first method uses a model to estimate the polarization resistance based on a transmission line (Feliu et al. 1988; Feliu et al. 1989), and the second method is to use a guard ring to confine the distribution of electrical signal to a given area of the structure located below the counter electrode (Feliu et al. 1990). Sehgal et al. (1992) used the guard ring technique on-site and indicated that the accuracy could be improved by using a planar concrete surface, decreasing the contact resistance between the probe and concrete surface, making measurements after the steady-state potential was reached, and symmetric positioning of the probe over the reinforcement. However, a more recent study that evaluated the linear polarization resistance technique with guarded and un-guarded procedures against gravimetric results indicated that the accuracy of corrosion estimation with linear polarization resistance measurements performed without the guard ring were more accurate (Liu and Weyers 2003).

## 2.3 CORROSION TESTS

Evaluating the corrosion of reinforcing steel completely embedded in concrete has some inherent difficulties. Evaluation procedures are difficult, time-consuming, and subject to uncertainties of interpretation. Several experimental procedures have been used to measure corrosion performance of concrete/reinforcement systems utilizing different corrosion monitoring techniques discussed in the previous section. These experimental procedures have to deal with the slowness and variability of the penetration of aggressive ions such as chlorides and carbon dioxides into the concrete and with the difficulties of designing and using electrochemical monitoring systems in concrete/reinforcement systems (Chappelow et al. 1992).

The ASTM C 876 method evaluates the corrosion status of metal reinforcement in concrete. The method uses half-cell potential measurements and does not provide information on the extent and rate of corrosion. Also the method is intended for use on existing structures, and it does not provide any information on how to fabricate and expose laboratory test specimens.

Different approaches were used by researchers in the laboratory to study the corrosion of reinforcement embedded in concrete; some studies were performed in simulated concrete pore solutions, some studies tried to extract pore solutions from fresh concrete and mortar samples, and some studies were performed on reinforcement that was embedded in concrete or mortar samples. The only ASTM standard to evaluate corrosion performance of reinforcement

steel embedded in concrete is the ASTM G 109 method, which uses half-cell measurements and macro cell measurements.

A major issue with the ASTM G 109 method is the long duration of testing that makes it very difficult for state highway agencies to evaluate new corrosion protection methods being offered by industry. A recent study performed in Canada evaluated corrosion protection methods for reinforced concrete bridges, including chemical corrosion inhibitors, and used ASTM G 109 samples in addition to the on-site measurements. The report indicated that the ASTM G 109 samples containing corrosion inhibitors did not show any activation after 10 years of testing. The control samples that did not contain any inhibitors showed corrosion activation only after seven years of testing (Qian and Cusson 2007).

As stated earlier many researchers are using different corrosion testing methods utilizing different corrosion monitoring methods. These studies try to accelerate the corrosion testing to obtain results much quicker compared to the standard ASTM G 109 method. Researchers are trying different methods to accelerate the corrosion testing, such as application of an electrical field to accelerate chloride penetration into the concrete (Castellote et al. 2002; Trejo and Pillai 2003) and different drying and wetting regimes to utilize different transport mechanisms in addition to diffusion (Nygaard and Geiker 2005). However, these new methods have to be evaluated for the actual time of testing, their complexity, and for the correlation of their results with the results obtained from the standard ASTM G 109 method to be implemented by state highway agencies. A study performed by Soleymani and Ismail (2004) used different corrosion tests on ordinary and high performance concrete samples and stated that different corrosion tests assessed the same level of corrosion activity only in 24 percent of samples.

### 2.3.1 Accelerated Chloride Threshold Level Test

The accelerated chloride threshold (ACT) test was developed to determine the critical chloride threshold of steel samples embedded in mortar in a relatively short time compared to the standard corrosion test methods (Trejo and Miller 2003). This test accelerates the transfer of chloride ions to the steel surface using an electrical field. Chloride ions migrate under the effect of an electrical field to the steel surface instead of slowly diffusing into concrete due to concentration differences.

Steel reinforcement samples are embedded in 3 x 6 in (75 x 150 mm) mortar cylinders that have attached chloride solution reservoirs at the top. Chloride reservoirs are filled with 3.5 percent by weight sodium chloride solution. Figure II-1 shows the layout of ACT test setup. An electrical field is generated by applying a potential difference of 20V between an anode at the reinforcement level and a cathode in the chloride reservoir. Negatively charged chlorides migrate to the anode, and when they reach the chloride threshold level, they initiate corrosion of the steel reinforcement. Corrosion of steel reinforcement is monitored through polarization resistance method. A counter electrode and Haber-Luggin probe, which contains a reference electrode, are embedded in the mortar above the steel reinforcement to run the polarization resistance tests. The anode, cathode, and counter electrodes are fabricated from Ni-Cr mesh.

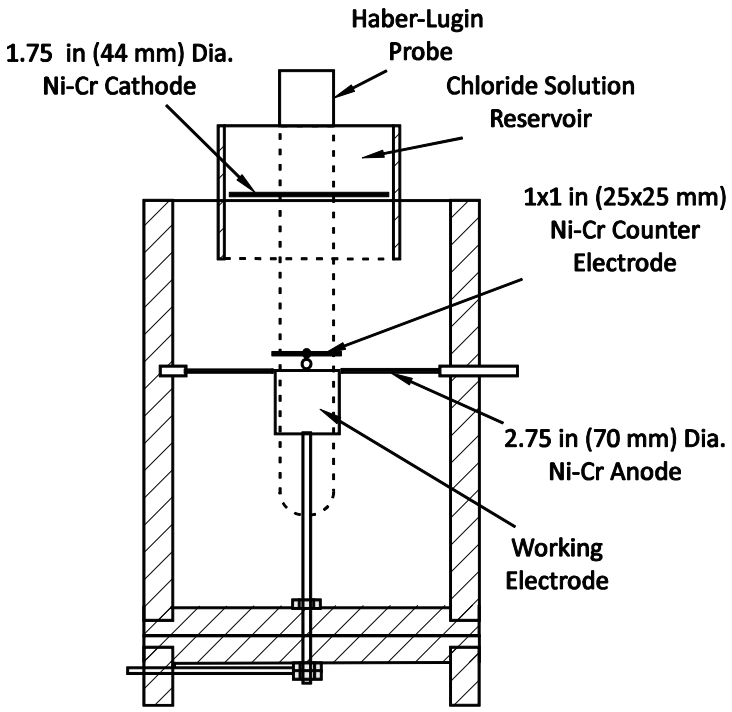


**Figure II-1 ACT Test Layout.**

An electrical field is applied in intervals of 6 hours, and polarization resistance of reinforcement is measured at the end of a wait period of 42 hours after each application of the electric field. Testing is stopped when initiation of corrosion is detected. The amount of

chlorides at the steel reinforcement level is then measured to determine the chloride threshold value.

Castellote et al. (2002) also developed a similar chloride threshold measurement method that uses an electrical field to accelerate the transfer of chloride ions. This method uses mortar cubes with an embedded steel reinforcement, and it monitors corrosion initiation through polarization resistance. It should be noted that in this test method the anode and the reference electrode are not embedded in the mortar. The anode is underneath the sample, and the cathode and the reference electrodes are placed in the chloride reservoir. Castellote et al. recommends the use of 10 to 13 V potential difference to drive the chlorides and uses a 1 M Sodium Chloride solution. Trejo and Pillai (2003) evaluated the use of 1, 5, 10, 20, and 40 V potential differences for the electrical field and determined that up to 10 V the chloride profile development in the mortar did not change significantly.

The use of an electrical field to accelerate the transport of chlorides into the mortar or concrete also causes polarization of the steel reinforcement that is being tested for chloride threshold. In the literature it is reported that chloride threshold is independent from the potential of the reinforcement for potential values greater than -200 ±50 mV vs. SCE (Alonso et al. 2002) and that it linearly increases with decreasing potential for potential values less than -200 ±50 mV vs. SCE (Izquierdo et al. 2004). The ACT test minimizes the polarization of reinforcement by placing the anode at the same level as the reinforcement and by connecting the anode to the ground terminal of the power source (Trejo and Pillai 2003). Castellote et al. (2002) reported that, although applied, the electrical field polarized the reinforcement being tested in direct proportion to the applied voltage, the reinforcement potential returned to its original value soon after the power supply was switched off. They also reported that because of this reversibility of potential the electrical field can be switched off when a drop in the potential is observed and that this way the chloride threshold could be measured in a quasi-natural state. Because the ACT test also measures the polarization resistance when the electrical field is switched off, the same claim about the quasi-natural state of reinforcement can be made for the ACT test.

Another issue with the use of an electrical field to accelerate chloride transfer is the effect of the electrical field on the pH of the mortar environment. In the literature many researchers reported that chloride threshold levels change proportionally with the hydroxyl ion concentration of the environment and proposed to state chloride threshold levels as chloride to

hydroxyl ratios (Glass and Buenfeld 1997). Trejo and Pillai (2003) reported that the pH of the environment around the reinforcement was decreasing with increasing magnitude of applied electrical field and with increasing time of application due to the oxidation of hydroxyl ions at the anode. Similar to chlorides, negatively charged hydroxyl ions are also attracted to the anode and if the rate of their oxidation is higher than their rate of transportation, the pH around the anode (same level as the reinforcement) decreases. On the contrary, Castellote et al. (1999; Castellote et al. 2002) recommended addition of HCl to the chloride solution to neutralize the environment around the reinforcement. They suggested that the extra hydroxyl ions generated at the cathode through reduction of water molecules were being attracted into the mortar causing an increase of the pH of the environment. Due to their higher transference numbers, hydroxyl ions were also slowing the penetration rate of chlorides.

ACT test was used to determine chloride threshold values of conventional and corrosion-resistant reinforcements embedded in mortars with a water-cement ratio of 0.5. Mean critical chloride threshold for ASTM A 615 and ASTM A 706 steels were 0.87 lb/yd$^3$ (0.52 kg/m$^3$) and 0.34 lb/yd$^3$ (0.20 kg/m$^3$), respectively. The 95 percent confidence intervals of the means for the ASTM A 615 and A 706 steels were 0.51 to 1.20 lb/yd$^3$ (0.3 to 0.71 kg/m$^3$) and 0.25 to 0.40 lb/yd$^3$ (0.15 to 0.24 kg/m$^3$), respectively. The 95 percent confidence interval shows the range of values that includes the mean value with 95 percent probability and is a good indicator of variability of results, i.e., the bigger the interval the more variability. Mean critical chloride threshold values for microcomposite steel, stainless steel 316LN (SS 316LN), and stainless steel 304 (SS304) were 7.7 lb/yd$^3$ (4.6 kg/m$^3$), 8.5 lb/yd$^3$ (5.0 kg/m$^3$), and 18.1 lb/yd$^3$ (10.8 kg/m$^3$), respectively. Their 95 percent confidence intervals were 6.5 to 9 lb/yd$^3$ (3.8 to 5.3 kg/m$^3$), 6.9 to 10.1 lb/yd$^3$ (4.1 to 6 kg/m$^3$), and 16 to 20.2 lb/yd$^3$ (9.5 to 12 kg/m$^3$), respectively. Corrosion resistant steel exhibited higher chloride threshold values as expected but with a higher variability compared to the ASTM A 615 and A 706 steels. The duration of the ACT test for conventional steel samples was approximately 7 weeks and approximately 16 weeks for corrosion resistant steel types (Trejo and Pillai 2003; Trejo and Pillai 2004). Although the ACT test was used on different types of steel reinforcement, it was not evaluated for different mortar mixtures with or without corrosion inhibiting admixtures, and its results were not compared with long-term standard test results. This study aims to do both of these evaluations for the ACT method.

Castellote et al. (2002) used their chloride threshold determination method only with conventional corrugated steel rebar embedded in mortar with a water-cement ratio of 0.37, but they also tested some of their samples without the application of an electrical field, where chlorides diffused into the mortar similar to longer term standard corrosion tests. They reported that the results of the accelerated test method were similar to the results of the standard diffusion method. Chloride threshold for the accelerated test method was 0.152 percent by weight of sample and 0.227 percent by weight of sample for the diffusion method. Chloride thresholds expressed as chloride to hydroxyl ion ratio for the accelerated and diffusion tests were 2.0 and 1.5, respectively (Castellote et al. 2002). Viedma et al. (2006) also tested similar samples using an electrical field to accelerate the test and using only diffusion of chlorides into the mortar with a water-cement ratio of 0.45. The chloride threshold for the embedded conventional corrugated steel rebar was 2 and 1.07 percent by weight of cement for the diffusion and accelerated samples, respectively. Similar to Castellote et al.'s results, the chloride threshold determined by the diffusion method was higher compared to the result of the accelerated method. Initiation of corrosion for the diffusion samples took 432 days, and the coefficient of variation of the results was 50 percent. For the accelerated samples, initiation of corrosion took place at 1 to 6 days, and the coefficient of variation was only 23 percent.

### 2.3.2 Rapid Macrocell Test

The rapid macrocell test was originally developed at the University of Kansas under the Strategic Highway Research Program (SHRP) (Martinez et al. 1990). Reinforcing bars placed in two separate containers, filled with simulated concrete pore solution, were intended to represent the top and bottom reinforcement mats of a bridge deck. Reinforcing bars were either bare or covered with mortar. Sodium chloride was added to one of the containers to initiate corrosion of reinforcing bars in this container (anode). The other container was supplied with scrubbed air to ensure adequate supply of oxygen necessary for reduction reactions (cathode). Reinforcing bars in separate containers were electrically connected over a resistor, and the solutions were connected over a salt bridge. The corrosion potential of reinforcing bars and the macrocell current flowing between the containers through the resistor were monitored. Figure II-2 shows the rapid macrocell test setup.

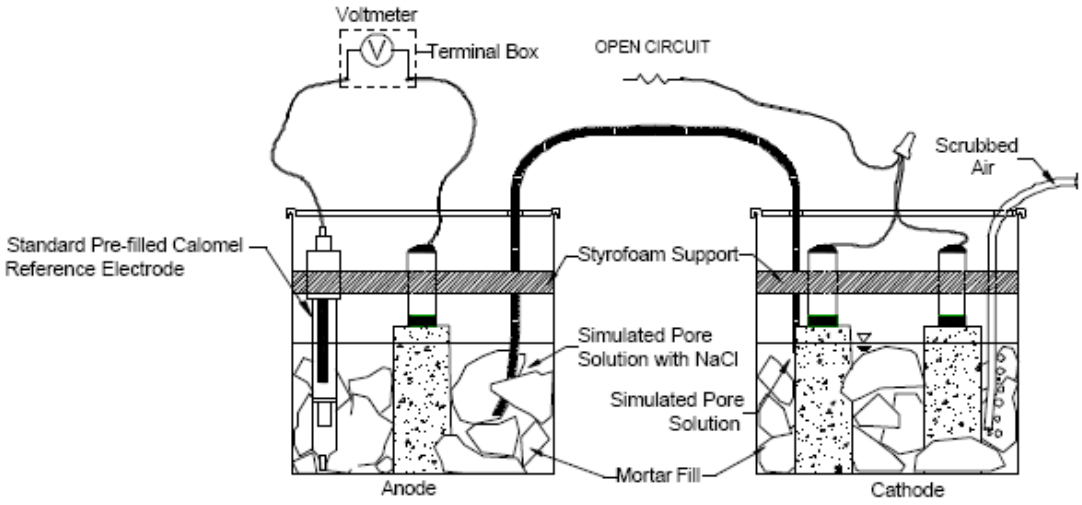


**Figure II-2 Rapid Macrocell Test Setup (Balma et al. 2004).**

Different aspects of the test method such as the number and diameter of reinforcing bars in containers, the magnitude of the resistor, salt concentration in anodic container, and the height of solution were all modified by different researchers, who used this method in later studies to improve the consistency and repeatability of the results (Schwensen et al. 1995; Senecal et al. 1995; Smith et al. 1995). Reinforcing bars used in initial studies were only partially covered with mortar (lollipop samples) but later it was decided to embed the reinforcing bars completely within the mortar (wrapped samples) to prevent corrosion of reinforcing bars at the steel-mortar interface (Darwin et al. 2002).

Kahrs et al. (2001) used the rapid macrocell method to evaluate corrosion performance of 304 stainless steel clad bars. Lollipop type samples and bare samples were exposed to 1.6 molal chloride solutions. Different mortar cover thicknesses and different protection methods for the cut end of reinforcing bars were evaluated. The study also evaluated the corrosion potential and macrocell current of sandblasted and damaged stainless steel clad samples. The study concluded that stainless steel 304 clad reinforcing bars have significant chloride corrosion resistance compared to conventional bars.

In another study the rapid macrocell method was used to evaluate the corrosion performance of micro-composite steel (MMFX) against conventional steel and epoxy coated reinforcement (Darwin et al. 2002; Gong et al. 2002). Mortar wrapped conventional steel, MMFX steel, and epoxy coated steel samples were exposed to 1.6 molal chloride solution for

15 weeks. Epoxy coated bars were combined with uncoated bars as cathodes, and the study also evaluated combinations of MMFX steel and conventional steel. In addition to rapid macrocell tests, the reinforcing bars were also tested with the southern exposure method and the cracked beam test method, which required more time to activate when compared to the rapid macrocell method. Results indicated that MMFX steel performed better than conventional steel samples and worse than epoxy coated samples. The results of the rapid macrocell tests and the long-term bench scale tests (southern exposure test and cracked beam test) were in good agreement. Results also indicated that combining MMFX steel with conventional steel reduced the corrosion performance of MMFX steel.

In 2005, Balma et al. used the rapid macrocell test method in addition to southern exposure and cracked beam tests to evaluate different corrosion protection systems, such as different water-cement ratios, corrosion inhibitors, and different steel types. Three different microalloyed thermex treated steels, thermex treated conventional steel, MMFX microcomposite steel, epoxy coated steel, two duplex steels, and uncoated normalized steel were evaluated for corrosion performance using rapid macrocell test. Samples were exposed to 0.4M and 1.6M NaCl solutions for 100 days during which their corrosion potential and corrosion rates were monitored. Total corrosion loss of samples was lower in mortar and concrete with lower water-cement ratios and in mortar and concrete containing corrosion inhibitors (there were no cracks in mortar or concrete). Epoxy coated reinforcing bars exhibited lower corrosion loss compared to conventional bars. The study also indicated that the correlation of total corrosion loss obtained from rapid macrocell corrosion test, southern exposure test, and cracked beam test were good in most cases and had similar variability.

Gong et al. (2006) also used the rapid macrocell test to evaluate the effectiveness of different corrosion inhibitors and different steel types to decrease corrosion. In addition to rapid macrocell tests, benchscale tests such as southern exposure test, cracked beam test, and ASTM G 109 tests were performed. The study evaluated conventional epoxy coated reinforcing bars, stainless steel 316LN clad bars, different corrosion inhibitors, bars coated with conventional epoxy over a primer coat that contains microencapsulated calcium nitrite, bars coated with different increased adhesion epoxies, and galvanized bars with blue epoxy coating. Linear polarization tests were also performed on benchscale test samples to measure microcell corrosion. Results indicated that stainless steel clad reinforcement exhibited superior corrosion performance if the cladding was not damaged compared to conventional reinforcement and

epoxy coated reinforcement. An interesting finding of this study was that the measured microcell corrosion rates for conventional steel samples in southern exposure and ASTM G 109 samples was one order of magnitude higher compared to the macrocell corrosion rates. Trejo and Pillai (2003) also found that the macrocell corrosion rates are not representative of actual corrosion rates.

Guo et al. (2006) did a very similar study evaluating different epoxy coated reinforcements and other corrosion protection systems using rapid macrocell test, southern exposure test, cracked beam test, and ASTM G 109 test. The results of the study were very similar to the results of Gong's study (Gong et al. 2006). However, there were a couple of contradicting results. The results of this study indicated that the corrosion performance of epoxy coated reinforcing bars with primer containing microencapsulated calcium nitrite improved for uncracked samples with water-cement ratio of 0.35 compared to conventional steel samples. Gong et al. noted that there was no significant improvement in their corrosion performance. Guo et al. also stated that although there was good correlation between the results of the rapid macrocell test and benchscale tests, the rapid macrocell test was better in identifying differences between corrosion protection systems.

### 2.3.3 Chloride Ion Threshold Test

The subcommittee G01.14 of the ASTM committee G 01 is currently working on work item WK995 to produce a standard for determining the chloride-ion threshold for corrosion of reinforcing steel in concrete. This new test method is being developed to supplement the existing protocol ASTM G 109 and is focusing on chloride ion threshold determination to evaluate the effectiveness of different corrosion protection systems, such as admixtures (Berke et al. 2003). The proposed test method involves placement of two reinforcement bars at two layers in cylindrical test specimens that are cast using a standard mortar mixture. The only alteration allowed to the standard mortar is the incorporation of the material (inhibitor, mineral admixture, etc.) being evaluated. Specimens are moist cured and dried at a laboratory standard environment before they are exposed to cyclic wetting and drying with a chloride solution. Macrocell current flowing between the two layers of reinforcement over a 10 ohm (Ω) resistor, open circuit potential of the top reinforcement, and the linear polarization resistance of the top reinforcement are monitored throughout the test to determine the initiation of corrosion. Figure II-3 shows the test layout. Testing of samples is stopped, and the chloride ion content at the top

reinforcement level is determined when all of the electrochemical measurements indicate corrosion initiation for two consecutive weeks. The draft standard for this test states that the method is intended to evaluate the relative performance of corrosion protection systems and that the measured results do not translate to corrosion rates occurring in structures.

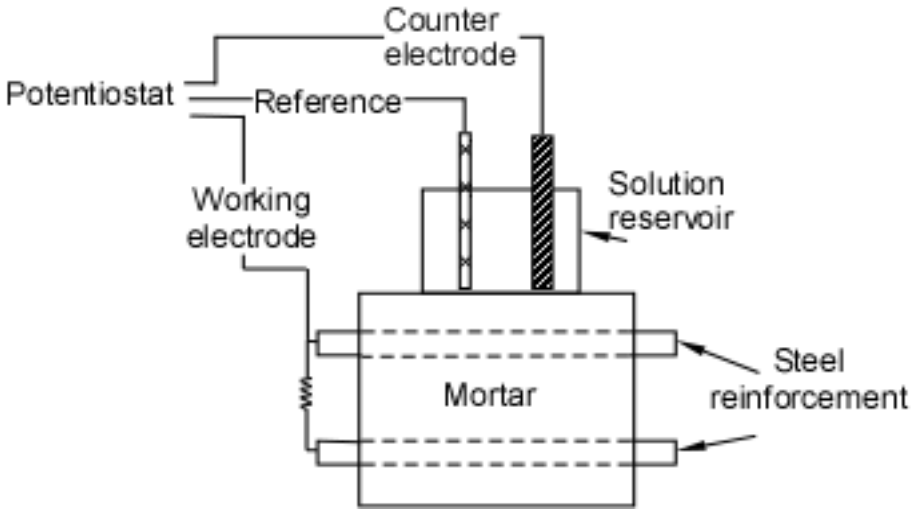


**Figure II-3 Chloride Ion Threshold Test Layout.**

As stated earlier, this is a new test method being developed and revised, and currently there are no published reports or papers with results obtained using this method.

### 2.3.4 ASTM G 109 and Modified G 109 Test

ASTM G 109 is the standard test method for determining effects of chemical admixtures on corrosion of embedded steel reinforcement in concrete exposed to chloride environments. In 1992 (and revised again in 2007), the ASTM committee published the standard. This is a widely used standard in corrosion studies to evaluate many corrosion protection methods, including different concrete properties, supplementary cementing materials, corrosion inhibitors, and corrosion resistant reinforcement steels. The method uses 11 x 6 x 4.5 in (280 x 150 x 115 mm) concrete samples with two layers of reinforcement. The top layer consists of one reinforcing bar with a 0.75 in (19 mm) concrete cover and two bottom layer bars. The two layers of reinforcement are electrically connected over a 100 Ω resistor. The samples are

ponded with a sodium chloride solution for two weeks and kept dry for two weeks. Macrocell corrosion current and the half-cell potential of the bars against a CSE reference electrode are monitored. Figure II-4 shows the ASTM G 109 setup. ASTM committee G 01 has performed an inter-laboratory and intra-laboratory study for the ASTM G 109 method and reported that the maximum end of the 95 percent confidence interval for time to failure for control specimens with 0.75 in (19 mm) cover was six months for both intra- and inter-laboratory tests.

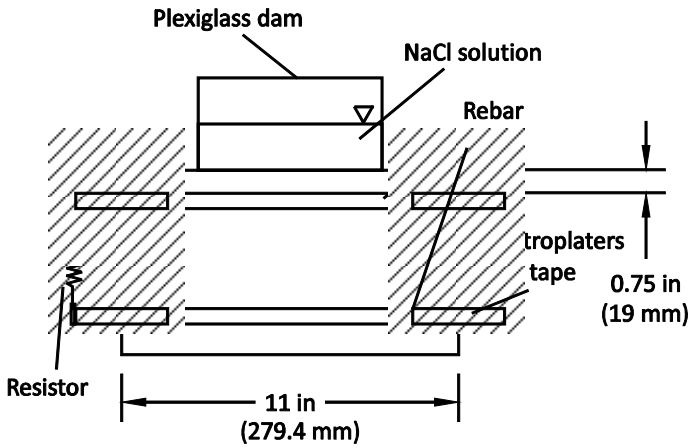


**Figure II-4 ASTM G 109 Sample.**

This test method has been extensively used by many researchers to evaluate different corrosion protection methods and many modifications of it were implemented. The number of bars at the top and bottom layer, the magnitude of resistor between the layers, chloride concentration of ponding solution, and wetting and drying cycles were all modified by different researchers. Although the standard notes that the time to failure is six months, the literature indicates that this time is much longer, and organizations that evaluate products to prevent corrosion of reinforcing steel in concrete are resistant to use this method.

## 2.4 CORROSION PROTECTION METHODS IN CONCRETE

Two key parameters are necessary to evaluate the corrosion performance of steel reinforcement embedded in concrete. These parameters are the chloride concentration required to initiate active corrosion (critical chloride threshold) and the rate of corrosion after initiation. The

service life of a reinforced concrete structure exposed to chlorides is typically evaluated as two separate phases. The first phase is the amount of time for chloride ions to reach the steel interface in sufficient quantities to initiate active corrosion. The second phase is the time required to cause sufficient cracking or spalling of the concrete cover such that the structure is no longer serviceable. A conventional plot of the service life for a reinforced concrete structure is shown in Figure II-5.

The initiation phase of the service life is dependent on the rate of chloride migration through the cementitious material and the corrosion resistance characteristics of the reinforcement in the cementitious environment. The propagation phase is mainly dependent on the rate of corrosion of the reinforcement. After initiation, corrosion protection systems are designed to increase the length of one or both of these phases to increase the service life of reinforced concrete structures.

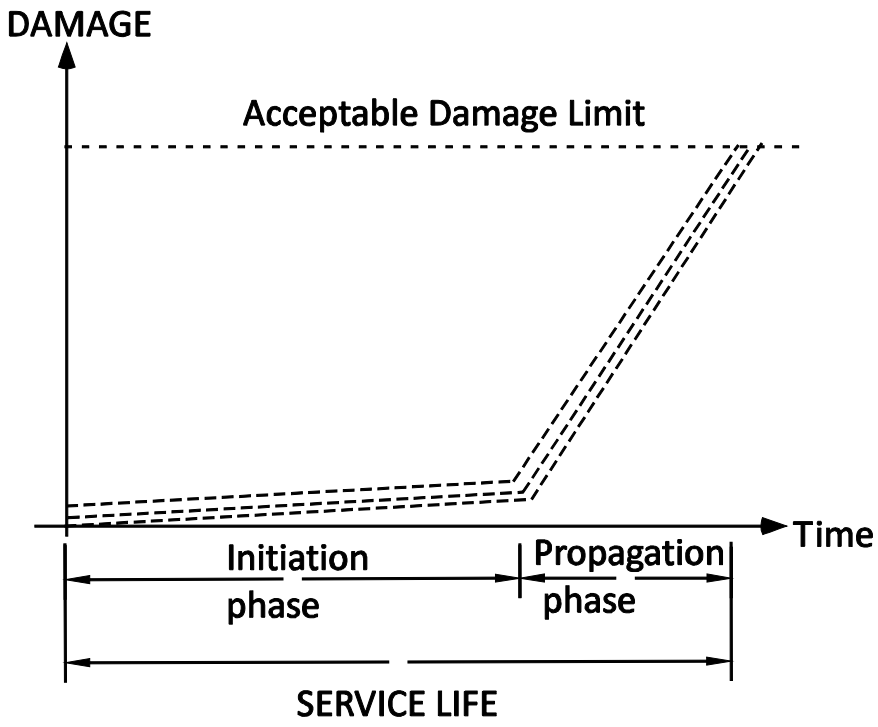


**Figure II-5 Conventional Schematic of the Service Life of a Reinforced Concrete Structure.**

Three main corrosion protection methods currently being used in the construction industry include the addition of corrosion inhibitors (chemical admixtures) into the concrete, use of alternative corrosion resistant reinforcement types, and reducing the permeability of concrete. These methods can be used separately or together for improved corrosion performance and longer service lives.

Cathodic protection can also be used to protect metals against corrosion. This method protects metals by making them cathodes in an electrochemical cell. This is achieved either by connecting the metal to a sacrificial anode or to an anode connected to a power source. Unlike the three earlier methods, cathodic protection requires continuous monitoring and maintenance and will not be further addressed in this report.

### 2.4.1 Alternative Corrosion Resistant Steel

Reinforcement steel meeting the requirements of ASTM A 615 specification is the most commonly used reinforcement type in the construction industry. ASTM A 615 specification requires only carbon, manganese, phosphorus, and sulfur contents to be reported but does not put any limits on them with the exception of sulfur. Sulfur content is limited at a maximum of 0.06 percent. ASTM A 706 puts many limits on steel chemistry to create a steel that is easily weldable and more ductile when compared with ASTM A 615 steel (Gamble 2003).

One of the methods to increase the corrosion resistance of reinforced concrete structures is to coat these commonly used steels that meet the ASTM A 615 or A 706 standards. Coatings can be organic or metallic. Coatings create a barrier against moisture, oxygen, and chloride ions and can electrically isolate the underlying steel. Another method to protect the reinforced concrete structures against corrosion is to use inherently corrosion resistant steels that are obtained through alloying and through different manufacturing processes.

#### *2.4.1.1 Corrosion resistant reinforcement*

##### *2.4.1.1.1 Stainless steel*

Stainless steels by definition contain a minimum of 12 percent chromium. The high chromium contents of stainless steel results in the formation of a passive layer on the surface of the steel that resists further oxidation (corrosion). According to their metallurgical structure, stainless steels are divided into four groups: ferritic, ferritic-austenitic, martensitic, and austenitic.

Historically, the most commonly used stainless steels in the construction industry are austenitic steels such as 304, 316, and 316 LN stainless steels (Smith and Tullman 1999). These steels are low in carbon and contain approximately 18 percent chromium and 8 percent nickel. Ferritic-austenitic stainless steels have also been used as concrete reinforcing steel. These are called duplex stainless steels and contain 21 to 28 percent chromium and 1 to 8 percent nickel. Ferritic steels have less than 17 percent chromium, and martensitic steels have 12 to 18 percent chromium. Neither has been used as concrete reinforcement steel.

An FHWA study evaluated the use of 304 and 316 stainless steels in concrete bridge decks. The study reported that the reinforcement in the decks built using only 304 stainless steel for the bottom and top reinforcement exhibited high corrosion resistance. However, the conventional reinforcement in the decks built using stainless steel 304 for the top reinforcement only and coupled with conventional steel at the bottom exhibited low corrosion resistance. Stainless steel 316 performed well in both cases (McDonald et al. 1998). Another study evaluated 304, 316LN, and duplex stainless steel 2205 and reported that solid stainless steel showed no signs of corrosion when the chloride concentration in the concrete adjacent to the stainless steel bars was 15 times higher than the corrosion initiation threshold of conventional steel (Clemena and Virmani 2002).

Although many studies reported superior corrosion performance of stainless steels in concrete, the main impediment to its use in reinforced concrete structures is their high initial costs.

#### *2.4.1.1.2 Microcomposite steel*

MMFX microcomposite steel was developed by the MMFX Steel Corporation and contains approximately 9 percent chromium. A proprietary chemical composition and production process controls the martensitic microcomposite microstructure that consists of untransformed nano sheets of austenite between laths of dislocated martensite, resulting in a virtually carbide free steel. Due to its microstructure, forming of microgalvanic cells is prevented, which makes the steel corrosion resistant.

Studies performed at Texas A&M University reported that the chloride threshold of MMFX was approximately nine times that of conventional steel and very close to that of 304 stainless steel (Trejo and Pillai 2004). Studies performed at the University of Kansas reported

that MMFX steel had a higher corrosion threshold and a lower corrosion rate compared to conventional steel reinforcement (Darwin et al. 2002; Gong et al. 2002).

#### *2.4.1.2 Coated reinforcement*

##### *2.4.1.2.1 Epoxy-coated reinforcement*

Epoxy-coated reinforcement (ECR) is used in many bridges in the U.S. ECR is produced by applying epoxy powder on freshly blasted steel surfaces at high temperatures. Reinforcing bars covered with melted epoxy are quenched, usually in a water spray bath. ASTM A 775 (*Standard Specification for Epoxy-Coated Steel Reinforcing Bars*) and A 934 (*Standard Specification for Epoxy-Coated Prefabricated Steel Reinforcing Bars*) provide specifications to control the quality of epoxy coatings during coating, handling, shipping, and storage (Manning 1996).

Although ECR has been commonly used since the 1970s in bridge decks, recent studies reported that ECR may not provide the desired service life due to cathodic disbondment problems. A Florida Department of Transportation study stated that electrochemical disbondment of epoxy coatings could initiate due to exposure to salt water and subsequent macrocell corrosion during service in bridge substructures (Sagues et al. 1994). However, later studies of cathodic disbondment of ECR reported that the adhesion reduction was related to water penetrating the coating and oxidation of the underlying steel, rather than the presence of the chloride ions or excessive coating damage (CRSI 1995; Weyers et al. 1998). If the coating had already disbonded when chloride ions arrived at the surface of the reinforcement, corrosion could occur under the coating (Pyc et al. 2000). Clear (1992) concluded that the life of ECR structures would exceed that of structures with conventional steel by only three to six years in marine environments in Canada and the northern U.S. He reported that the failure mechanisms of ECR included cathodic disbondment, loss of epoxy's insulative properties under macrocell action, and the evolution of hydrogen at secondary cathodes developed on the macro anode after the pH decreased due to macrocell action.

Although cathodic disbondment of ECR was reported by many researchers, an FHWA study performed in 1996 reported that ECR incorporating reinforced concrete structures performed well. The study evaluated a total of 92 bridge decks, two bridge barrier walls, and one noise barrier wall located in 11 states and three provinces that were built with ECR and found that overall, the structures were in good condition, and only two percent of evaluated

ECR segments exhibited significant corrosion. These were extracted from locations of heavy cracking, shallow concrete cover, high concrete permeability, and high chloride concentrations (Smith and Virmani 1996). In another FHWA study it was reported that to get the best performance from ECR, it should be used not only for the top mat but for both top and bottom mats. The study also recommended the repair of cracks and damaged areas of ECR (McDonald et al. 1998).

Currently many companies are trying to develop modified ECR bars to solve the cathodic disbondment and corrosion problem and bringing new products to the market. The objective of this study is to identify a cost and time efficient evaluation system for state highway agencies so that these products can be evaluated in a timely manner and incorporated into new construction projects.

#### *2.4.1.2.2 Metal-coated reinforcement*

Metallic coatings can either be sacrificial or noble. Metals that have a more negative corrosion potential than conventional steel will act as sacrificial coatings, i.e., if the coating is broken, the coating will corrode, protecting the conventional base steel. Noble coatings have a more positive potential than conventional steel, which means that they are less likely to corrode in concrete than conventional steel. If the coating is broken, the conventional base steel will become anodic and corrode.

A widely used sacrificial coating is galvanized steel. Galvanized coatings are produced by hot dip galvanizing processes where steel is immersed in a bath of molten zinc metal. Steel is first cleaned to remove oils, greases, soils, mill scale, and rust. Galvanized coating is metallurgicaly bonded to the steel substrate and consists of a series of zinc-iron alloy layers with a surface layer of zinc. When coating is damaged and the underlying steel starts to corrode, zinc corrodes sacrificially and a layer of zinc hydroxide ($Zn(OH)_2$) layer forms on the active corrosion site preventing further corrosion (McCrum and Arnold 1993). However, studies that evaluated galvanized steel in concrete concluded that this method may be inadequate to obtain the desired service life. It was reported that using galvanized steel in concrete with high concentrations of chloride only delay concrete failure by a limited period of time and did not provide a permanent solution (McCrum et al. 1995; Rasheeduzzafar et al. 1992). Another study found that the chloride threshold level for galvanized steel in concrete was approximately 2.5 times that of conventional steel, and that zinc coating increased the

corrosion initiation phase 4 to 5 times compared to conventional steel in equivalent conditions (Yeomans 1994).

An example for noble coating is stainless steel clad reinforcement. Because of the high initial cost of using solid stainless steel reinforcement, the use of stainless steel clad reinforcement was evaluated as a cheaper alternative. A field study reported that samples of 304 stainless steel clad bars taken from a bridge after 11 years of service exhibited no sign of corrosion (McDonald et al. 1995). Laboratory studies reported that 304 stainless steel clad reinforcement had a much higher chloride threshold and superior corrosion performance compared to conventional steel (Kahrs et al. 2001; Rasheeduzzafar et al. 1992). However, challenges with breaks or holidays in the stainless steel cladding have prevented its widespread use.

### 2.4.2 Low Permeability/Diffusivity Concrete

Another corrosion protection method is to decrease the permeability or diffusivity of the concrete. Lower permeability/diffusivity values will slow the ingress of water, oxygen, chloride ions, and other chemicals that initiate corrosion of reinforcement. A lower permeability also reduces the electrical conductivity of the concrete. Use of lower water-cement ratios (with the help of superplasticizers) and supplementary cementing materials can also decrease the permeability/diffusivity of concrete. Studies showed that the use of concretes with a water-cement ratio of 0.3 and 0.32 exhibited practically impermeable concrete (Sherman et al. 1996). However, crack surveys at bridge decks indicated that concretes with necessary cement contents to obtain these water-cement ratios may exhibit excessive cracking, which would allow faster ingress of water, oxygen, and other chemicals into the concrete.

Application of concrete surface treatments such as polymer membranes, penetrating sealers, and modified cementitious or acrylic coatings can also prevent the ingress of water, oxygen, and other chemicals into the concrete. Use of a larger cover depth by design can also extend the corrosion initiation phase by increasing the distance that needs to be travelled by chlorides and other chemicals to initiate corrosion.

### 2.4.3 Corrosion Inhibitor

An ideal chemical inhibitor is a chemical compound that can prevent corrosion of embedded steel when added in adequate amounts and, at the same time, has no adverse effect on the fresh

and hardened properties of concrete (Al-Amoudi et al. 2003). It also needs to be effective at the pH and temperature of the concrete environment. Corrosion inhibitors can affect several factors of the corrosion process including: rate of chloride ingress, degree to which chlorides are chemically bound in the concrete cover, chloride threshold of the steel/concrete system, electrical resistance of concrete, and chemical composition of the electrolyte (Hansson et al. 1998).

Corrosion inhibitors can be divided into three types: anodic, cathodic, and mixed. The type is determined based on whether they interfere with the corrosion reaction preferentially at the anodic or cathodic sites, or at both sites (Ramachandran 1984). Anodic inhibitors act by forming an oxide film barrier on anodic surfaces of the reinforcing steel or by promoting the stabilization of the natural passivating layer of the steel, thereby delaying corrosion initiation and controlling the rate of corrosion. Cathodic inhibitors often precipitate at the cathode sites and limit the availability of oxygen necessary for the cathodic reaction to occur (Brown 1999; Daigle et al. 2004). Mixed corrosion inhibitors form a corrosion resistant film that adheres to the metal surface physically and/or chemically to block both the anodic and the cathodic reations (Nmai et al. 1992).

Corrosion inhibitors may be inorganic or organic compounds. Evaluated inorganic compounds include sodium nitrite, potassium chromate, sodium benzoate, stannous chloride, dinitrobenzoic acid, sodium molybdate, and sodium florophophite. Organic inhibitors include amines, esters, and sulfonates, and they are typically classified as mixed corrosion inhibitors.

This study used a commercial inorganic corrosion inhibitor DCI-S, a product of W.R. Grace, and evaluated its effects with different corrosion test methods. DCI-S is a calcium nitrite based inhibitor and also includes a set retarder to counteract the accelerator effect of calcium nitrite that was shown in earlier studies (Ann et al. 2006). The solid content of DCI-S is approximately 33 percent, and its specific gravity is 1.2. The manufacturer recommended dosages vary from 2 to 5 gal/yd$^3$ (10 to 30 L/m$^3$) of concrete, depending on the chloride exposure level.

Calcium nitrite is an anodic inhibitor that minimizes the anodic reaction by reacting with ferrous ions to form a γ-ferric oxide layer at the anode, as shown in Eq. (2.12):

$$Fe^{++} + OH^- + NO_2^- \rightarrow NO\uparrow + \gamma FeOOH \tag{2.12}$$

Calcium nitrite increases the chloride concentration necessary to initiate corrosion by competing with the chloride ions reacting with the steel. Because the relative concentration of

chloride and nitrite ions determines which ion will react with steel, the minimal dosage of calcium nitrite to prevent corrosion is usually expressed as the concentration ratio of chloride to nitrite ions. Different studies reported different chloride to nitrite ratios for corrosion prevention. El-Jazairi and Berke (1990) reported a ratio of 1 to 2. Another study indicated that a chloride to nitrite ratio higher than 1.6 would result in the corrosion of reinforcing steel in concrete (Gaidis and Rosenberg 1987). An FHWA study reported that for chloride to nitrite ratios less than 1.5, calcium nitrite was able to inhibit corrosion (Virmani 1990; Virmani et al. 1983). Another study evaluated calcium nitrite in oxygenated limewater with added calcium chloride and reported a chloride to nitrite ratio of 1.1 to 1.4 prevented corrosion. The same study reported that calcium nitrite could also repassivate the steel after corrosion initiated by exposure to calcium chloride (Hope and Ip 1989). A more recent study that evaluated the chloride threshold of nitrite in mortar and concrete reported a chloride to nitrite ratio range from 1.5 to 3 (Ann et al. 2006). Other researchers cautioned about the possibility of accelerated pitting of steel reinforcement in the presence of chlorides when nitrite was "under dosed" and expressed reservations with regard to the possible migration and leaching out of nitrite from concrete (Cigna et al. 1994; Nurnberger and Beul 1991).

Calcium nitrite has been used in concrete in Europe and the U.S. for a long time, and it is preferred as an inhibitor because of its compatibility with concrete properties. Extensive testing showed that it protects the steel against chloride induced corrosion, its efficiency increases as the concrete quality improves, it lowers the corrosion rate once corrosion begins, and it works in the presence of cracks (Berke et al. 1988; Berke and Rosenberg 1989; Burke 1994; El-Jazairi and Berke 1990; Pfeifer et al. 1987; Trepanier et al. 2001).

Comparing the effectiveness of calcium nitrite with ECR reinforcement as a corrosion protection method, a study showed that use of calcium nitrite was better than using ECR with 2 percent coating damage and equivalent to using ECR without damage. The study also stated that calcium nitrite cannot prevent coating disbondment or corrosion underneath the coating when used together with ECR (Berke 1998).

Al-Amoudi et al. (2003) evaluated different corrosion inhibitors including calcium nitrite in concrete that was contaminated with chlorides, sulfates, seawater, brackish water, and unwashed aggregates. He stated that the use of ASTM C 876 corrosion potential method did not give reliable results. Linear polarization testing indicated that calcium nitrite was distinctly

efficient in delaying corrosion and decreasing corrosion rates in chloride and chloride plus sulfate contaminated concrete.

Another study evaluated DCI-S for inhibition effects, influence on the chloride transport, compressive strength, and setting time of concrete. The corrosion rate was reduced at all levels of chloride ions in the mortar, and the chloride threshold level was elevated by increasing the dosage of corrosion inhibitor from 0.22 percent to 1.95 percent by weight of cement. Nitrite-free specimens resulted in critical chloride threshold values ranging from 0.18 to 0.33 percent. ASTM C 1202 exhibited increased total charge and heating for inhibitor containing samples (Ann et al. 2006). These results are contradictory to an earlier study that stated that DCI-S did not significantly affect the chloride ingress and permeability based on rapid chloride permeability tests (Zemajtis et al. 1999). Ann et al. (2006) also reported that the long-term strength (900 days) of concrete containing nitrites was lower compared to control samples although it was higher at early ages. Also, the setting time of inhibitor containing mixtures was reported to decrease by approximately one hour.

# CHAPTER III. EXPERIMENTAL WORK

## 3.1 INTRODUCTION

Corrosion monitoring methods evaluated in this study used either concrete or mortar mixtures to assess the corrosion performance of different steel types in different environments. Mortar and concrete mixture proportions and information on materials, used to produce these mixtures, will be provided in this section. In addition to the corrosion monitoring methods two material characterization tests were performed on the mortar and concrete mixtures. These material characterization tests were:

- ASTM C 1202, Standard Test Method for Electrical Indication of Concrete's Ability to Resist Chloride Ion Penetration and
- ASTM C 1556, Standard Test Method for Determining the Apparent Chloride Diffusion Coefficient of Cementitious Mixtures by Bulk Diffusion.

Information on the experimental design, specimen preparation, and testing procedure of corrosion monitoring test methods will also be provided. The five corrosion monitoring methods evaluated in this study are divided into two groups based on their duration: short-term and longer-term tests. These tests are:

- Short-Term Tests
  - Accelerated Chloride Threshold Level Test (ACT),
  - Rapid Macrocell Test, and
  - Chloride Ion Threshold Test;
- Long-Term Tests
  - ASTM G 109, Standard Test Method for Determining the Effects of Chemical Admixtures on the Corrosion of Embedded Steel Reinforcement in Concrete Exposed to Chloride Environments, and
  - Modified ASTM G 109 Test.

## 3.2 CONCRETE MIXTURES

Concrete mixtures were prepared at two different water-cement ratios (0.45 and 0.55) and with three different amounts of corrosion inhibitor admixtures (0, 2, and 4 gal/yd$^3$ [0, 10, and 20 l/m$^3$]). Table III-1 shows the mixture proportions of all concrete mixtures. Type I cement was used for all the mixtures. Table III-2 shows the chemical composition of the cement.

**Table III-1 Concrete Mixture Proportions.**

| Materials | Water-Cement Ratio | | | | | |
|---|---|---|---|---|---|---|
| | 0.45 | | | 0.55 | | |
| | Admixture Content, gal/yd$^3$ [l/m$^3$] | | | | | |
| | 0 [0] | 2 [10] | 4 [20] | 0 [0] | 2 [10] | 4 [20] |
| Cement,lb/yd3 [kg/m3] | 855.6 [507.6] | 855.6 [507.6] | 855.6 [507.6] | 700 [415.3] | 700 [415.3] | 700 [415.3] |
| Coarse Aggregate, lb/yd3 [kg/m3] | 1114.6 [661.3] | 1114.6 [661.3] | 1114.6 [661.3] | 1114.6 [661.3] | 1114.6 [661.3] | 1114.6 [661.3] |
| Fine Aggregate, lb/yd3 [kg/m3] | 1464.3 [868.7] | 1421.8 [843.5] | 1379.2 [818.2] | 1590.3 [943.5] | 1547.7 [918.2] | 1505.2 [892.9] |
| Water, lb/yd3 [kg/m3] | 385 [228.4] | 385 [228.4] | 385 [228.4] | 385 [228.4] | 385 [228.4] | 385 [228.4] |

**Table III-2 Chemical Composition of Type I Cement.**

| Chemical Compounds, (%) | Spec. Limit | Test Result |
|---|---|---|
| $Al_2O_3$ | 6 max | 5.12 |
| $Fe_2O_3$ | 6 max | 1.76 |
| MgO | 6 max | 1.18 |
| $SO_3$ | | 3.16 |
| CaO | | 64.97 |
| Loss on Ignition | 3 max | 1.42 |
| Insoluble Residue | 0.75 max | 0.24 |
| $C_3A$ | | 11.00 |
| $C_3S$ | | 61.00 |
| Total Alkalines ($Na_2O$ equiv.) | 0.6 max | 0.47 |

Concrete sand complying with the size distribution requirements of ASTM C 33, *Standard Specification for Concrete Aggregates,* was used as fine aggregate. Figure III-1 shows the size distribution of fine aggregate. The fineness modulus and absorption coefficient of the concrete sand were 3.14 and 1.1 percent, respectively. Crushed limestone with a size distribution meeting size number 8 requirements of ASTM C 33 was used as coarse aggregate. Figure III-2 shows the size distribution of the coarse aggregate. The absorption coefficient of the coarse aggregate was 1.65 percent. The maximum aggregate size was 3/8 in (9.5 mm). Laboratory tap water was used to prepare the concrete mixtures. Because concrete samples were going to be used to determine the critical chloride threshold values for different steel types, determining the amount of chloride ions in the tap water was important. Table III-3 shows ion chromatography results for the laboratory tap water used in this research.

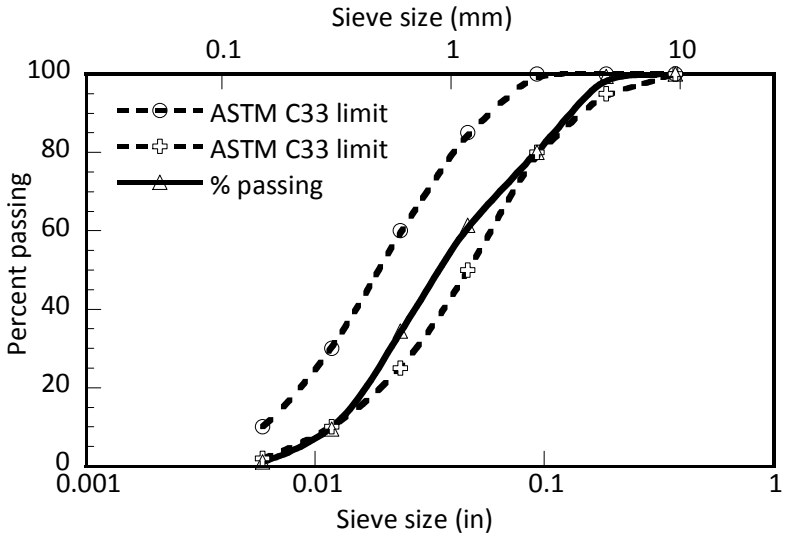


**Figure III-1 Size Distribution of Fine Aggregate.**

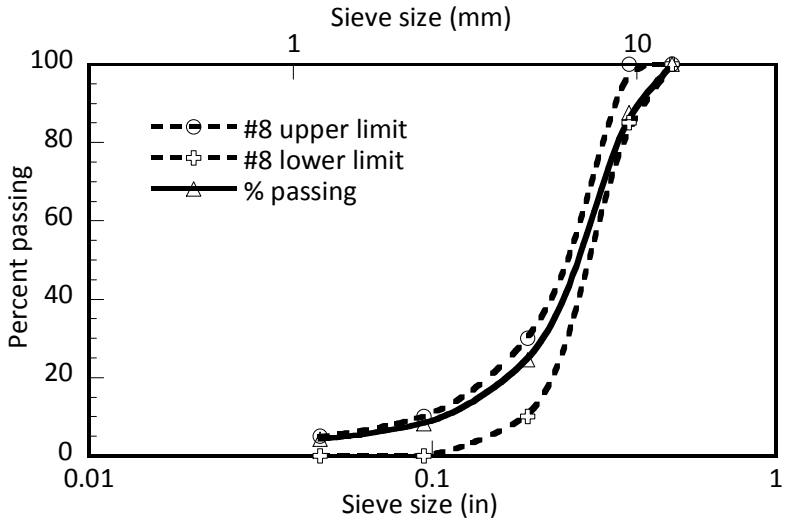


**Figure III-2 Size Distribution of Coarse Aggregate.**

**Table III-3 Ion Chromatography Results for Laboratory Tap Water.**

| Sample Number | Concentration (mg/L or ppm) | | | | | | |
|---|---|---|---|---|---|---|---|
| | F | Cl | $NO_2$ | Br | $NO_3$ | $HPO_4$ | $SO_4$ |
| 1 | 0.192 | 58.590 | - | 0.055 | 0.848 | 0.604 | 11.175 |
| 2 | 0.220 | 58.470 | - | 0.016 | 0.851 | 0.456 | 11.247 |
| 3 | 0.152 | 58.567 | - | 0.034 | 0.698 | 0.346 | 11.187 |
| Average | 0.188 | 58.542 | - | 0.035 | 0.799 | 0.469 | 11.203 |

The corrosion inhibitor evaluated in this study, DCI-S, was a calcium-nitrite based chemical admixture. DCI-S, in liquid form, was added to the batch water of concrete mixtures using graduated cylinders. The manufacturer's recommended addition rate of DCI-S ranged from 2 to 6 gal/yd$^3$ (10 to 30 L/m$^3$). The batch water was reduced to compensate for the water in the DCI-S. According to the manufacturer, DCI-S improves the oxide layer of reinforcing steel and increases the tolerance of steel to chloride ions. Therefore, it should delay the initiation of corrosion and keep corrosion rates low compared to an environment without the admixture. This product is reported to not affect setting time and is reported to be compatible with other admixtures.

Due to limited production capacity and large number of concrete samples evaluated in this study, each concrete mixture shown in Table III-1 was produced in multiple batches of 2.5

$ft^3$ (0.07 $m^3$) following the ASTM C 192, *Standard Practice for Making and Curing Concrete Test Specimens in the Laboratory*. A total of 84 batches were cast to prepare all concrete samples evaluated in this study. Air content and slump values of each batch were measured and compared as a quality control measure to ensure similarity of different batches of the same mixture. Slump and air content were measured following ASTM C 143 (*Standard Test Method for Slump of Hydraulic-Cement Concrete*) and ASTM C 231 (*Standard Test Method for Air Content of Freshly Mixed Concrete by the Pressure Method)* – the pressure method was used. Also 4 × 8-in. (100 × 200 mm) cylinders were prepared to determine compressive strength of each mixture at 7 and 28 days. Concrete samples were cured at 73°F (23°C) and 100 percent relative humidity following ASTM C 192.

## 3.3 MORTAR MIXTURES

Similar to concrete mixtures, mortar mixtures were also prepared at two different water-cement ratios (0.45 and 0.55) and with three different amounts of corrosion inhibitor admixture (0, 2, and 4 gal/$yd^3$ [0, 10, and 20 l/$m^3$]). Table III-4 shows the mixture proportions of all mortar mixtures used in this study. Note that the design quantity of the batch water provided in Table III-4 was further adjusted to compensate for the water content in the DCI-S and the moisture content of aggregates.

**Table III-4 Mortar Mixture Proportions.**

| Materials | Water-Cement Ratio | | | | | |
|---|---|---|---|---|---|---|
| | 0.45 | | | 0.55 | | |
| | Admixture Content, gal/$yd^3$ [l/$m^3$] | | | | | |
| | 0 [0] | 2 [10] | 4 [20] | 0 [0] | 2 [10] | 4 [20] |
| Cement,lb/$yd^3$ [kg/$m^3$] | 924.8 [548.7] | 924.8 [548.7] | 924.8 [548.7] | 817.2 [484.8] | 817.2 [484.8] | 817.2 [484.8] |
| Fine Aggregate, lb/$yd^3$ [kg/$m^3$] | 2401.5 [1424.8] | 2401.5 [1424.8] | 2401.5 [1424.8] | 2401.5 [1424.8] | 2401.5 [1424.8] | 2401.5 [1424.8] |
| Water, lb/$yd^3$ [kg/$m^3$] | 416.2 [246.8] | 416.2 [246.8] | 416.2 [246.8] | 449.5 [266.6] | 449.5 [266.6] | 449.5 [266.6] |

Type I cement was used for all mortar mixtures. The chemical composition of cement is shown in Table III-2. The same laboratory tap water that was used to prepare the concrete mixtures was used to prepare the mortar mixtures. Due to the high number of concrete and mortar samples, sand purchased for concrete mixtures was not enough to prepare mortar mixtures. The sand purchased to prepare mortar mixtures also complied with the size distribution requirements of ASTM C 33. The fineness modulus and absorption coefficient of sand used in the mortar samples were 3.5 and 0.7, respectively. Figure III-3 shows the size distribution of the sand used for the mortar mixtures. Corrosion inhibitor, DCI-S, was added to the batch water.

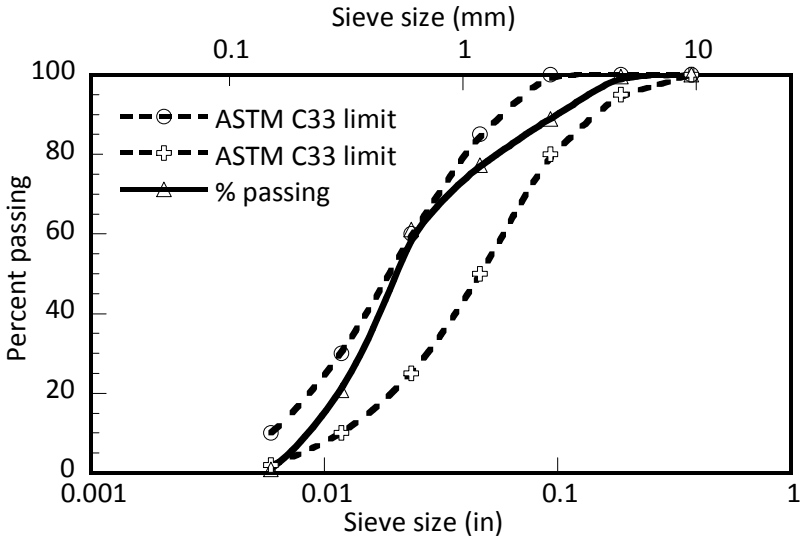


**Figure III-3 Size Distribution of Mortar Sand.**

The air content and the flow of mortar mixtures were determined following the ASTM C 185 (*Standard Test Method for Air Content of Hydraulic Cement Mortar*) and ASTM C 1437 (*Standard Test Method for Flow of Hydraulic Cement Mortar*). Strength of mortar mixtures was determined after 7 and 28 days of curing using 2-in. (50 mm) cubes following ASTM C 109. Samples were cured at 73°F (23°C) and 100 percent relative humidity following ASTM C 192, *Standard Practice for Making and Curing Concrete Test Specimens in the Laboratory*. Mortar cubes were removed from the molds one day after casting. Mortar was cast in a total of 16 batches to produce all mortar samples evaluated in this study.

## 3.4 STEEL TYPES

This study examined coated and uncoated steel reinforcement types for their apparent corrosion performance embedded in concrete and mortar mixtures using different corrosion monitoring methods. Three types of uncoated steel, ASTM A 615, ASTM A 706, and Stainless Steel 304 (SS304), were evaluated in this study. Two types of coated steel were evaluated: epoxy coated and galvanized.

Types of uncoated steel reinforcement were evaluated in concrete and mortar mixtures shown in Table III-1 and Table III-4. Coated steel reinforcement types were evaluated only in concrete and mortar mixtures without corrosion inhibitor (0 l/m$^3$ [0 gal/yd$^3$]). However, coated reinforcement was evaluated in damaged and undamaged conditions. One percent of the coating of reinforcement was damaged using either a file (file damaged, FD) or a drill (drill damaged, DD). File damaged conditions simulated damages sustained by reinforcement due to dragging of reinforcement on the ground on construction sites. The drill damaged condition simulated puncture type damage or holidays that could occur on coated reinforcement. Epoxy coated reinforcement was evaluated in not-damaged, file-damaged, and drill-damaged conditions. Galvanized reinforcement was evaluated in not-damaged and drill-damaged conditions.

## 3.5 MATERIAL CHARACTERIZATION TESTS

### 3.5.1 Electrical Indication of Concrete's Ability to Resist Chloride Ion Penetration (ASTM C 1202)

Although this method was developed for concrete, in this study it was used to evaluate both the mortar and concrete mixtures shown in Table III-1 and Table III-4. Cylindrical mortar and concrete samples, 4 x 8 in (100 x 200 mm) were cast at the same time as the corrosion monitoring test samples. A total of six samples were cast from each mixture. Three samples were tested for rapid permeability at 28 days after casting, and the rest were tested at 56 weeks after casting. Samples were stored in a curing room at 73$^o$F (23$^o$C) and 100 percent relative humidity until testing time.

A water-cooled band saw was used to cut a 2 ± 1/8-in (51 ± 3 mm) slice from the top of each cylindrical specimen. After 1 hour of drying at laboratory environmental conditions the sides of the samples were coated with a two-part, high-viscosity epoxy. The next day, samples

were placed in a vacuum desiccators, and vacuum was applied for three hours. Later, water that was de-aerated through boiling and was let into the desiccator to cover the samples while the samples were still under vacuum. After one hour, the vacuum was turned off, and samples were kept under water for 18 hours.

A test instrument and cells produced by Germann Inc. was used to apply a constant voltage of 60 V across the samples for 6 hours and to measure the total charge passing through the samples. Figure III-4 shows a typical test cell. Each cell contained a 3 percent sodium chloride solution in the side that was connected to the negative pole of the power source and a 0.3 N sodium hydroxide solution in the other side that was connected to the positive pole of the power supply.

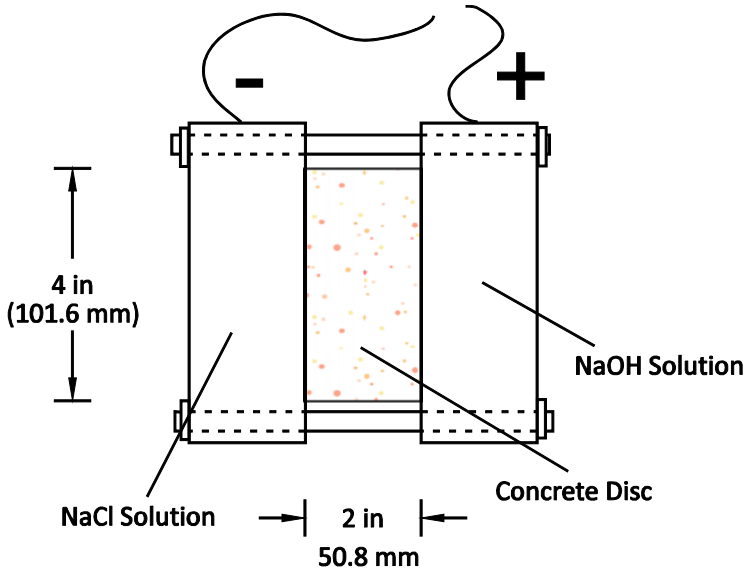


**Figure III-4 ASTM C 1202 Test Cell.**

Permeability of each sample was classified from negligible to high based on the total charge that passed through the sample as shown in Table III-5. Figure III-5 shows assembled test cells being tested.

**Table III-5 Chloride Ion Permeability Classification Following ASTM C 1202.**

| Charge Passed (Coulombs) | Chloride Ion Permeability |
|---|---|
| >4000 | High |
| 2000-4000 | Moderate |
| 1000-2000 | Low |
| 100-1000 | Very Low |
| <100 | Negligible |


**Figure III-5 Assembled Test Cells Being Tested.**

### 3.5.2 Apparent Chloride Diffusion Coefficient of Cementitious Mixtures by Bulk Diffusion (ASTM C 1556)

Cylindrical samples, 4 x 8 in (100 x 200 mm) in size, were cast for each of the concrete and mortar mixtures shown in Table III-1 and Table III-4. A total of three cylinders were cast for

each of the mortar and concrete mixtures. Samples were cured for 28 days in a curing room at 73°F (23°C) and 100 percent relative humidity.

At the end of the curing period, a 3-in (75 mm) long section was cut from the top of each cylinder, and a 1-in (25 mm) long section was cut from the rest of the sample. These 1-in (25 mm) sections were used to determine the initial chloride content of the samples. The 3-in (75 mm) long sections were dried for 24 hours at the laboratory room temperature and humidity. The sides of dried samples were coated with a two-part, high-viscosity epoxy. Samples were then placed in a saturated calcium hydroxide solution and periodically weighed until the change in their mass was less than 0.1 percent in 24 hours. Fully saturated samples were rinsed, surface dried, and put into plastic containers filled with 3 percent by weight sodium chloride solution. After 35 days of exposure samples were removed from the containers, rinsed, dried, and placed into sealed high density polyethylene bags.

Concrete and mortar powder samples were collected from different depths of the 3-in (75 mm) samples using a profile grinder (Germann Instruments Inc, Metabo D-72622). This grinder used a diamond bit and allowed the depth to which the concrete or mortar samples were ground to be accurately set. Figure III-6 shows the profile grinder. Powder samples were collected from different depth ranges for concrete and mortar mixtures that had different water-cement ratios. Table III-6 shows the depth ranges that were used to collect the powder samples for mortar and concrete mixtures based on water-cement ratio. Powder samples were tested for chloride ion content using a computer controlled potentiometric auto-titrator with a sample changer (Metrohm-Brinkmann, Titrando 808) following ASTM C 1152, *Standard Test Method for Acid-Soluble Chloride in Mortar and Concrete*. Figure III-7 shows the auto-titrator used for chloride ion analysis.

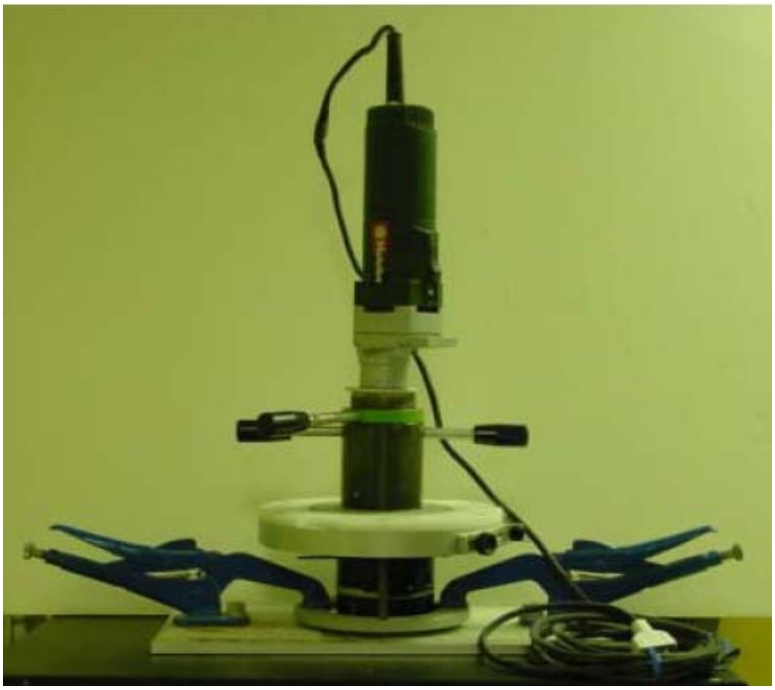

**Figure III-6 Profile Grinder by Germann Instruments, Inc.**

**Table III-6 Depth Intervals for Chloride Ion Testing.**

| Depth | Water-Cement Ratio | |
|---|---|---|
| | 0.45 | 0.55 |
| 1 | 0-0.04 in (0-1 mm) | 0-0.04 in (0-1 mm) |
| 2 | 0.04-0.12 in (1-3 mm) | 0.04-0.12 in (1-3 mm) |
| 3 | 0.12-0.20 in (3-5 mm) | 0.12-0.20 in (3-5 mm) |
| 4 | 0.20-0.28 in (5-7 mm) | 0.20-0.31 in (5-8 mm) |
| 5 | 0.28-0.39 in (7-10 mm) | 0.31-0.47 in (8-12 mm) |
| 6 | 0.39-0.51 in (10-13 mm) | 0.47-0.63 in (12-16 mm) |
| 7 | 0.51-0.63 in (13-16 mm) | 0.63-0.79 in (16-20 mm) |
| 8 | 0.63-0.79 in (16-20 mm) | 0.79-1.0 in (20-25 mm) |

**Figure III-7 Metrohm-Brinkmann Auto-Titrator.**

## 3.6 CORROSION TESTS

### 3.6.1 Accelerated Chloride Threshold Level Test

This test method is reported to determine the critical chloride threshold level of reinforcing steel embedded in mortar. Under constant potential difference, which is applied in 6-hour intervals, chloride ions migrate from a chloride solution ponded on the surface of the mortar to the reinforcing steel surface. Initiation of corrosion is monitored through polarization resistance measurements. Application of potential is stopped when polarization resistance measurements indicate initiation of corrosion. Samples are then separated, and the chloride concentration at the steel reinforcement, which is the critical chloride threshold level, is determined.

#### *3.6.1.1 Experimental design*

The ACT test was performed in two phases. A total of 84 samples were tested in the first phase using the six different mortar mixture proportions (two water-cement ratios and three admixture quantities) shown in Table III-4. Water-cement ratio of the mortar mixture, amount of corrosion inhibitor, reinforcement steel type, and damage of coated steel were variables evaluated for their effect on corrosion performance. The experimental design and the number

of samples evaluated for each condition is shown in Table III-7 and Table III-8 for uncoated and coated steel samples, respectively.

A total of 36 samples were tested in the second phase using the same six mortar mixtures with only two types of uncoated steel types. The main objective of the second phase was to evaluate the repeatability of the test results. Table III-9 shows the experimental design and number of samples evaluated for each condition.

**Table III-7 Experimental Design for Uncoated Steel in Phase I.**

| Water-cement ratio | Admixture content, gal/yd$^3$ (l/m$^3$) | Rebar type | No. of samples |
|---|---|---|---|
| 0.45 | 0 (0) | A 615 | 3 |
| | | A 706 | 3 |
| | | SS304 | 3 |
| | 2 (10) | A 615 | 3 |
| | | A 706 | 3 |
| | | SS304 | 3 |
| | 4 (20) | A 615 | 3 |
| | | A 706 | 3 |
| | | SS304 | 3 |
| 0.55 | 0 (0) | A 615 | 3 |
| | | A 706 | 3 |
| | | SS304 | 3 |
| | 2 (10) | A 615 | 3 |
| | | A 706 | 3 |
| | | SS304 | 3 |
| | 4 (20) | A 615 | 3 |
| | | A 706 | 3 |
| | | SS304 | 3 |

**Table III-8 Experimental Design for Coated Steel in Phase I.**

| Water-cement ratio | Damage type[1] | Rebar Type[2] | No. of samples |
|---|---|---|---|
| 0.45 | ND | ECR | 3 |
| | | GR | 3 |
| | DD | ECR | 3 |
| | | GR | 3 |
| | FD | ECR | 3 |
| 0.55 | ND | ECR | 3 |
| | | GR | 3 |
| | DD | ECR | 3 |
| | | GR | 3 |
| | FD | ECR | 3 |

[1]ND: not damaged, DD: drill damaged
[2]ECR: epoxy coated, GR: galvanized reinforcement

**Table III-9 Experimental Design of Phase II.**

| Water-cement ratio | Admixture content gal/yd$^3$ (l/m$^3$) | Rebar type | No. of samples |
|---|---|---|---|
| 0.45 | 0 (0) | A 615 | 3 |
| | | SS304 | 3 |
| | 2 (10) | A 615 | 3 |
| | | SS304 | 3 |
| | 4 (20) | A 615 | 3 |
| | | SS304 | 3 |
| 0.55 | 0 (0) | A 615 | 3 |
| | | SS304 | 3 |
| | 2 (10) | A 615 | 3 |
| | | SS304 | 3 |
| | 4 (20) | A 615 | 3 |
| | | SS304 | 3 |

### *3.6.1.2 Specimen preparation and test procedure*

Steel reinforcement was cut in 0.75-in (19 mm) long specimens using a band saw with a liquid cooling system to prevent heating of steel specimens. Steel specimens were then drilled and tapped using a #38 drill bit and #5-40 tap. During the drilling process, a coolant solution was continuously applied onto the specimen to prevent overheating. After being cleaned in ethyl alcohol using an ultrasonic cleaner, specimens were attached to #5-40 threaded stainless steel

rods. A rectangular area of approximately 0.35x0.67 in (9x17 mm) in size was marked as the exposure surface on the top surface of the steel specimens. Steel specimens (with the exception of exposure surface) and part of threaded rods were then coated using a two-part epoxy as shown in Figure III-8. Exact dimensions of exposed surface were measured for each specimen after the application of epoxy coating. Epoxy coated reinforcement samples were not coated with two-part epoxy. For the damaged coated bars 1 percent of the total exposed surface was damaged. Coating of drill damaged specimens was drilled with a gauge 54 drill bit to produce the required damage area.

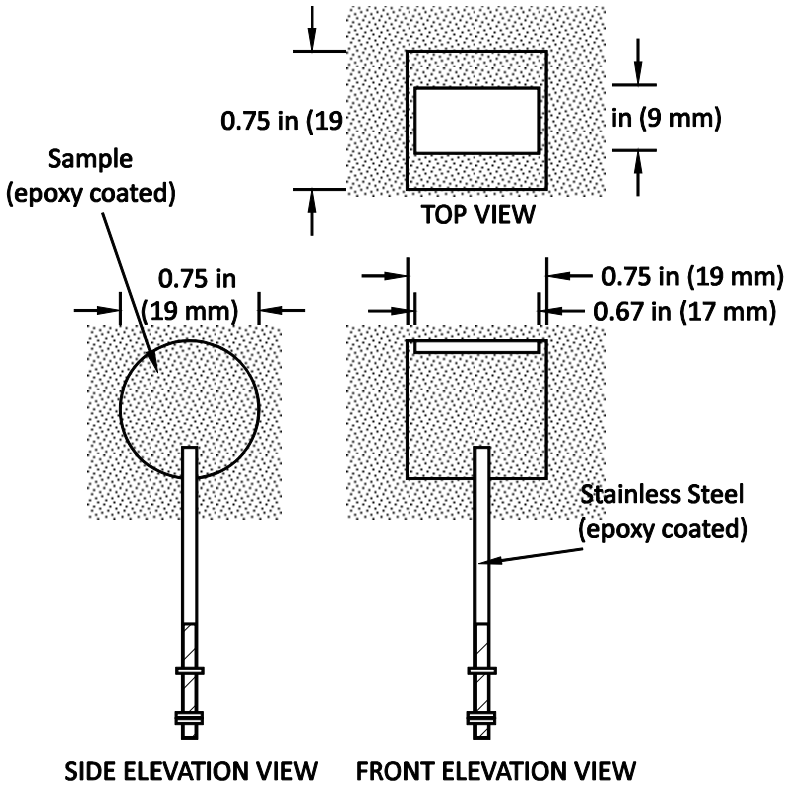


**Figure III-8 Steel Specimen of ACT Test (Pillai 2003).**

Three-part, prefabricated 3x4.5 in (75x115 mm) Acrylonitrile-Butilene-Styrene (ABS) cylinder molds were used to cast the mortar samples for the ACT testing. Figure 3-9 shows the three-part cylinder mold and different parts of ACT sample. Part number 9 shows the steel specimen (shown in Figure III-8) attached to the bottom part of cylinder mold. The anode (Part number 10 shown in Figure III-9) was prepared using a 2.8-in (69 mm) diameter Nichrome

mesh with a 1x1-in (25x25 mm) section removed from the center. The anode mesh disk was soldered to two copper wires and attached to the middle part of the ABS mold. The 1x1-in (25x25 mm) section removed from the anode was soldered to two copper wires and was used as the counter electrode (Part number 5 shown in Figure III-9). The counter electrode was attached to the top part of the ABS mold. All copper wires and connections were coated with a two-part epoxy.

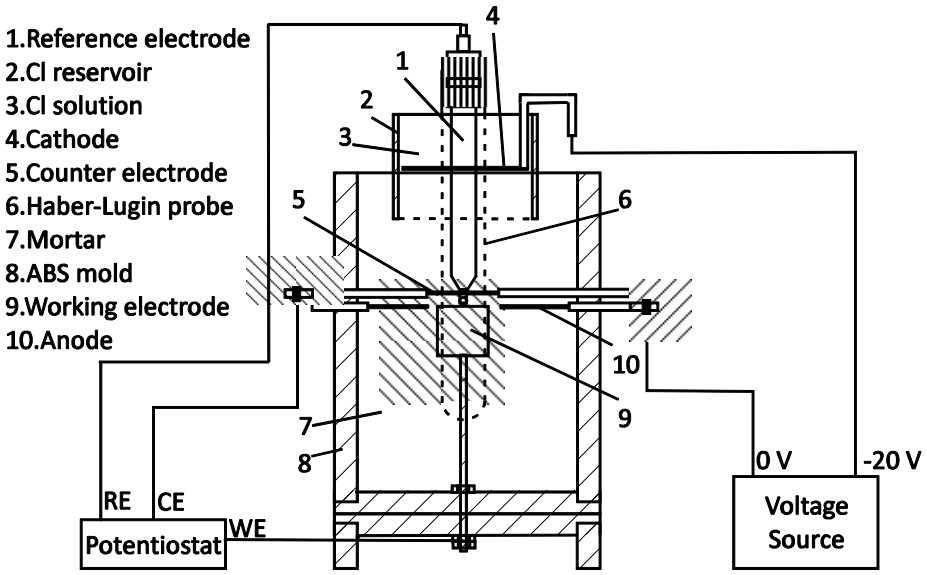


**Figure III-9 ACT Test Sample (Pillai 2003).**

Mortar mixtures were batched and mixed following ASTM C 305, *Standard Practice for Mechanical Mixing of Hydraulic Cement Pastes and Mortars of Plastic Consistency*. The bottom part of the ABS molds were filled in three layers with mortar with the steel specimens inside and the molds were tapped 10 times with a rubber mallet to improve consolidation. Approximately 0.3 $in^3$ (5 $cm^3$) of mortar was placed in the mold before the placement of the middle part of the ABS mold forcing mortar through the anode mesh disk.

Haber-Lugin probes (Part number 6 shown in Figure III-9) were then inserted through a pre-drilled hole in the middle part of the ABS mold. The Haber-Lugin probe is a glass tube with a fine glass tip extending from its side into the mortar. The tip of the probe is placed approximately 1/32 in (1 mm) above the exposed surface of the steel specimen and was fitted with a porous frit. Heat shrinking tube was used to hold the frit and probe together. Figure

III-10 shows the Haber-Lugin probe. When filled with a conductive solution, Haber-Lugin probes acts as a conductive bridge between the reference electrode (Part number 1 shown in Figure III-9) and the steel specimen (working electrode) for polarization resistance measurements.

Approximately 0.6 $in^3$ (10 $cm^3$) of mortar was placed on the steel specimen and Haber-Lugin probe before the placement of the top part of the mold forcing mortar through the counter electrode mesh. The top part was filled with mortar and tapped slightly. A 2-in (50 mm) diameter plastic mold was used as the chloride solution reservoir system (Part number 2 shown in Figure III-9). These pieces were inserted 0.24 in (6 mm) into the mortar at the center of the ABS mold.

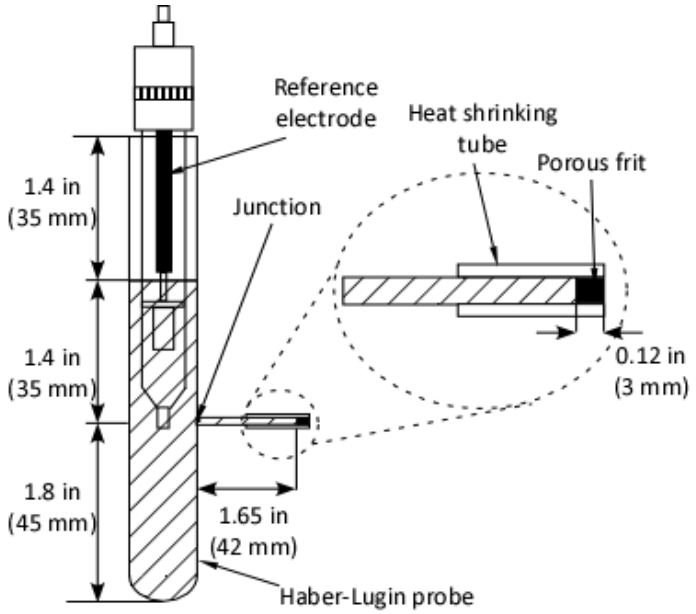


**Figure III-10 Haber-Lugin Probe and Reference Electrode (Pillai 2003).**

Samples were moved immediately after casting to a curing room and stored at 73°F (23°C) and 100 percent relative humidity for 28 days. Nichrome mesh with a 1.8-in (44 mm) diameter was used as cathode (Part number 4 shown in Figure III-9). Cathode mesh disks soldered to copper wires for electrical connection were placed into the chloride solution reservoirs at the end of the curing period. Reservoirs were filled with a 3.5 percent by weight chloride solution that was prepared by mixing 2.16 ounces (61.23 g) of NaCl in 0.26 gal (1000

ml) of distilled water. Haber-Lugin probes were filled with a 0.1 percent by weight chloride solution.

The cathode and anode mesh disks in the samples were connected to the negative and ground terminals of a DC power source through distribution boxes. Saturated calomel electrodes were placed in Haber-Lugin probes as reference electrodes. Reference electrodes, steel specimens (working electrodes), and counter electrodes were connected to a Solartron SI 287 potentiostat as shown in Figure III-9. Initial polarization resistance ($R_p$) of the samples was then measured. A potential difference of 20 V was applied between the anode and cathode of samples for 36 hours in three 12-hour periods with a wait period of 42 hours between additional voltage applications. After the second $R_p$ measurement the potential was applied in periods of 6 hours with 42-hour wait periods between the applications (each cycle took 2 days). After each voltage application electrochemical measurements were performed. The potentiostat was programmed to first determine the open circuit potential (OCP) of the steel specimen against the calomel electrode for a 60-second period, then to keep the potential of the specimen constant at the last measured OCP level for 30 seconds, and then to run a potential scan from -15 mV to +15 mV against the OCP to determine the $R_p$. The scan rate used for testing was 0.167 mV/s. Cumulative hours of voltage application and the measured $R_p$ values over time were recorded.

A statistically significant increase of the reciprocal of $R_p$ was used as the activation criteria. When a sample was deemed active (initiation of corrosion), testing was stopped and the sample was disconnected from the power source and potentiostat. Active samples were broken at the level of anode mesh disk and steel specimen, i.e., the middle and top parts of the ABS mold were kept together and separated from the bottom section. Using a profile grinder, mortar was ground into a powder from the middle part of the mortar in the ABS mold (from the section that was above the steel specimen). Ground mortar powder (approximately 0.053 ounce [1.5 g]) was collected from a depth of 78.7 mils (2 mm). The chloride content of ground mortar was determined using a chloride ion specific electrode following a rapid chloride content determination method developed by the Strategic Highway Research Program (Herald et al. 1993). A detailed description of the ACT test procedure is provided in Appendix A in the format of ASTM standards (Pillai 2003).

The ACT test procedure was modified slightly in the second phase of the testing. After 28 days of curing, the OCP values of ACT samples were monitored until they became stable. On the average it took one month to obtain stable OCP readings from ACT samples. Testing

for $R_p$ and application of potential difference was started after the stabilization of the OCP readings.

### 3.6.2 Rapid Macrocell Test

This test method measures the corrosion rate and half cell potential of steel reinforcement embedded in mortar mixtures. Steel reinforcement specimens covered with a thin layer of mortar are placed in separate containers to act as anodes and cathodes. The cathode container contains two specimens to increase the cathode to anode surface ratio. The cathode containers are filled with simulated concrete solution and were purged with scrubbed air. Anode containers were filled with simulated pore solution and salt solution. Steel specimens acting as anodes and cathodes were connected with a 10 Ω resistor, and containers were connected with a salt bridge to close the circuit. The corrosion was then determined by measuring the current flowing through the resistor and with half cell potential measurements.

#### *3.6.2.1 Experimental design*

The rapid macrocell test was performed in two phases. A total of 18 test conditions were evaluated for uncoated steel specimens in the first phase using six different mortar mixtures and three different steel types (ASTM A 615, A 706, and SS304). Three test setups, shown earlier in Figure II-2, were prepared for each condition, i.e., 162 mortar coated steel specimens were prepared. Table III-10 shows the experimental design for 54 test setups prepared using uncoated steel specimens. For coated samples a total of 10 test conditions were evaluated in the first phase as shown in Table III-11.

The three test setups were prepared for each condition, i.e., 90 mortar coated steel specimens were prepared. The water-cement ratio of the mortar mixture, the amount of corrosion inhibitor, the reinforcement steel type, and the damage of the coated steel were variables evaluated for their effect on corrosion rate and OCP of steel specimens.

It should be noted that three mortar covered steel specimens are necessary for each complete test setup. Mortar covered specimens were cast for 84 test setups. However, removing samples from molds turned out to be a very difficult task due to very brittle nature of thin mortar covers around the specimens and only 24 test setups could not be assembled due to the loss of one of the three steel specimens necessary for a complete setup. The mortar around the galvanized steel specimens tended to consistently break at the level where the steel

specimen ended in mortar. This cracking is likely due to the formation of hydrogen gas from the corrosion of the zinc in the high pH mortar environment. As a result only two test setups could be tested with galvanized steel specimens in the first phase.

**Table III-10 Experimental Design for Uncoated Rapid Macrocell Samples.**

| Water-Cement Ratio | Admixture Content, Gal/yd$^3$ (l/m$^3$) | Rebar Type | No. of Test Setups |
|---|---|---|---|
| 0.45 | 0 (0) | A 615 | 3 |
| | | A 706 | 3 |
| | | SS304 | 3 |
| | 2 (10) | A 615 | 3 |
| | | A 706 | 3 |
| | | SS304 | 3 |
| | 4 (20) | A 615 | 3 |
| | | A 706 | 3 |
| | | SS304 | 3 |
| 0.55 | 0 (0) | A 615 | 3 |
| | | A 706 | 3 |
| | | SS304 | 3 |
| | 2 (10) | A 615 | 3 |
| | | A 706 | 3 |
| | | SS304 | 3 |
| | 4 (20) | A 615 | 3 |
| | | A 706 | 3 |
| | | SS304 | 3 |

**Table III-11 Experimental Design for Coated Rapid Macrocell Samples.**

| Water-Cement Ratio | Damage Type[1] | Rebar Type[2] | No. of Test Setups |
|---|---|---|---|
| 0.45 | ND | ECR | 3 |
| | | GR | 3 |
| | DD | ECR | 3 |
| | | GR | 3 |
| | FD | ECR | 3 |
| 0.55 | ND | ECR | 3 |
| | | GR | 3 |
| | DD | ECR | 3 |
| | | GR | 3 |
| | FD | ECR | 3 |

[1]ND: Not damaged, DD: Drill damaged, FD: File Damaged
[2]ECR: Epoxy coated, GR: Galvanized reinforcement

The second phase testing of ASTM A 615 and SS304 samples was planned to check repeatability of test results. However due to the loss of almost all galvanized steel specimens in the first phase, testing of undamaged galvanized steel specimens was added to the second phase plan. Table III-12 shows the 18 different conditions tested in the second phase with three test setups for each condition.

**Table III-12 Experimental Design of Phase II for Rapid Macro Cell Test**

| Water-Cement Ratio | Admixture Content Gal/yd$^3$ (l/m$^3$) | Rebar Type[1] | No. of Samples |
|---|---|---|---|
| 0.45 | 0 (0) | A 615 | 3 |
| | | SS304 | 3 |
| | | GR | 3 |
| | 2 (10) | A 615 | 3 |
| | | SS304 | 3 |
| | | GR | 3 |
| | 4 (20) | A 615 | 3 |
| | | SS304 | 3 |
| | | GR | 3 |
| 0.55 | 0 (0) | A 615 | 3 |
| | | SS304 | 3 |
| | | GR | 3 |
| | 2 (10) | A 615 | 3 |
| | | SS304 | 3 |
| | | GR | 3 |
| | 4 (20) | A 615 | 3 |
| | | SS304 | 3 |
| | | GR | 3 |

[1]GR: Galvanized reinforcement

### *3.6.2.2 Specimen preparation and test procedure*

No. 5 (No. 16M) reinforcement was used to prepare the rapid macrocell samples. Steel reinforcement was cut to obtain 5-in (127 mm) long specimens using a liquid cooled band saw. One end of specimens was drilled and tapped to receive a 3/8-in (9.5 mm) long No. 8-32 stainless steel machine screw. Steel specimens were cleaned in ethyl alcohol using an ultrasonic cleaner. A 0.6-in (15.24 mm) band centered 2-in (50.8 mm) from the top of each steel specimen was coated with a two-part, high-viscosity epoxy. This coating was applied to prevent accelerated corrosion of steel specimens due to galvanic corrosion at the section where they protrude from the mortar. Figure III-11 shows the mortar covered steel specimens.

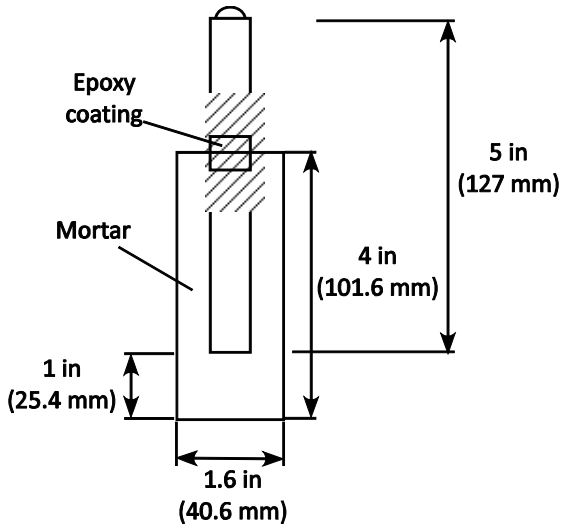


**Figure III-11 Mortar Covered Steel Specimen.**

A plastic mold assembly consisting of two parts (bottom and top) was used with PVC pipes to cast the mortar cover around the steel specimens. The bottom part was a 13.8 x 8.75 x 2-in (351 x 222 x 51 mm) plastic slab with 15 holes drilled in three rows of five holes. The holes had a diameter of 0.7 in (18 mm), and were 2 in (51 mm) deep. At the center of the bottom of each hole there was a smaller hole with a diameter of 0.12 in (3 mm) that went through the rest of the thickness of the slab. Figure III-12 shows the bottom part of the mold.

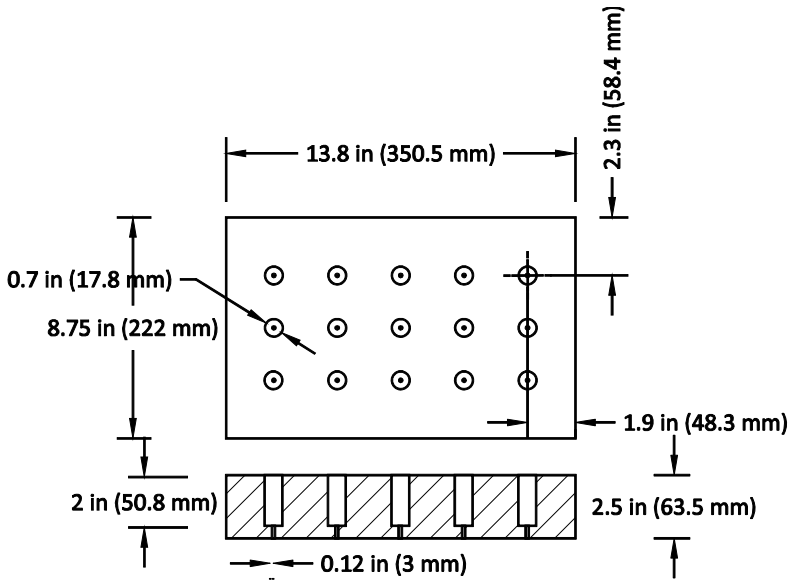


**Figure III-12 Bottom Part of the Mold.**

The top part of the mold had the same dimensions as the bottom part but its thickness was 1 in (25 mm). It had three rows of five holes with a diameter of 1.6 in (40.6 mm). The holes of the bottom and top were aligned at the center. During casting the two parts were fixed together, and the steel reinforcing bars were inserted into the bottom part of the mold. A PVC pipe with an outside diameter of 1.6 in (41 mm) was cut into 4-in (102 mm) pieces and 8-in (203 mm) long pieces were prepared by taping two 4-in (101.6 mm) pieces together. PVC pipe pieces (8-in [203 mm] long) were inserted into the top part of the mold around the steel specimens. The entire assembly was placed on a vibrating table. Mortar was placed into the PVC pipe pieces in three layers, and each layer was vibrated 3 to 4 seconds at 60 Hz. The top 4-in (101.6-mm) long PVC pipe was used to overfill the bottom part during the placement of the third layer to make sure that the bottom part was completely filled with consolidated mortar. At the end of casting, the top PVC pipe pieces were discarded, and the mortar was finished flush with the top of the bottom PVC pipe pieces. Figure III-13 shows the casting setup for the rapid macrocell corrosion test.

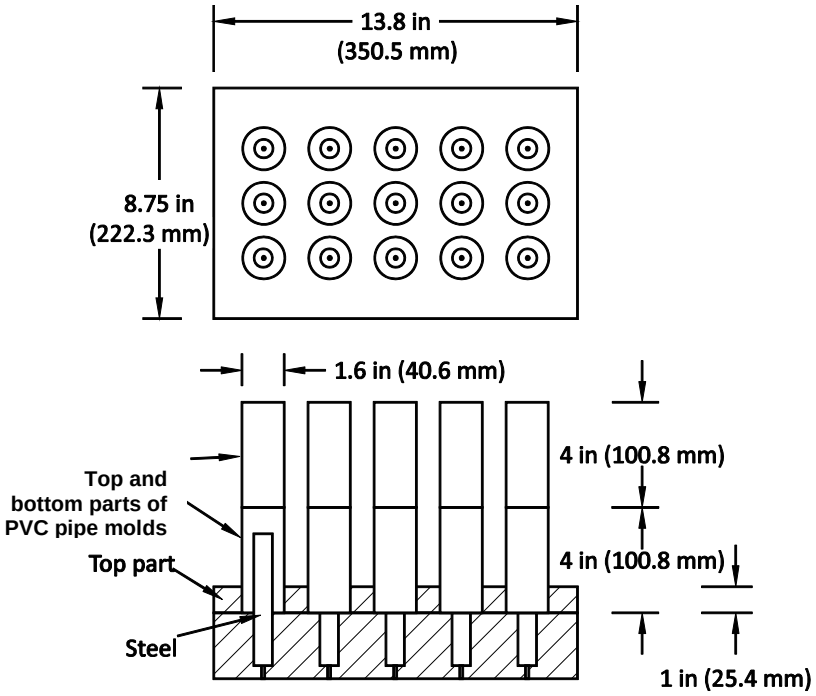


**Figure III-13 Casting Setup for Rapid Macrocell Samples.**

Immediately after casting, samples were covered with wet burlap and after initial set they were moved to a curing room. Samples were removed from the molds 72 hours after casting. Samples were cured at 73°F (23°C) and 100 percent humidity for 28 days.

Cylindrical containers, 6 x 4.5 in (150x114 mm), with lids were used to hold the samples for the rapid macrocell test setup (Figure III-14). Containers were made out of high density polyethylene. Each test setup consisted of two containers to house the anode and cathode. One specimen was placed in a container to act as the anode and two specimens were placed in another container to act as cathodes. The lids were drilled to hold No. 5 (No. 16 metric) steel reinforcement. Plastic O-rings were placed between the steel specimens and plastic lids to hold specimens straight. Cathode containers were filled with simulated concrete pore solution and mortar pieces. Anode containers were filled with a simulated concrete pore solution with a 1.6 molal concentration of sodium chloride and mortar fill. A salt bridge provided the ionic path between the anode and cathode containers to complete the electrical circuit.

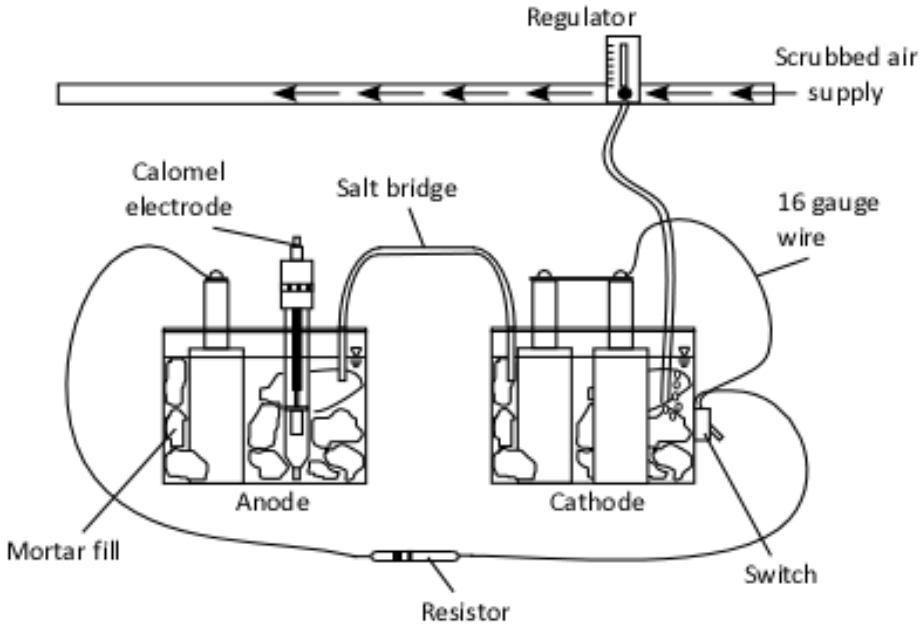


**Figure III-14 Rapid Macrocell Setup.**

The two mortar covered steel specimens in the cathode container were electrically connected using a 2-in (50.8 mm) stainless steel pipe strap and stainless steel screws. A stainless steel O-ring terminal and 16 gauge insulated copper wire was used to connect the two specimens to an electrical switch. The specimens in the anode container were also connected to the switch using an O-ring terminal and copper wire over a 10 Ω resistor. The switch was kept in the "on" position to complete the circuit. It was turned off two hours before the open circuit potential was measured.

Scrubbed air was obtained by passing pressurized air through a 1 M sodium hydroxide solution. This solution was prepared by mixing 0.0882 lb (40 g) of sodium hydroxide with 2.2046 lb (1000 g) of distilled water. Pressurized air was connected to the bottom of a 30-gal (113.6 L) container using vinyl tubing and a barbed fitting. Perforated vinyl tubing was used to bubble pressurized air through the solution inside the container. Vinyl tubing was attached to the top of the container with a barbed fitting to convey the scrubbed air to the cathode containers by means of a series of smaller size diameter vinyl tubing and air regulators. Test setups were stored on the racks of a steel shelf throughout the test, and a separate air line from the container was used to feed scrubbed air to a set of 12 samples on each rack. Figure III-15 shows the rapid macro cell test setups on shelves.


**Figure III-15 Picture of Rapid Macrocell Test Setup on the Rack.**

Broken mortar samples used to fill the anode and cathode containers were cast at the same time as the mortar covered steel specimens. Simulated concrete pore solution was prepared by mixing 0.0415 lb (18.81 g) of potassium hydroxide (KOH) and 0.0391 lb (17.87) of sodium hydroxide (NaOH) with 2.1491 lb (974.8 g) of distilled water (Farzammehr 1985). Simulated concrete pore solution that was described in Farzammehr's study also included 0.00031 lb (0.14 g) of sodium chloride but it was not mixed into the solution in this study. Cathode and anode containers were filled with broken mortar pieces and simulated concrete solution to a depth of 3.72 in (95 mm). However, 0.1005 lb (45.6 g) of sodium chloride was added to 0.2642 gal (1 l) of simulated concrete pore solution that was used to fill the anode containers. This addition of sodium chloride resulted in a 1.6 Molal sodium chloride solution in the anode containers.

For each test setup one salt bridge was placed between the anode and cathode containers to provide an ionic path for current flow. Salt bridges were prepared following a procedure described in a report by Kahrs et al. (2001).

Open circuit potential and macrocell corrosion current of all samples were monitored for a minimum of 100 days. To determine the macro cell corrosion current, the voltage drop across the 10 Ω resistors was measured by connecting the positive lead of a voltmeter to the

anode side and the negative lead to the cathode side. After the completion of the voltage drop readings, all the switches were turned off and after a wait period of two hours OCP readings were collected using a voltmeter and a saturated calomel electrode. After the collection of OCP readings from all the samples, the switches were turned on again and left at the on position until the next reading. During the first phase, data were collected weekly and in the second phase three times a week.

### 3.6.3 Chloride Ion Threshold Test Method (CIT)

This test measures the chloride ion threshold of steel reinforcement embedded in mortar and determines activation through monitoring macro cell corrosion, half cell potential, and polarization resistance of reinforcement. Reinforcement is placed in a mortar cylinder at two levels and this was exposed to cyclic ponding with chloride solution and drying on a weekly basis. Once it is determined that a sample is actively corroding, testing is stopped and the chloride ion concentration at the steel mortar interface at the top reinforcement level is determined. Currently there is no standard procedure to determine the chloride ion threshold for corrosion of reinforcing steel in concrete, and ASTM committee G01 is considering a standard based on this method as work item WK995.

#### *3.6.3.1 Experimental design*

This test was performed in two phases. Similar to the ACT and rapid macrocell tests, the second phase was performed to evaluate the repeatability of test results. Three types of uncoated steel reinforcement (ASTM A 615, A 706, and SS304) were evaluated in six different mortar mixtures as shown earlier in Table III-4. Table III-13 shows the 18 different conditions evaluated for uncoated steel types. Coated reinforcement types (epoxy coated and galvanized) were evaluated in two mortar mixtures with different water-cement ratios. These mixtures did not contain corrosion inhibitor admixture. Coated samples were evaluated in undamaged and damaged conditions.

Table III-14 shows the experimental design used for coated samples in the first phase. Four samples were prepared for each test condition of uncoated and coated reinforcement sample. Two of the samples in each group were used to determine the chloride threshold of samples, and the other two samples were used to monitor corrosion rate of samples.

Table III-15 shows the experimental design used in the second phase of the study. ASTM A 615 and SS304 samples were evaluated in six different mortar mixtures (two water-cement ratios and three different corrosion inhibitor amounts). Triplicate samples were prepared, and all of the samples were used to determine the critical chloride threshold values.

**Table III-13 Experimental Design of Uncoated Steel for CIT Test.**

| Water-Cement Ratio | Admixture Content, gal/yd$^3$ (l/m$^3$) | Rebar Type | No. of Test Setups |
|---|---|---|---|
| 0.45 | 0 (0) | A 615 | 4 |
| | | A 706 | 4 |
| | | SS304 | 4 |
| | 2 (10) | A 615 | 4 |
| | | A 706 | 4 |
| | | SS304 | 4 |
| | 4 (20) | A 615 | 4 |
| | | A 706 | 4 |
| | | SS304 | 4 |
| 0.55 | 0 (0) | A 615 | 4 |
| | | A 706 | 4 |
| | | SS304 | 4 |
| | 2 (10) | A 615 | 4 |
| | | A 706 | 4 |
| | | SS304 | 4 |
| | 4 (20) | A 615 | 4 |
| | | A 706 | 4 |
| | | SS304 | 4 |

**Table III-14 Experimental Design of Coated Steel for CIT Test.**

| Water-Cement Ratio | Damage Type[1] | Rebar Type[2] | No. of Test Setups |
|---|---|---|---|
| 0.45 | ND | ECR | 4 |
| | | GR | 4 |
| | DD | ECR | 4 |
| | | GR | 4 |
| | FD | ECR | 4 |
| 0.55 | ND | ECR | 4 |
| | | GR | 4 |
| | DD | ECR | 4 |
| | | GR | 4 |
| | FD | ECR | 4 |

[1]ND: Not damaged, DD: Drill damaged,
[2]ECR: Epoxy coated, GR: Galvanized reinforcement

**Table III-15 Experimental Design for Phase II CIT Test.**

| Water-cement ratio | Admixture content gal/yd$^3$ (l/m$^3$) | Rebar type | No. of samples |
|---|---|---|---|
| 0.45 | 0 (0) | A 615 | 3 |
| | | SS304 | 3 |
| | 2 (10) | A 615 | 3 |
| | | SS304 | 3 |
| | 4 (20) | A 615 | 3 |
| | | SS304 | 3 |
| 0.55 | 0 (0) | A 615 | 3 |
| | | SS304 | 3 |
| | 2 (10) | A 615 | 3 |
| | | SS304 | 3 |
| | 4 (20) | A 615 | 3 |
| | | SS304 | 3 |

### *3.6.3.2 Specimen preparation and test procedures*

No. 4 (No. 13M) steel reinforcement was cut into 8-in (200 mm) long pieces using a liquid cooled band saw. One end of the reinforcement was drilled and tapped to receive 3/8-in (9.5 mm) long No. 8-32 stainless steel machine screw. Steel specimens were cleaned in ethyl alcohol using an ultrasonic cleaner. Two-inch (50 mm) sections from each end of the steel specimens were covered with electroplater's tape leaving a 4-in (100 mm) long piece of specimen exposed for testing.

Plastic cylinder molds, 6x12 in (150x300 mm), were used to cast the samples. Molds were drilled at 1.25 in (31.75 mm) and 3.75 in (95.25 mm) from the bottom using a 5/8-in (15.875 mm) drill bit. Steel specimens were inserted at both levels. Molds were cut along the holes and taped back together with electrical tape to make removal of molds easier. Figure III-16 shows the cylindrical mold prepared to cast the CIT test samples.

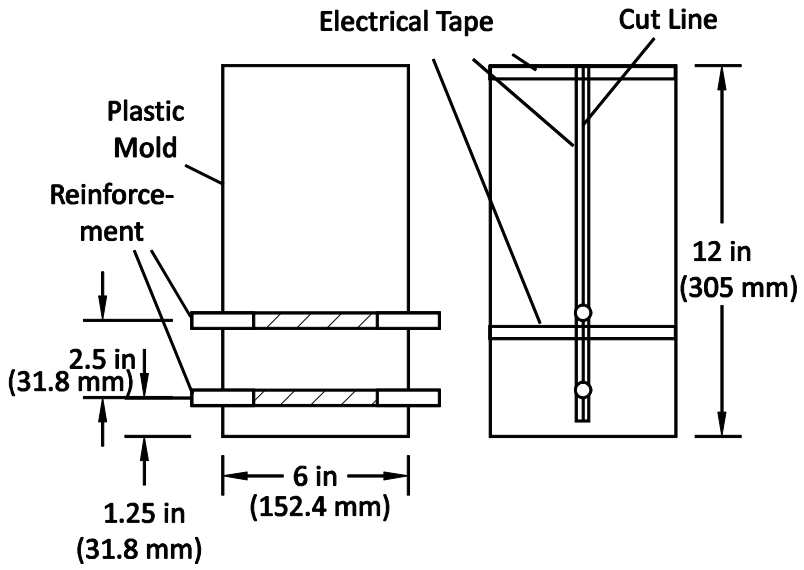


**Figure III-16 Mold for CIT Sample.**

Steel specimens were inserted into the molds right before casting to ensure that the drilled and tapped ends of both specimens are facing the same direction. The 4-in (100 mm) long exposed surface was centered with the center of the cylindrical molds. For samples that received damaged (file or drill damaged) coated steel specimens, steel specimens were placed in such a way that their damaged areas were facing upward.

Mortar was mixed following ASTM C 305 and placed into the molds in three layers. Each layer was rodded 25 times using a 5/8-in (15.875 mm) diameter steel rod. Each layer was tapped with a rubber mallet to remove air bubbles. After casting, samples were covered with wet burlap and after initial set they were moved to curing rooms. Samples were removed from molds the next day and were cured at 73$^{o}$F (23$^{o}$C) and 100 percent humidity for a total of 28 days.

At the end of the curing period, samples were removed from the curing room and cut using a water-cooled masonry saw to leave a mortar cover of 0.75 in (20 mm) over the top steel specimen. Cut portions of the samples were retained for later chloride content determination to determine the initial chloride content of samples before exposure to the chloride solution. Samples were dried for two weeks at laboratory room temperature and humidity. A 4-in (100 mm) PVC pipe was cut into 3-in (75 mm) long pieces to be used as a chloride solution reservoir. At the end of the drying period, chloride solution reservoirs were attached to the top

of the samples using silicone caulk and two-part high viscosity epoxy. The sides and the top of the samples (with the exception of the area inside the chloride solution reservoir) were coated using a two-part high viscosity epoxy.

The top reinforcement of each sample was connected to an electrical switch, attached to the side of the sample, using a No. 8-32 stainless steel screw, an O-ring electrical terminal, and a 2-in (50 mm) long 16 gauge copper wire. A 10 Ω resistor was attached to the bottom reinforcement using a No. 8-32 stainless screw and two stainless steel washers at one end. At the other end the resistor was clamped to a 2-in (50 mm) long 16 gauge copper wire that was connected to the switch. Also, another 2-in (50 mm) long copper wire with a female banana plug was attached to the top reinforcement of each sample. Figure III-17 shows the CIT test sample.

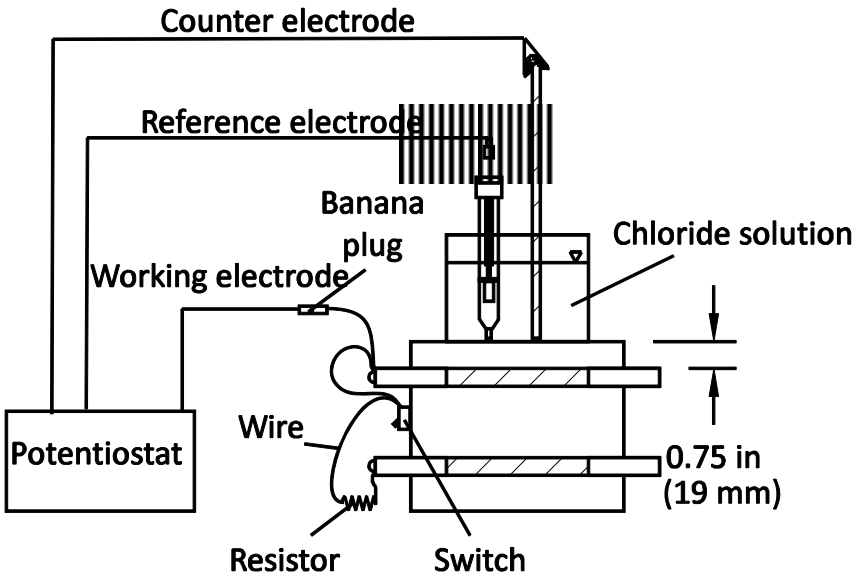


**Figure III-17 CIT Test Sample and Setup.**

Samples were stored on steel wire shelves, exposing the bottom of samples to air. Samples were ponded with a 3 percent sodium chloride solution every Monday morning and dried every Friday morning, exposing the samples to a four days wet and three days dry weekly schedule. Drying of samples was performed using a wet/dry shop vacuum. Electrochemical measurements were performed every Tuesday (1 day after ponding samples). The 3 percent sodium chloride solution was prepared by mixing 0.106 oz (3 g) sodium chloride with 3.42 oz

(97 g) distilled water. Fresh sodium chloride solution was prepared in a 50-gal (189 l) nalgene container every week.

Macrocell corrosion current, OCP, and the polarization resistance ($R_p$) of the samples were measured weekly. While the electrical switch was in the "on" position, the voltage drop across the resistor was measured by connecting the positive terminal of a voltmeter to the bottom reinforcement and the negative terminal to the other end of the resistor. Macrocell current was calculated by dividing the voltage drop by the resistance of the resistor. After measuring the voltage drop across the resistor, the electrical switch was turned off. Two hours later the OCP and $R_p$ of the top reinforcement was measured using a Solartron SI 287 potentiostat. A saturated calomel reference electrode and graphite counter electrode were inserted into the sodium chloride solution reservoir, and the top reinforcement was connected to the potentiostat as the working electrode using the banana plug. The potentiostat was programmed to first determine the OCP of the steel specimen against the calomel electrode over 60 seconds, then to keep the potential of the specimen constant at the last measured OCP level for 30 seconds, and then to run a potential scan from -15 mV to +15 mV against the OCP to determine the $R_p$. Scan rate used for testing was 0.167 mV/s. At the completion of electrochemical measurements the electrical switch was switched back to the "on" position.

The criteria to determine the initiation of corrosion (activation criteria) was either a macrocell current greater than 1µA and a sudden drop in the OCP (<-350 mV SCE) or a sharp decrease in $R_p$ (<5kOhm). When a sample satisfied the activation criteria for two consecutive weeks, testing was stopped and the sample was cut at the level of top reinforcement after discarding the chloride solution reservoir. A minimum of 0.35 oz (10 g) of mortar powder was collected from the top portion of the sample for chloride content determination using a profile grinder. First the profile grinder was used to grind the mortar to the bottom of the reinforcement trace, and the obtained mortar powder was discarded. Then mortar powder was collected from a depth of 78.7 mils (2 mm) as shown in Figure III-18, and its chloride content was analyzed following ASTM C 1152.

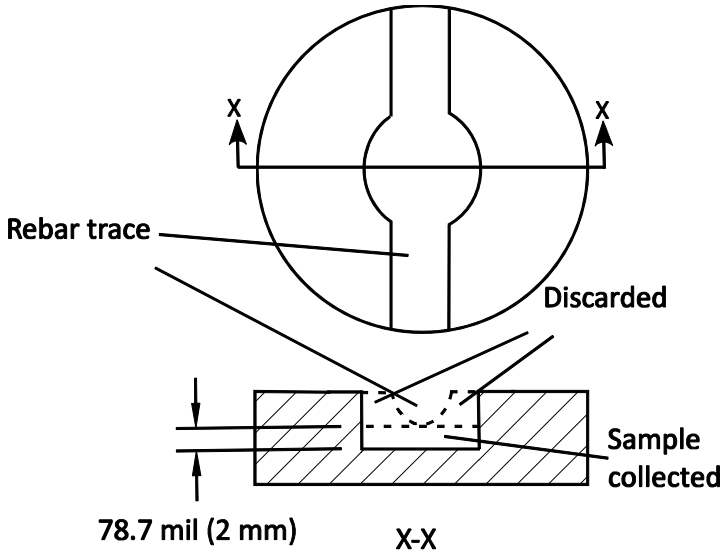


**Figure III-18 Mortar Powder Collected from the Top Part.**

### 3.6.4 Standard ASTM G 109 Test and Modified ASTM G 109 Test

The ASTM G 109 test is an established test method that is commonly used to evaluate materials that are intended to inhibit chloride induced corrosion of steel in concrete. This method monitors the current flow (macro cell corrosion current) between a lower and upper mat of reinforcing steel embedded in concrete that is exposed to cyclic ponding and drying with a sodium chloride solution. Initiation of corrosion of the top reinforcement is determined by an increase of current flow between the upper and lower reinforcements. After initiation, testing is stopped, and the reinforcement is removed to examine the extent of corrosion and to determine the amount of chlorides at the steel concrete interface of the top reinforcement (chloride threshold level). The only difference between the ASTM G 109 test and the modified G 109 test method is the environment where samples are kept during the test. ASTM G 109 samples are kept at laboratory room temperature and humidity conditions, and the modified ASTM G 109 samples are kept at a high temperature and high humidity environment to accelerate the initiation of corrosion.

#### *3.6.4.1 Experimental design*

Due to the long test duration, the G109 and modified G109 samples were evaluated only in the first phase of this study, and testing of these samples continued during the preparation and

testing of the second phase samples of other tests. Also, as stated earlier, the ASTM G 109 test is a well-established test, and there are extensive data on the repeatability of test results. Section 11 of the test method provides repeatability and reproducibility limits based on earlier test results. Therefore, casting samples in a second phase to evaluate repeatability of test results was not deemed necessary.

Three types of uncoated steel reinforcement (ASTM A 615, A 706, and SS304) were tested using six different concrete mixtures as shown in Table III-1. For each of the evaluated 18 conditions 12 replicate samples were prepared which resulted in a total of 216 samples. Epoxy-coated and galvanized-coated reinforcement were not evaluated using the ASTM G 109 test method. Table III-16 shows the experimental design used for ASTM G 109 testing.

Uncoated and coated steel types were evaluated for their corrosion performance embedded in the six different concrete mixtures using the modified G109 test method. Concrete mixtures evaluated using this method are shown in Table III-1 and Table III-17. Table III-18 shows the experimental design and number of tested samples for the uncoated and coated steel samples, respectively. A total of 336 samples were cast and tested using the SE method.

**Table III-16 Experimental Design for ASTM G 109 Test.**

| Water-Cement Ratio | Admixture Content, gal/yd$^3$ (l/m$^3$) | Rebar Type | No. of Test Setups |
|---|---|---|---|
| 0.45 | 0 (0) | A 615 | 12 |
| | | A 706 | 12 |
| | | SS304 | 12 |
| | 2 (10) | A 615 | 12 |
| | | A 706 | 12 |
| | | SS304 | 12 |
| | 4 (20) | A 615 | 12 |
| | | A 706 | 12 |
| | | SS304 | 12 |
| 0.55 | 0 (0) | A 615 | 12 |
| | | A 706 | 12 |
| | | SS304 | 12 |
| | 2 (10) | A 615 | 12 |
| | | A 706 | 12 |
| | | SS304 | 12 |
| | 4 (20) | A 615 | 12 |
| | | A 706 | 12 |
| | | SS304 | 12 |

**Table III-17 Experimental Design for MG109 Samples with Uncoated Steel.**

| Water-Cement Ratio | Admixture Content, gal/yd$^3$ (l/m$^3$) | Rebar Type | No. of Test Setups |
|---|---|---|---|
| 0.45 | 0 (0) | A 615 | 12 |
| | | A 706 | 12 |
| | | SS304 | 12 |
| | 2 (10) | A 615 | 12 |
| | | A 706 | 12 |
| | | SS304 | 12 |
| | 4 (20) | A 615 | 12 |
| | | A 706 | 12 |
| | | SS304 | 12 |
| 0.55 | 0 (0) | A 615 | 12 |
| | | A 706 | 12 |
| | | SS304 | 12 |
| | 2 (10) | A 615 | 12 |
| | | A 706 | 12 |
| | | SS304 | 12 |
| | 4 (20) | A 615 | 12 |
| | | A 706 | 12 |
| | | SS304 | 12 |

**Table III-18 Experimental Design for MG109 Samples with Coated Steel.**

| Water-Cement Ratio | Damage Type[1] | Rebar Type[2] | No. of Test Setups |
|---|---|---|---|
| 0.45 | ND | ECR | 4 |
| | | GR | 4 |
| | DD | ECR | 4 |
| | | GR | 4 |
| | FD | ECR | 4 |
| 0.55 | ND | ECR | 4 |
| | | GR | 4 |
| | DD | ECR | 4 |
| | | GR | 4 |
| | FD | ECR | 4 |

[1]ND: Not damaged, DD: Drill damaged,
[2]ECR: Epoxy coated, GR: Galvanized reinforcement

### *3.6.4.2 Specimen preparation and test procedures*

No. 4 (No. 13M) steel reinforcement were cut into 14-in (360 mm) long pieces using a liquid cooled band saw. One end of specimens was drilled using a drill press and No. 27 drill bit and tapped to receive 3/8-in (9.5 mm) long No. 8-32 stainless steel machine screws. Steel specimens were cleaned in ethyl alcohol using an ultrasonic cleaner. Three inches (75 mm) from each end of the steel specimens were covered with electroplater's tape leaving an 8-in (200 mm) long piece of specimen exposed for testing. The ends of the steel reinforcement and electrical connections were coated with a two-part, high-viscosity epoxy before the initiation of test.

Steel reinforcement bars were placed into 11 x 6 x 4.5-in (280 x 150 x 115 mm) (inner dimensions) molds in two layers making sure that the exposed areas of reinforcement bars were in the middle of the mold. Molds were fabricated with plywood. The bottom reinforcement layer consisted of two steel reinforcement bars that were placed 1.25 in (31.75 mm) from the center from the bottom of the mold. The top layer consisted of one steel reinforcement bar with a clear cover depth of 0.75 in (20 mm). Damaged coated reinforcement bars were placed into the molds making sure that the damaged part of the exposed surface was facing upward. It should also be noted that for the samples with damaged coated reinforcement only the bar at the top layer was damaged, and the bars at the bottom layer were intact. Figure III-19 shows the setup of an ASTM G 109 test sample.

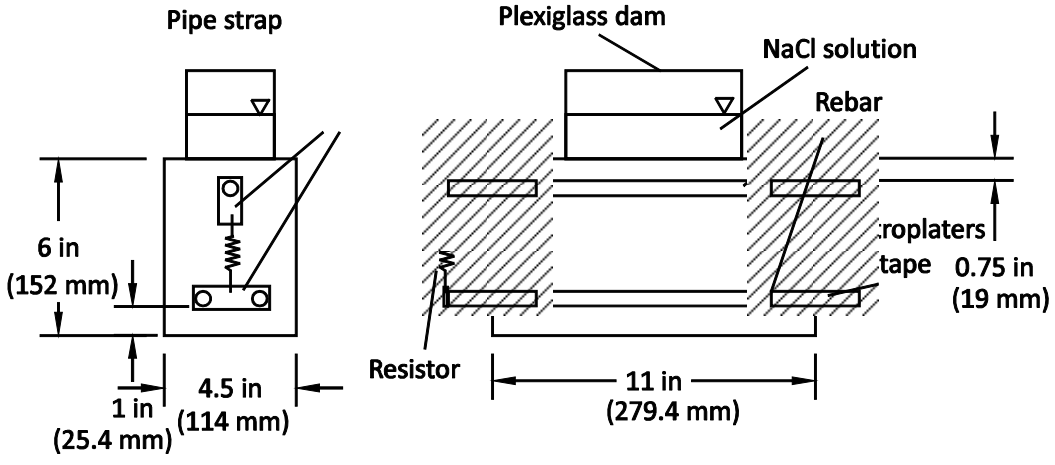


**Figure III-19 Test Setup of an ASTM G 109 Sample.**

Concrete was mixed following ASTM C 192 and was placed into the molds in three layers. Each layer was rodded 25 times (without hitting the reinforcement) and tapped 10 times using a rubber mallet. Samples were finished using a wood float. Samples were covered with wet burlap until they were moved to a curing room. Samples were then cured until 28 days after casting at 73°F (23°C) and 100 percent humidity.

After curing, the samples were dried for two weeks at laboratory room temperature and humidity. Plexiglass dams, 3 x 6 x 3 in (75 x 150 x 75 mm), were attached to the top of the samples using silicone caulk. The top surface outside the dam and the vertical sides of the samples were coated with a two part high viscosity epoxy. Stainless steel pipe straps and No. 8-32 screws were used to electrically connect the top and bottom layers of reinforcement with 100 Ω (±5 percent) resistors.

Epoxy coating of samples and attachment of the dams and resistors were completed during the two weeks after drying, and the test was started one month after the end of curing period. ASTM G 109 samples were stored on wire shelves in the laboratory where their bottom surfaces were exposed to air. The modified G109 test samples were stored on similar wire shelves in a 100°F (37.8°C) controlled environment room.

Samples were exposed to two weeks of ponding following by two weeks of drying resulting in a monthly test cycle. During the two-week wet cycle the dams of the samples were filled with a 3 percent by weight sodium chloride solution 1.5 in (38 mm) deep. The 3 percent sodium chloride solution was prepared by mixing 0.106 oz (3 g) sodium chloride with 3.42 oz (97 g) distilled water. New sodium chloride solution was prepared every week. Once a month, at the end of each first wet week, the voltage drop across the 100 Ω resistor between the top and bottom reinforcement was measured. Macrocell current was calculated from the measured voltage drop and plotted against the time since the start of the test. Testing of each sample was stopped when the average integrated current over time was 150 coloumbs or greater.

At the end of the test, each sample was cut at the level of top reinforcement and 0.35 oz (10 g) of concrete powder was collected from the top portion of the sample for chloride content determination using a profile grinder. The profile grinder was used to grind the concrete to the bottom of the reinforcement trace. Concrete powder was then collected from a depth of 78.7 mils (2 mm) similar to the procedure shown in Figure III-18 for mortar samples. The chloride content of the collected concrete powder was analyzed following ASTM C 1152.

# CHAPTER IV. EXPERIMENTAL RESULTS

## 4.1 MATERIAL CHARACTERIZATION TESTS

### 4.1.1 Rapid chloride permeability test (ASTM C 1202)

Rapid chloride permeability of mortar and concrete samples was determined after 28 days and 56 weeks of curing. The rapid chloride permeability test is an indicator of conductivity of a mixture and is based on the total charge that passes through the sample in a 6-hour period. The results are used to qualitatively assess the chloride ion permeability.

Figure IV-1 and Figure IV-2 show the box plots of the total charge passed at 28 days and 56 weeks, respectively (units are coulombs). At 28 days the average total charge passed for all concrete samples was above 4000 coulombs, indicating high chloride ion permeability. Although some of the differences were not statistically significant, the average chloride ion permeability of the concrete samples with a water-cement ratio of 0.55 was higher compared to samples with water-cement ratio of 0.45. After 56 weeks of curing, the permeability of all samples decreased to moderate and low permeability values. The total charge passed through the concrete samples with a water-cement ratio of 0.45 is statistically significantly lower compared to the concrete samples with water-cement ratio of 0.55. Among the samples with the same water-cement ratio, samples containing 4 gal/yd$^3$ (19.8 L/m$^3$) of corrosion inhibitor exhibited significantly higher total charge values compared to the other samples. However, researchers believe that this is not an indication of higher permeability but more an indication of higher concentration of charge carrying ions in the solution due to the high amount of corrosion inhibitor.

Figure IV-3 and Figure IV-4 show the box plots of total charge that passed through mortar samples after 28 days and 56 weeks of curing, respectively. Testing of the mortar samples at 28 days with a water-cement ratio of 0.55 could not be completed due to very high amounts of current flowing through the samples, which indicates extremely high conductivity. The permeability of mortar samples with a water-cement ratio of 0.45 was high and unlike the concrete samples the permeability of these samples decreased with increasing corrosion inhibitor contents. After 56 weeks, the mortar samples with a water-cement ratio of 0.45 exhibited the same trend but the chloride permeability of the mortar samples containing 2 and 4

gal/yd$^3$ (9.9 and 19.8 L/m$^3$) corrosion inhibitor exhibited moderate permeability. Samples with a water-cement ratio of 0.55 exhibited high chloride permeability, and the samples with 4 gal/yd$^3$ (19.8 L/m$^3$) corrosion inhibitor exhibited statistically significantly lower permeability values.

Results of concrete and mortar samples after 56 weeks of curing are contradictory. Results obtained from concrete samples indicated that higher corrosion inhibitor addition increased the chloride ion permeability, and results obtained from mortar samples indicated that the permeability decreased with increasing corrosion inhibitor levels. The effect of water-cement ratio on the permeability was similar for both mortar and concrete samples; the chloride permeability of samples increased with increasing water-cement ratio.

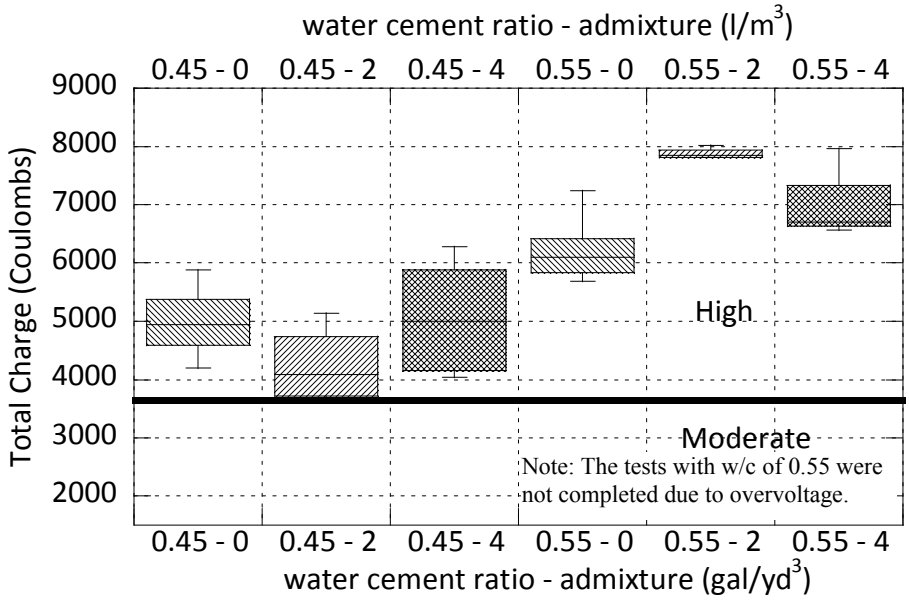


**Figure IV-1 The 28-Day Permeability of Concrete Samples.**

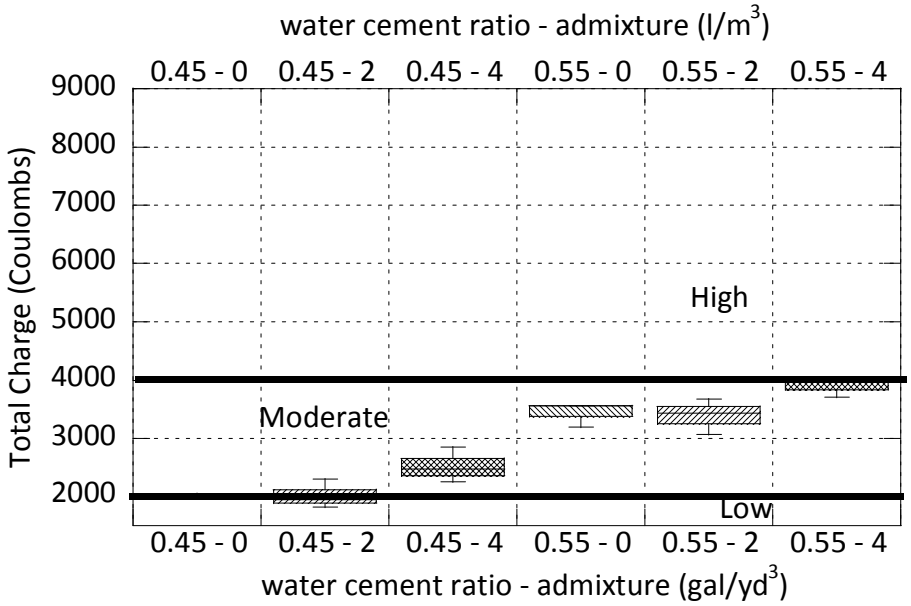


**Figure IV-2 The 56-Week Permeability Values of Concrete Samples.**

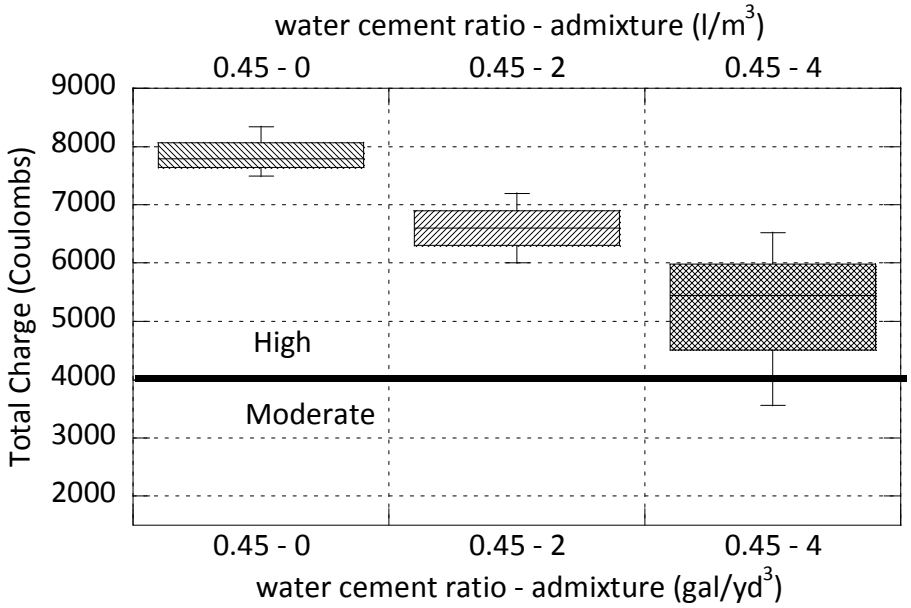


**Figure IV-3 The 28-Day Permeability of Mortar.**

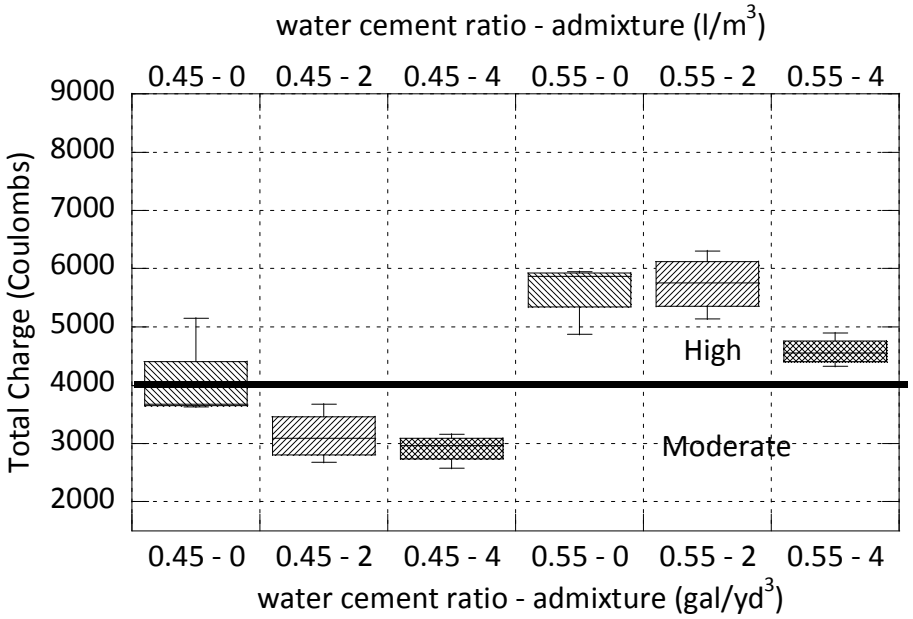


**Figure IV-4 The 56-Week Permeability Values of Mortar.**

### 4.1.2 Diffusion coefficient test (ASTM C 1556)

As explained earlier in section 3.4.2, mortar and concrete samples were exposed to a chloride solution for 35 days. The sides of the samples were epoxy coated allowing diffusion only in one direction (from the top surface to the bottom surface of the samples). At the end of exposure period, samples were cut, ground, and their chloride contents were determined by titration. After determining chloride contents at different depths from the top surface, Fick's second law was used to determine a diffusion coefficient for each of the samples. Figure IV-5 and Figure IV-6 show the ranges of diffusion coefficients and their average values determined for each testing condition (water-cement ratio and inhibitor combination) for concrete and mortar mixtures, respectively.

Results clearly indicate that for concrete samples the magnitude of the apparent diffusion coefficient increases with increasing water-cement ratios. However due to the large variances in the data, the difference between the samples embedded in the mortar with a water-cement ratio of 0.45 containing 4 gal/yd$^3$ (19.8 L/m$^3$) corrosion inhibitor and samples embedded in mortar with water-cement ratio of 0.55 containing 0 and 2 gal/yd$^3$ (9.9 L/m$^3$) of corrosion inhibitor were not statistically significant. Also, although not statistically significant, for

samples embedded in mortar with a water-cement ratio of 0.55, the average diffusion coefficient seemed to increase with increasing corrosion inhibitor level.

Results were similar for the mortar samples. The average apparent diffusion coefficient increased with increasing water-cement ratio; however, due to large variances only the samples embedded in mortar with a water-cement ratio of 0.45 and without corrosion inhibitor had a statistically significantly smaller diffusion coefficient compared to the samples embedded in mortar with a water-cement ratio of 0.55. For the samples embedded in mortar with water-cement ratio of 0.55, apparent diffusion coefficient increased statistically significantly from 2 to 4 gal/yd$^3$ corrosion inhibitor level but samples without corrosion inhibitor were not statistically different from other samples.

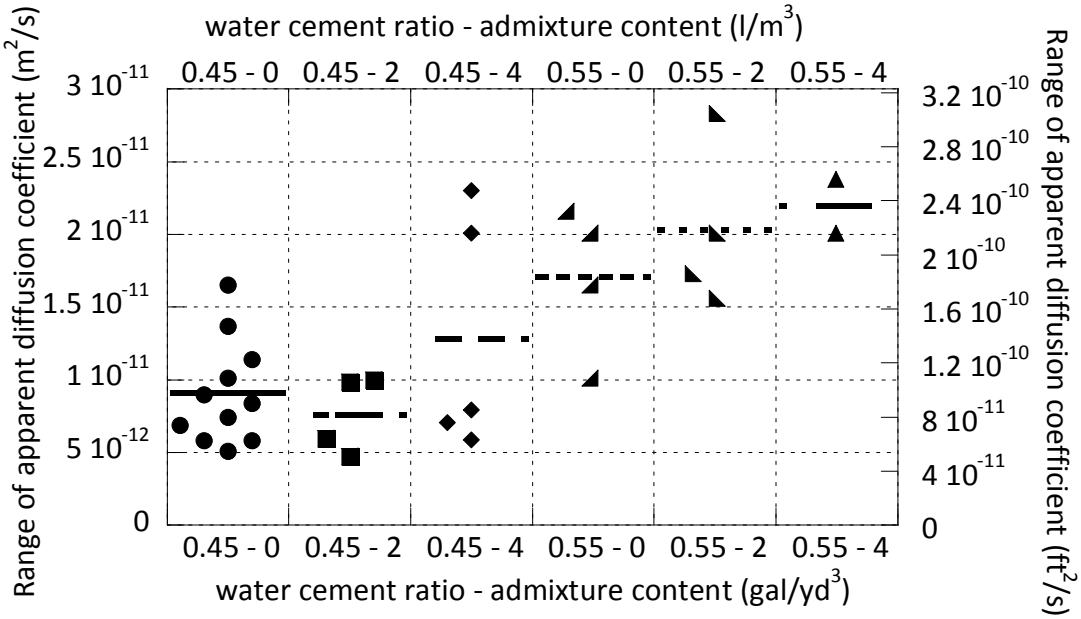


**Figure IV-5 Diffusion Coefficient of Concrete Samples Determined after 35 Days.**

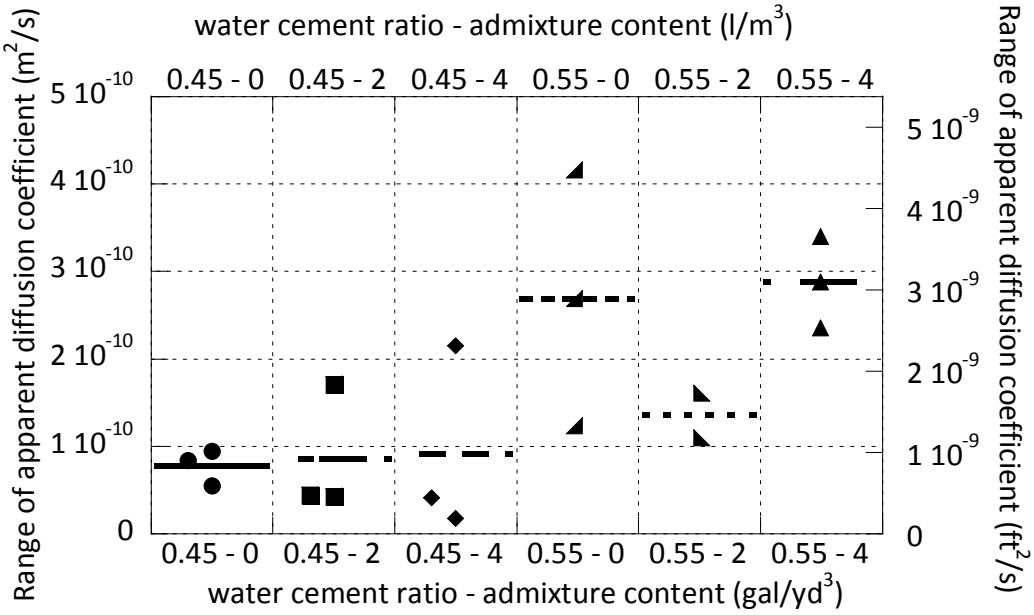


**Figure IV-6 Diffusion Coefficient of Mortar Samples Determined after 35 Days.**

### 4.1.3 Compressive strength

Compressive strength results at 7 and 28 days are shown in Figure IV-7 and Figure IV-8, respectively. Three samples were used to determine the compressive strength at each testing age. Comparison of compressive strength values assuming a normal distribution and using Tukey's method at 95 percent level showed that although the difference in strength between samples containing 0 and 2 gal/yd3 (9.9 L/m3) corrosion inhibitor was not statistically significant, the difference between the samples containing 0 and 4 gal/yd3 (19.8 L/m3) was statistically significant at both water-cement ratio values and at both ages. The compressive strength decreased with increasing corrosion inhibitor level.

Figure IV-9 and Figure IV-10 show the compressive strength values of mortar cubes at 7 and 28 days. Strength measurements of mortar cubes exhibited greater variability compared to the concrete samples, and there were no significant trends in compressive strength related to the corrosion inhibitor content.

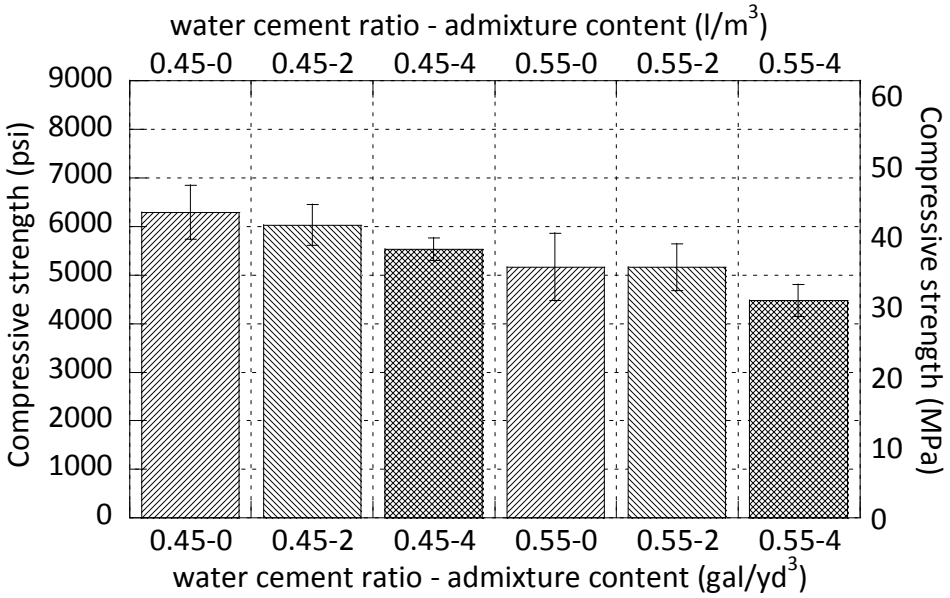


**Figure IV-7 Compressive Strength of Concrete Mixtures at 7 Days.**

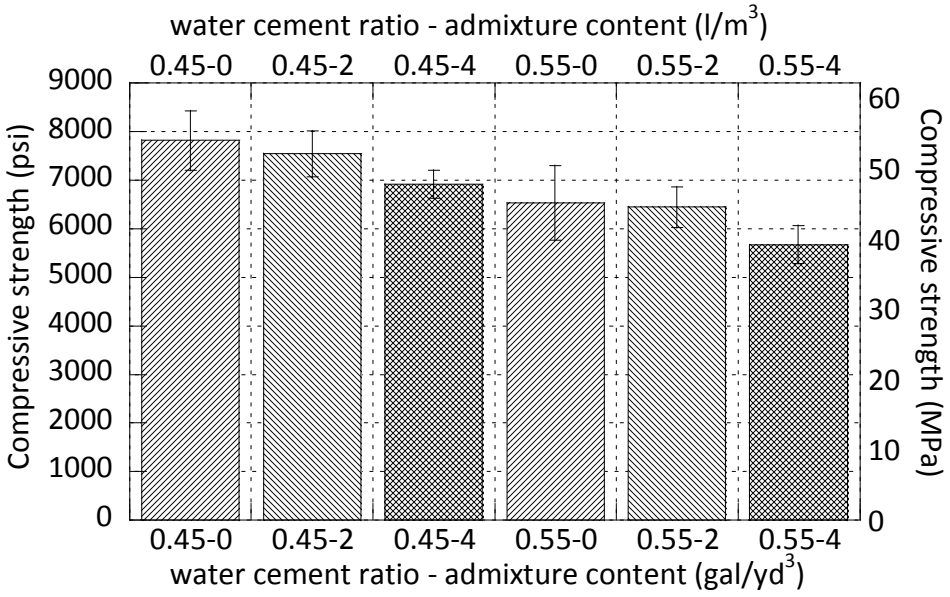


**Figure IV-8 Compressive Strength of Concrete Mixtures at 28 Days.**

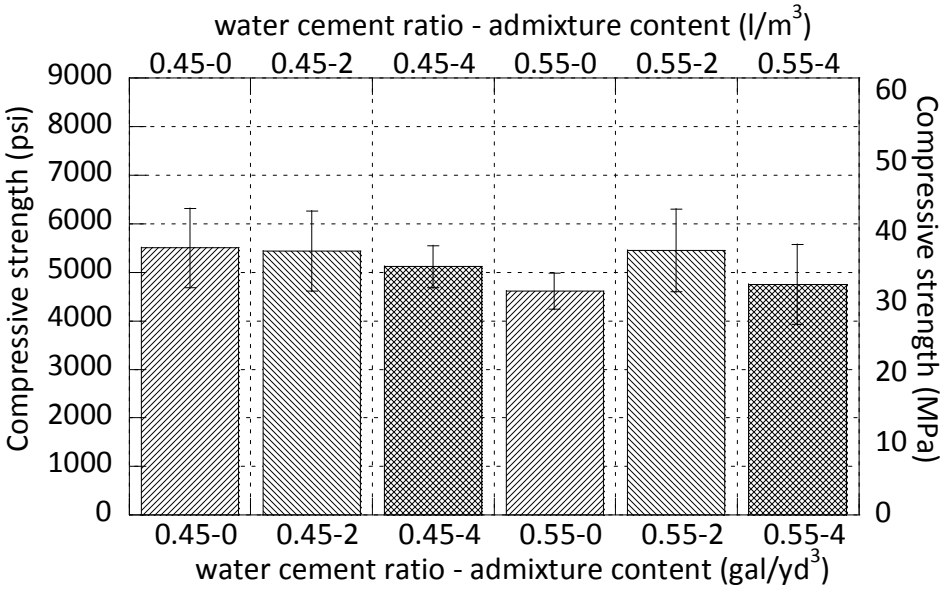


**Figure IV-9 Compressive Strength of Mortar Mixtures at 7 Days.**

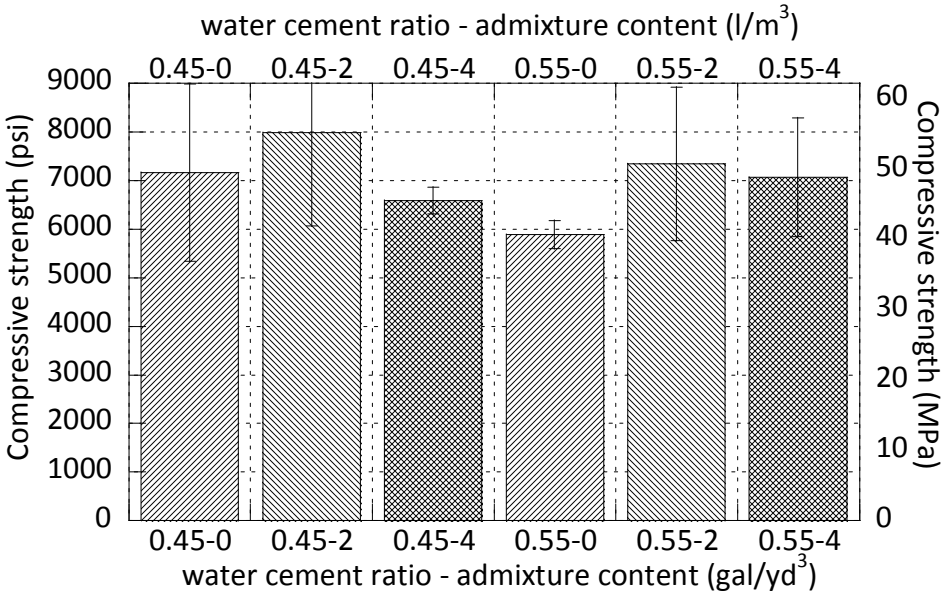


**Figure IV-10 Compressive Strength of Mortar Mixtures at 28 Days.**

## 4.2 CORROSION TESTS

### 4.2.1 Rapid macrocell test

#### *4.2.1.1 Phase I*

A total of 84 samples consisting of 54 uncoated and 30 coated samples were tested in Phase I of the study as shown in Table III-10 and Table III-11. Uncoated bars, ASTM A 615, A 706, and stainless steel 304, were tested at two different water-cement ratios and with three different levels of corrosion inhibitor. Coated bars (i.e., galvanized and epoxy coated) were also tested at two water-cement ratios. Drill damaged and file damaged epoxy coated bars and drill damaged galvanized bars were also included in the test program. It should be noted again that although the experimental design shown in Table III-10 and Table III-11 required three samples for each condition, due the breakage of some samples during de-molding. some conditions had less tested samples. A large percentage of galvanized steel samples were damaged when de-molded. Therefore, additional galvanized reinforcement samples were evaluated in the second phase testing of this study.

The open circuit potential of anode and macrocell current across the 10 Ω resistor were measured weekly for a period of 15 weeks for each sample. Macrocell current values were converted to current density by dividing current values to the exposed area of steel in mortar. The exposed area of steel samples was 39.935 $cm^2$ (6.19 $in^2$). For the coated samples that had a damaged coating, the area of exposed surface was 1 percent of the area of uncoated samples, i.e., 0.39935 $cm^2$ (0.0619 $in^2$). The current density values were converted to macrocell corrosion rate, $r$, using Faraday's law as shown in Eq. (4.1).

$$r = \frac{ia}{nFD} \tag{4.1}$$

where

$a$ = atomic weight,

$i$ = current density ($A/cm^2$),

$n$ = number of ion equivalents exchanged,

$F$= Faraday's constant, and

$D$ = density of metal.

Eq. (4.1) becomes Eq. (4.2) when appropriate values are given for atomic weight, equivalence number, Faraday's constant, and the density of the metal as follows:

$$r = \alpha i \tag{4.2}$$

where

$r$ = corrosion rate in μm/yr

$$\alpha = \begin{cases} 11.59 \text{ for conventional reinforcement} \\ 14.98 \text{ for galvanized reinforcement} \\ 10.59 \text{ for stainless steel reinforcement} \end{cases}$$

$i$ = current density in μA/cm$^2$

For galvanized steel samples the atomic weight and density of zinc is used. Actually, when the galvanization is corroded away the underlying steel will start to corrode; however, for a galvanized rebar prepared according to ASTM A 767 (*Standard Specification for Zinc-Coated (Galvanized) Steel Bars for Concrete Reinforcement*), the average thickness of the galvanization is 4.7 to 5.9 mils (120 to 150 μm), which is higher than the total corrosion loss values obtained in this experiment. Because stainless steel 304 is an alloy, to calculate its corrosion rate its equivalent mass $a/n$ was calculated based on its composition. The calculated equivalent mass was 0.06 lb (25.82 g). The average density of stainless steel 304 was assumed to be 1612 lb/ft$^3$ (8.03 g/cm$^3$). The stainless steel used in this study had an average of 18.43 percent Cr, 8.64 percent Ni, and 70.236 percent Fe. The equivalent mass of stainless steel 304 was calculated as follows:

$$\text{Equivalent mass} = a/n = \frac{1}{\sum\left(\frac{f_i n_i}{a_i}\right)} \tag{4.3}$$

where

$a_i$ = atomic mass for element i

$n_i$ = number of exchanged electrons for element i

$f_i$ = mass fraction of element i

Figure IV-11 shows the average corrosion rates of ASTM A 706 samples embedded in six different mortars. Two water-cement ratios and three levels of corrosion inhibitors were evaluated. Samples without corrosion inhibitor exhibited very high initial corrosion rates but they stabilized starting from the second week on. Figure IV-12 shows the average corrosion

loss values of ASTM A 706 samples. Table IV-1 shows the average corrosion rates and their standard deviation starting from week 2 and their total corrosion loss values at the end of the test. Total corrosion loss of samples decreased with decreasing water-cement ratio for each level of corrosion inhibitor addition. For samples with water-cement ratio of 0.45, total corrosion loss of samples decreased with increasing corrosion inhibitor level. Results from these tests indicated that corrosion inhibitor did not affect the total corrosion loss of the samples with a water-cement ratio of 0.55. Insignificant effect of calcium nitrite based corrosion inhibitors on concrete with high water-cement ratios has been reported in the literature.

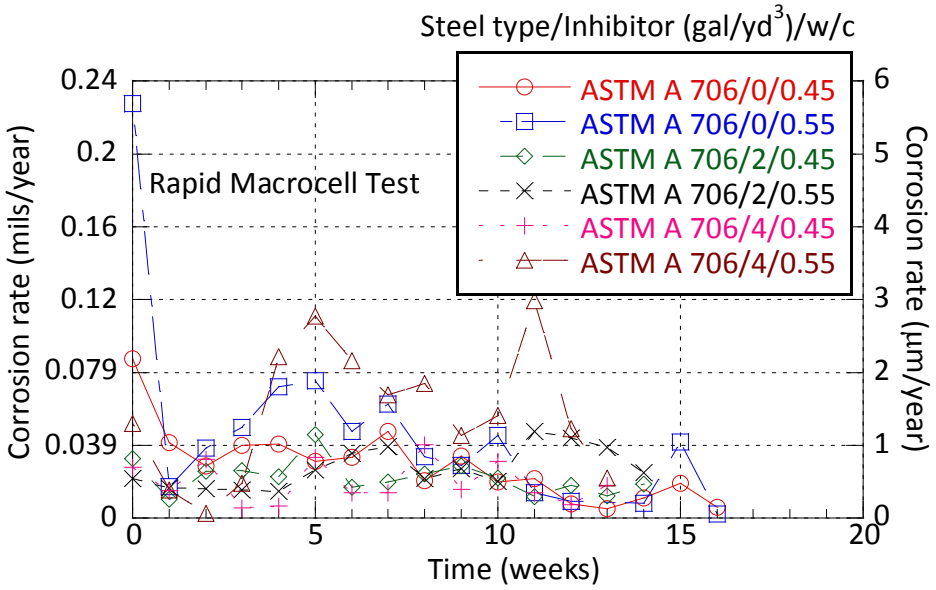


**Figure IV-11 Average Corrosion Rates of ASTM A 706 Samples.**

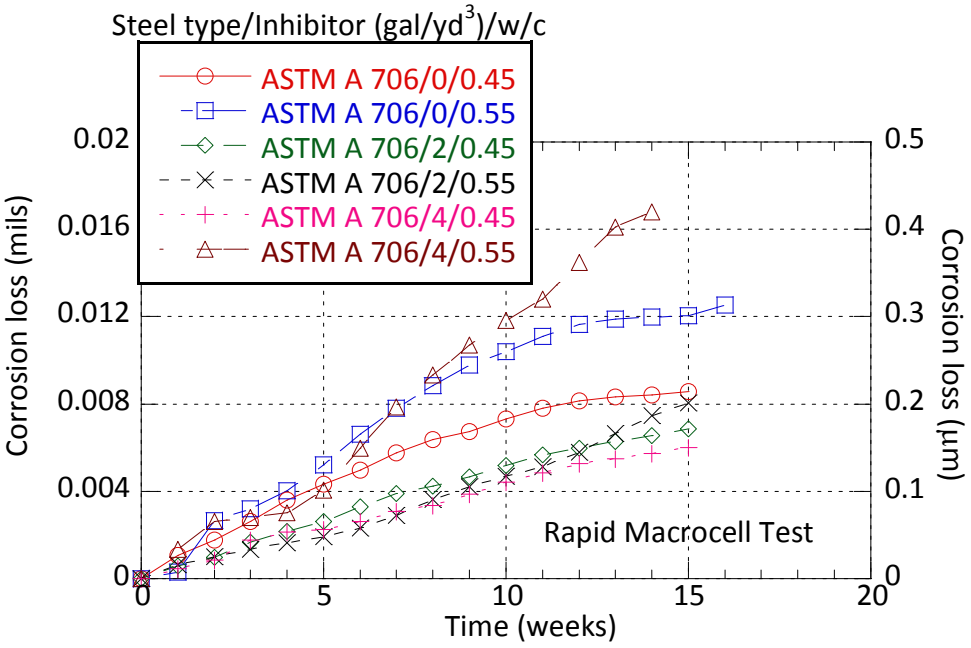


**Figure IV-12 Average Corrosion Loss of ASTM A 706 Samples.**

**Table IV-1 Average Corrosion Rate and Total Corrosion Loss of ASTM A 706 Samples.**

| Corrosion Inhibitor gal/yd$^3$ [kg/m$^3$] | Water-Cement Ratio | Average Corrosion Rate mils/year [µm/year] | Standard Deviation | Total Corrosion Loss mils [µm] |
|---|---|---|---|---|
| 0 [0] | 0.45 | 0.029 [0.727] | 0.020 [0.501] | 0.011 [0.271] |
| | 0.55 | 0.048 [1.210] | 0.052 [1.319] | 0.012 [0.314] |
| 2 [10] | 0.45 | 0.021 [0.540] | 0.009 [0.224] | 0.007 [0.171] |
| | 0.55 | 0.027 [0.693] | 0.011 [0.282] | 0.008 [0.202] |
| 4 [20] | 0.45 | 0.019 [0.474] | 0.011 [0.284] | 0.006 [0.150] |
| | 0.55 | 0.057 [1.456] | 0.037 [0.929] | 0.027 [0.687] |

Figure IV-13 shows the open circuit potential values of ASTM A 706 samples. Starting at week 5 the open circuit potential of all samples was below -275 mV vs. the SCE electrode,

indicating a high probability of corrosion following the interpretation of ASTM C 876. The open circuit potentials of all samples were between -400 and -600 mV vs. SCE at the end of the test.

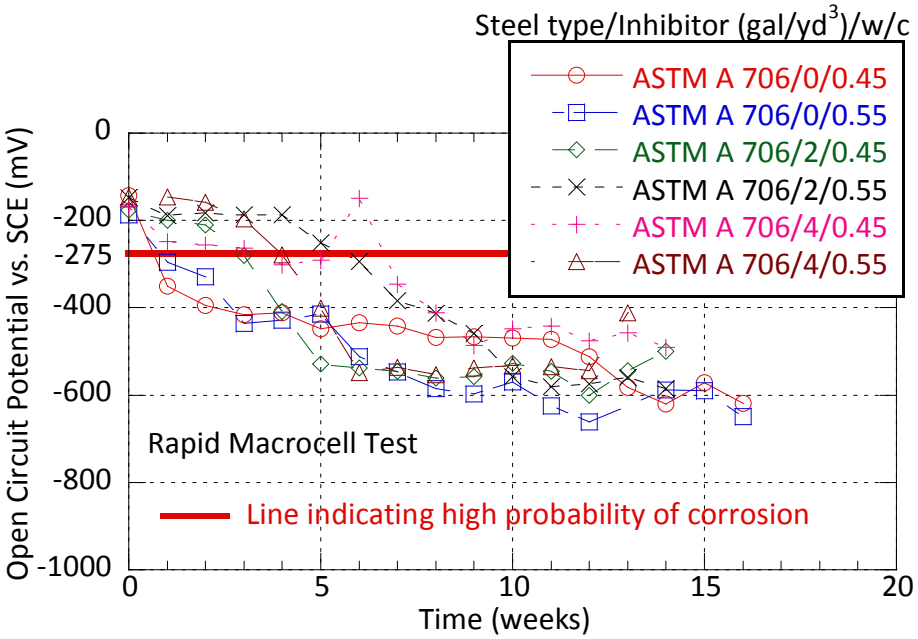


**Figure IV-13 Open Circuit Potential of ASTM A 706 Samples.**

Figure IV-14 shows the average corrosion rates of ASTM A 615 samples embedded in mortars tested with the rapid macrocell test. Mortars were prepared at two different water-cement ratios and contained three different levels of corrosion inhibitors. Figure IV-15 shows the average corrosion loss values of ASTM A 615 samples. Table IV-2 shows the standard deviation and average of observed corrosion rates and total corrosion loss values for ASTM A 615 samples. ASTM A 615 samples do not exhibit any clear trends based on the water-cement ratio or corrosion inhibitor level. Figure IV-16 shows the open circuit potential values of the ASTM A 615 samples. This figure shows that most of the samples remained passive until the 11$^{th}$ week of testing. The samples with the highest amount of corrosion inhibitor showed early activation around weeks 4 to 5, and these are the samples that exhibited the highest total average corrosion loss values. Samples with a water-cement ratio of 0.55 and without corrosion inhibitor showed activation based on the average OCP at week 7, which coincides with the sharp increase of corrosion rate of these samples. The same is true for samples with a water-

cement ratio of 0.45 and 2 gal/yd$^3$ (10 kg/m$^3$) corrosion inhibitor. The results of the rapid macrocell test containing ASTM A 615 samples show a good agreement between the OCP measurements and corrosion rate readings.

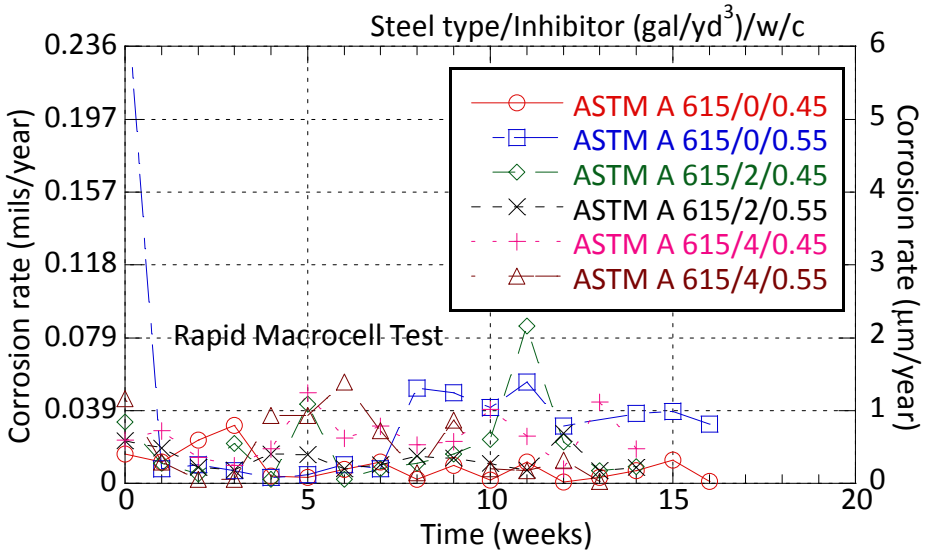


**Figure IV-14 Average Corrosion Rates of ASTM A 615 Samples.**

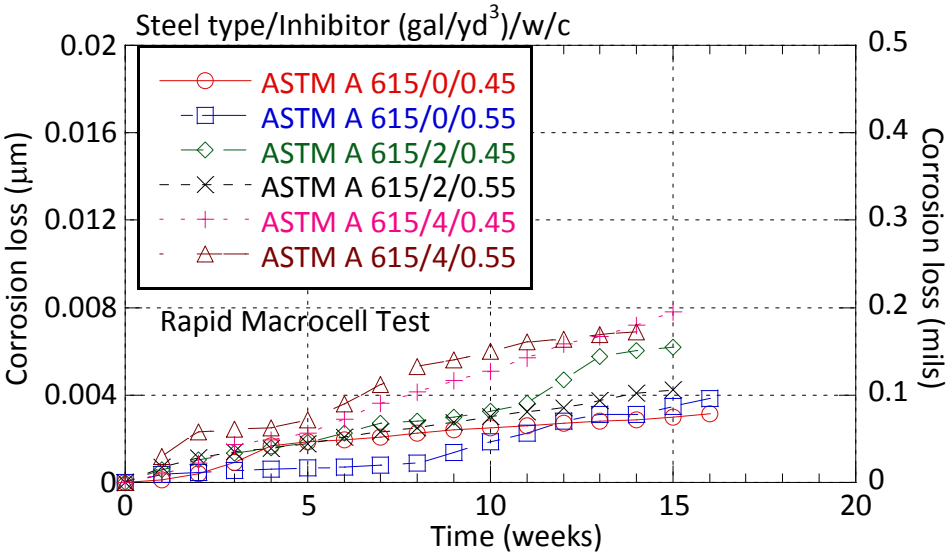


**Figure IV-15 Average Corrosion Loss of ASTM A 615 Samples.**

**Table IV-2 Average Corrosion Rate and Total Corrosion Loss of ASTM A 615 Samples Evaluated with Rapid Macrocell Test.**

| Corrosion Inhibitor gal/yd$^3$ [kg/m$^3$] | Water-Cement Ratio | Average Corrosion Rate mils/year [µm/year] | Standard Deviation | Total Corrosion Loss Mils [µm] |
|---|---|---|---|---|
| 0 [0] | 0.45 | 0.009 [0.226] | 0.008 [0.214] | 0.003 [0.079] |
| | 0.55 | 0.026 [0.656] | 0.019 [0.484] | 0.004 [0.096] |
| 2 [10] | 0.45 | 0.019 [0.485] | 0.022 [0.557] | 0.006 [0.155] |
| | 0.55 | 0.012 [0.316] | 0.006 [0.146] | 0.004 [0.106] |
| 4 [20] | 0.45 | 0.025 [0.647] | 0.012 [0.311] | 0.007 [0.180] |
| | 0.55 | 0.019 [0.471] | 0.017 [0.443] | 0.007 [0.172] |

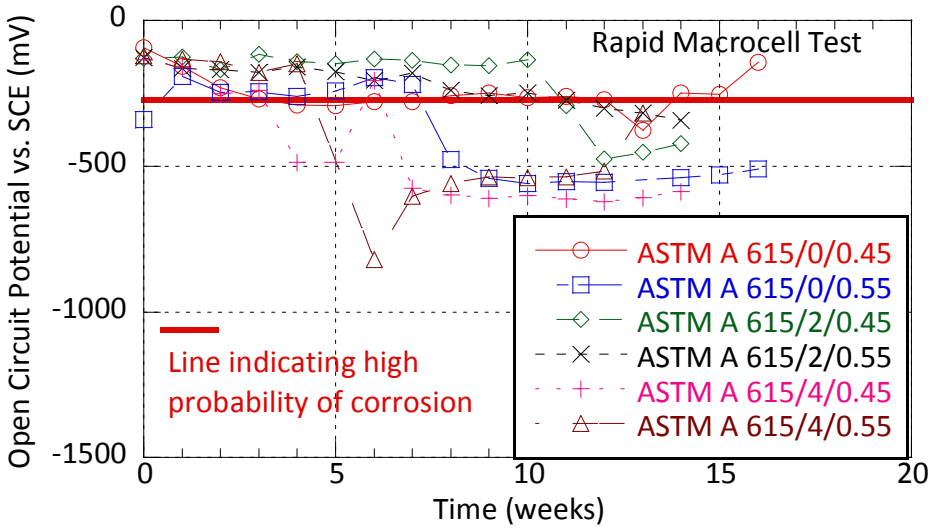


**Figure IV-16 Open Circuit Potential of ASTM A 615 Samples.**

Average corrosion rates of SS304 samples embedded in mortars are shown in Figure IV-17. Figure IV-18 shows the average corrosion loss values of SS304 samples. Table IV-3 shows the average corrosion rates, standard deviations, and total corrosion loss values of the SS304 samples evaluated with the rapid macrocell corrosion test. Figure IV-19 shows the open circuit potential values of the SS304 samples. Results indicate that the stainless steel samples

remained passive for the entire test and exhibited very small corrosion rates and corrosion loss values. Corrosion inhibitor level and water-cement ratio do not seem to affect the average corrosion loss and corrosion rate values of samples.

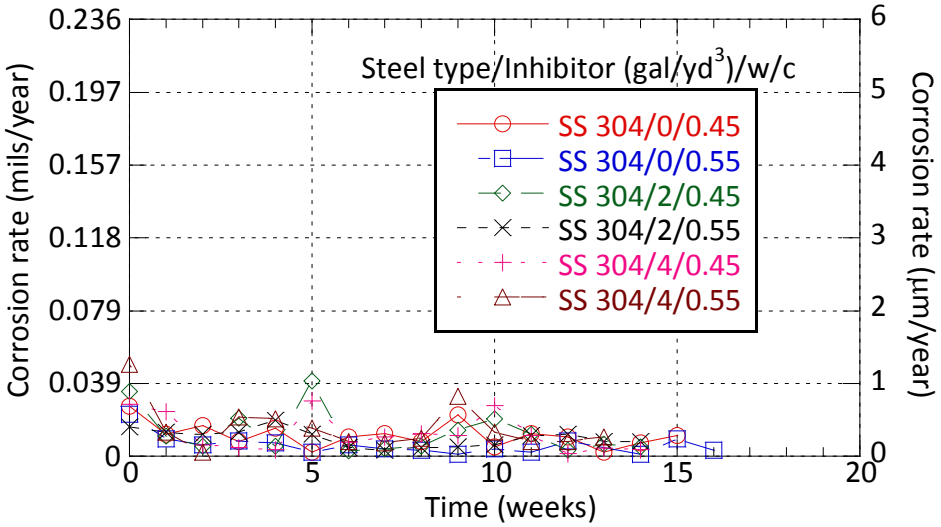


**Figure IV-17 Average Corrosion Rates of SS304 Samples.**

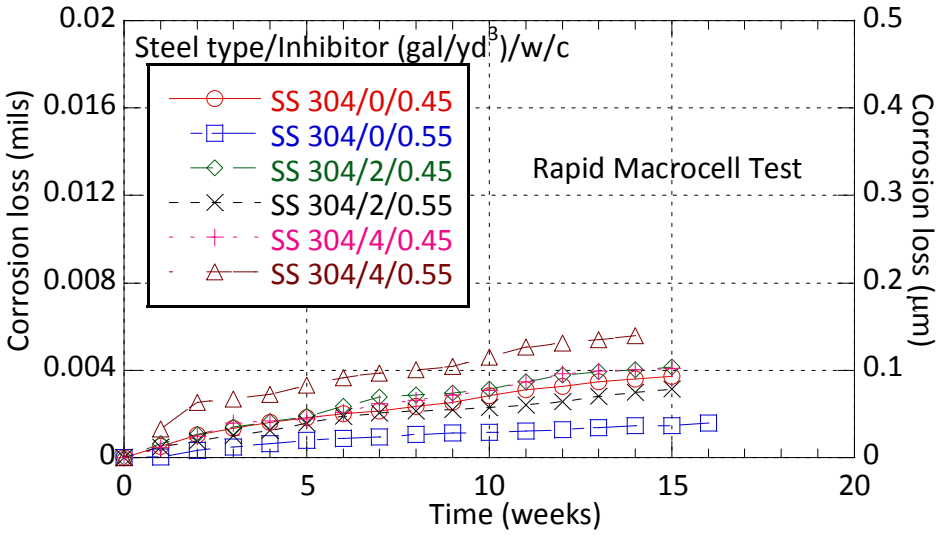


**Figure IV-18 Average Corrosion Loss of SS304 Samples.**

**Table IV-3 Average Corrosion Rate and Total Corrosion Loss of SS304 Samples.**

| Corrosion Inhibitor gal/yd$^3$ [kg/m$^3$] | Water-Cement Ratio | Average Corrosion Rate mils/year [µm/year] | Standard Deviation | Total Corrosion Loss mils [µm] |
|---|---|---|---|---|
| 0 [0] | 0.45 | 0.005 [0.132] | 0.003 [0.077] | 0.004 [0.093] |
| | 0.55 | 0.010 [0.262] | 0.005 [0.136] | 0.001 [0.037] |
| 2 [10] | 0.45 | 0.011 [0.285] | 0.010 [0.261] | 0.004 [0.104] |
| | 0.55 | 0.009 [0.240] | 0.005 [0.116] | 0.003 [0.079] |
| 4 [20] | 0.45 | 0.012 [0.303] | 0.009 [0.238] | 0.004 [0.100] |
| | 0.55 | 0.013 [0.328] | 0.008 [0.202] | 0.005 [0.140] |

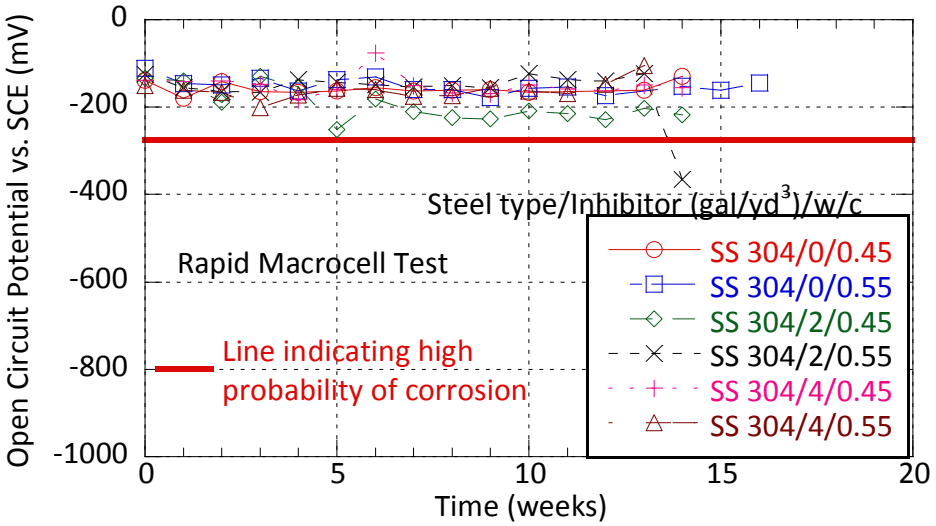


**Figure IV-19 Open Circuit Potential of SS304 Samples.**

As noted in the experimental setup section, most of the samples containing galvanized reinforcement were damaged during de-molding of samples in the first phase. Therefore, only one drill damaged galvanized sample and one galvanized sample with no damage could be tested at a water-cement ratio of 0.45. Figure IV-20 shows the average corrosion rates of samples with galvanized reinforcement. Figure IV-21 shows their average corrosion loss values. Average corrosion rate of drill damaged galvanized reinforcement samples was

0.038 mils/yr (0.975 µm/yr), and their standard deviation was 0.041 (1.043). Total corrosion loss of drill damaged galvanized reinforcement was 0.013 mils (0.325 µm). Average corrosion rate of undamaged galvanized reinforcement samples was 0.040 mils/yr (1.015 µm/yr) and their standard deviation was 0.037 (0.935). Total corrosion loss of drill damaged and undamaged galvanized reinforcement was 0.013 mils (0.323 µm). Figure IV-22 shows the open circuit potential values of samples containing galvanized reinforcement.

OCP values indicate that according to ASTM C 876 limits both samples were actively corroding from the beginning of the test, which is due to the corroding zinc layer. Although both samples indicated high corrosion rates for the first couple of weeks, starting from week 4 corrosion rates stabilized at lower values. Based on the average corrosion rate and total corrosion loss, damaging the galvanized coating with a drill did not have a significant effect on the corrosion performance. Considering that the average thickness of the galvanized layer is 4.7 to 5.1 mils (120 to 130 µm), no significant reduction of galvanization occurred in 15 weeks. and this was also confirmed by visual inspection of samples. It should be noted that because of the high potential for damage of the samples, the rapid macrocell test is likely not appropriate for evaluating the corrosion performance of galvanized reinforcement.

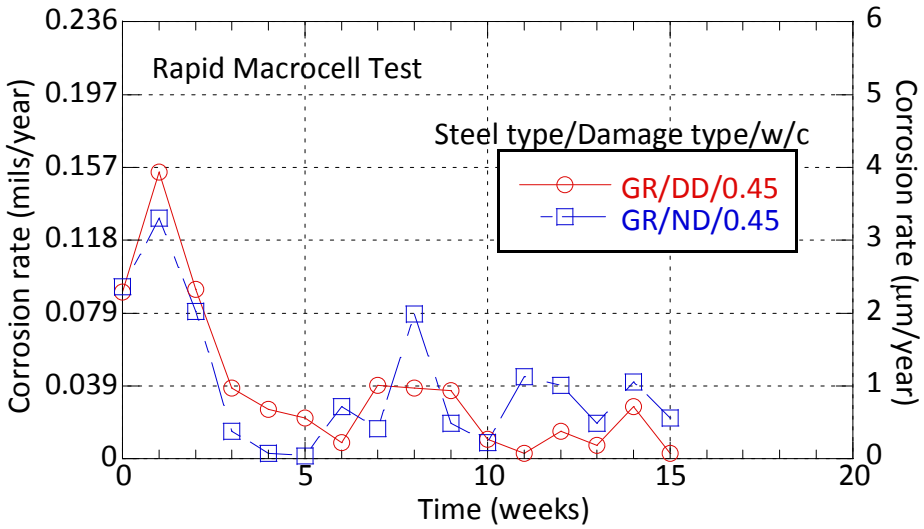


**Figure IV-20 Average Corrosion Rates of Samples Containing Galvanized Reinforcement.**

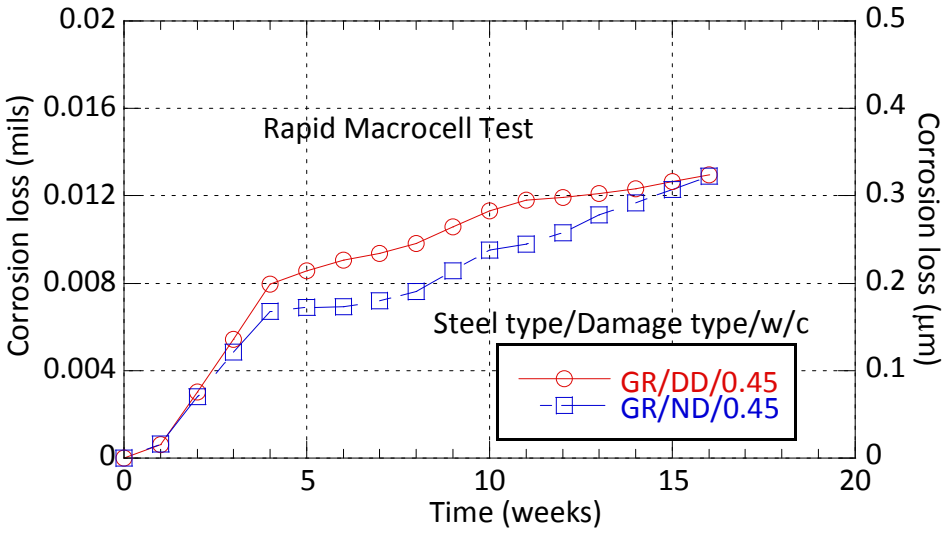


**Figure IV-21 Average Corrosion Loss of Samples Containing Galvanized Reinforcement.**

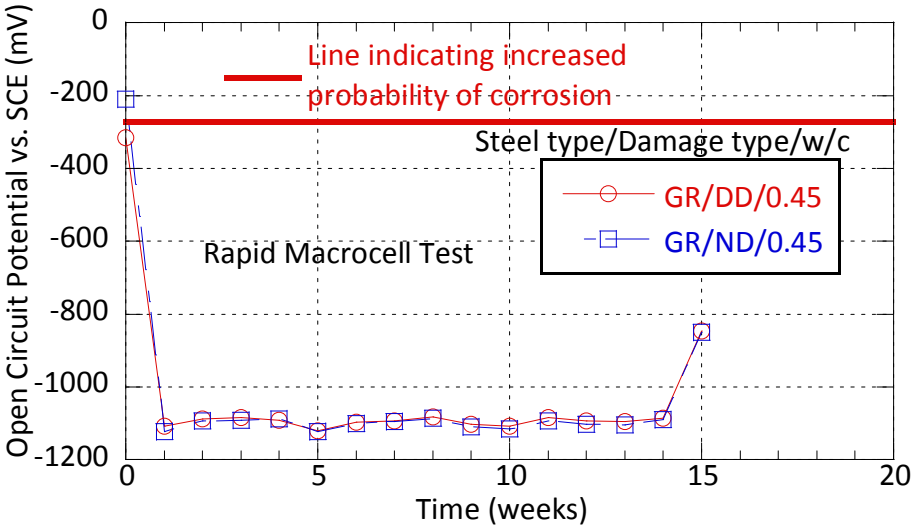


**Figure IV-22 Open Circuit Potential of Samples Containing Galvanized Reinforcement.**

Figure IV-23 shows the average corrosion rates of ECR samples embedded in mortars for the rapid macrocell test. The corrosion rates of damaged samples (drill damaged and file damaged) are calculated based on the exposed surface (1 percent of the exposed surface of uncoated samples). Figure IV-24 also shows the average corrosion rates of ECR samples, but these corrosion rates are calculated based on the total embedded surface of the reinforcement

and not just the damaged surface area. Figure IV-25 and Figure IV-26 show the average corrosion loss values of the ECR samples calculated based on the exposed surface area and based on the total embedded surface area, respectively. Table IV-4 shows the average corrosion rates and corrosion loss values of ECR samples at the end of the test based on the damaged and total surface area. Visual inspection of the samples indicated that none of the ECR samples exhibited cathodic disbondment and under coating corrosion. Although damaged samples had a much higher corrosion rate and corrosion loss compared to undamaged samples when assessments were based on total exposed surface area, results indicate that the corrosion loss was similar. Although file damaged samples looked clean during visual inspection, corrosion products were observed at drill damaged areas of ECR bars. Figure IV-27 shows one of the drill damaged ECR bars with corrosion products accumulated at the drill damaged area.

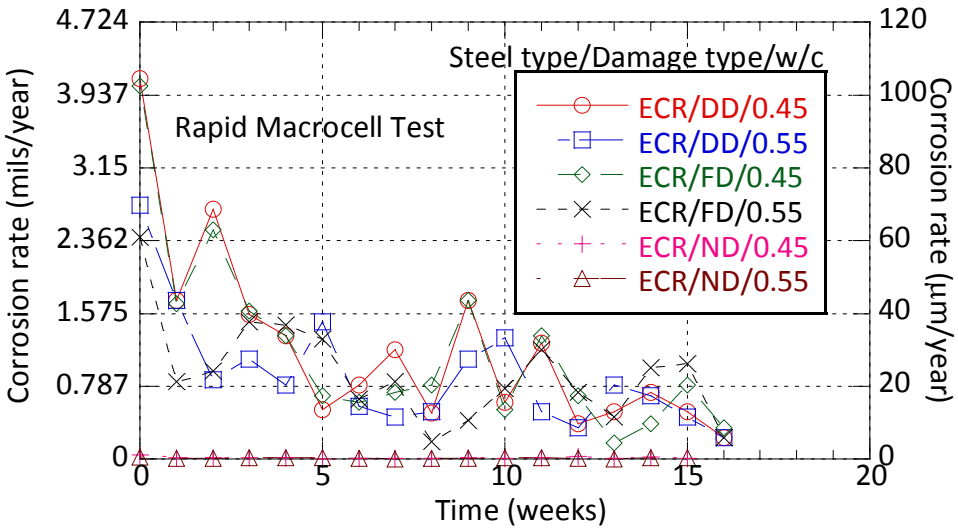


**Figure IV-23 Average Corrosion Rates of ECR Samples. Corrosion Rates of Damaged Samples Are Calculated Based on the Damaged Exposed Surface Area.**

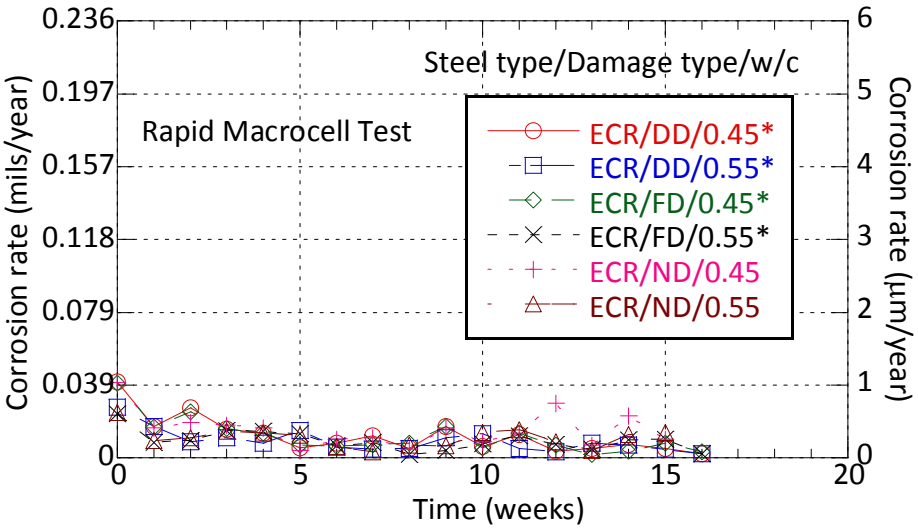


**Figure IV-24 Average Corrosion Rates of ECR Samples. Corrosion Rates of Damaged Samples Are Calculated Based on the Total Embedded Reinforcement Surface Area.**

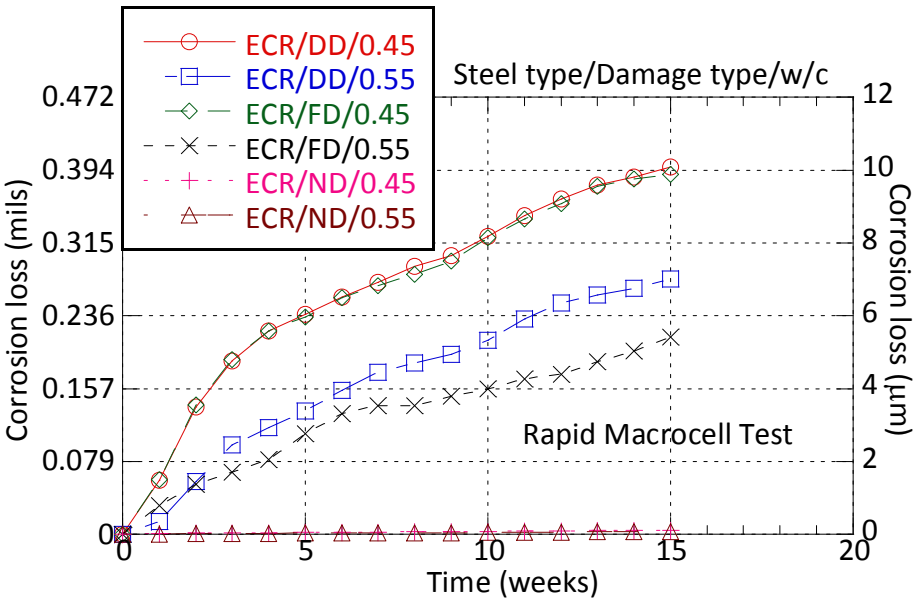


**Figure IV-25 Average Corrosion Loss of ECR Samples. Corrosion Loss of Damaged Samples Are Calculated Based on the Damaged Exposed Surface Area.**

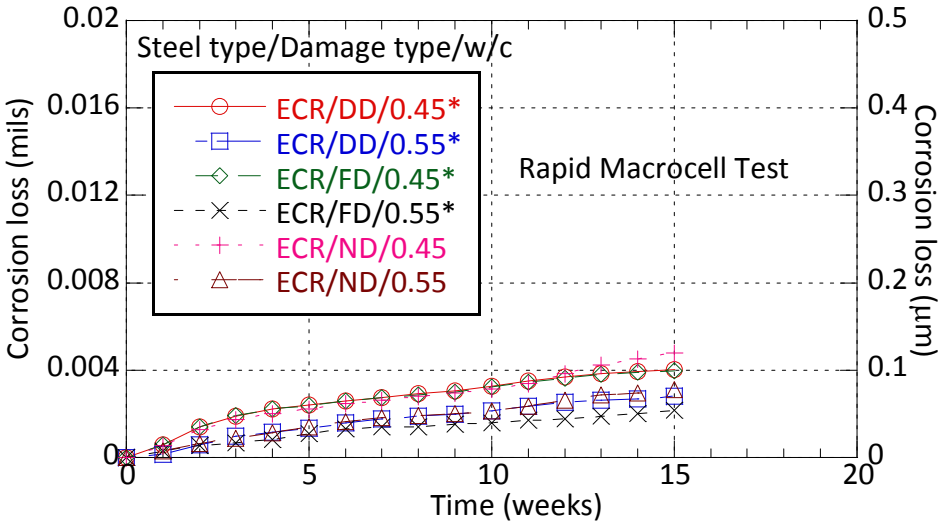


**Figure IV-26 Average Corrosion Loss of ECR Samples. Corrosion Loss of Damaged Samples Are Calculated Based on the Total Embedded Reinforcement Surface Area.**

**Table IV-4 Average Corrosion Rate and Total Corrosion Loss of Epoxy Coated Samples.**

| Damage Type[1] | Water-Cement Ratio | Average Corrosion Rate mils/year [µm/year] | Standard Deviation | Total Corrosion Loss mils [µm] | Average Corrosion Rate mils/year [µm/year][2] | Standard Deviation[2] | Total Corrosion Loss mils [µm][2] |
|---|---|---|---|---|---|---|---|
| DD | 0.45 | 0.846 [21.49] | 0.47 [11.98] | 0.397 [10.084] | 0.010 [0.258] | 0.007 [0.169] | 0.003 [0.083] |
| | 0.55 | 0.739 [18.76] | 0.37 [9.57] | 0.276 [7.009] | 0.008 [0.205] | 0.004 [0.108] | 0.002 [0.048] |
| FD | 0.45 | 0.991 [25.18] | 0.63 [16.00] | 0.389 [9.889] | 0.010 [0.252] | 0.006 [0.160] | 0.003 [0.080] |
| | 0.55 | 0.843 [21.404] | 0.39 [10.07] | 0.214 [5.425] | 0.008 [0.214] | 0.004 [0.101] | 0.002 [0.043] |
| ND | 0.45 | 0.014 [0.351] | 0.007 [0.18] | 0.005 [0.117] | | | |
| | 0.55 | 0.010 [0.256] | 0.004 [0.10] | 0.002 [0.060] | | | |

[1]DD: Drill damaged, FD: File damaged, ND: Not damaged
[2]Based on total embedded surface area of reinforcement

**Figure IV-27 Drill-Damaged #5 Epoxy-Coated Reinforcement.**

Figure IV-28 shows the open circuit potential values of ECR samples. The OCP values remained close to passive potentials throughout the test. Although at week 13 some of the averages exhibited a sharp decrease, this decrease did not correspond to a sharp increase in corrosion rate or corrosion loss values.

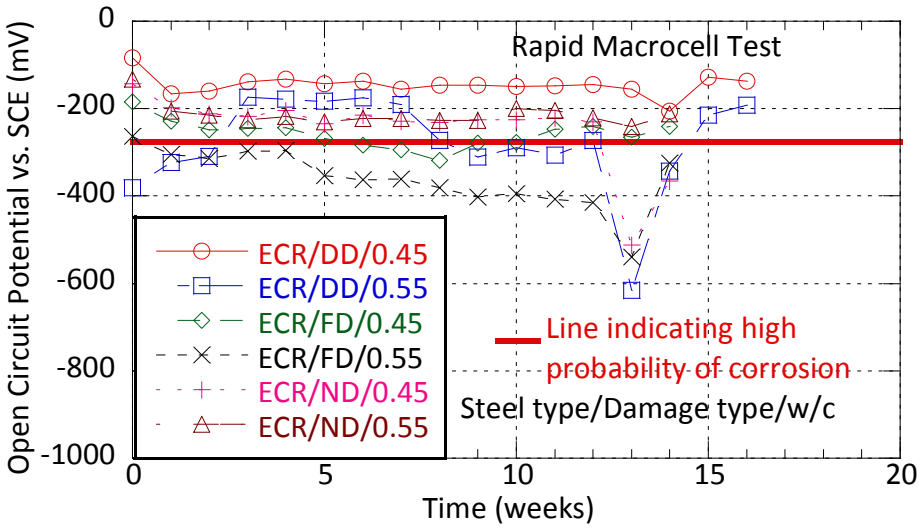


**Figure IV-28 Open Circuit Potential of ECR Samples.**

#### *4.2.1.2 Phase II – Rapid macrocell tests*

A total of 54 samples consisting of ASTM A 615, stainless steel 304, and undamaged galvanized steel reinforcement were tested in the second phase in mortars with two different water-cement ratios and three different corrosion inhibitor levels. Macrocell current and open circuit values were measured for 36 weeks, and readings were collected three times a week to monitor the change of the instantaneous corrosion rate of samples. Corrosion rate and corrosion loss values for all samples were calculated following the methodology discussed in the first phase.

Figure IV-29 shows the average corrosion rates of the ASTM A 615 samples embedded in mortars. Figure IV-30 shows the average corrosion loss values of ASTM A 615 samples calculated based on the average corrosion rates. Table IV-5 shows the average of corrosion rates over the duration of testing, their standard deviation, and the total corrosion loss values at 15 weeks and at 36 weeks. The total corrosion loss values at 15 weeks are shown to compare the results with the results of the first phase testing. Although this was not the case in the first phase, results indicated that average total corrosion loss decreased with decreasing water-cement ratio and increasing corrosion inhibitor level. Results also indicate that at the second phase of testing the ASTM A 615 samples exhibited much higher average corrosion rates and corrosion loss values. At the end of 15 weeks the total corrosion loss values of the first phase samples ranged from 0.006 to 0.027 mils (0.150 to 0.687 μm) whereas the total corrosion values of second phase samples ranged from 0.025 to 0.058 mils (0.637 to 1.485 μm). The highest corrosion loss was exhibited by the samples without corrosion inhibitor and with a water-cement ratio of 0.55.

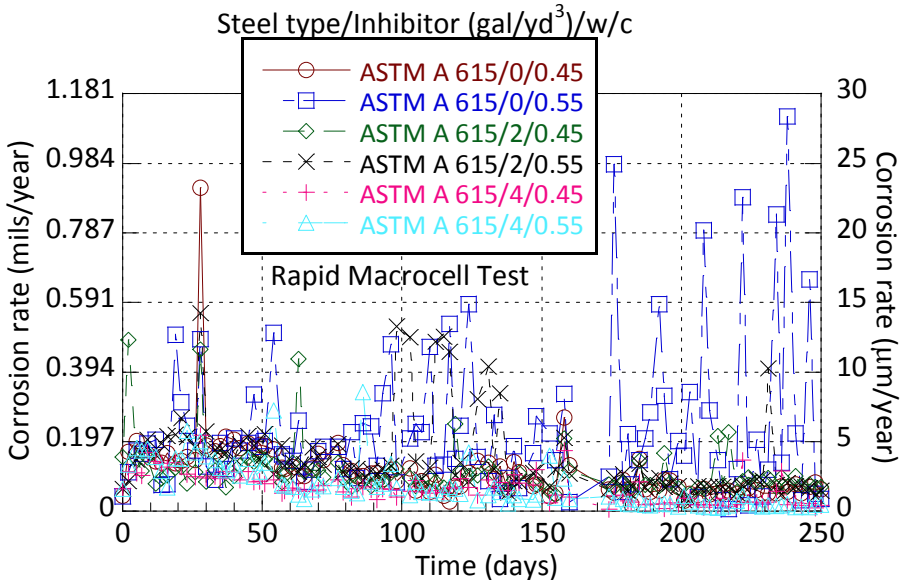


**Figure IV-29 Average Corrosion Rates of Phase II ASTM A 615 Samples.**

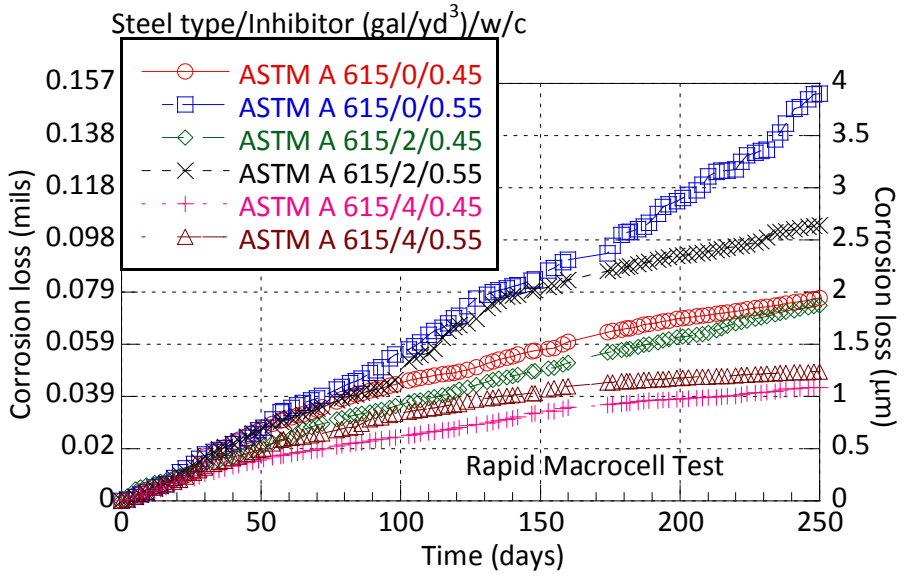


**Figure IV-30 Average Corrosion Loss of Phase II ASTM A 615 Samples.**

**Table IV-5 Average Corrosion Rate and Total Corrosion Loss of ASTM A 615 Samples.**

| Corrosion Inhibitor gal/yd$^3$ [kg/m$^3$] | Water-Cement Ratio | Average Corrosion Rate mils/year [µm/year] | Standard Deviation | Total Corrosion Loss at 15 weeks mils [µm] | Total Corrosion Loss at 36 weeks mils [µm] |
|---|---|---|---|---|---|
| 0 [0] | 0.45 | 0.112 [2.838] | 0.096 [2.446] | 0.046 [1.165] | 0.077 [1.953] |
| | 0.55 | 0.229 [5.821] | 0.210 [5.345] | 0.058 [1.485] | 0.154 [3.906] |
| 2 [10] | 0.45 | 0.109 [2.771] | 0.073 [1.847] | 0.038 [0.958] | 0.074 [1.885] |
| | 0.55 | 0.149 [3.784] | 0.114 [2.893] | 0.054 [1.380] | 0.104 [2.651] |
| 4 [20] | 0.45 | 0.064 [1.635] | 0.041 [1.050] | 0.025 [0.637] | 0.043 [1.089] |
| | 0.55 | 0.071 [1.814] | 0.063 [1.592] | 0.034 [0.865] | 0.049 [1.242] |

Figure IV-31 shows the open circuit potential values of ASTM A 615 samples. In the first phase the average OCP of some conditions remained passive until the 11$^{th}$ week of testing while the average OCP of samples of three conditions fell below -275 mV earlier and came down to -600 mV. In the second phase the average OCP values of all samples went down to –600 mV within 1 to 2 weeks and stabilized at this value.

Figure IV-32 shows the average corrosion rates of the SS304 samples embedded in six different mortars. It should be noted that the scale of y-axis of this figure is smaller compared to the y-axis of the other corrosion rate figures from the second phase because of the small magnitudes of observed corrosion rates of stainless steel samples. Figure IV-33 shows the average corrosion loss values of the SS304 samples, and Table IV-6 shows the average corrosion rate, standard deviation, and total average corrosion loss at 15 weeks and at the end of the testing period. Similar to the first phase results for the rapid macrocell test the average corrosion rates and total corrosion loss values of the stainless steel samples were very low. Although at these small magnitudes and large standard deviations the differences are statistically not significant, results indicated an increase in the total average corrosion loss with increasing water-cement ratio and increasing corrosion inhibitor level. Figure IV-34 shows the open circuit potential values of ASTM A 615 samples. Similar to the first phase results the average OCP values were above -275 mV indicating passive conditions throughout the test.

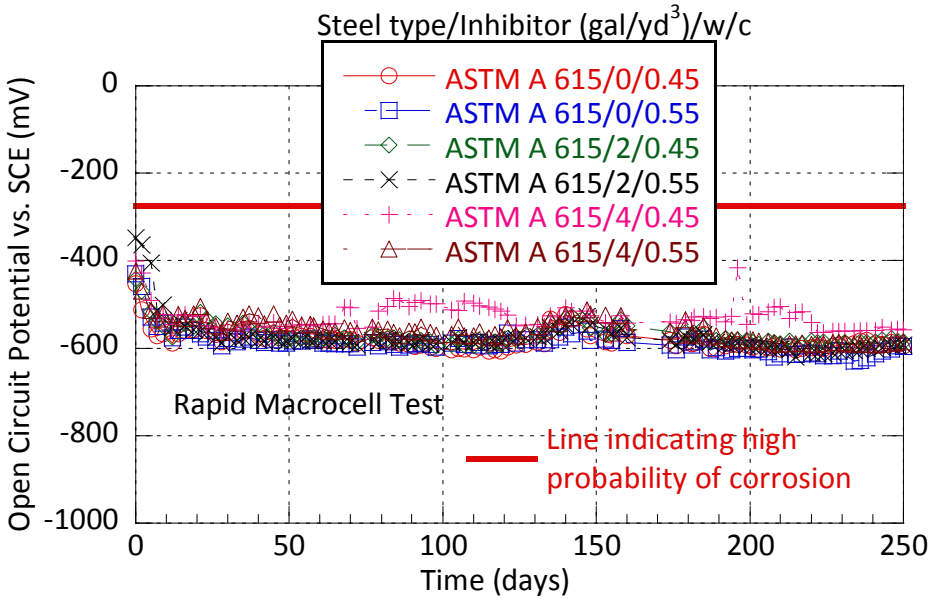


**Figure IV-31 Open Circuit Potential of Phase II ASTM A 615 Samples.**

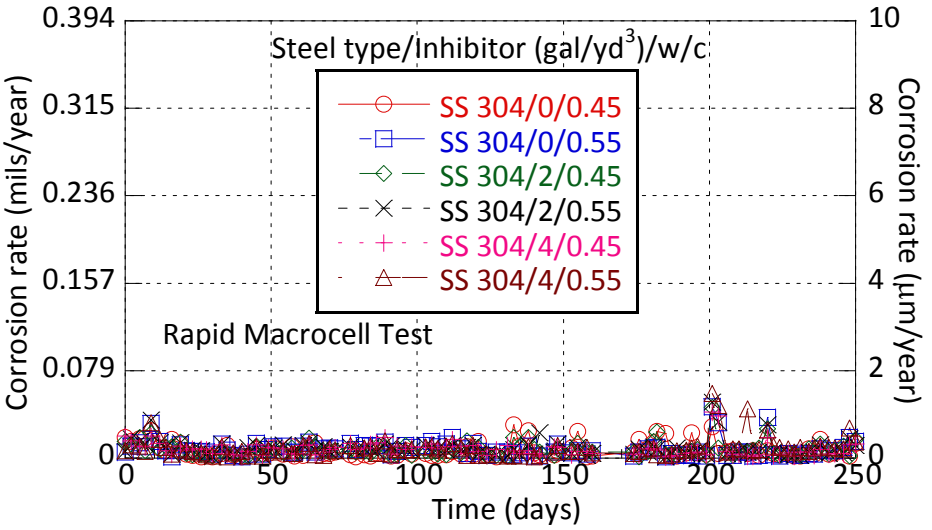


**Figure IV-32 Average Corrosion Rates of Phase II SS304 Samples.**

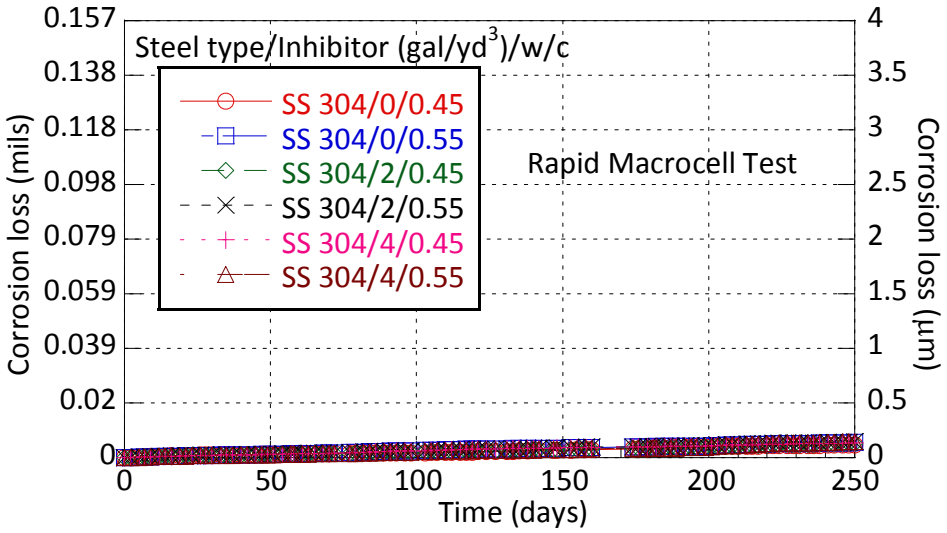


**Figure IV-33 Average Corrosion Loss of Phase II SS304 Samples.**

**Table IV-6 Average Corrosion Rate and Total Corrosion Loss of SS304 Samples.**

| Corrosion Inhibitor gal/yd$^3$ [kg/m$^3$] | Water-Cement Ratio | Average Corrosion Rate mils/year [µm/year] | Standard Deviation | Total Corrosion Loss at 15 weeks mils [µm] | Total Corrosion Loss at 36 weeks mils [µm] |
|---|---|---|---|---|---|
| 0 [0] | 0.45 | 0.008 [0.192] | 0.007 [0.175] | 0.002 [0.047] | 0.005 [0.121] |
| | 0.55 | 0.008 [0.212] | 0.007 [0.184] | 0.003 [0.068] | 0.006 [0.142] |
| 2 [10] | 0.45 | 0.008 [0.199] | 0.006 [0.162] | 0.002 [0.053] | 0.005 [0.129] |
| | 0.55 | 0.009 [0.218] | 0.007 [0.184] | 0.003 [0.067] | 0.006 [0.147] |
| 4 [20] | 0.45 | 0.008 [0.204] | 0.006 [0.161] | 0.003 [0.067] | 0.005 [0.135] |
| | 0.55 | 0.009 [0.231] | 0.009 [0.224] | 0.002 [0.057] | 0.006 [0.151] |

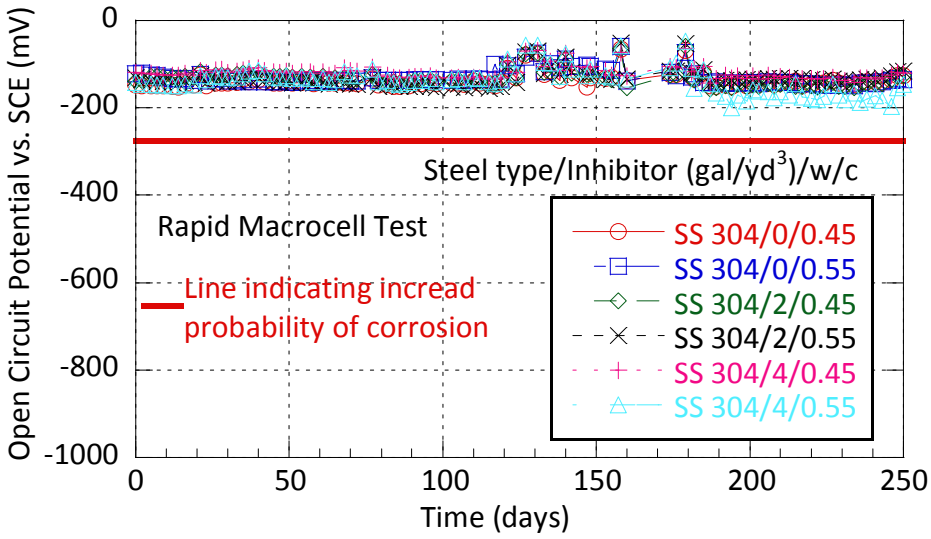


**Figure IV-34 Open Circuit Potential of Phase II SS304 Samples.**

Figure IV-35 shows the average corrosion rates of galvanized reinforcement samples embedded in mortars from the macrocell test. Figure IV-36 shows the average corrosion loss values of galvanized reinforcement samples and Table IV-7 shows average corrosion rate, standard deviation, and average total corrosion loss values at 15 weeks and at the end of testing. Due to challenges with demolding of samples in the first phase, sufficient data from the galvanized reinforcement samples were not available to make any conclusions. In the first phase study only one undamaged galvanized sample could be tested at a water-cement ratio of 0.45, and its total corrosion loss at 15 weeks was 0.013 mils (0.323 μm). Results of the second phase testing indicate that at the end of 15 weeks all galvanized samples exhibited an average total corrosion loss higher than 0.02 mils (0.5 μm). Evaluation of the total corrosion loss values also indicate that total corrosion loss increased with increasing water-cement ratio. However, this was not the case with corrosion inhibitor level. The average total corrosion loss decreased when the corrosion inhibitor level was increased from 0 to 2 gal/yd$^3$ (0 to 10 kg/m$^3$) and increased when the inhibitor level was further increased from 2 to 4 gal/yd$^3$ (10 to 20 kg/m$^3$). Figure IV-37 shows the open circuit potential values of galvanized reinforcement samples. The average OCP values were below -275 mV from the beginning of the test, and they remained between -600 and -1000 mV throughout the test.

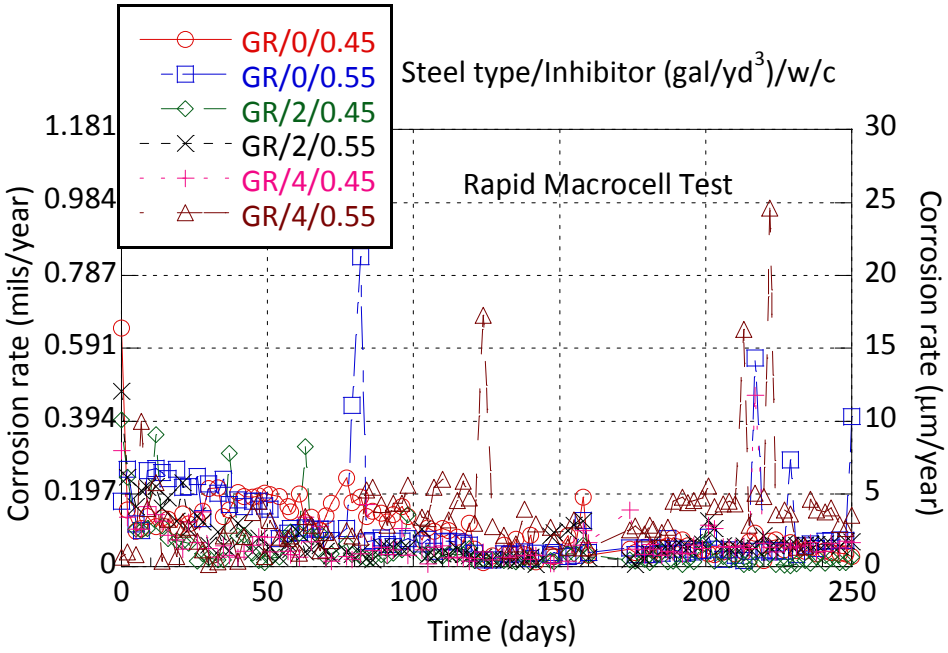


**Figure IV-35 Average Corrosion Rates of Phase II Samples containing Galvanized Reinforcement.**

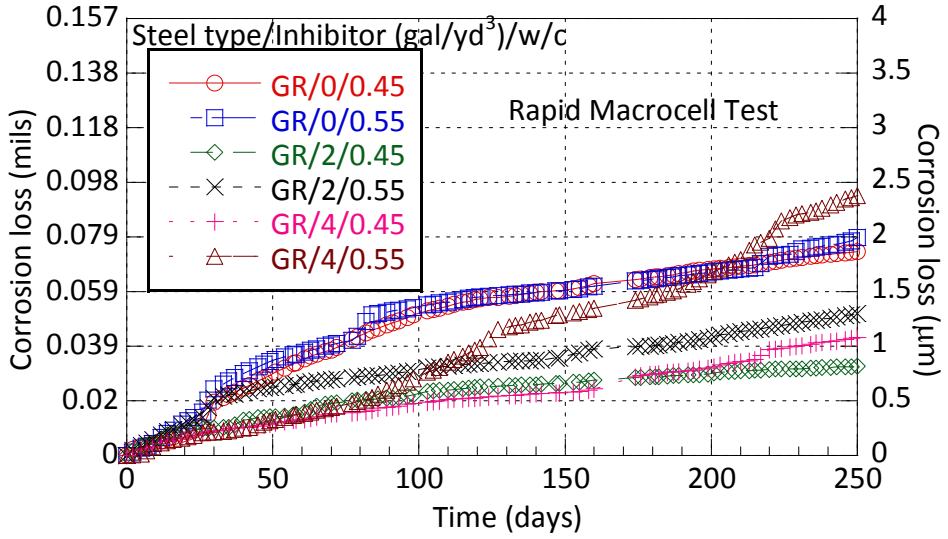


**Figure IV-36 Average Corrosion Loss of Phase II Samples containing Galvanized Reinforcement.**

**Table IV-7 Average Corrosion Rate and Total Corrosion Loss of Samples containing Galvanized Reinforcement.**

| Corrosion Inhibitor gal/yd$^3$ [kg/m$^3$] | Water-Cement Ratio | Average Corrosion Rate mils/year [µm/year] | Standard Deviation | Total Corrosion Loss at 15 weeks mils [µm] | Total Corrosion Loss at 36 weeks mils [µm] |
|---|---|---|---|---|---|
| 0 [0] | 0.45 | 0.115 [2.913] | 0.161 [4.096] | 0.053 [1.335] | 0.074 [1.870] |
| | 0.55 | 0.123 [3.126] | 0.169 [4.302] | 0.055 [1.386] | 0.080 [2.027] |
| 2 [10] | 0.45 | 0.050 [1.259] | 0.070 [1.787] | 0.023 [0.591] | 0.032 [0.819] |
| | 0.55 | 0.082 [2.078] | 0.131 [3.320] | 0.032 [0.809] | 0.051 [1.306] |
| 4 [20] | 0.45 | 0.064 [1.616] | 0.060 [1.516] | 0.019 [0.495] | 0.043 [1.092] |
| | 0.55 | 0.140 [3.551] | 0.130 [3.295] | 0.031 [0.781] | 0.094 [2.397] |

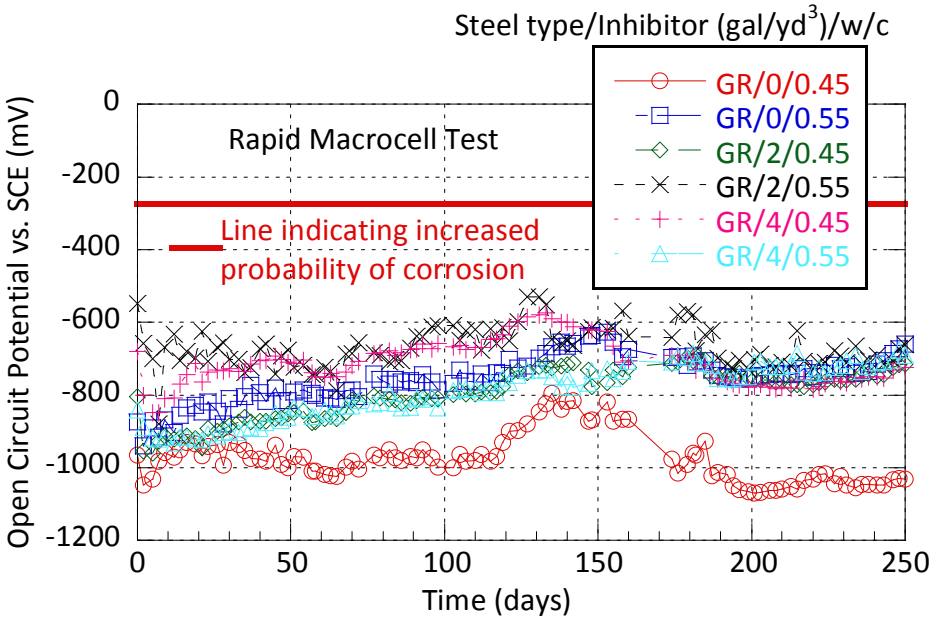


**Figure IV-37 Open Circuit Potential of Phase II Samples Containing Galvanized Reinforcement.**

Figure IV-38 shows the average total corrosion loss values obtained from the first phase testing with different steel types embedded in mortar without corrosion inhibitor (galvanized steel is not included due to the low number of samples available in the first phase). Figure IV-39 shows the average total corrosion loss of undamaged steel types evaluated in the second phase without a corrosion inhibitor. ASTM A 706 embedded in mortar with a water-cement ratio of 0.55 exhibited the worst corrosion performance in the first phase, and ASTM A 615 embedded in mortar with a water-cement ratio of 0.55 exhibited the worst corrosion performance in the second phase. It should be noted that if actual damaged surface area is taken into account then epoxy coated reinforcement with drill damage exhibited the worst corrosion performance in the first phase.

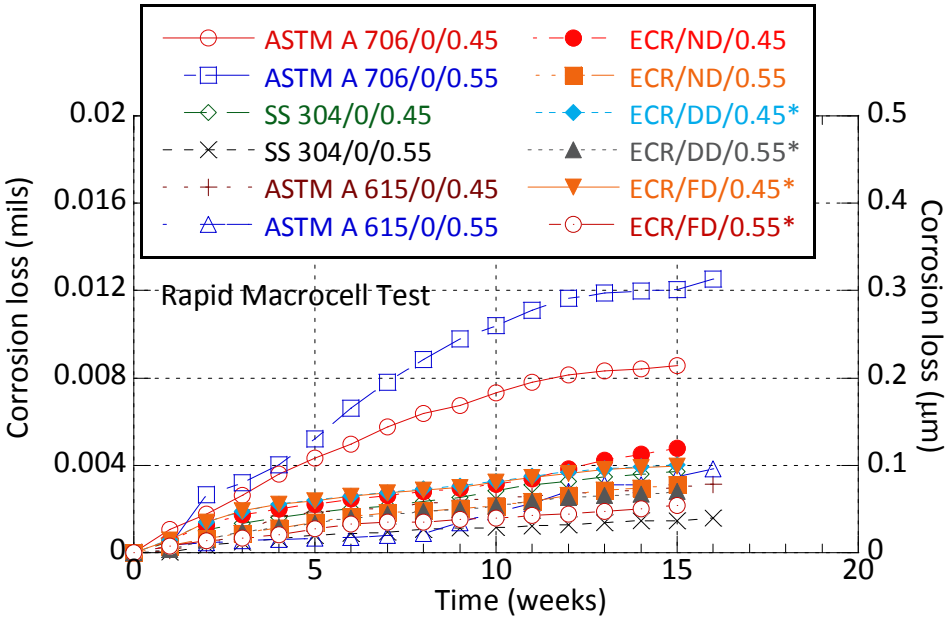


**Figure IV-38 Average Total Corrosion Loss of Different Steel Types in Phase I.**

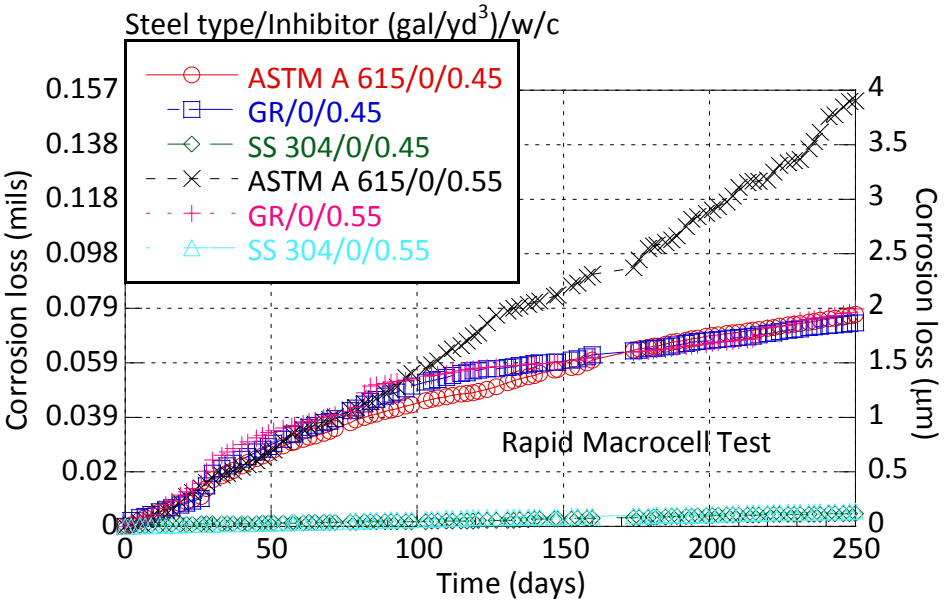


**Figure IV-39 Average Total Corrosion Loss of Different Steel Types in Phase II.**

These results indicate that the rapid macrocell test is an adequate test to assess the corrosion rate of steel embedded in mortar. However, due to the challenges with the galvanized steel samples embedded in mortar, the rapid macrocell test is not recommended for assessing the corrosion rate of galvanized steel products or other sacrificial coatings.

### 4.2.2 Accelerated chloride threshold test (ACT)

#### *4.2.2.1 Phase I*

Coated and uncoated steel samples were tested at two different water-cement ratio values. Uncoated samples were embedded in mortar containing three different levels of corrosion inhibitor. Coated samples were tested in the "as received" condition and in damaged conditions as noted in the rapid macrocell test section. Epoxy coated samples were tested in drill damaged and file damaged conditions, and galvanized samples were tested in drill damaged condition. In the Phase I testing, a potential difference of 20 V was initially applied between the anodes and cathodes of samples for 36 hours in three periods of 12-hour intervals. After the 12-hour potential application, a 42-hour wait period (no potential application) was observed. After the initial potential application, a 20 V potential was applied in periods of 6 hours with 42-hour wait periods between these applications (each cycle took 2 days). The polarization resistance

was measured after each cycle. As shown earlier in Eq. (2.9) inverse of polarization resistance is directly related to the corrosion rate. A sudden increase in the inverse of polarization resistance value was accepted as an indicator of corrosion initiation.

Current density was calculated using an exposed area of 0.23 $in^2$ (1.5 $cm^2$). To determine the time to initiation of corrosion based on the increase of inverse of polarization resistance, a statistical method that is commonly used for quality control purposes was implemented. Initial inverse polarization resistance values were used to forecast the next reading using the sum of least squares method, and the next actual reading was compared to the estimated value. If the measured value was higher than the estimated value, and the difference was higher than three times the standard error of the forecast, the sample was deemed actively corroding, and the test was stopped. Activated samples were cut at the level of reinforcement, and the chloride content of the mortar immediately above the reinforcement was measured to determine the chloride threshold of the system.

Figure IV-40 and Figure IV-41 show the inverse of polarization resistance versus the total time of applied voltage for the ASTM A 615 samples embedded in mortar with water-cement ratios of 0.45 and 0.55, respectively. A total of three samples were tested for each inhibitor level. The statistical procedure indicated activation of samples after approximately the same time of voltage application for samples at both water-cement ratio levels.

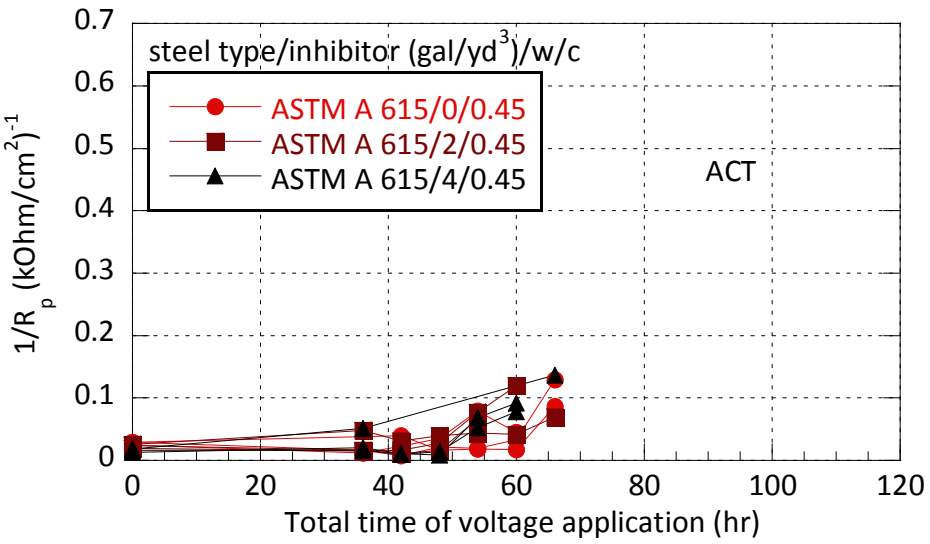


**Figure IV-40 ASTM A 615 Samples Embedded in Mortar with w/c of 0.45.**

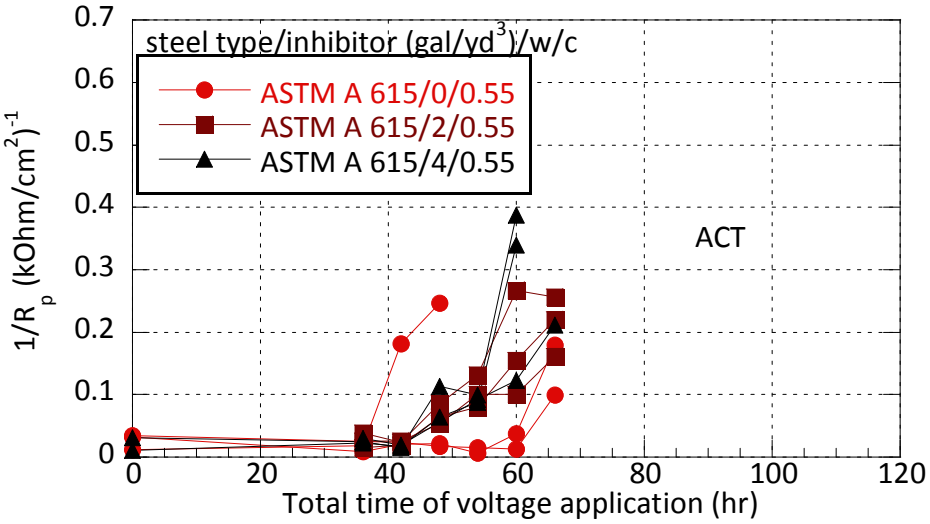


**Figure IV-41 ASTM A 615 Samples Embedded in Mortar with w/c of 0.55.**

Figure IV-42 shows the measured critical chloride threshold values as percent chloride content by weight of mortar. Each point represents one sample, and the lines show the average chloride content for each condition. Samples embedded in mortar with a water-cement ratio of 0.55 exhibited much higher variability and higher average chloride content values. These results indicate that after approximately the same time of voltage application, more chlorides were driven to the level of steel in mortars with a higher water-cement ratio. Because the statistical method used to determine activation indicated activation after approximately the same time of voltage application, samples in mortar with higher water-cement ratio seemed to have higher critical chloride threshold values.

The researchers believe that the statistical procedure used to determine activation may not be reliable because of the long initial 36-hour potential application. For the statistical method to properly indicate a change in the system, obtaining several initial stable data points is essential. This is less likely with the long potential applications at the beginning of the test. Therefore, in the Phase II testing, measurement of polarization resistance was started without the initial 36 hours of voltage application. Results also indicated that there was no clear trend of chloride content values based on the corrosion inhibitor amount for samples embedded in mortar with a water-cement ratio of 0.45. For samples embedded in mortar with a water-cement ratio of 0.55, samples containing 4 gal/yd$^3$ (20 kg/m$^3$) corrosion inhibitor exhibited higher

average chloride threshold values compared to other samples embedded in mortar with water-cement ratios of 0.55.

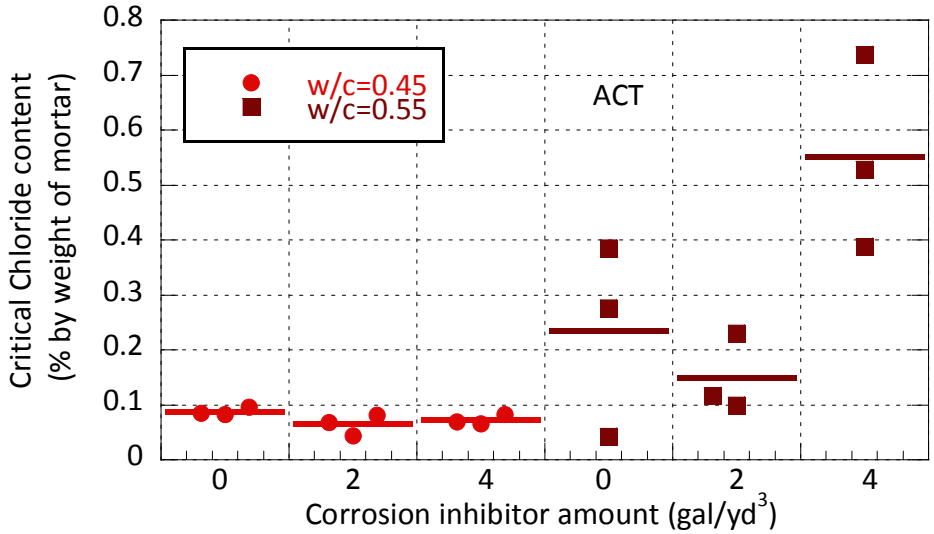


**Figure IV-42 Percent Chloride Content of ASTM A 615 Samples.**

Figure IV-43 and Figure IV-44 show the inverse polarization resistance values plotted against the total time of applied voltage for the ASTM A 706 samples embedded in mortar with a water-cement ratio of 0.45 and 0.55, respectively. Results indicate a very similar behavior to the ASTM A 615 samples with most of the samples activating after approximately 60 hours of voltage application and samples embedded in mortar with a water-cement ratio of 0.55 exhibiting higher corrosion rates.

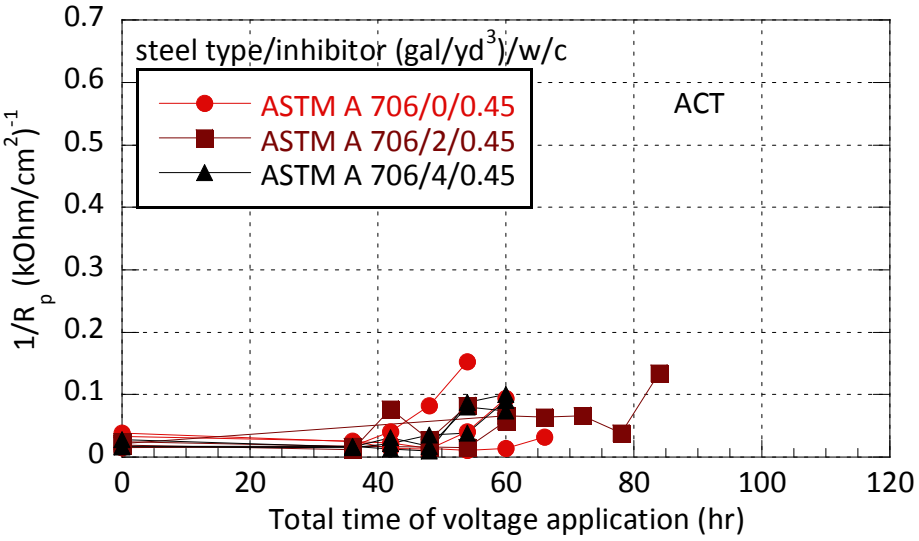


**Figure IV-43 ASTM A 706 Samples Embedded in Mortar with w/c of 0.45.**

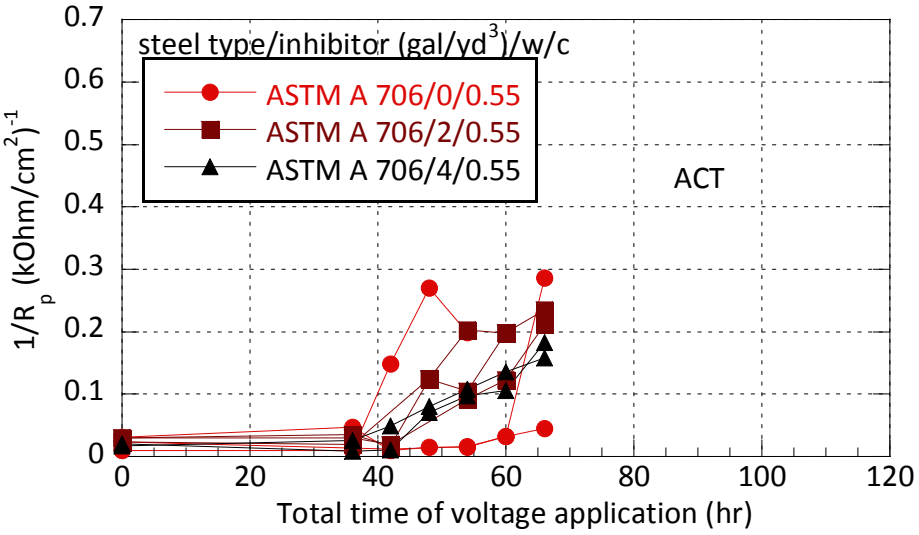


**Figure IV-44 ASTM A 706 Samples Embedded in Mortar with w/c of 0.55.**

Figure IV-45 shows the chloride content values measured at the end of the test as a percent weight of mortar. Similar to ASTM A 615 samples, samples embedded in mortar with a water-cement ratio of 0.45 exhibited very low critical chloride threshold values. Samples

embedded in mortar with a water-cement ratio of 0.55 exhibit higher variability and higher average chloride threshold values. Also samples embedded in mortar with a water-cement ratio of 0.55 and containing 4 gal/yd$^3$ (20 kg/m$^3$) inhibitor exhibited higher average chloride threshold value compared to other samples.

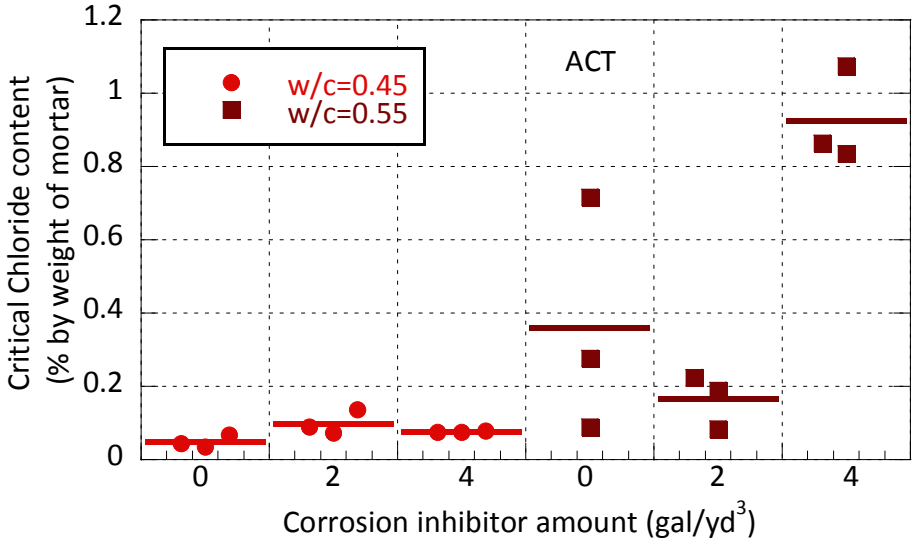


**Figure IV-45 Percent Chloride Content of ASTM A 706 Samples.**

Figure IV-46 and Figure IV-47 show the inverse of polarization resistance values plotted against total time of voltage application for stainless steel samples embedded in mortar with water-cement ratio of 0.45 and 0.55, respectively. Except for one sample in each group, the statistical method did not show activation for any of the samples even after application of voltage for 120 hours. Testing was stopped after 120 hours of voltage application, and chloride content was determined in samples as shown in Figure IV-48. However, note that these chloride content values are not critical chloride threshold values since the samples did not show activation.

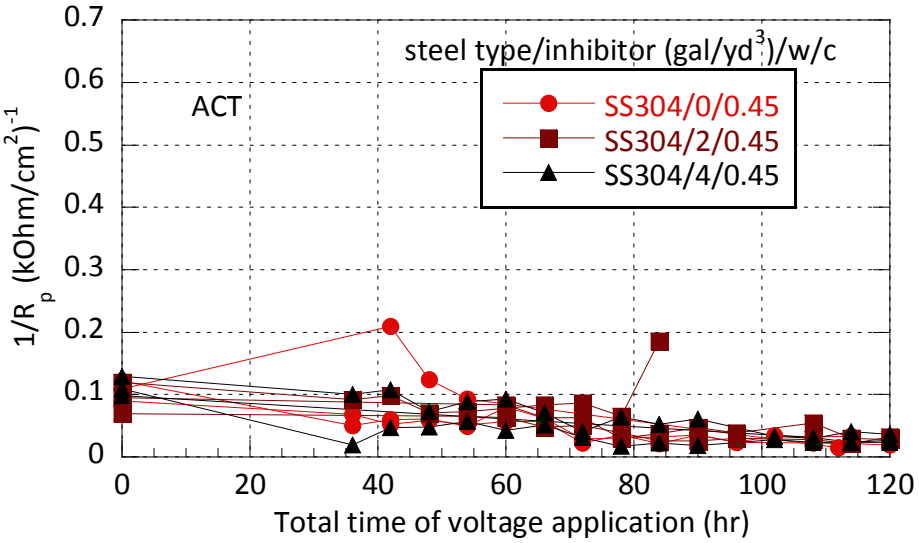


**Figure IV-46 SS304 Samples Embedded in Mortar with w/c of 0.45.**

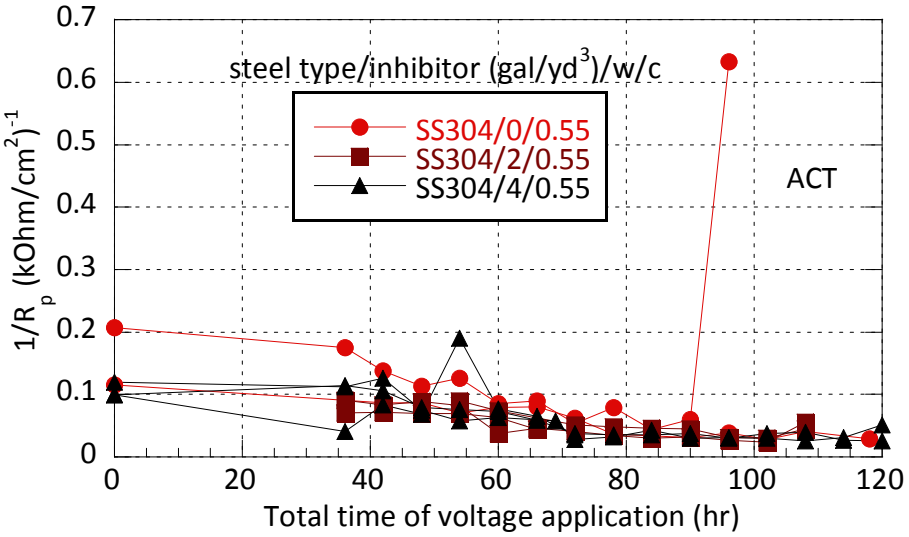


**Figure IV-47 SS304 Samples Embedded in Mortar with w/c of 0.55.**

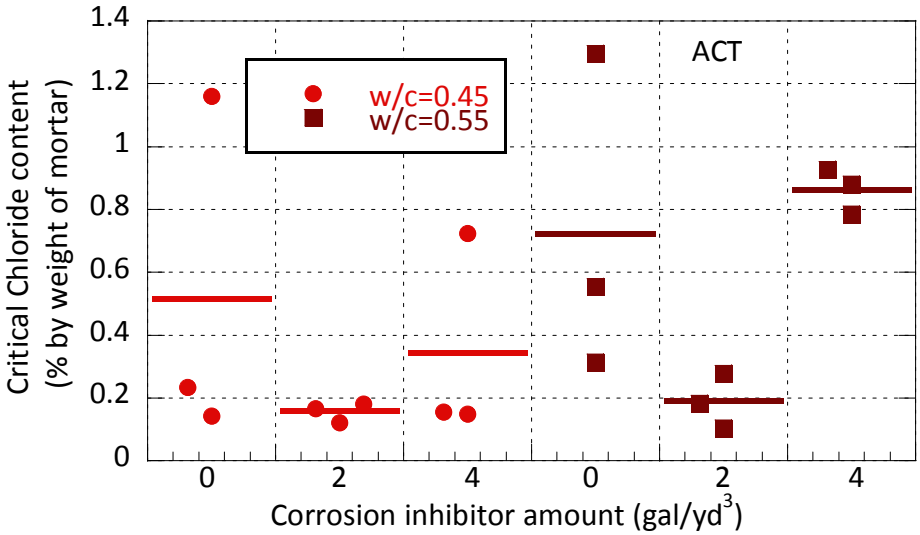


**Figure IV-48 Percent Chloride Content of SS304 Samples.**

Inverse polarization resistance values were calculated and plotted against the total time of applied voltage for the ECR samples embedded in mortar with water-cement ratios of 0.45 and 0.55 in Figure IV-49 and Figure IV-50, respectively. It should be noted that when calculating the polarization resistance, the current density of the damaged ECR samples were calculated based on the actual exposed damaged surface area. Because of the difference in exposed areas, damaged samples exhibited much higher corrosion rate values. Comparison of results with other steel types indicated that the variability of corrosion rates of ECR samples was much higher, making determination of activation much more difficult and less reliable. Figure IV-51 shows the chloride content values measured from the ECR samples. Similar to other steel types the variability of results was much higher for samples embedded in mortar with a water-cement ratio of 0.5. Critical chloride threshold values of samples were similar for the damage types for each group of water-cement ratio.

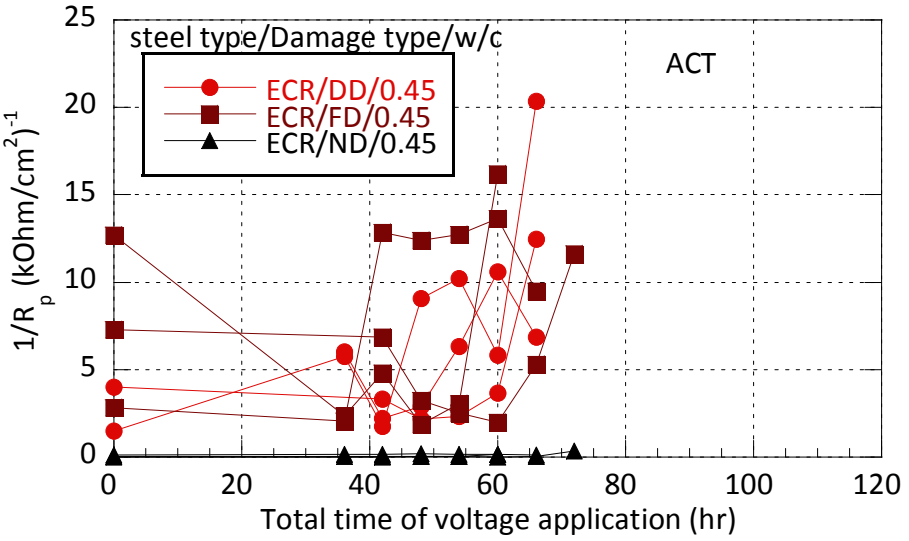


**Figure IV-49 Epoxy Coated Samples Embedded in Mortar with w/c of 0.45.**

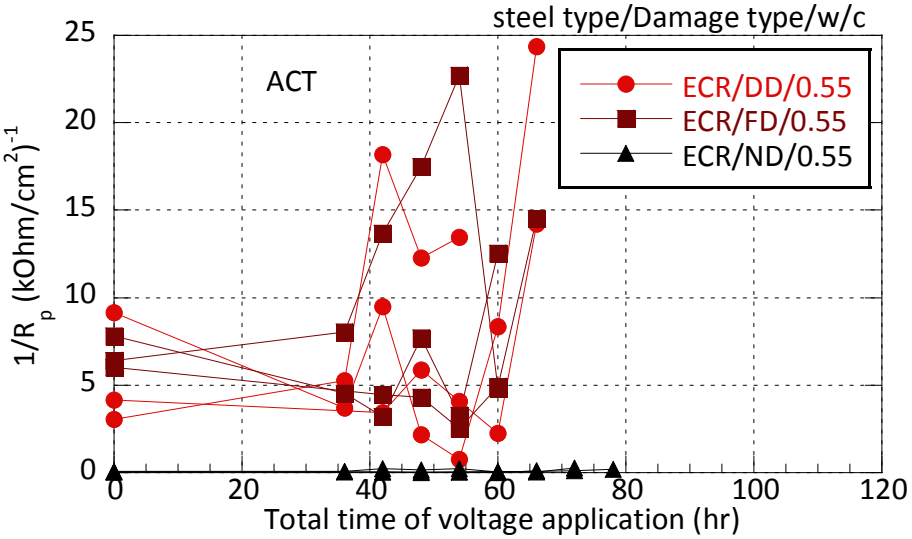


**Figure IV-50 Epoxy Coated Samples Embedded in Mortar with w/c of 0.55.**

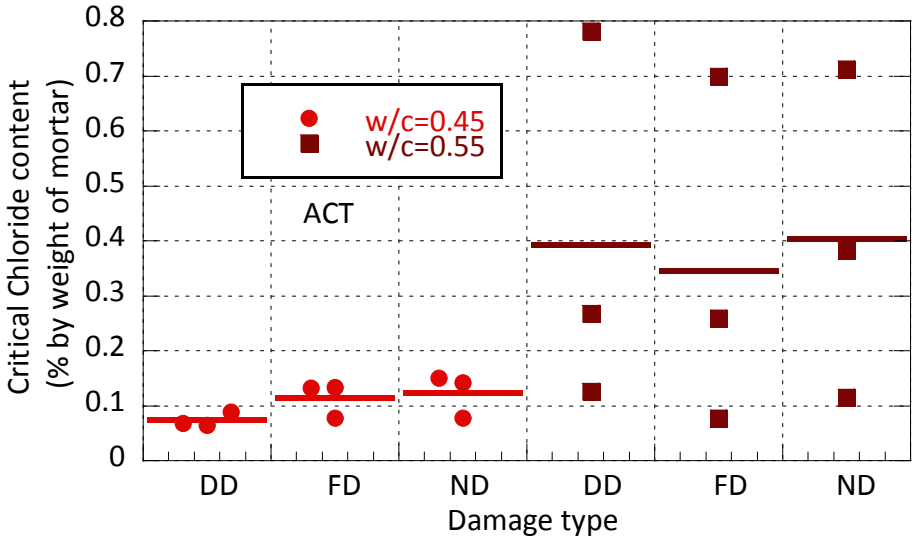


**Figure IV-51 Percent Chloride Content of Epoxy Coated Samples.**

Inverse polarization resistance values of galvanized samples embedded in mortar with a water-cement ratio of 0.45 are plotted against the total potential application time in Figure IV-52. Changes in the inverse polarization resistance values with applied voltage for samples embedded in mortar with a water-cement ratio of 0.55 are shown in Figure IV-53. Unlike epoxy coated samples, corrosion is assumed to take place over the total surface of reinforcement and not only at the damaged areas, therefore current density of damaged samples was calculated using the total exposed surface area of the samples. Two of the drill damaged samples took much longer to activate compared to all other steel types. However, it should also be noted that the inverse polarization resistance values measured for the galvanized samples were much lower compared to all other steel types. Evaluation of chloride threshold values shown in Figure IV-54 indicates that the averages for samples embedded in mortar with water-cement ratios of 0.45 and 0.55 were similar but with increased variance for samples embedded in mortar with a water-cement ratio of 0.55.

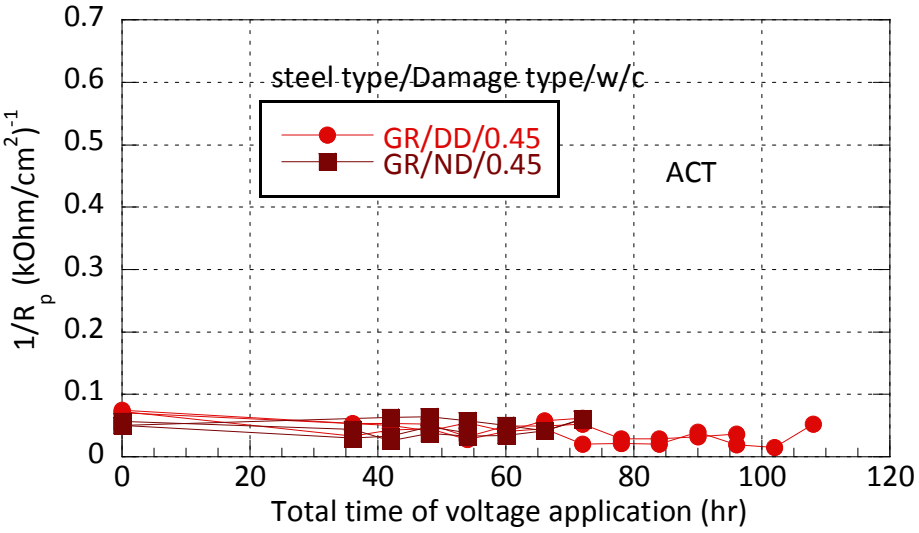


**Figure IV-52 Galvanized Samples Embedded in Mortar with w/c of 0.45.**

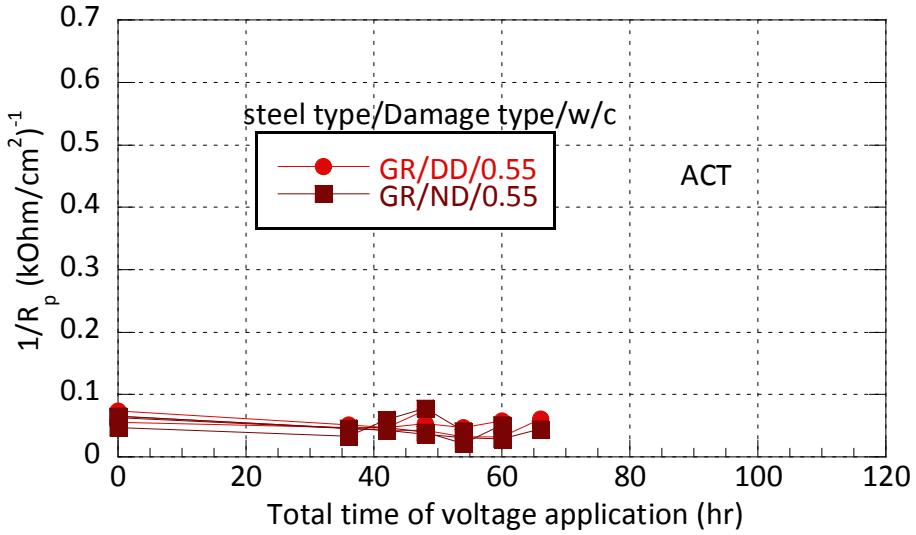


**Figure IV-53 Galvanized Samples Embedded in Mortar with w/c of 0.55.**

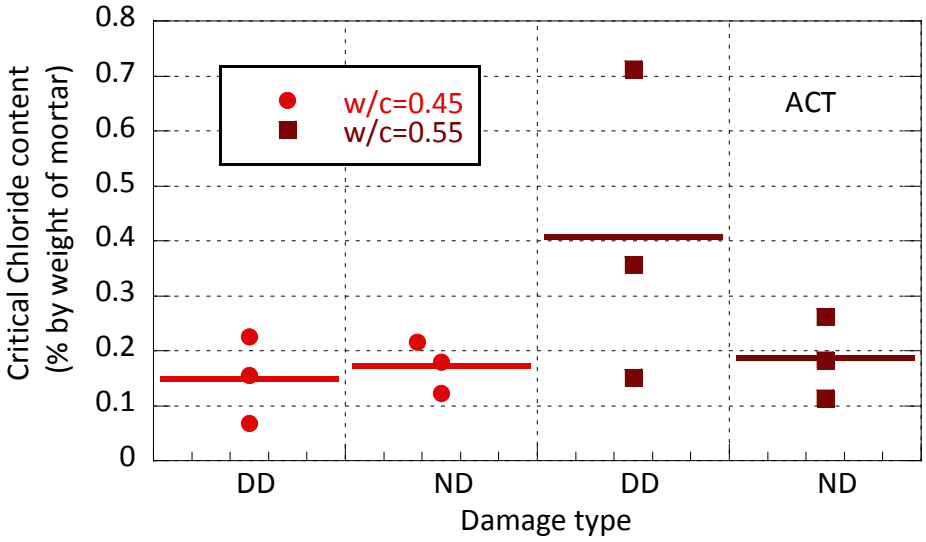


**Figure IV-54 Percent Chloride Content of Galvanized Samples.**

Because the evaluation of results indicated that chloride content values were similar across the different corrosion inhibitor levels and damage types, chloride content data were pulled together for each steel type and divided only by the water-cement ratio as shown in Figure IV-55. After applying a logarithmic transformation to bring the data closer to a normal distribution, t-tests were performed at the 95 percent level between the different water-cement ratio values. Results indicate that the critical chloride content of samples embedded in mortar with water-cement ratio of 0.45 at activation was statistically significantly lower compared to the samples embedded in mortar with a water-cement ratio of 0.55 for the ASTM A 615, A 706, and epoxy coated samples. The difference was not statistically significant for galvanized samples. Because the stainless steel samples did not activate during the test, they are not shown in Figure IV-55.

Results indicate that for mortar with a water-cement ratio of 0.45, chloride content was not significantly different between ASTM A 615, A 706, and epoxy coated steel samples. Galvanized steel samples exhibited significantly higher chloride content values compared to ASTM A 615 and A 706 samples but were not statistically significantly different from the epoxy coated samples.

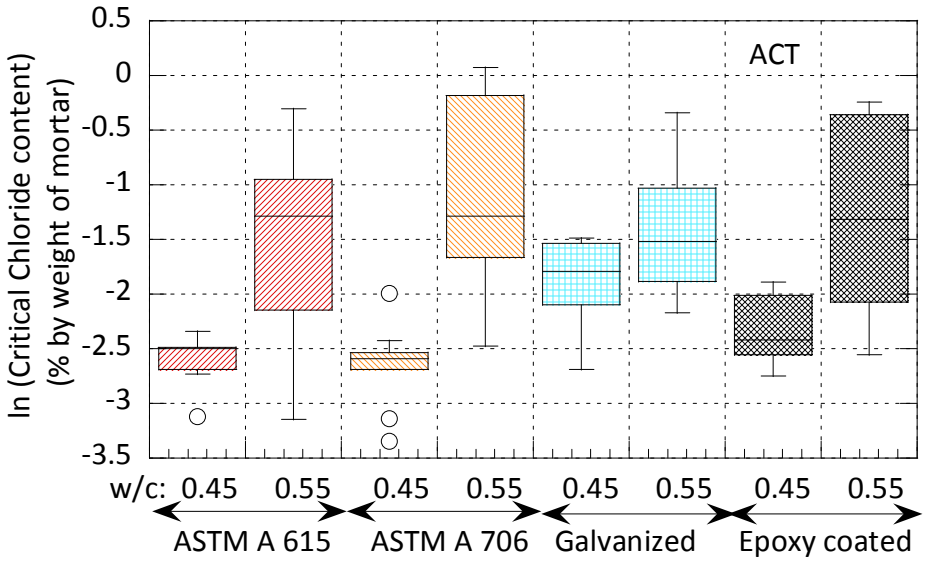


**Figure IV-55 Comparison of Chloride Threshold Values for Different Steel Type and w/c Values.**

### *4.2.2.2 Phase II*

ASTM A 615 and stainless steel 304 samples embedded in mortar with water-cement ratios of 0.45 and 0.55 were tested in the second phase. As discussed earlier, the initial application of voltage for 36 hours was not performed in the second phase to collect more readings at the stable condition of samples. In addition to application of voltage in 6-hour intervals from the beginning of the test, the open circuit potential of samples was also monitored starting at the end of the curing period. The test was not started (the initial six hours of voltage application was not started) until all the samples reached a stable OCP reading.

Figure IV-56 and Figure IV-57 show the inverse polarization resistance values for ASTM A 615 samples embedded in mortar with a water-cement ratio of 0.45 for the ACT tests. The inverse polarization resistance is plotted against total time of voltage application and their open circuit potential readings during this time. The zero point on the abscissa on both figures shows the start of the first voltage application, and the first polarization reading was collected six hours after this time. The OCP readings of all samples increased and stabilized before the start of the test. Collecting data at every six hours of potential application from the start of the test provided stable data points to establish the baseline for forecasting further data. Testing

was stopped when the statistical method indicated initiation of active corrosion. The OCP data of all samples exhibited a small dip at the beginning of the test but then increased. The OCP curves did not indicate activation at the same time as the inverse of polarization resistance curves.

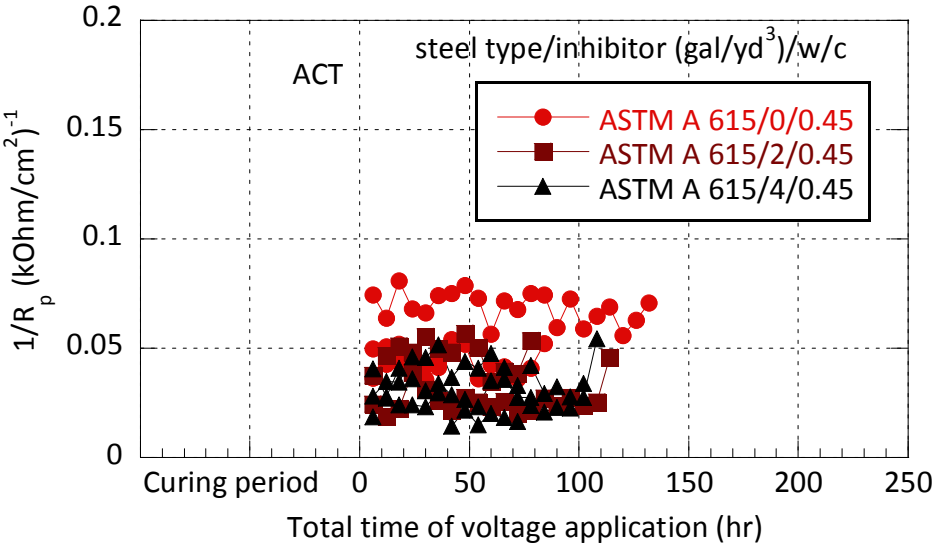


**Figure IV-56 ASTM A 615 Samples Embedded in Mortar with w/c of 0.45 in Phase II.**

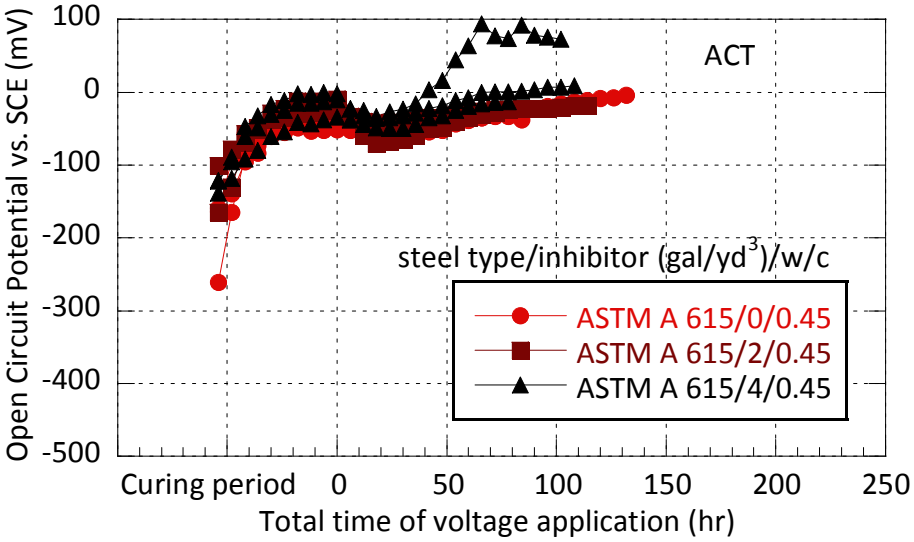


**Figure IV-57 OCP of ASTM A 615 Samples Embedded in Mortar with w/c of 0.45 in Phase II.**

Figure IV-58 and Figure IV-59 show the inverse polarization resistance values and OCP values plotted against the total time of voltage application for samples embedded in mortar with water-cement ratio of 0.55. The inverse polarization resistance values exhibited a similar trend as the samples were embedded in mortar with a water-cement ratio of 0.45. Figure IV-60 shows the measured chloride content values at the activation of ASTM A 615 samples in Phases I and II. The variation of samples embedded in mortar with a water-cement ratio of 0.55 was much smaller in the second phase but still clearly higher compared to the samples embedded in mortar with a water-cement ratio of 0.45.

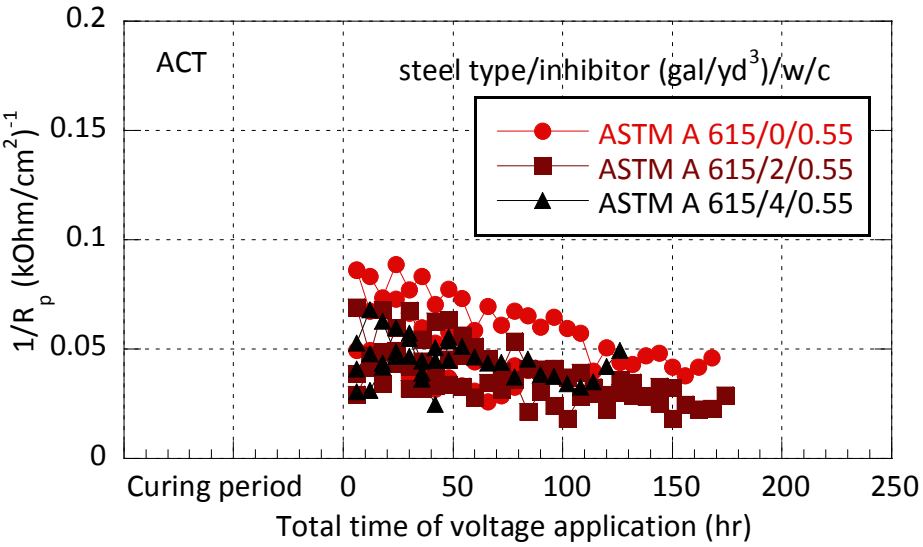


**Figure IV-58 ASTM A 615 Samples Embedded in Mortar with w/c of 0.55 in Phase II.**

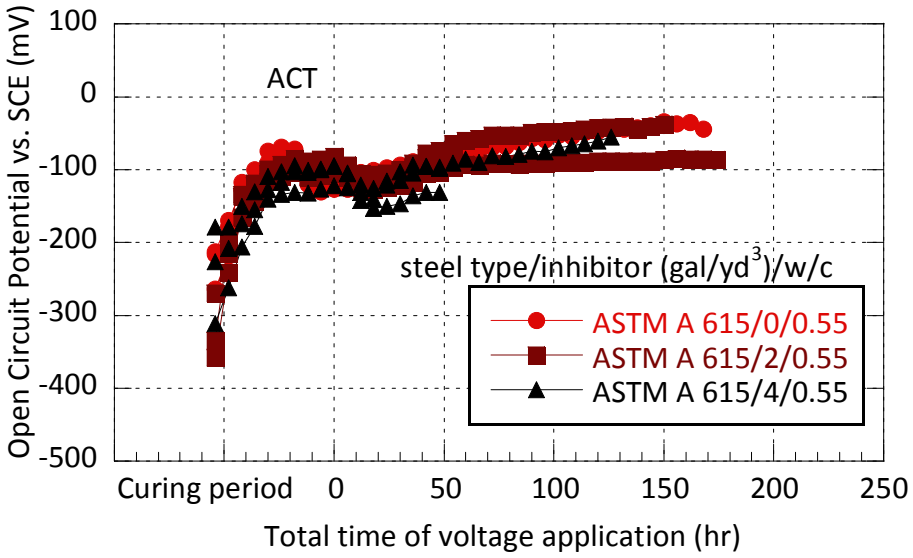


**Figure IV-59 OCP of ASTM A 615 Samples Embedded in Mortar with w/c of 0.55 in Phase II.**

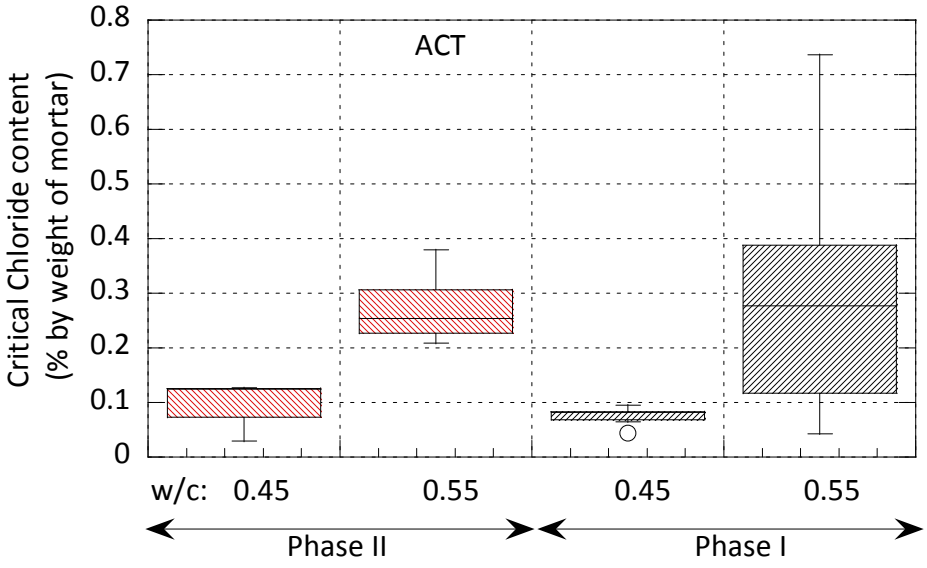


**Figure IV-60 Comparison of Chloride Thresholds of ASTM A 615 Samples in Phase I and II.**

Figure IV-61 and Figure IV-62 show the inverse polarization resistance and OCP values plotted against total time of voltage application for SS304 samples embedded in mortar with a water-cement ratio of 0.45. In the first phase, stainless steel samples did not show activation after 120 hours of voltage application with the exception of two samples. In the second phase, testing was continued beyond 120 hours, and most of the stainless steel samples showed activation approximately after 150 hours of voltage application. The average activation time for SS304 samples embedded in mortar with a water-cement ratio of 0.55 was shorter compared to SS304 samples embedded in mortar with a water-cement ratio of 0.45 as shown in Figure IV-63. Figure IV-64 shows the OCP values of samples embedded in mortar with a water-cement ratio of 0.55. OCP values of SS304 samples embedded in both mortars with different water-cement ratio values started to increase with the start of the test and did not exhibit the small dip that was observed for the ASTM A 615 samples. Figure IV-65 shows the chloride content values measured at the time of activation of Phase II samples. Comparison of chloride contents of ASTM A 615 and stainless steel samples under the assumption of normal distribution indicates that the chloride threshold values of SS304 samples were statistically significantly higher compared to ASTM A 615 samples indicating that the ACT procedure is capable of distinguishing the corrosion performance between different reinforcement types.

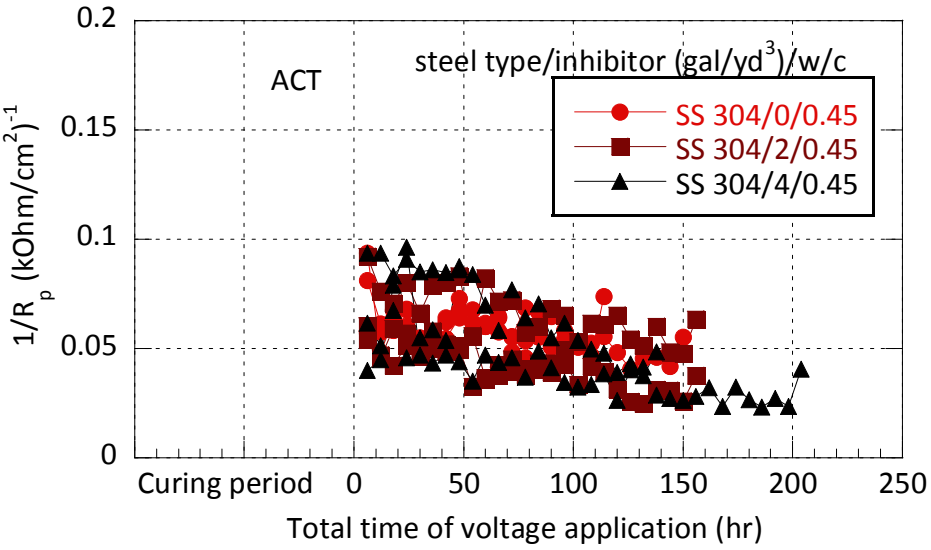


**Figure IV-61 SS304 Samples Embedded in Mortar with w/c of 0.45 in Phase II.**

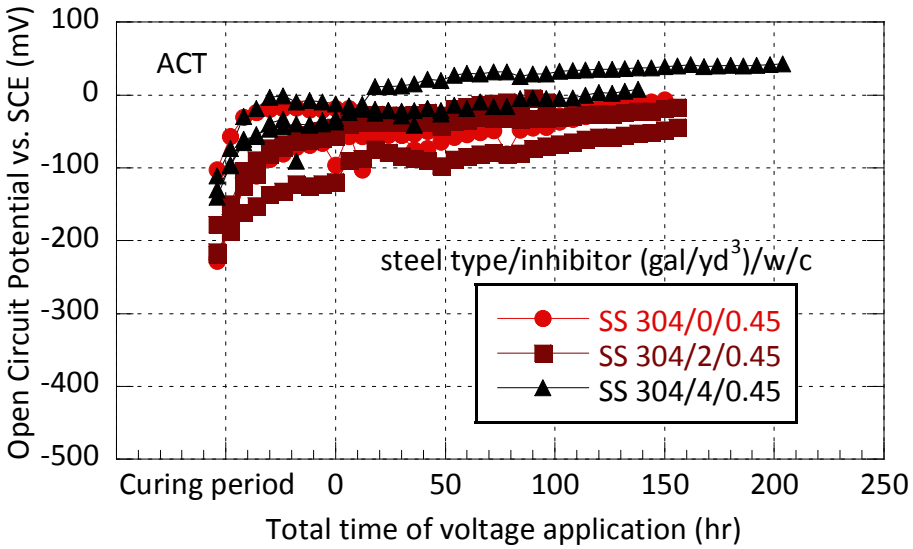


**Figure IV-62 OCP of SS304 Samples Embedded in Mortar with w/c of 0.45 in Phase II.**

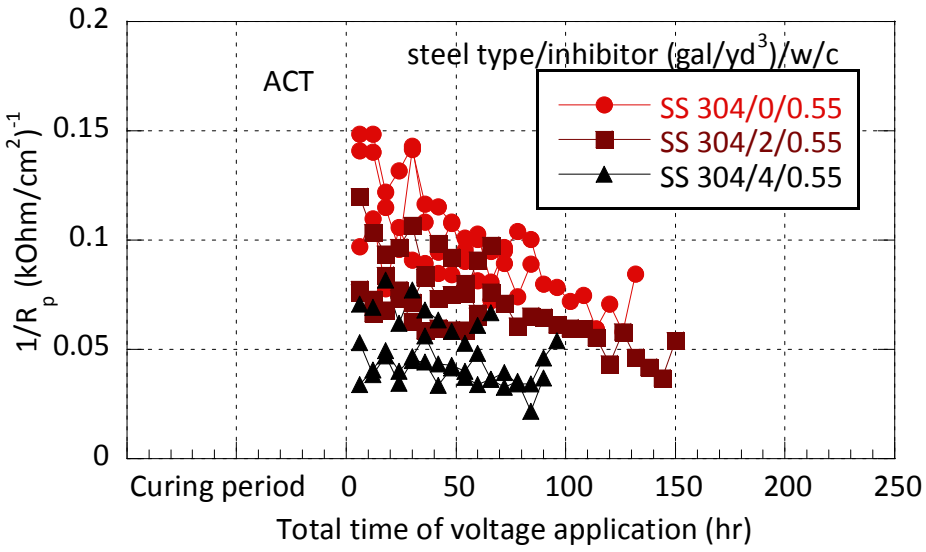


**Figure IV-63 SS304 Samples Embedded in Mortar with w/c of 0.55 in Phase II.**

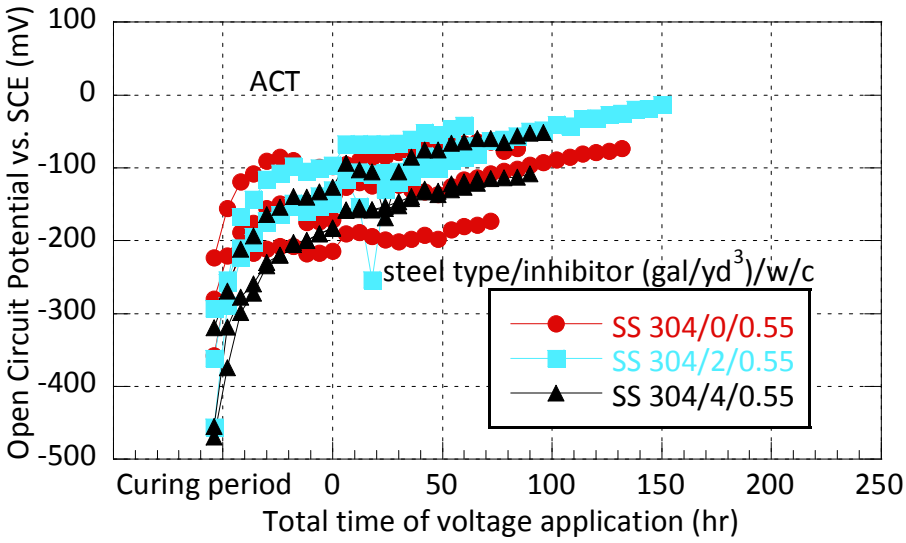


**Figure IV-64 OCP of SS304 Samples Embedded in Mortar with w/c of 0.55 in Phase II.**

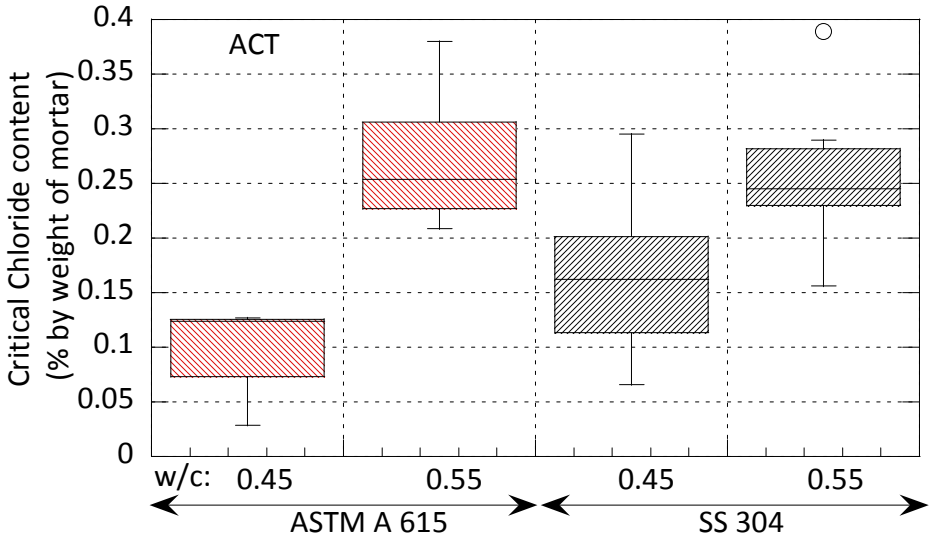


**Figure IV-65 Critical Chloride Content of Phase II Samples at Activation.**

Evaluation of results of both phases indicate that the measured chloride threshold values for samples that were embedded in mortar with a water-cement ratio of 0.55 exhibited very high variability, and, therefore, the test method was not able to differentiate between different types of steel at this high water-cement ratio level. Results of both phases indicated that the test

method was able to differentiate between different types of steel when they were embedded in mortar with water-cement ratio of 0.45. Chloride threshold values of ASTM A 615 and A 706 were not statistically different from each other. Galvanized and epoxy coated reinforcement performed better compared to ASTM A 615 and A 706, and results of the Phase II testing indicated that the SS304 samples had the highest average chloride threshold value among all the different steel types. Open circuit potential values observed in the second phase of the testing did not show a correlation with the inverse of polarization resistance data. The researchers believe that monitoring of polarization resistance from the beginning of the test without the initial 36 hours of voltage application could improve the results of the statistical method used to determine activation. The test was not effective in distinguishing difference in performance of the 0.55 water-cement ratio mixtures. However, for the lower water-cement ratio, the test did show an improvement in corrosion resistance with higher inhibitor levels. This is reasonable as the manufacturer of the inhibitor states that it should be used with lower water-cement ratios.

### 4.2.3 Chloride ion threshold test method (CCIA)

#### *4.2.3.1 Phase I*

In the first phase of the CCIA testing a total of four samples were tested for each steel type, inhibitor quantity, and water-cement ratio combination. Testing of two samples from each group was stopped as soon as they satisfied the corrosion initiation criteria and the other two samples were tested beyond activation to observe the corrosion rates. Samples were ponded weekly with chloride solution and their macrocell current, polarization resistance, and OCP values were measured. A sample was deemed actively corroding if the macrocell current was higher than 1 μA or the OCP was lower than −300 mV vs. SCE and the polarization resistance was lower than 5 kΩ for two consecutive weeks. It should be noted that the standard asks for calculation of polarization resistance by measuring the change in current and not current density, therefore the unit of polarization resistance is kΩ and not kΩ/cm$^2$. A total of 112 samples were tested in the first phase including ASTM A 615, A 706, SS304, galvanized, and epoxy coated reinforcement.

Figure IV-66 through Figure IV-68 show the macrocell current, OCP, and polarization resistance values of ASTM A 615 samples embedded in mortar with a water-cement ratio of 0.45 plotted against time to activation in weeks. All three figures clearly show that corrosion inhibitor level has an effect on the time to activation, and the time to activation increases with

increasing inhibitor level. It should also be pointed out that for most of the samples all three activation criteria indicates corrosion activity after very similar testing periods. The samples that were tested beyond activation clearly show that once all three indicators show corrosion for two consecutive weeks, the ASTM A 615 samples remain active for the remainder of the test period.

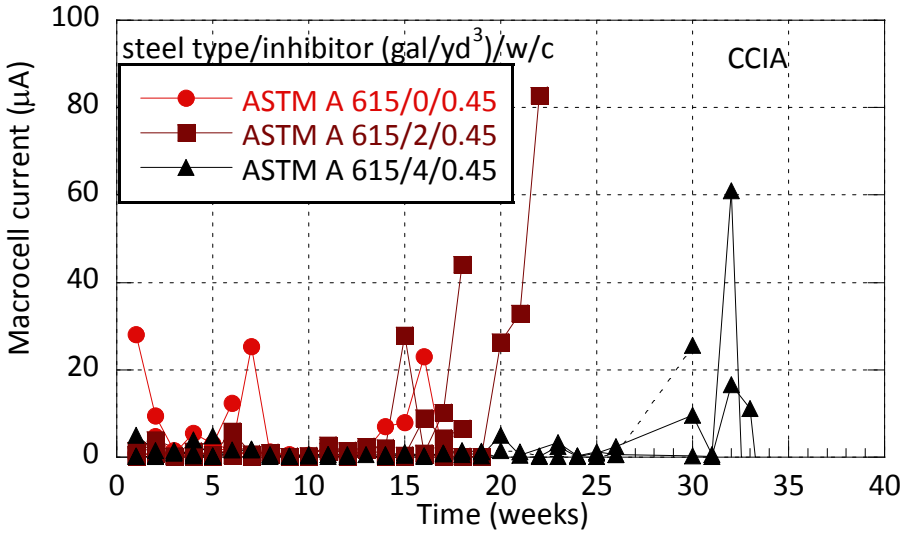


**Figure IV-66 CCIA Phase I - Macrocell Current of ASTM A 615 Samples with w/c of 0.45.**

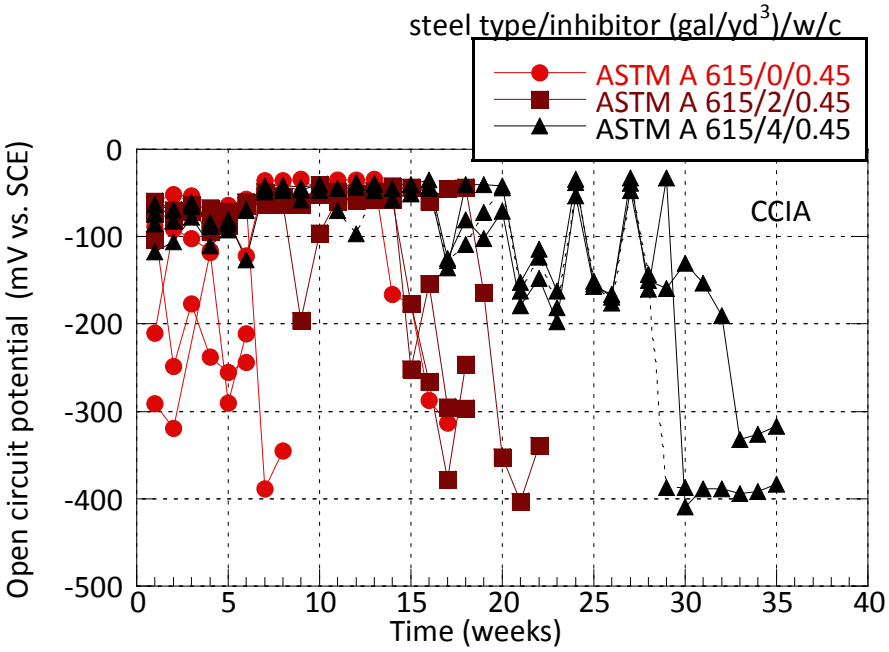


**Figure IV-67 CCIA Phase I – OCP Values of ASTM A 615 Samples with w/c of 0.45.**

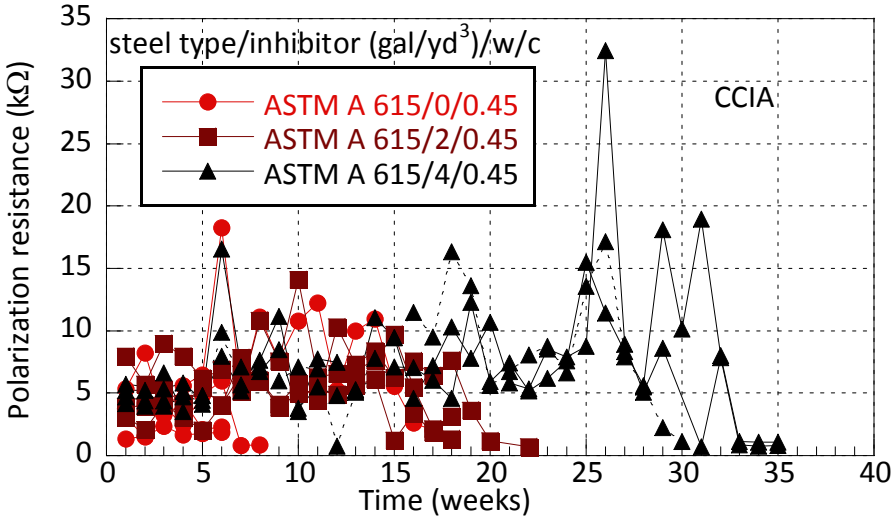


**Figure IV-68 CCIA Phase I – Polarization Resistance of ASTM A 615 Samples with w/c of 0.45.**

Figure IV-69 through Figure IV-71 show the macrocell current, OCP, and polarization resistance values of ASTM A 615 samples embedded in mortar with a water-cement ratio of 0.55. Similar to the samples embedded in mortar with a water-cement ratio of 0.45, all three indicators exhibited the same trend as the samples with a water-cement ratio of 0.45. Examination of these results indicates that the time to activation of samples that were embedded in mortar with a water-cement ratio of 0.55 was shorter on the average when compared to the samples that were embedded in mortar with water-cement ratio of 0.45. Figure IV-72 shows the chloride content values measured at the time of activation at the level of top reinforcement for samples embedded in mortar. The results clearly indicate that the average chloride content increases with increasing corrosion inhibitor level at the water-cement ratio level of 0.45 similar to time to activation values. There is no clear trend among the averages of samples with a water-cement ratio of 0.55, indicating that the corrosion inhibitor was not effective at a water-cement ratio of 0.55. This finding is similar to earlier results reported in the literature about the use of calcium nitrites at high water-cement ratio values. The average chloride contents of ASTM A 615 samples embedded in mortar with a water-cement ratio of 0.55 was higher than the averages of samples embedded in mortar with a water-cement ratio of 0.45, although the average time to activation for the samples with a water-cement ratio of 0.55 was shorter. This was also the case for the samples that were tested using the ACT method.

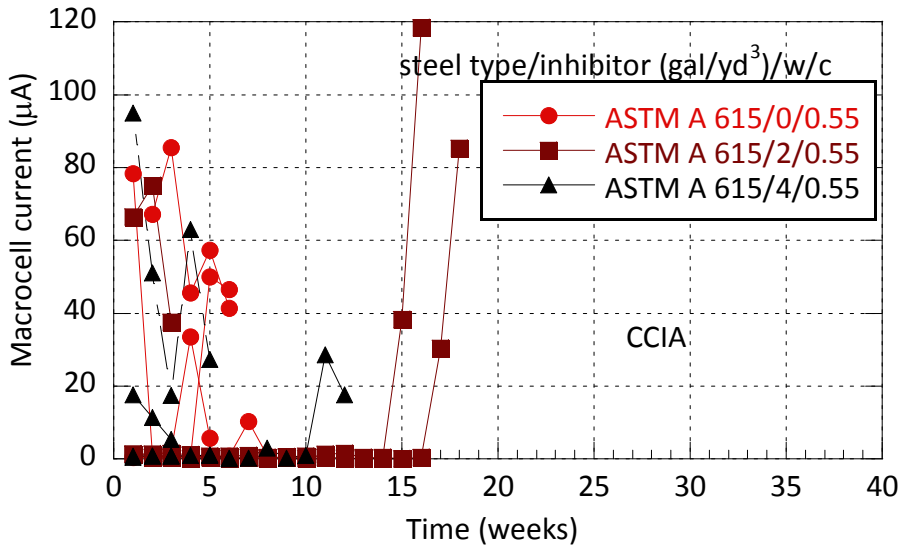


**Figure IV-69 CCIA Phase I - Macrocell Current of ASTM A 615 Samples with w/c of 0.55.**

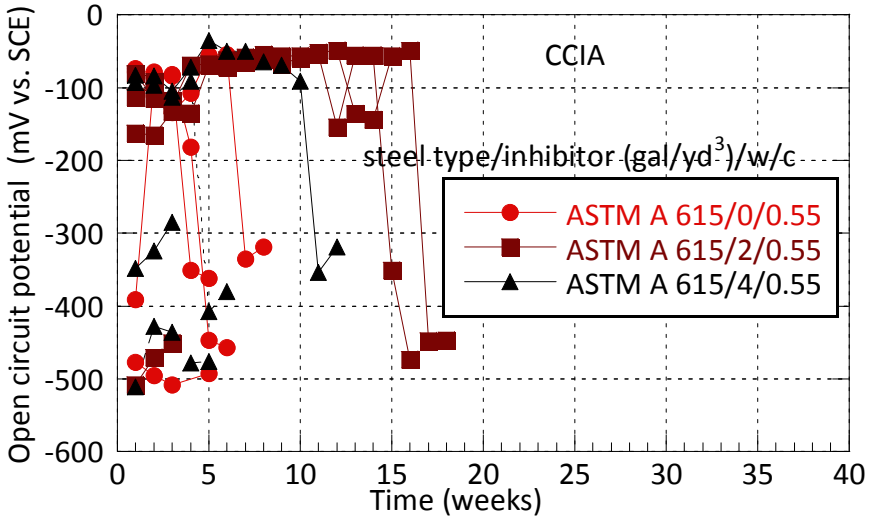


**Figure IV-70 CCIA Phase I – OCP Values of ASTM A 615 Samples with w/c of 0.55.**

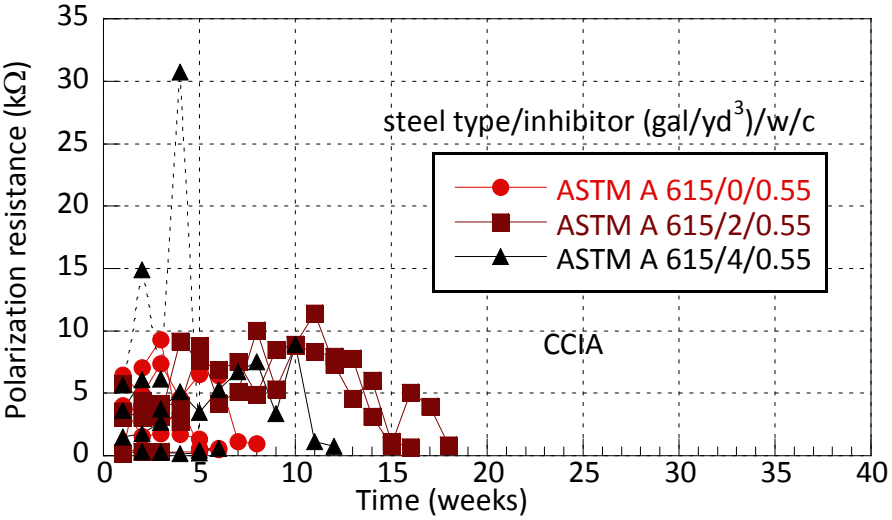


**Figure IV-71 CCIA Phase I – Polarization Resistance of ASTM A 615 Samples with w/c of 0.55.**

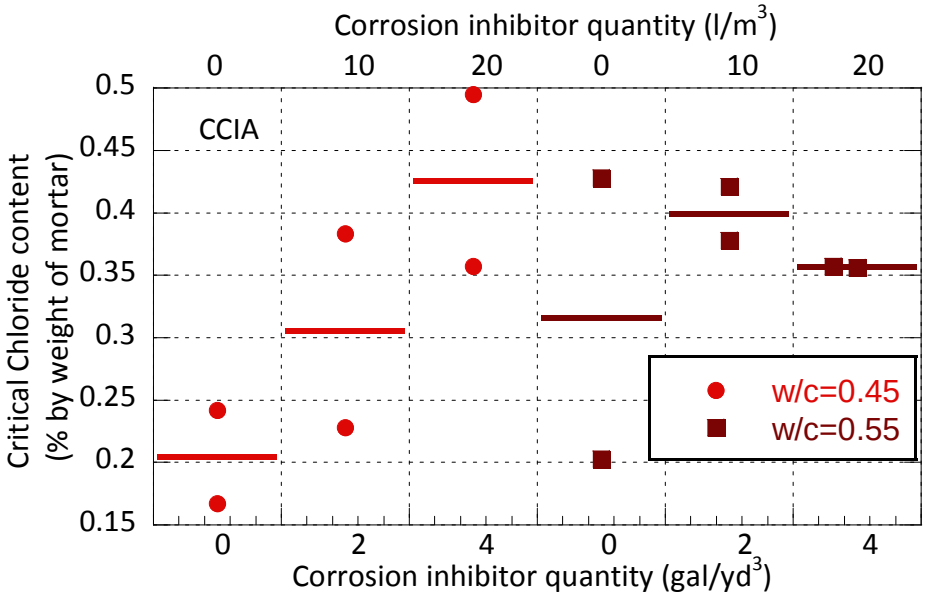


**Figure IV-72 CCIA Phase I – Chloride Content of ASTM A 615 Samples at Activation.**

Figure IV-73 through Figure IV-75 show the macrocell current, OCP, and polarization resistance of ASTM A 706 samples embedded in mortar with a water-cement ratio of 0.45. One of the samples without corrosion inhibitor activated from the very beginning of the test; however, the sample had consistently high macrocell current, OCP lower than -500 mV, and polarization resistance less than 1 kΩ from the beginning of the test. Although a second sample without corrosion inhibitor activated at the 5th week of testing, the other two samples without inhibitor did not activate until after 21 and 26 weeks of testing. This irregularity is similar to the ASTM A 615 samples where the average time to activation increased with increasing corrosion inhibitor for samples embedded in mortar with a water-cement ratio of 0.45.

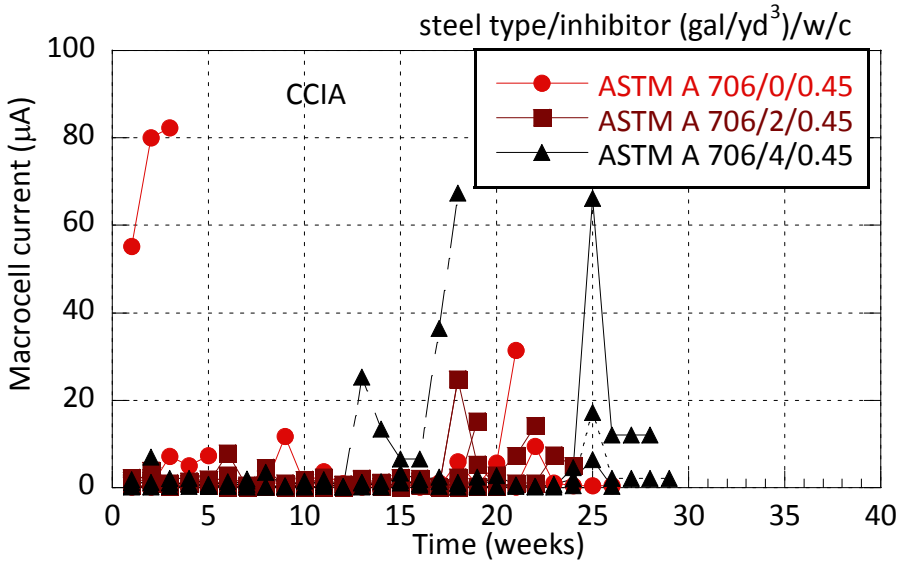


**Figure IV-73 CCIA Phase I - Macrocell Current of ASTM A 706 Samples with w/c of 0.45.**

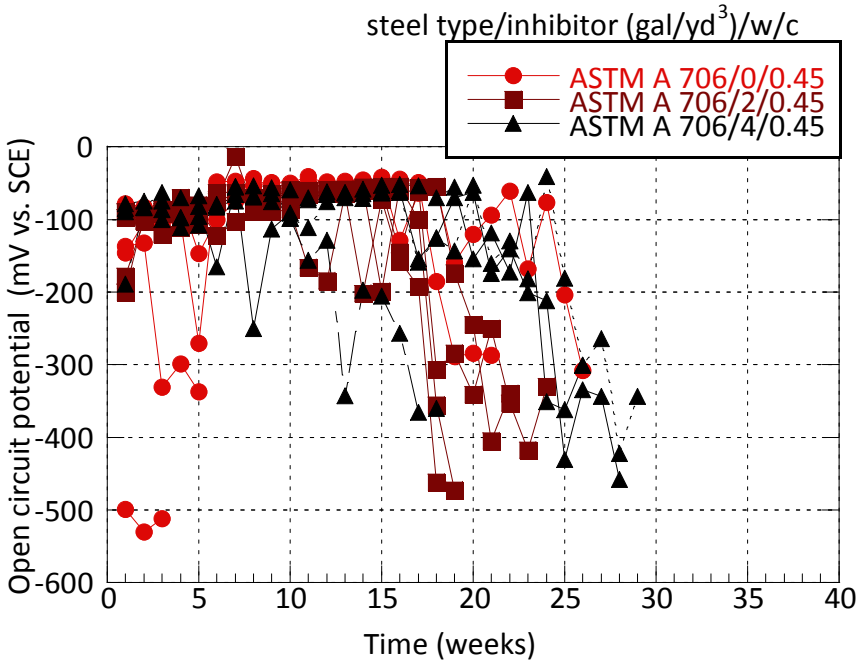


**Figure IV-74 CCIA Phase I – OCP Values of ASTM A 706 Samples with w/c of 0.45.**

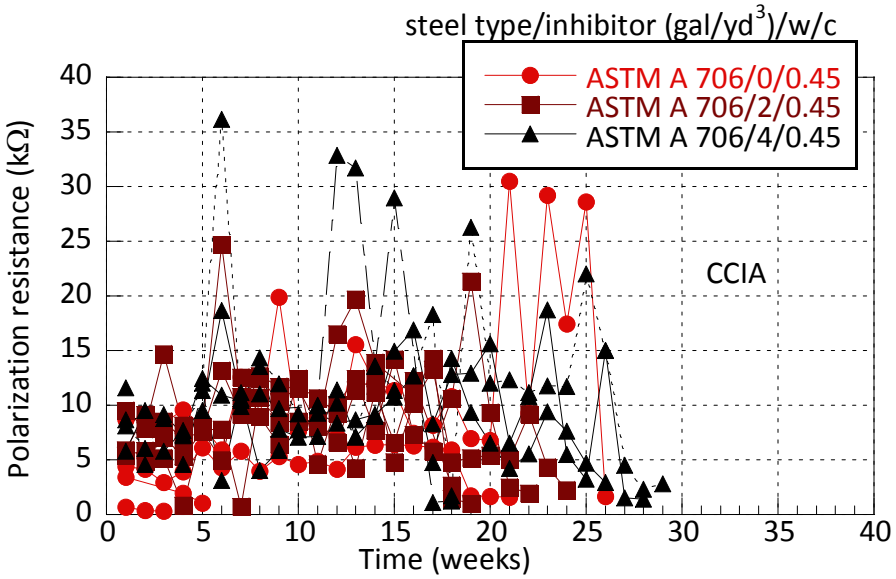


**Figure IV-75 CCIA Phase I – Polarization Resistance of ASTM A 706 Samples with w/c of 0.45.**

Figure IV-76 through Figure IV-78 show the macrocell current, OCP, and inverse polarization resistance values for CCIA samples containing ASTM A 706 samples that were embedded in mortar with water-cement ratio of 0.55. Three of the samples without inhibitor, one sample from the group with 2 gal/yd$^3$ (10 kg/m$^3$) inhibitor, and one sample with 4 gal/yd$^3$ (20 kg/m$^3$) inhibitor satisfied the activation criteria at the beginning or at the 1st week of testing. For the samples embedded in mortar with a water-cement ratio of 0.55 the average time to activation did not show dependence on the corrosion inhibitor level. This is also shown in Figure IV-79 which shows the chloride content values measured at the level of top reinforcement at the time of activation. Average chloride content at activation increases with increasing corrosion inhibitor level for samples embedded in mortar with a water-cement ratio of 0.45 and does not exhibit a trend for the samples embedded in mortar with a water-cement ratio of 0.55. One of the samples that was selected for chloride threshold determination among the samples embedded in mortar with a water-cement ratio of 0.45 and no corrosion inhibitor activated very early, and the other sample did not activate for 21 weeks. This fact explains the large difference between the measured chloride contents of this group on Figure IV-79.

As noted earlier the CCIA samples were cast using 6 x 12 in cylindrical molds and were then cut to the correct height using a saw. Researchers believe that cracks, invisible to the eye,

created during the cutting process could be the reason for the unexpected early activation of some of the samples.

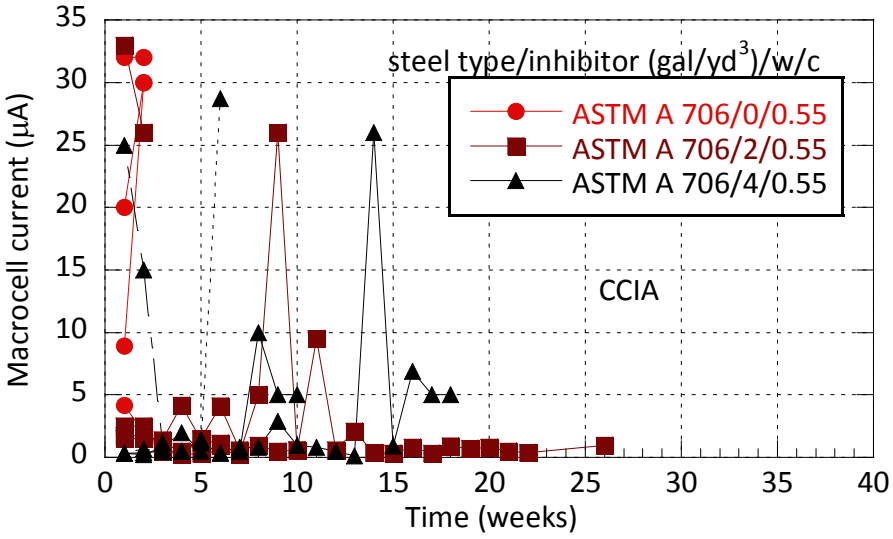


**Figure IV-76 CCIA Phase I - Macrocell Current of ASTM A 706 Samples with w/c of 0.55.**

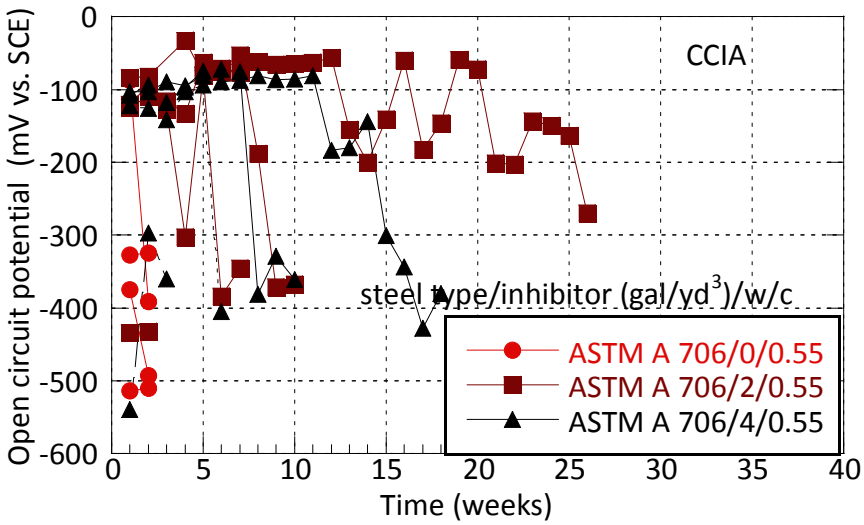


**Figure IV-77 CCIA Phase I – OCP Values of ASTM A 706 Samples with w/c of 0.55.**

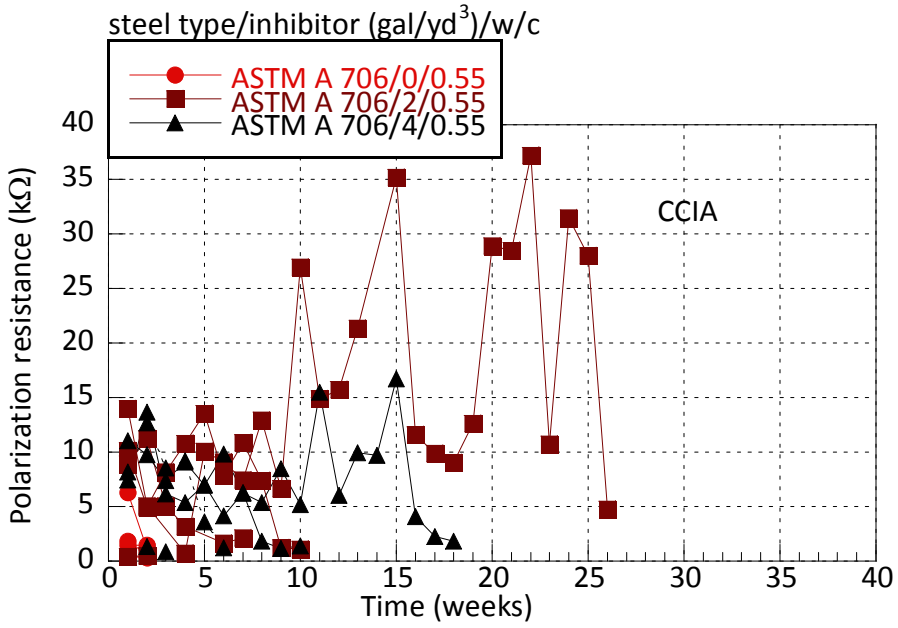


**Figure IV-78 CCIA Phase I – Polarization Resistance of ASTM A 706 Samples with w/c of 0.55.**

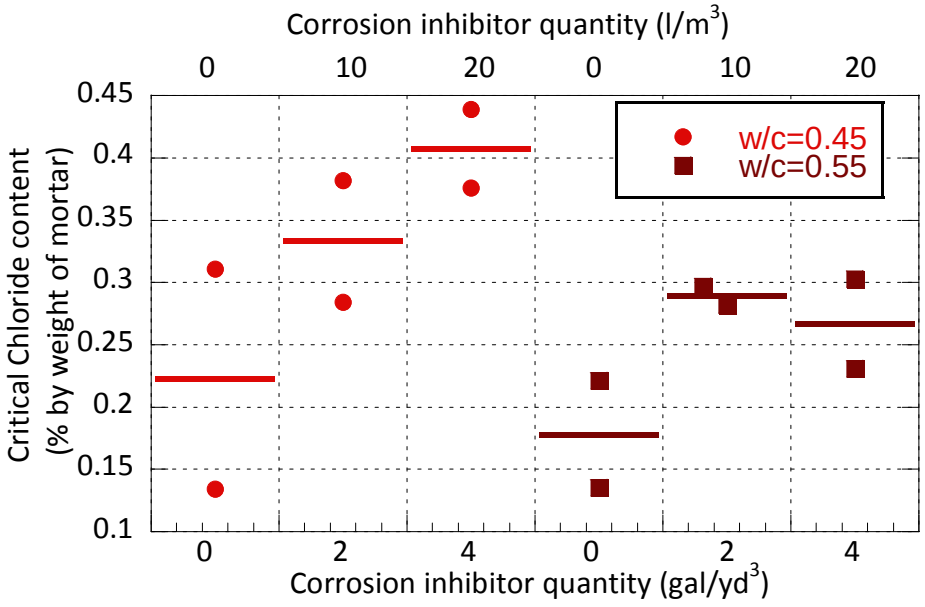


**Figure IV-79 CCIA Phase I – Critical Chloride Content of ASTM A 706 Samples at Activation.**

All epoxy coated reinforcement samples were tested embedded in mortar without corrosion inhibitor. Mortars with two different water-cement ratio values were used. Reinforcement samples were tested in three conditions: not damaged, drill damaged, and file damaged. Trials at the first phase showed that polarization resistance data could not be collected from undamaged (as received) epoxy coated reinforcement. Although larger scan ranges than 20 mV were tried, data collected from linear polarization did not cross the zero current line, and polarization resistance values could not be calculated. Also, as shown in Figure IV-80, the OCP values of undamaged epoxy coated samples in mortars with different water-cement ratio values changed within a range of ±1 mV indicating a passive state.

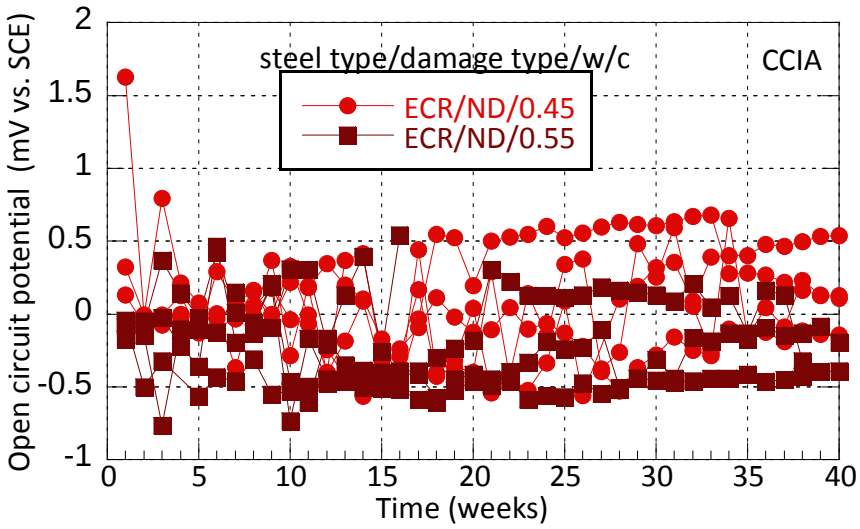


**Figure IV-80 CCIA Phase I – OCP Values of Undamaged ECR Samples.**

Figure IV-81 to Figure IV-83 show the macrocell current, OCP, and polarization resistance of drill damaged and file damaged epoxy coated samples embedded in mortar with a water-cement ratio of 0.45. None of the drill damaged samples showed activation for two consecutive weeks and testing of these samples were eventually stopped after 60 weeks of testing. Three of the four file damaged samples exhibited activation and two of them were stopped at activation to determine their chloride content. Evaluation of the figures clearly shows that although macrocell current, OCP, and polarization resistance reached values indicating activation, they did not all show activation at the same time.

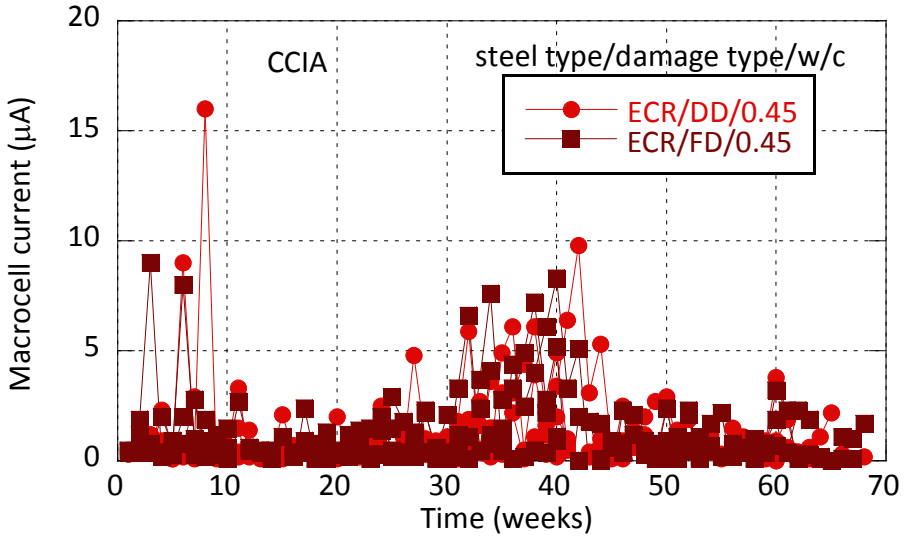


**Figure IV-81 CCIA Phase I - Macrocell Current of Drill and File Damaged ECR Samples with w/c of 0.45.**

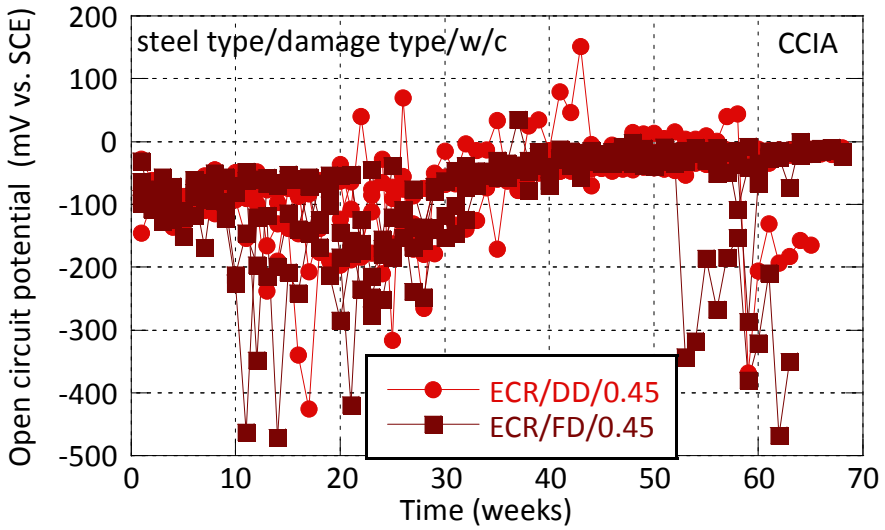


**Figure IV-82 CCIA Phase I – OCP Values of Drill and File Damaged ECR Samples with w/c of 0.45.**

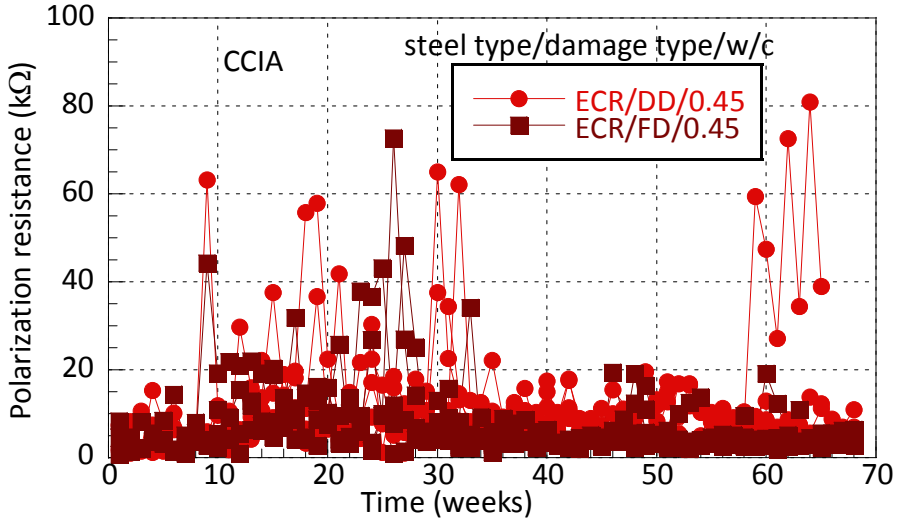


**Figure IV-83 CCIA Phase I – Polarization Resistance of File and Drill Damaged ECR Samples with w/c of 0.45.**

Figure IV-84 through Figure IV-86 show the macrocell current, OCP, and polarization resistance values of drill damaged and file damaged epoxy coated samples embedded in mortar with a water-cement ratio of 0.55. Chloride content data at activation could not be measured for the file damaged samples because these samples did not show activation for two consecutive weeks. All file damaged samples were tested for more than 60 weeks, and testing was eventually stopped. Drill damaged epoxy coated samples embedded in mortar with a water-cement ratio of 0.55 exhibited a wide range of activation times from 3 to 53 weeks. The two samples that activated at three and four weeks were stopped and tested for chloride contents, and the other two samples were further tested to observe the average corrosion. Evaluation of file damaged and drill damaged samples indicated that even the samples that showed activation following all three criteria became passive and active many times over the test period, unlike the ASTM A 615 and A 706 samples that remained active once they showed activation.

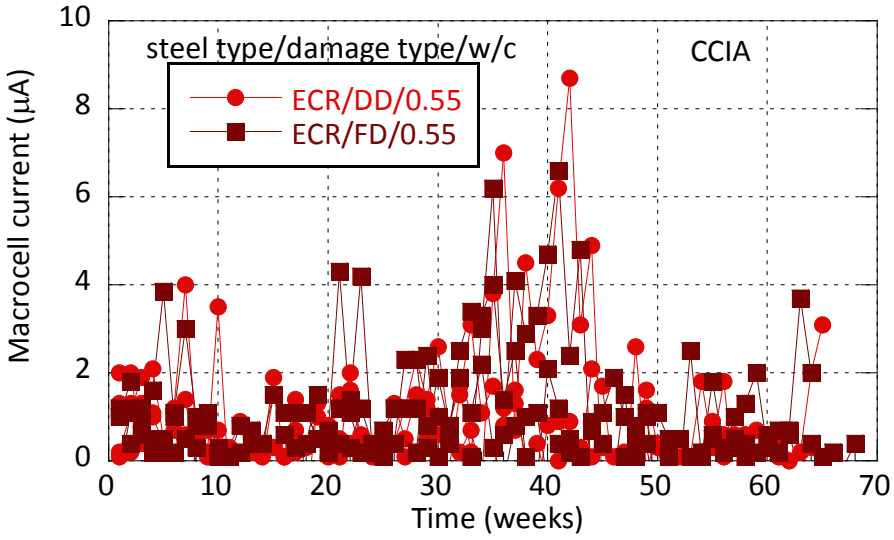


**Figure IV-84 CCIA Phase I - Macrocell Current of Drill and File Damaged ECR Samples with w/c of 0.55.**

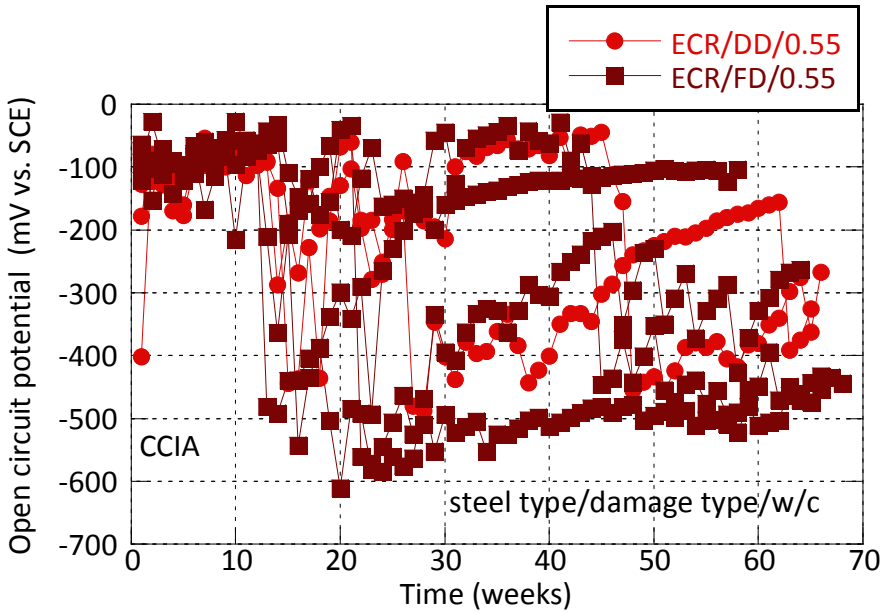


**Figure IV-85 CCIA Phase I – OCP Values of Drill and File Damaged ECR Samples with w/c of 0.55.**

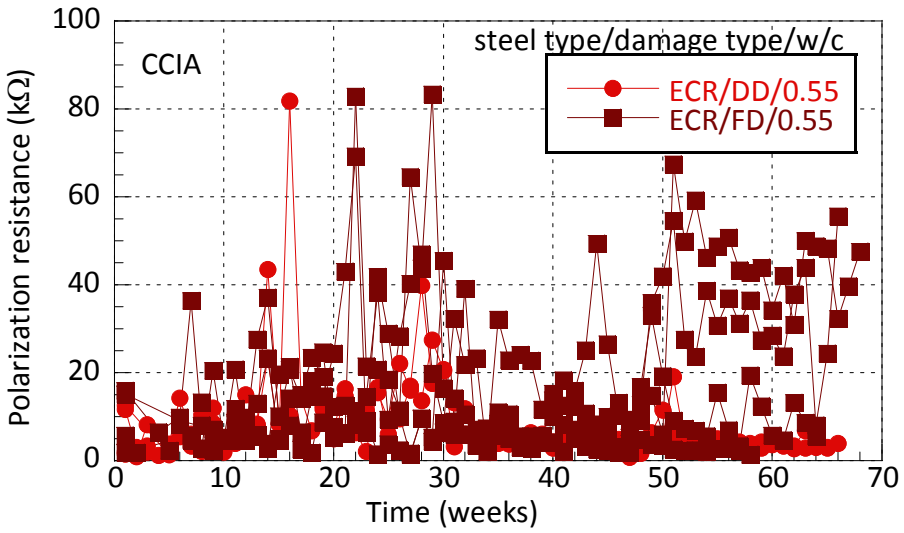


**Figure IV-86 CCIA Phase I – Polarization Resistance of File and Drill Damaged ECR Samples with w/c of 0.55.**

As noted earlier, the undamaged and drill damaged epoxy coated reinforcement samples embedded in mortar with a water-cement ratio of 0.45, and the file damaged samples embedded in mortar with a water-cement ratio of 0.55 did not show activation for two consecutive weeks; therefore their chloride threshold value (chloride content at the time of activation) could not be determined. Figure IV-87 shows the chloride content values measured from file damaged samples embedded in mortar with a water-cement ratio of 0.45 and drill damaged samples embedded in mortar with a water-cement ratio of 0.55. However, because samples tested at these conditions were tested beyond the activation point (to monitor their average corrosion rate), the chloride content values obtained are likely higher than the critical chloride threshold values for these samples. Because it took much longer (around 30 weeks) for the samples embedded in mortar with a water-cement ratio of 0.45 to activate, their chloride content was much higher compared to samples embedded in mortar with a water-cement ratio of 0.55 and that activated at three to four weeks.

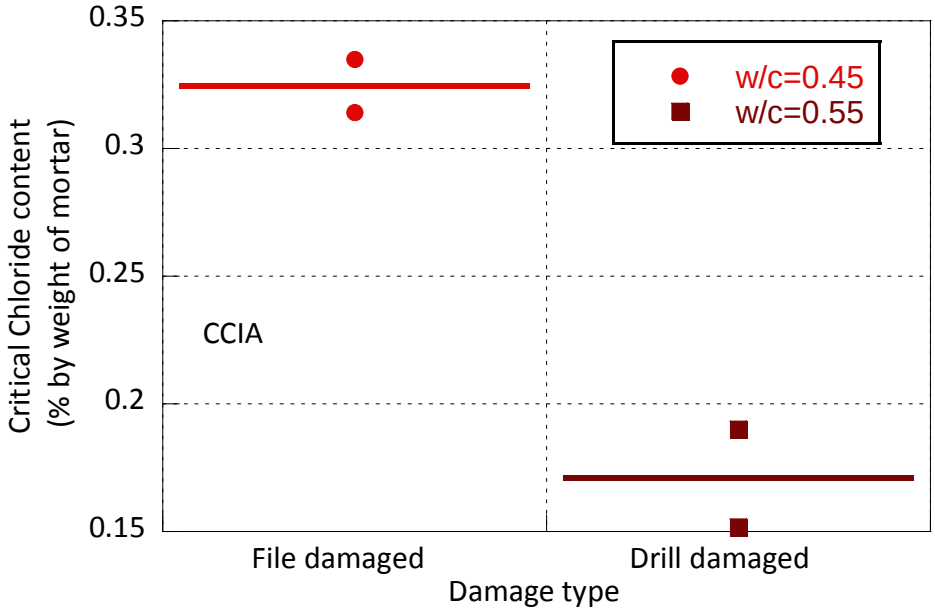


**Figure IV-87 CCIA Phase I – Chloride Content of Damaged ECR Samples at Activation.**

Galvanized samples were tested in mortar without corrosion inhibitor and only in two conditions, undamaged and drill damaged. Results indicate that the galvanized samples satisfied the activation criteria from the beginning of the test, and testing was stopped after the second week. Evaluation of the data from the samples that were further tested indicated that the samples remained active. Figure IV-88 through Figure IV-90 show the macrocell current, OCP, and polarization resistance of samples that were continued to be tested after activation. Figure IV-91 shows the measured chloride contents of the samples that were stopped after two to three weeks of testing. The research team believes that although the activation criteria was satisfied for these samples, these samples were not actively corroding but they satisfied the criteria because of a high corrosion rate of galvanization in high pH environment. Therefore the low chloride content values shown in Figure IV-91 are also not believed to be the actual chloride threshold values.

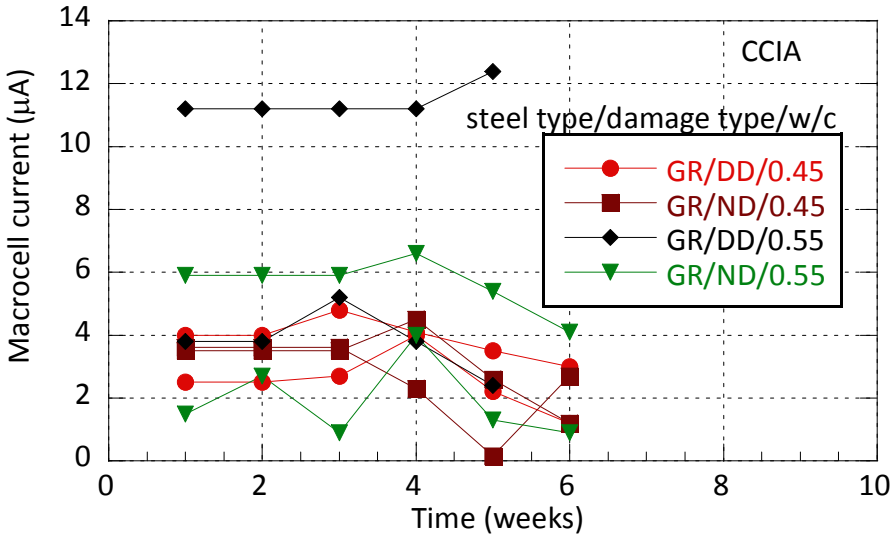


**Figure IV-88 CCIA Phase I - Macrocell Current of Galvanized Samples.**

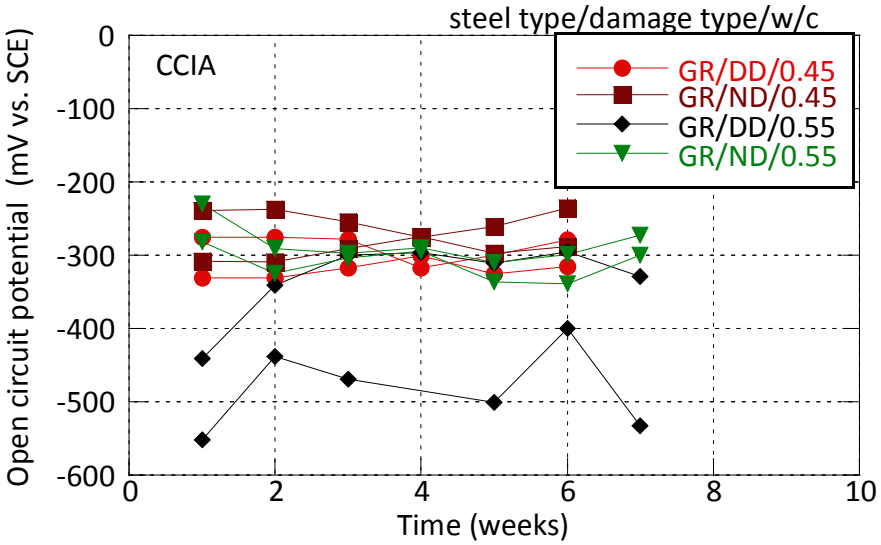


**Figure IV-89 CCIA Phase I – OCP Values of Galvanized Samples.**

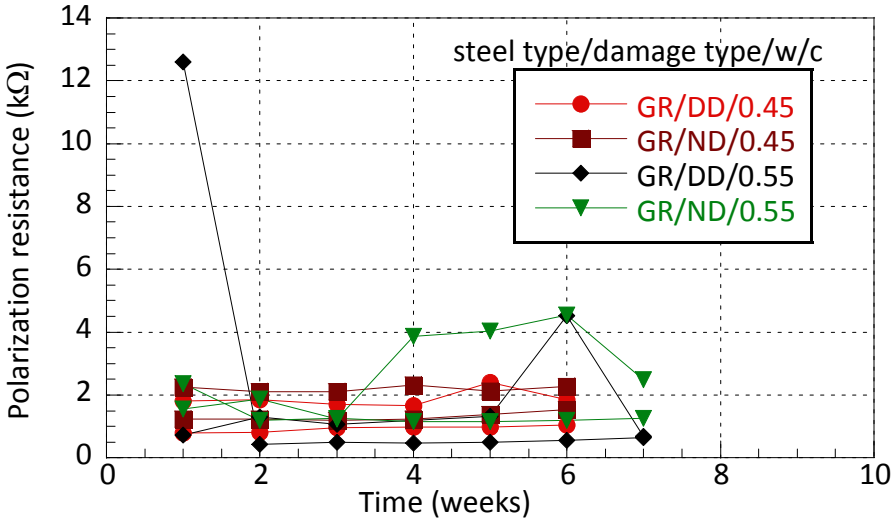


**Figure IV-90 CCIA Phase I – Polarization Resistance of Galvanized Samples.**

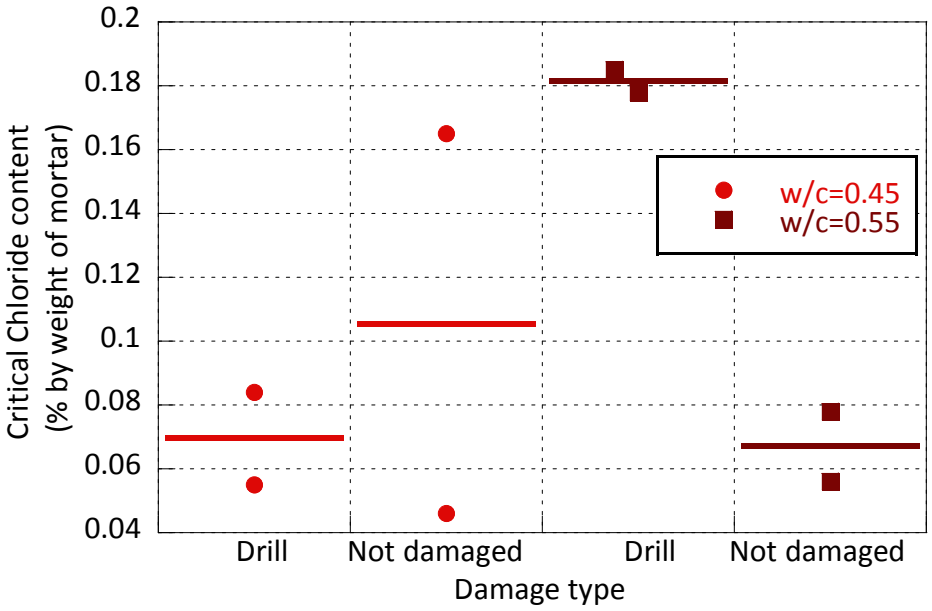


**Figure IV-91 CCIA Phase I – Chloride Content of Galvanized Samples at Activation.**

Figure IV-92 through Figure IV-94 show the macrocell current, OCP, and polarization resistance of stainless steel 304 samples embedded in mortar with water-cement ratio of 0.45, respectively. Figure IV-93 shows that the OCP values of stainless steel samples remained above -300 mV, which was the activation limit. On the average it took stainless steel samples much longer to satisfy the activation criteria for two consecutive weeks compared to the ASTM A 615 and A 706 samples. For the ASTM A 615 and A 706 samples all three variables, macrocell current, OCP, and polarization resistance, indicated activation around the same time. The SS304 samples activated at different times. Also, evaluation of continued samples indicated that samples that showed activation for two consecutive weeks immediately went back to passive afterward and became passive and active randomly thereafter.

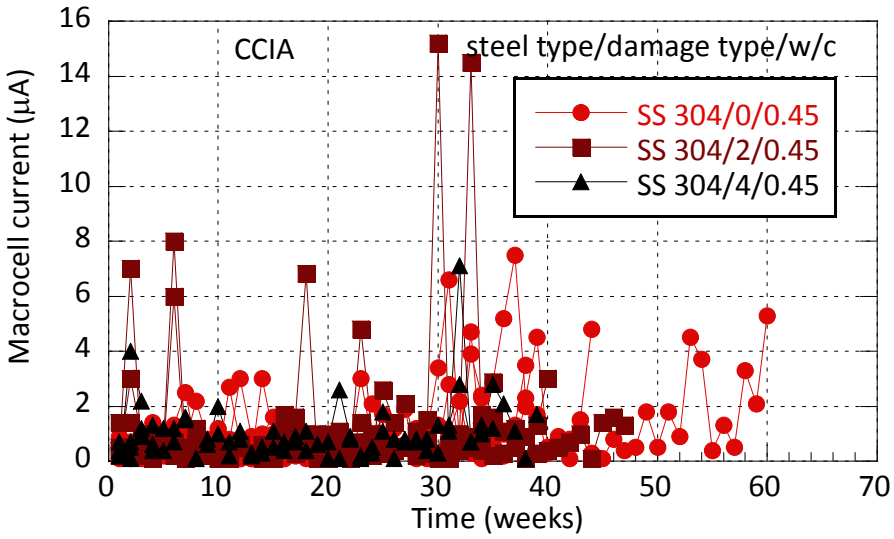


**Figure IV-92 CCIA Phase I - Macrocell Current of SS304 Samples Embedded in Mortar with w/c of 0.45.**

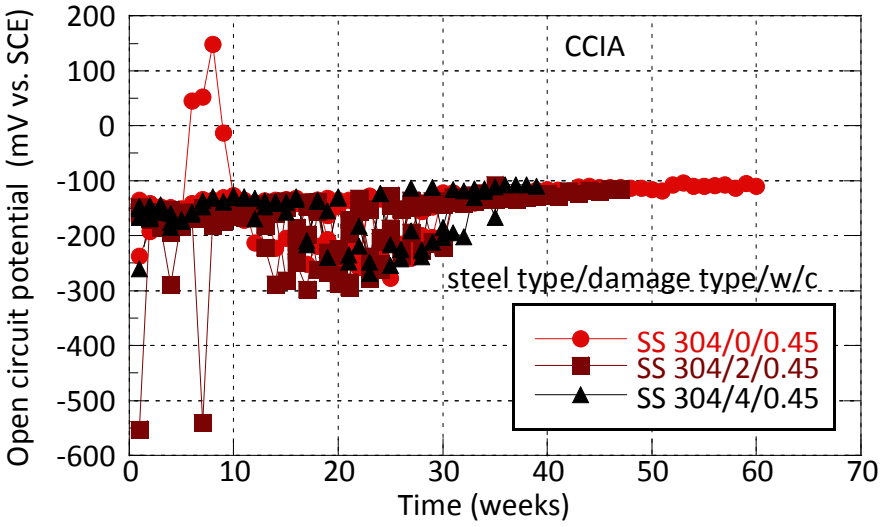


**Figure IV-93 CCIA Phase I – OCP Values of SS304 Samples Embedded in Mortar with w/c of 0.45.**

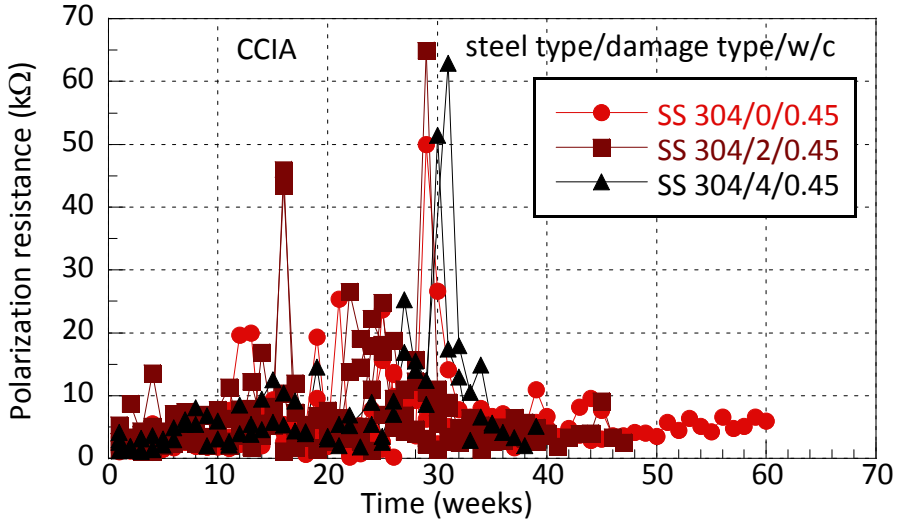


**Figure IV-94 CCIA Phase I – Polarization Resistance of SS304 Samples Embedded in Mortar with w/c of 0.45.**

Figure IV-95 to Figure IV-97 show the macrocell current, OCP, and polarization resistance of stainless steel samples embedded in mortar with water-cement ratio of 0.55, respectively. Similar to samples embedded in mortar with a water-cement ratio of 0.45, the OCP values mostly remained more positive than -300 mV. Macrocell current and polarization resistance values jumped above and below the activation limit throughout the test. Again similar to the samples embedded in mortar with a water-cement ratio of 0.45, the samples that were further tested became passive and active randomly after they indicated activation for two consecutive weeks. Based on these results the researchers believe that the activation criteria used in this test method may not be appropriate to test stainless steel samples and that it may need to be modified for better results. Stainless steel samples were also tested in the second phase of CCIA testing to evaluate repeatability. Figure IV-98 shows the chloride contents measured from the samples that were stopped at activation. Results indicate that the chloride contents of all samples were similar except the samples that were embedded in mortar without corrosion inhibitor and with a water-cement ratio of 0.55 exhibited lower chloride content compared to others. Still chloride content values of stainless steel samples measured at activation were much higher compared to other samples containing different kinds of reinforcement steel.

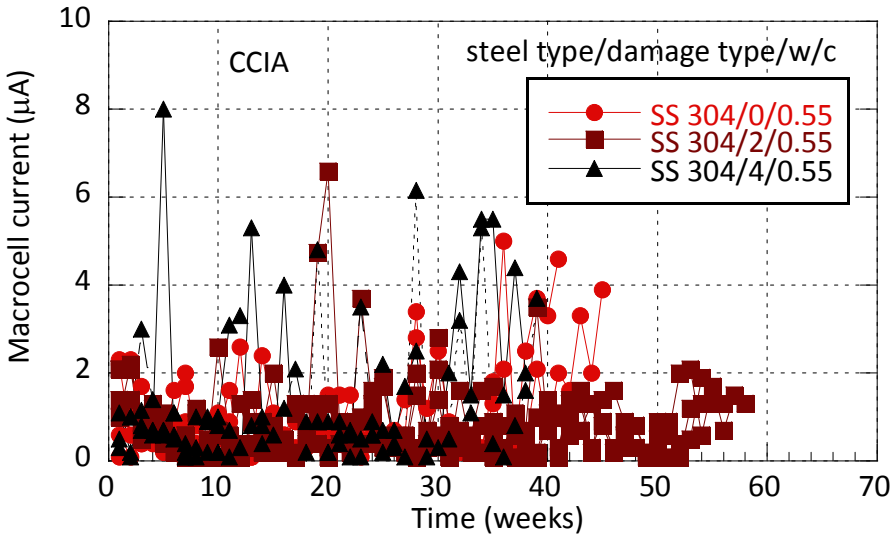


**Figure IV-95 CCIA Phase I - Macrocell Current of SS304 Samples Embedded in Mortar with w/c of 0.55.**

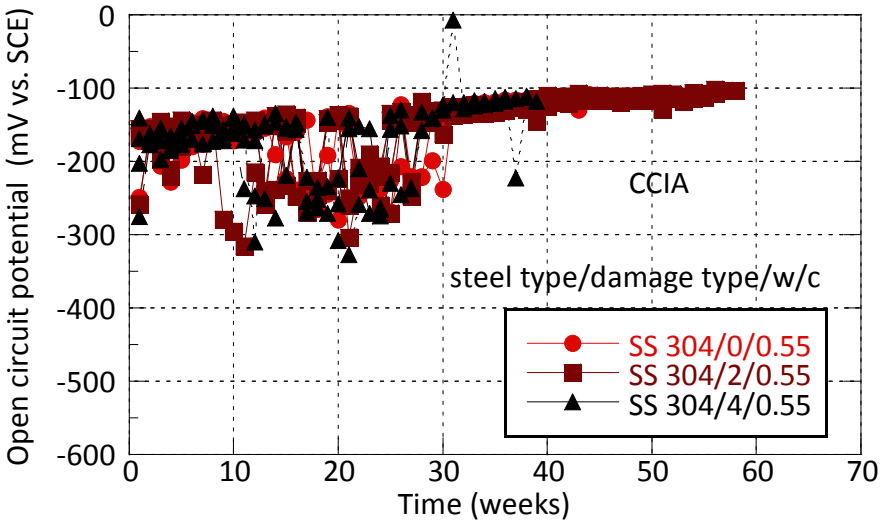


**Figure IV-96 CCIA Phase I – OCP Values of SS304 Samples Embedded in Mortar with w/c of 0.55.**

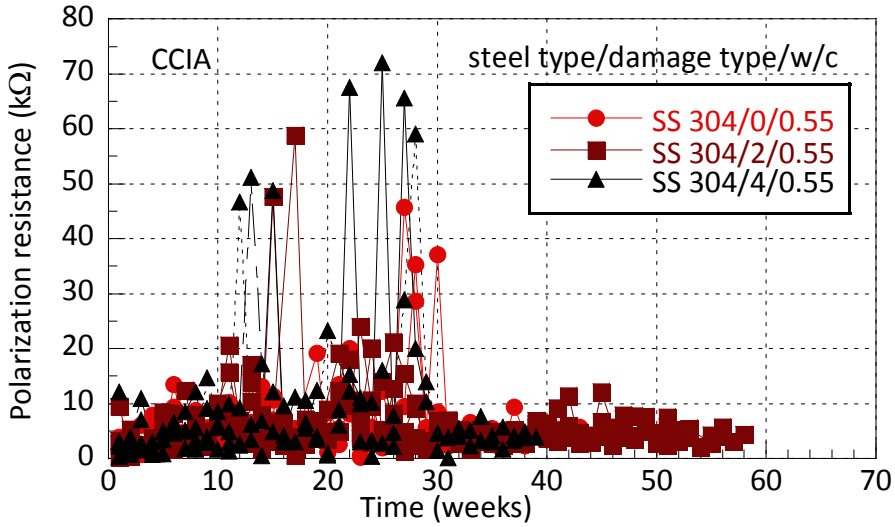


**Figure IV-97 CCIA Phase I – Polarization Resistance of SS304 Samples Embedded in Mortar with w/c of 0.55.**

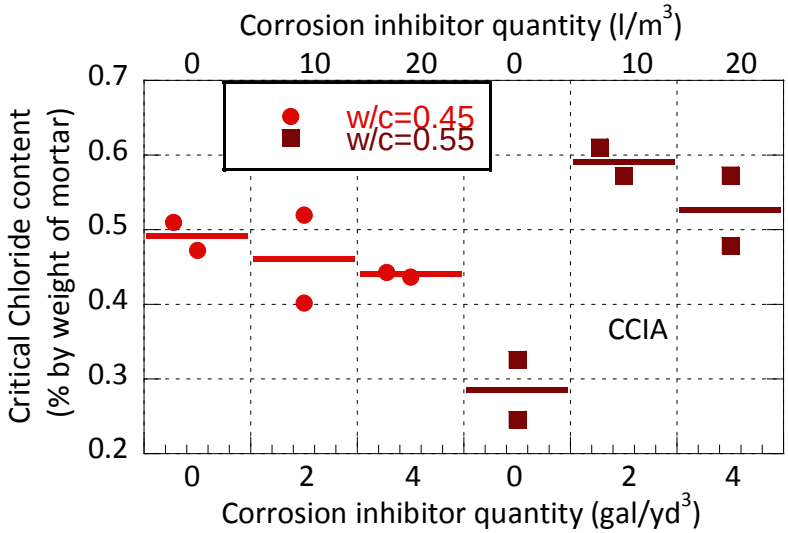


**Figure IV-98 CCIA Phase I – Chloride Content of SS304 Samples at Activation.**

### *4.2.3.2 Phase II CCIA*

A total of 36 samples were cast for the second phase of testing with two steel types, three corrosion inhibitor levels, and two water-cement ratio values. Three replicates were prepared for each condition. At the time of the writing of this report 27 of 36 samples showed activation. Testing of all activated samples was stopped, and their chloride threshold was determined. Table IV-8 shows the number of activated samples for each different test condition in Phase II.

Figure IV-99 through Figure IV-101 shows the macrocell current, OCP, and the polarization resistance of ASTM A 615 samples embedded in mortar with a water-cement ratio of 0.45, respectively. It should be noted that after 27 weeks of testing only two samples embedded in mortar containing 4 gal/yd$^3$ (20 L/m$^3$) of inhibitor activated. The figures also indicate that the macrocell current is decreasing, while the OCP values are slowly becoming more positive. The polarization resistance values are decreasing slowly but were generally still above 5 kΩ. The behavior of samples is very similar to the samples tested at the first phase. Based on the results obtained in the first phase, it can be said that these samples are very close to activation.

**Table IV-8 Activated Phase II CCIA Samples.**

| Water-Cement Ratio | Admixture Content gal/yd$^3$ (l/m$^3$) | Rebar Type | No. of Activated Samples |
|---|---|---|---|
| 0.45 | 0 (0) | A 615 | 0 |
| | | SS304 | 3 |
| | 2 (10) | A 615 | 0 |
| | | SS304 | 1 |
| | 4 (20) | A 615 | 2 |
| | | SS304 | 3 |
| 0.55 | 0 (0) | A 615 | 3 |
| | | SS304 | 3 |
| | 2 (10) | A 615 | 3 |
| | | SS304 | 3 |
| | 4 (20) | A 615 | 3 |
| | | SS304 | 3 |

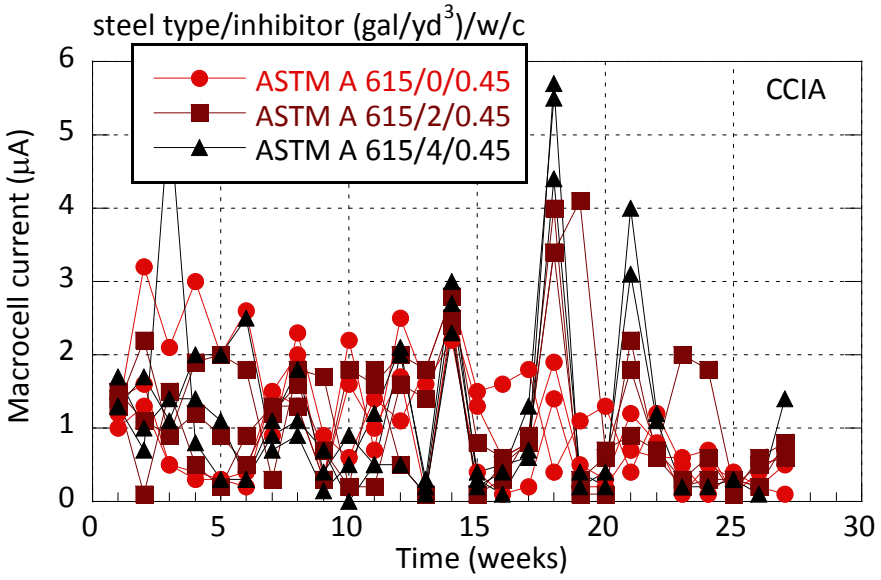


**Figure IV-99 CCIA Phase II - Macrocell Current of ASTM A 615 Samples Embedded in Mortar with w/c of 0.45.**

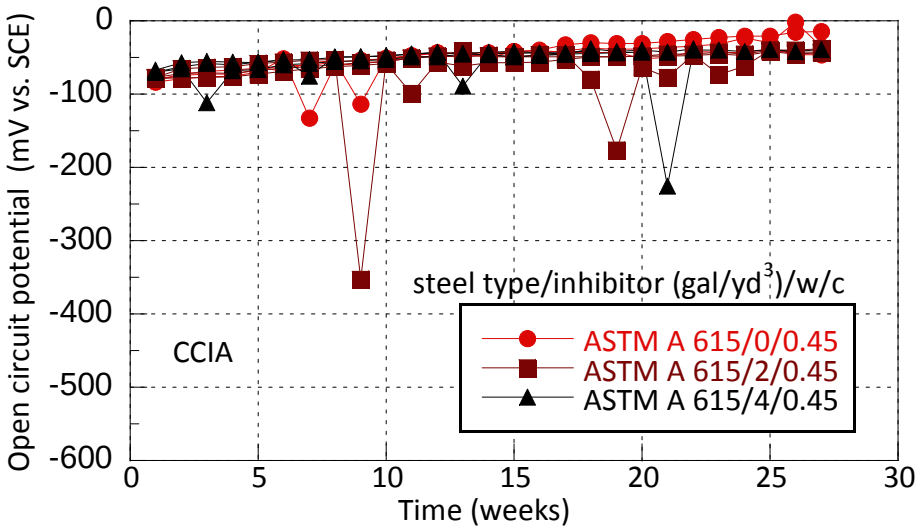


**Figure IV-100 CCIA Phase II – OCP Values of ASTM A 615 Samples Embedded in Mortar with w/c of 0.45.**

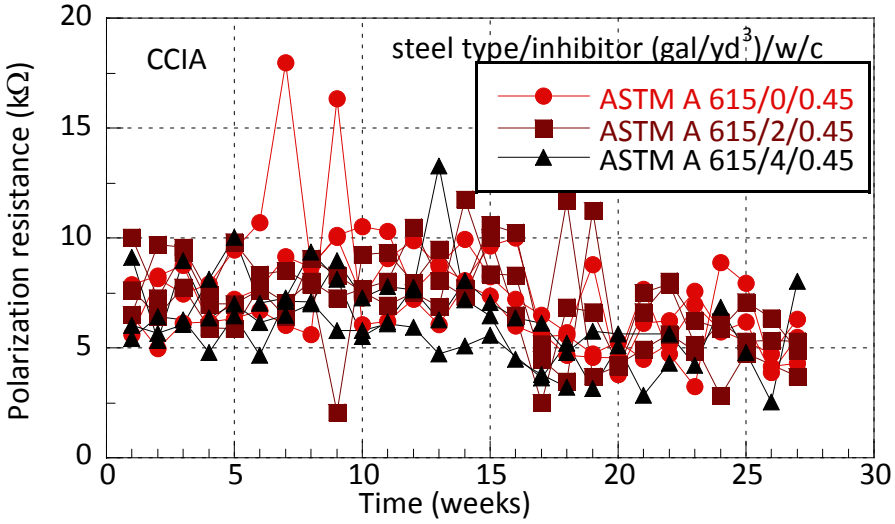


**Figure IV-101 CCIA Phase II – Polarization Resistance of ASTM A 615 Samples Embedded in Mortar with w/c of 0.45.**

Figure IV-102 to Figure IV-104 show the macrocell current, OCP, and the polarization resistance of ASTM A 615 samples embedded in mortar with a water-cement ratio of 0.55, respectively. Similar to the first phase, these samples activated faster compared to the samples embedded in mortar with a water-cement ratio of 0.45. Except one sample, all samples exhibited active conditions. It should be noted that similar to the first phase for the ASTM A 615 samples, all indicators provided consistent indicators of corrosion activation. Figure IV-105 shows the chloride content values obtained at the activation of samples. Limited data for the samples embedded in mortar with a water-cement ratio of 0.45 are available to date with only two samples satisfying the activation criteria. Similar to the Phase I results, the average chloride content values at the activation of samples embedded in mortar with a water-cement ratio of 0.55 do not change significantly with changing corrosion inhibitor level.

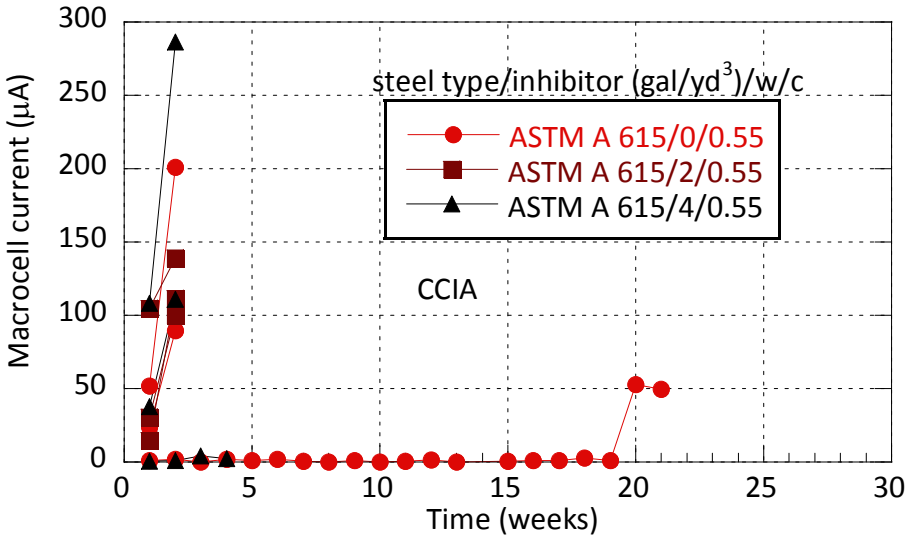


**Figure IV-102 CCIA Phase II - Macrocell Current of ASTM A 615 Samples Embedded in Mortar with w/c of 0.55.**

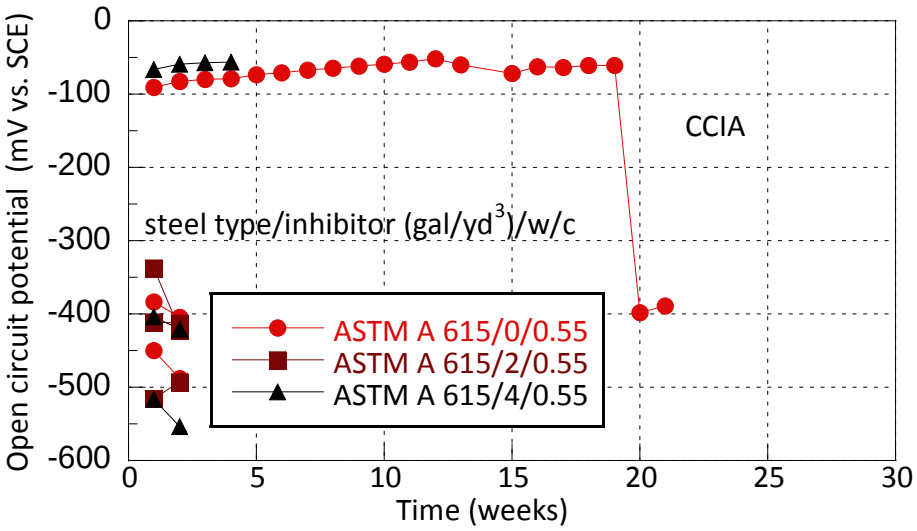


**Figure IV-103 CCIA Phase II – OCP Values of ASTM A 615 Samples Embedded in Mortar with w/c of 0.55.**

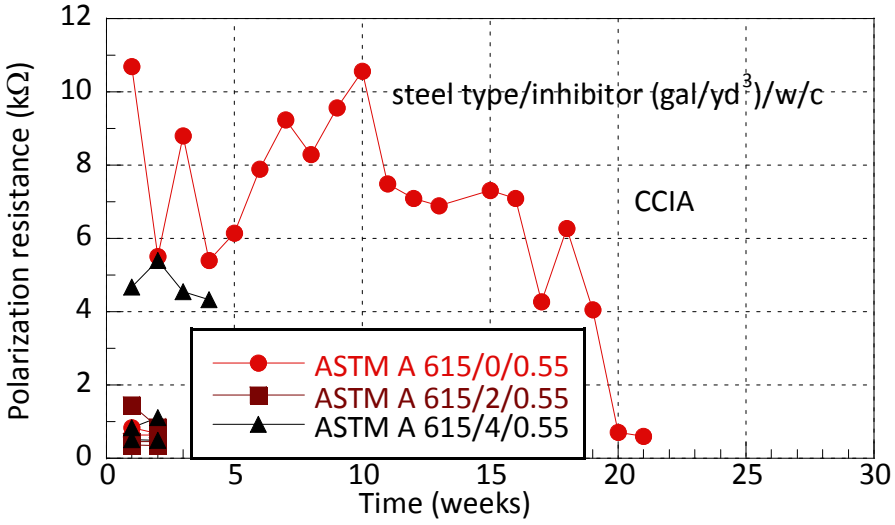


**Figure IV-104 CCIA Phase II – Polarization Resistance of ASTM A 615 Samples Embedded in Mortar with w/c of 0.55.**

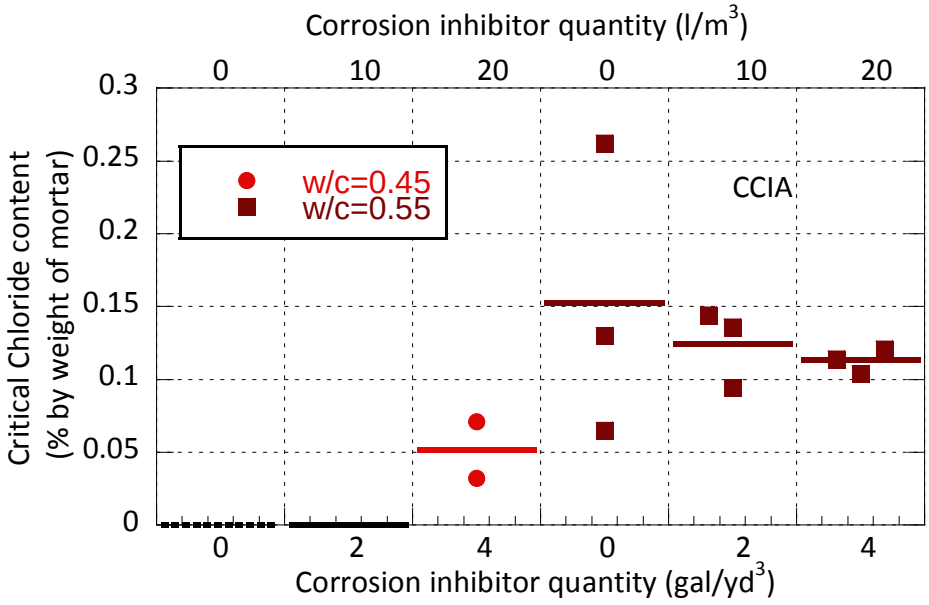


**Figure IV-105 CCIA Phase II – Chloride Content of ASTM A 615 Samples at Activation.**

Figure IV-106 to Figure IV-108 show the macrocell current, OCP, and the polarization resistance values of stainless steel samples embedded in mortar with a water-cement ratio of 0.45. Similar to the stainless steel samples tested in the first phase, the OCP values of samples are more positive than –300 mV, and the macrocell current values jump above and below the activation limit (1 μA). All samples satisfied the activation criteria for two consecutive weeks except two samples that contain 2 gal/yd$^3$ (20 kg/m$^3$) of corrosion inhibitor. Evaluation of the polarization resistance values shows that they also did not exhibit a clear trend but were going above and below the 5 kΩ limit of activation. Unlike the first phase, all samples that satisfied the activation criteria in the second phase were stopped and tested for chloride content.

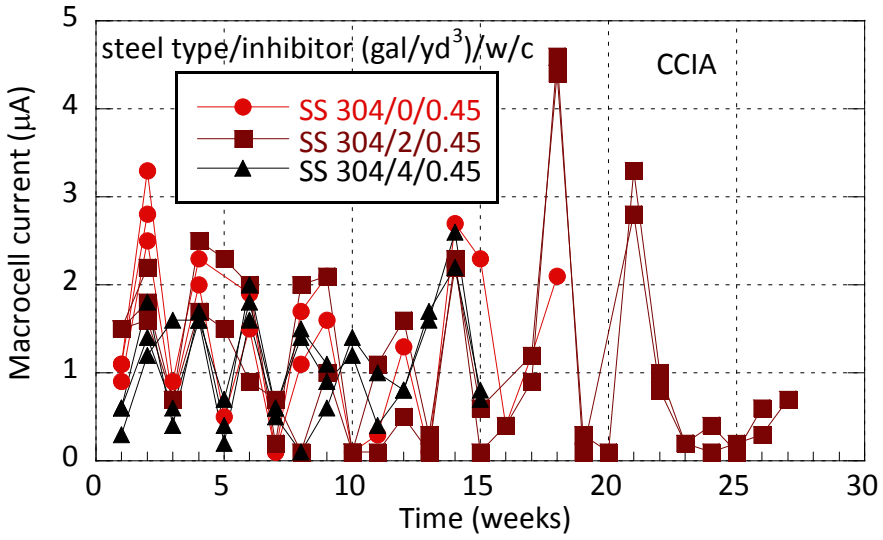


**Figure IV-106 CCIA Phase II - Macrocell Current of SS304 Samples Embedded in Mortar with w/c of 0.45.**

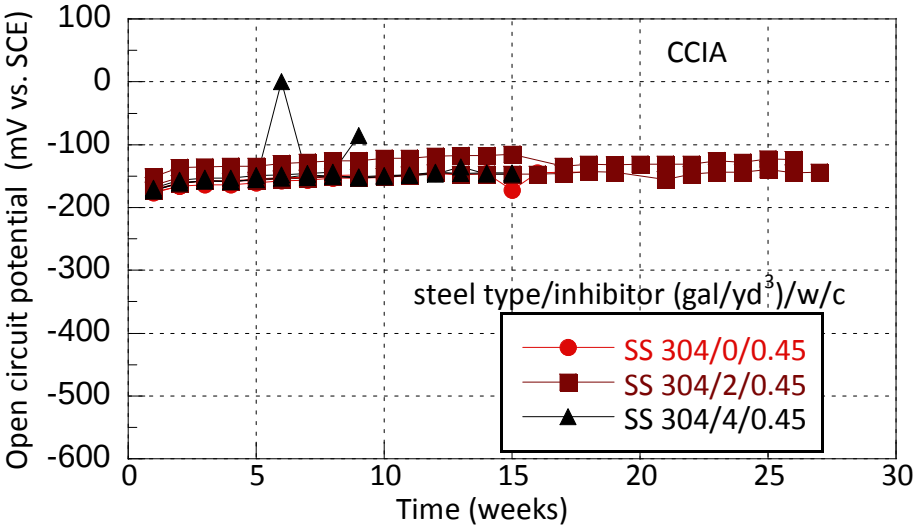


**Figure IV-107 CCIA Phase II – OCP Values of SS304 Samples Embedded in Mortar with w/c of 0.45.**

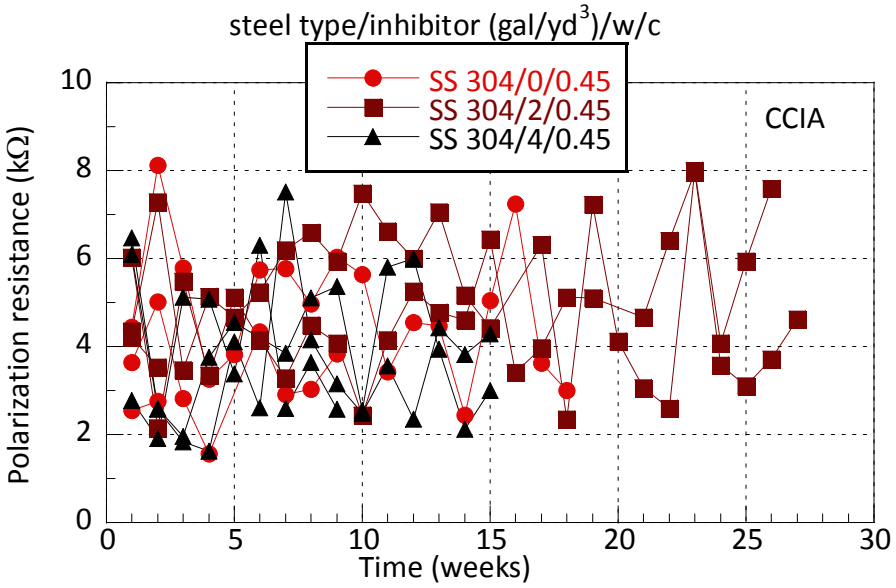


**Figure IV-108 CCIA Phase II – Polarization Resistance of SS304 Samples Embedded in Mortar with w/c of 0.45.**

Figure IV-109 through Figure IV-111 show the macrocell current, OCP, and the polarization resistance of stainless steel samples that were embedded in mortar with a water-cement ratio of 0.55 in the second phase, respectively. All samples activated and when compared to the results from the SS304 samples tested in the first phase with similar mortar mixtures these samples (Phase II samples) activated much faster. The OCP values were more positive than -300 mV for all samples throughout the test. Similar to the other stainless steel samples tested in this study the macrocell current values and the polarization resistance values went above and below the activation limits randomly. Figure IV-112 shows the chloride contents measured at the time of activation of stainless steel samples tested in the second phase of the study.

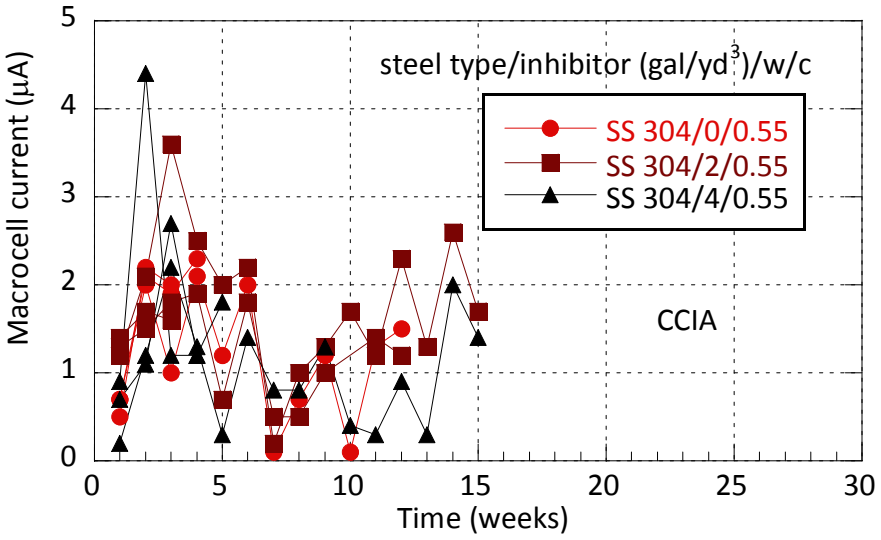


**Figure IV-109 CCIA Phase II - Macrocell Current of SS304 Samples Embedded in Mortar with w/c of 0.55.**

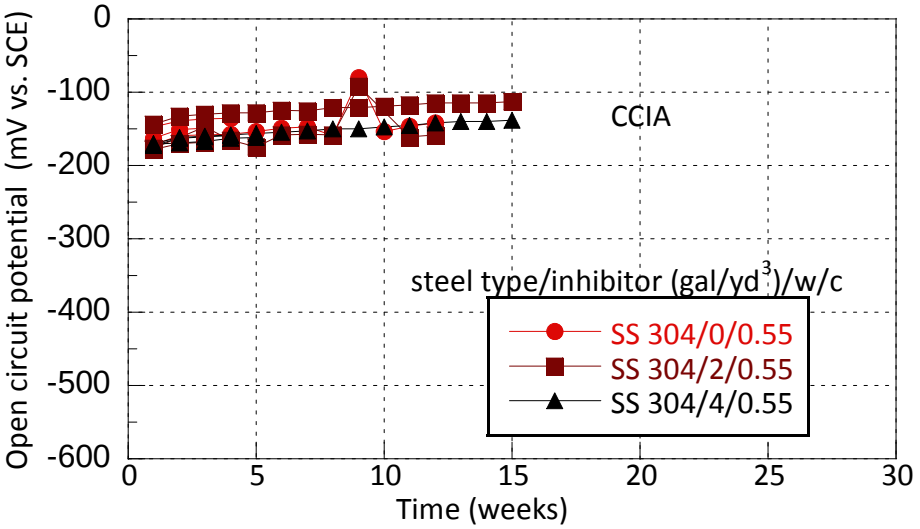


**Figure IV-110 CCIA Phase II – OCP Values of SS304 Samples Embedded in Mortar with w/c of 0.55.**

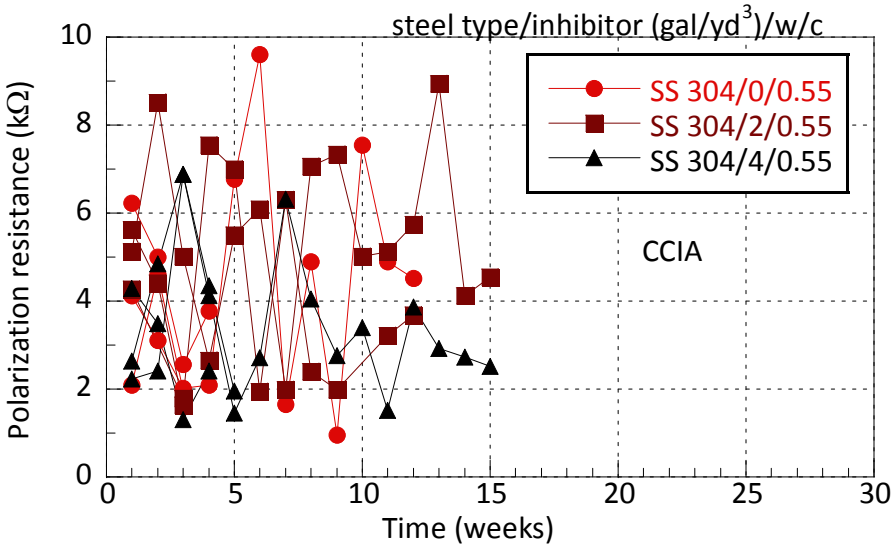


**Figure IV-111 CCIA Phase II – Polarization Resistance of SS304 Samples Embedded in Mortar with w/c of 0.55.**

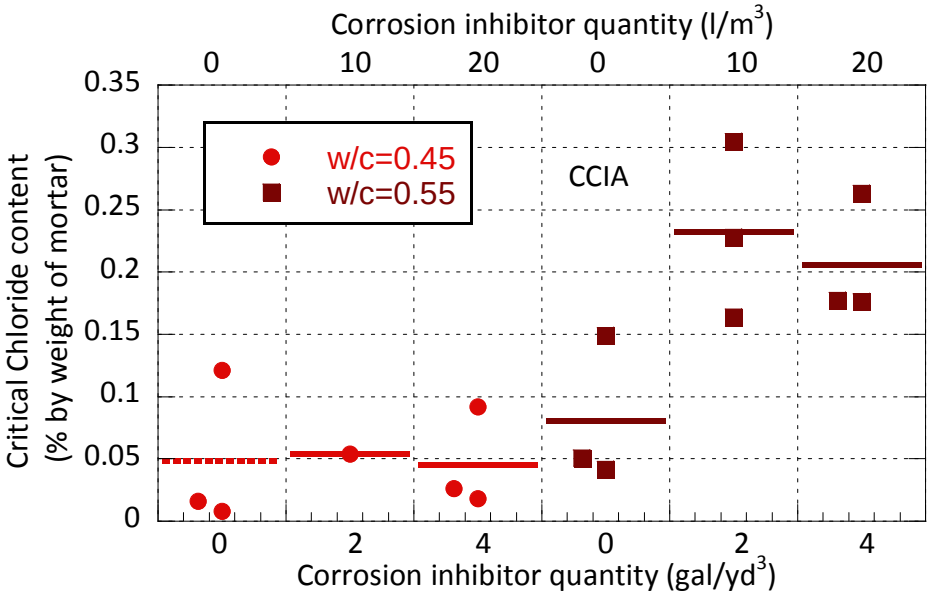


**Figure IV-112 CCIA Phase II – Chloride Content of SS304 Samples at Activation.**

A comparison of Figure IV-98 and Figure IV-112 indicate that the chloride threshold values determined for the SS304 samples in the two phases were very different. The inconsistency of activation indicators for these samples and the random active and passive behavior of continued samples in addition to the difference in results obtained from two phases indicate that the CCIA test may not be applicable to corrosion resistant steel samples. Similarly, comparison of Figure IV-72 and Figure IV-105 show that the chloride threshold values obtained for the ASTM A 615 samples from the two phases are very different, with the results obtained in the second phase being significantly lower. Researchers suspect that lower chloride threshold values and faster activation times may be due to cracks generated during the cutting of second phase samples. The relatively poor repeatability of the results may be an indicator of the susceptibility of this test method to small changes in the procedure when the testing is performed by different researchers and at different times.

Analysis of the results of both phases show that the CCIA test can be used to evaluate ASTM A 615 and A 706 samples and seems to be a reasonable test for evaluating the effect of calcium nitrite inhibitor. This test may be applicable for other inhibitor types. All indicators used to determine activation were consistent for these types of samples, however the results obtained from two phases for the ASTM A 615 samples were very different. Analysis showed that the test method was not applicable to epoxy coated samples because they either did not activate or could not be tested using linear polarization method. Use of CCIA test on galvanized steel samples is not recommended either, because these samples showed activation right from the beginning of the test due to the different corrosion rates and potentials of zinc in high pH environment. The use of CCIA test method to test stainless steel samples is also not recommended since the indicators used to determine activation were not consistent, and continued samples became active and passive randomly throughout the test. Also the results obtained from the two phases of testing were very different showing poor repeatability. The stainless steel (304) samples exhibited the highest chloride threshold values, higher than the ASTM A 706 and A 615 samples that were embedded in mortar with low water-cement ratios and highest corrosion inhibitor concentration. As such, this test may be applicable for assessing the corrosion performance of various reinforcement types assuming the potential issue with repeatability can be resolved.

### 4.2.4 ASTM G 109 and modified ASTM G 109

The ASTM G 109 samples and the modified G109 samples (MG 109) were only fabricated in Phase I of this research due to the very long duration these tests require to complete. After 49 months of testing, some samples still have not activated for both tests, G109 and MG109. At the time of writing of this report, 70 out of 216 G 109 samples (32 percent) were active and evaluated up to 49 months. A total of 159 samples out of 335 MG 109 samples (47 percent) activated. The total charge passed through the resistor between the two layers of reinforcement was monitored for both sample types, and samples were identified as being active when a total charge of 150 Coulombs or more passed through the resistor. Figure IV-113 shows as an example the total charge passing through G 109 samples containing ASTM A 615 rebar. These bars were embedded in mortar with a water-cement ratio of 0.55 and without a corrosion inhibitor. As the figure shows, the macrocell current and therefore the total charge passing through the samples at the beginning of the test are very small. Both begin increasing at the point of activation, and when the total charge passing through the resistor reaches 150 Coulombs, testing is stopped. Figures for the other activated samples showing the total charge passing through G109 and MG109 samples and their activation time are provided in Appendix B.

The MG 109 testing was performed following the standard of ASMT G 109; however, the samples were maintained at a high temperature environment to reduce the time to activation. Galvanized steel samples and epoxy coated steel samples were tested only using the MG 109 samples. Figure IV-114 and Figure IV-115 show the cumulative number of samples that activated over the duration of the test for G 109 and MG 109 samples, respectively.

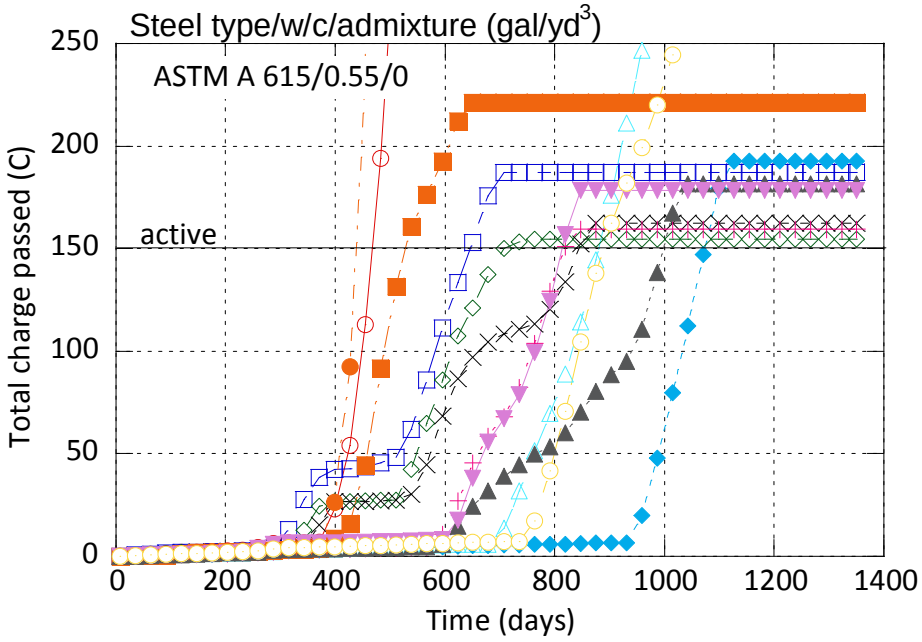


**Figure IV-113 Total Charge Passing through the Resistor for G109 Samples with ASTM A 615 Rebar.**

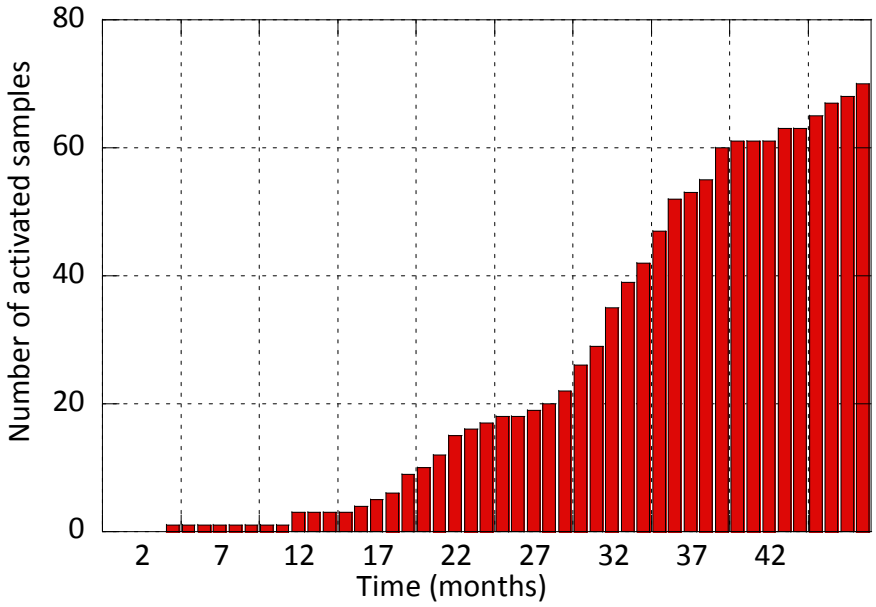


**Figure IV-114 Number of Activated G 109 Samples Plotted vs. Time.**

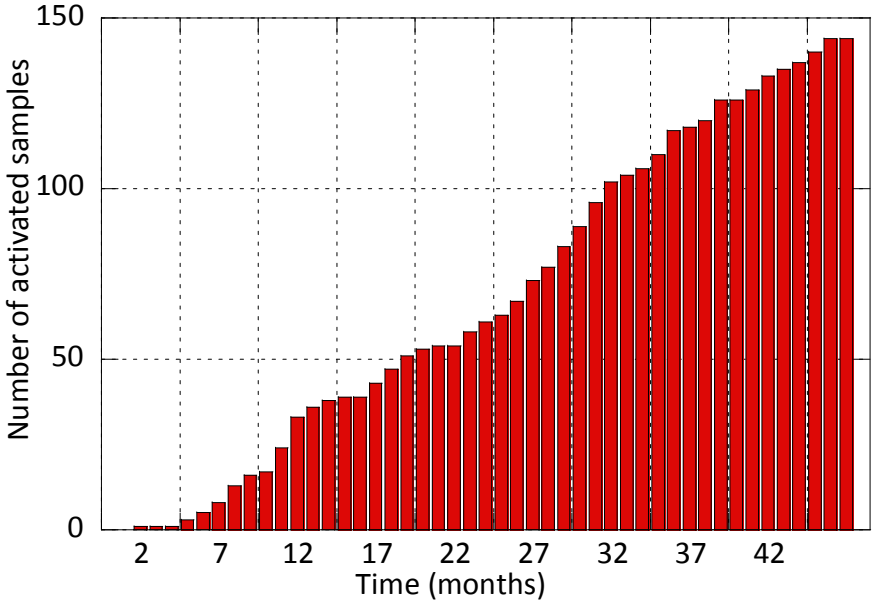


**Figure IV-115 Number of Activated MG 109 Samples Plotted vs. Time.**

Table IV-9 shows the number of active G 109 samples and their average time to activation for each reinforcement steel and concrete mixture combination. Evaluation of the results in this table clearly shows the important effect of water-cement ratio. Only two ASTM A 706 and one ASTM A 615 samples showed activation among the samples that were embedded in concrete with a water-cement ratio of 0.45. A large portion of the ASTM A 615 and A 706 samples that were embedded in concrete with a water-cement ratio of 0.55 activated. Although the average time to activation seems to increase for ASTM A 615 and A 706 samples when corrosion inhibitor level was increased from 0 to 2 and 4 gal/yd$^3$, (0 to 10 and 20 l/m$^3$) statistical analysis of chloride threshold values shown in Figure IV-116 and Figure IV-117 show that the difference between different corrosion inhibitor levels among the samples with a water-cement ratio of 0.55 was not significant. For ASTM A 706 samples, the average chloride threshold value increased with increasing corrosion inhibitor level, but due to increased variability the differences were not statistically significant. The 95 percent confidence interval for the mean chloride threshold of ASTM A 615 samples was 0.21 to 0.29 percent by weight of concrete. The 95 percent confidence interval for the mean chloride threshold of ASTM A 706 samples was 0.19 to 0.25 percent by weight of concrete. Comparison of the chloride threshold values for ASTM A 615 and A 706 samples indicated that their difference was statistically insignificant. With the exception of one sample, none of the G109 samples containing a

stainless steel rebar showed activation; therefore not much can be deduced from the results about the stainless steel samples except that they will not be active in 49 months.

**Table IV-9 Activated G 109 Samples and Their Average Activation Time.**

| Water-Cement Ratio | Admixture Content, gal/yd$^3$ (l/m$^3$) | Rebar Type | No. of Test Setups | Active Samples | Average Time to Activation (weeks) |
|---|---|---|---|---|---|
| 0.45 | 0 (0) | A 615 | 12 | 0 | - |
| | | A 706 | 12 | 2 | 21 |
| | | SS304 | 12 | 0 | -* |
| | 2 (10) | A 615 | 12 | 1 | 12 |
| | | A 706 | 12 | 0 | -* |
| | | SS304 | 12 | 0 | -* |
| | 4 (20) | A 615 | 12 | 0 | -* |
| | | A 706 | 12 | 0 | -* |
| | | SS304 | 12 | 0 | -* |
| 0.55 | 0 (0) | A 615 | 12 | 12 | 27.3 |
| | | A 706 | 12 | 11 | 24.5 |
| | | SS304 | 12 | 0 | -* |
| | 2 (10) | A 615 | 12 | 11 | 35 |
| | | A 706 | 12 | 9 | 36 |
| | | SS304 | 12 | 1 | 19 |
| | 4 (20) | A 615 | 12 | 8 | 32.6 |
| | | A 706 | 12 | 11 | 37 |
| | | SS304 | 12 | 0 | - |

"-*" Average time to activation cannot be calculated because there are no active samples.

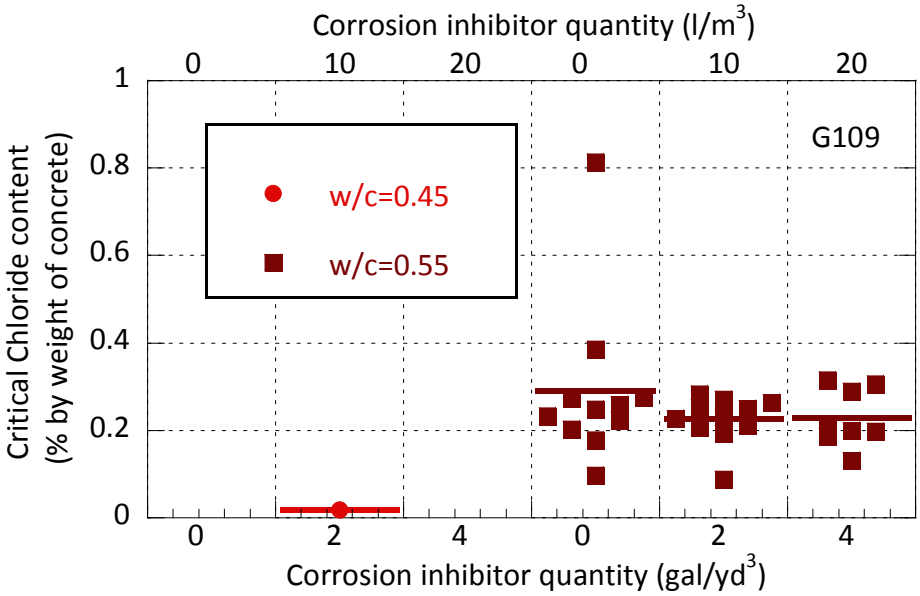


**Figure IV-116 G 109 Test: Chloride Content of ASTM A 615 Samples.**

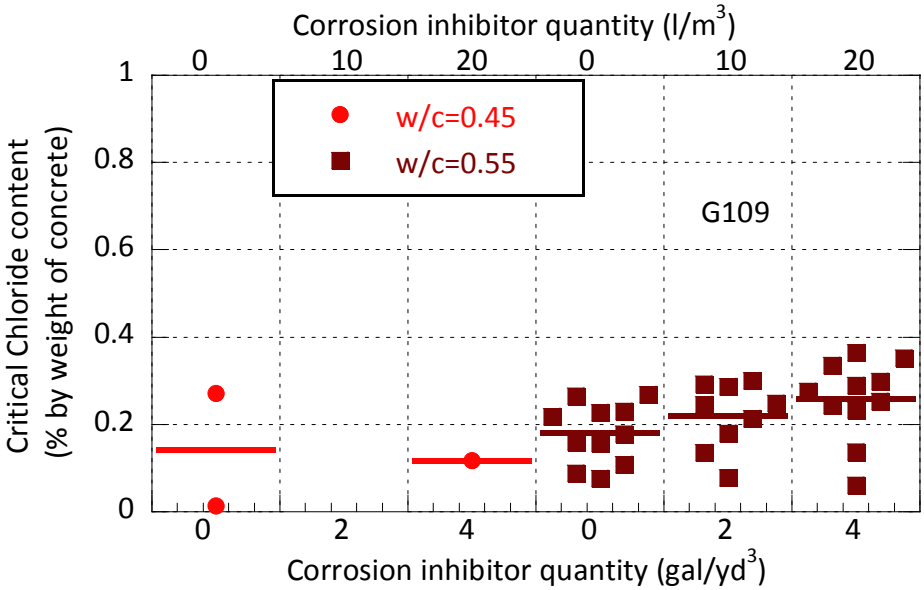


**Figure IV-117 G 109 Test: Chloride Content of ASTM A 706 Samples.**

Table IV-10 and Table IV-11 show the number of activated MG 109 samples and their average time to activation for each rebar concrete mixture combination. Table IV-10 shows that

when compared to the G 109 samples, the number of activated samples increases. This indicates that the concept of keeping the samples at an elevated temperature to accelerate the test is valid. Similar to the G 109 testing, none of the stainless steel samples activated. In addition to the stainless steel samples, none of the epoxy coated samples (damaged or undamaged activated in MG109 testing) activated. However, this may be a result of the area being used to calculate the corrosion rates.

Both the ASTM A 615 and A 706 samples exhibited similar average time to activation. Figure IV-118 and Figure IV-119 show the critical chloride threshold values measured from MG 109 samples containing A 615 and A 706 reinforcement. Mean critical chloride threshold values between different corrosion inhibitors and between different water-cement ratios are not statistically significantly different from each other for both types of rebar. The 95 percent confidence interval for ASTM A 615 samples with water-cement ratio of 0.45 (all corrosion inhibitor levels combined) was 0.38 to 0.51 percent chloride by weight of concrete. The 95 percent confidence interval for ASTM A 615 samples with a water-cement ratio of 0.55 (all corrosion inhibitor levels combined) was 0.32 to 0.43 percent chloride by weight of concrete. The mean chloride threshold data obtained using the MG 109 samples for ASMT A 615 bars embedded in concrete with a water-cement ratio of 0.55 is statistically significantly different and greater than the threshold value obtained from G 109 samples and greater. ASTM A 615 samples embedded in concrete with a water-cement ratio of 0.45 cannot be compared because most of the G 109 samples have not yet activated.

The 95 percent confidence interval for ASTM A 706 samples with a water-cement ratio of 0.45 (all corrosion inhibitor levels combined) was 0.33 to 0.48 percent chloride by weight of concrete. This data cannot be compared with G 109 data because of the lack of activated G 109 samples containing ASTM A 706. The 95 percent confidence interval for the ASTM A 706 samples with a water-cement ratio of 0.55 (all corrosion inhibitor levels combined) was 0.32 to 0.55 percent chloride by weight of concrete. The chloride threshold results obtained from the MG 109 samples with a water-cement ratio of 0.55 and containing A 706 is statistically significantly different and greater from the mean value obtained using the G 109 samples.

MG 109 samples containing galvanized reinforcement, except the two drill damaged samples embedded in concrete with a water-cement ratio of 0.45, exhibited activation as shown in Table IV-11. Figure IV-120 shows the measured chloride threshold values for damaged and undamaged galvanized steel samples. Only a limited number of galvanized steel samples were

tested, therefore comparisons of chloride threshold values were made on the assumption of normal distribution. Results indicated that the effect of the water-cement ratio and damage type were both statistically insignificant. The 95 percent confidence interval for the combined galvanized steel MG 109 data was 0.39 to 0.59 percent by weight of concrete.

**Table IV-10 Activated MG 109 Samples and Their Average Activation Time.**

| Water-Cement Ratio | Admixture Content, gal/yd$^3$ (l/m$^3$) | Rebar type | No. of Test Setups | Active Samples | Average Time to Activation (weeks) |
|---|---|---|---|---|---|
| 0.45 | 0 (0) | A 615 | 12 | 7 | 34.6 |
| | | A 706 | 12 | 9 | 30 |
| | | SS304 | 12 | 0 | - |
| | 2 (10) | A 615 | 12 | 9 | 33.3 |
| | | A 706 | 12 | 9 | 34.5 |
| | | SS304 | 12 | 0 | - |
| | 4 (20) | A 615 | 12 | 7 | 33.9 |
| | | A 706 | 12 | 10 | 36.8 |
| | | SS304 | 12 | 0 | - |
| 0.55 | 0 (0) | A 615 | 12 | 12 | 17.8 |
| | | A 706 | 12 | 11 | 24 |
| | | SS304 | 12 | 0 | - |
| | 2 (10) | A 615 | 12 | 10 | 22.8 |
| | | A 706 | 12 | 10 | 14 |
| | | SS304 | 12 | 0 | - |
| | 4 (20) | A 615 | 12 | 8 | 20.5 |
| | | A 706 | 12 | 6 | 23 |
| | | SS304 | 12 | 0 | - |

**Table IV-11 Activated MG 109 Samples Containing Coated Rebar and Their Average Activation Time.**

| Water-Cement Ratio | Damage Type[1] | Rebar Type[2] | No. of Test Setups | Active Samples | Average Time to Activation |
|---|---|---|---|---|---|
| 0.45 | ND | ECR | 4 | 0 | - |
| | | GR | 4 | 4 | 27.5 |
| | DD | ECR | 4 | 0 | - |
| | | GR | 4 | 2 | 38 |
| | FD | ECR | 4 | 0 | - |
| 0.55 | ND | ECR | 4 | 0 | - |
| | | GR | 4 | 4 | 26.3 |
| | DD | ECR | 4 | 0 | - |
| | | GR | 4 | 4 | 29.5 |
| | FD | ECR | 4 | 0 | - |

[1]ND: Not damaged, DD: Drill damaged, FD: File damaged
[2]ECR: Epoxy coated, GR: Galvanized reinforcement

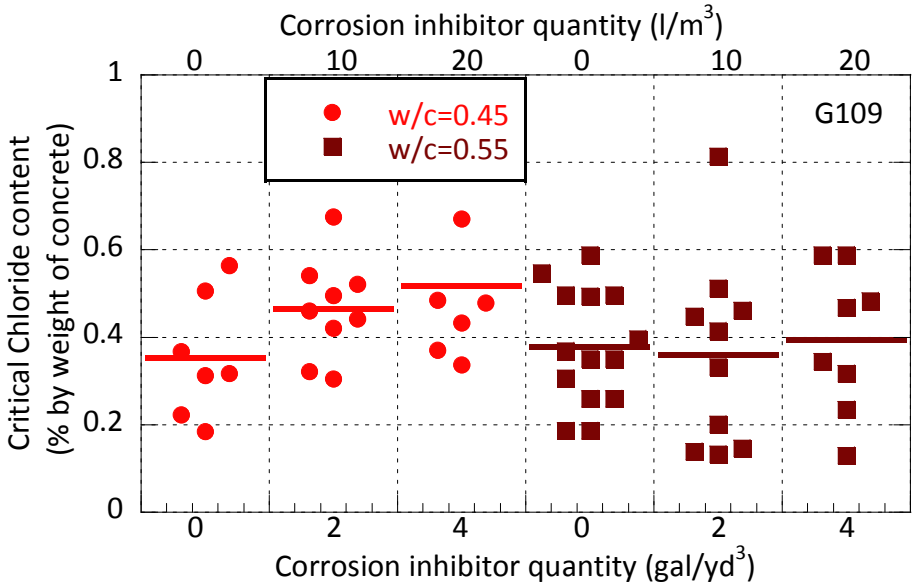


**Figure IV-118 MG 109 Test: Chloride Content of ASTM A 615 Samples.**

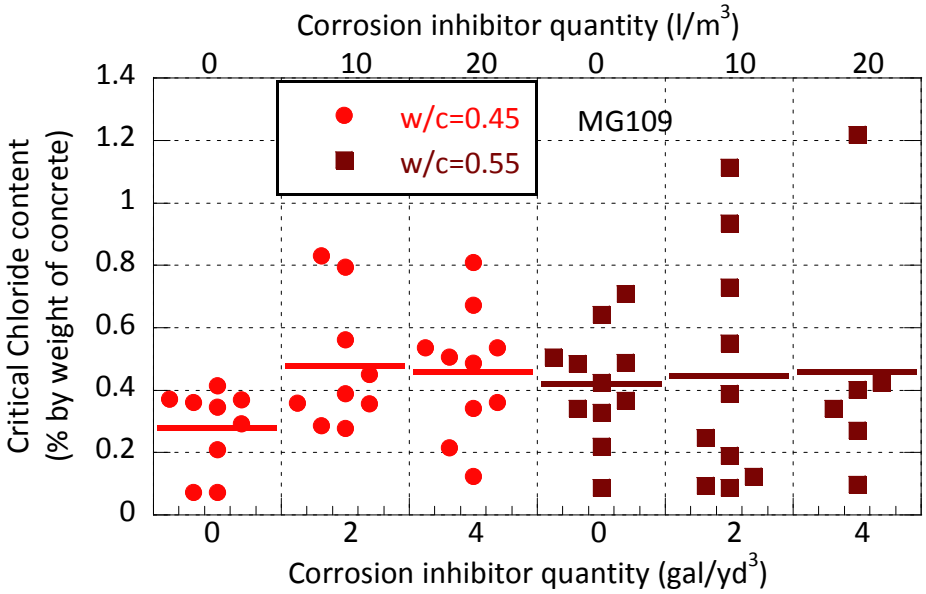


**Figure IV-119 MG 109 Test: Chloride Content of ASTM A 706 Samples.**

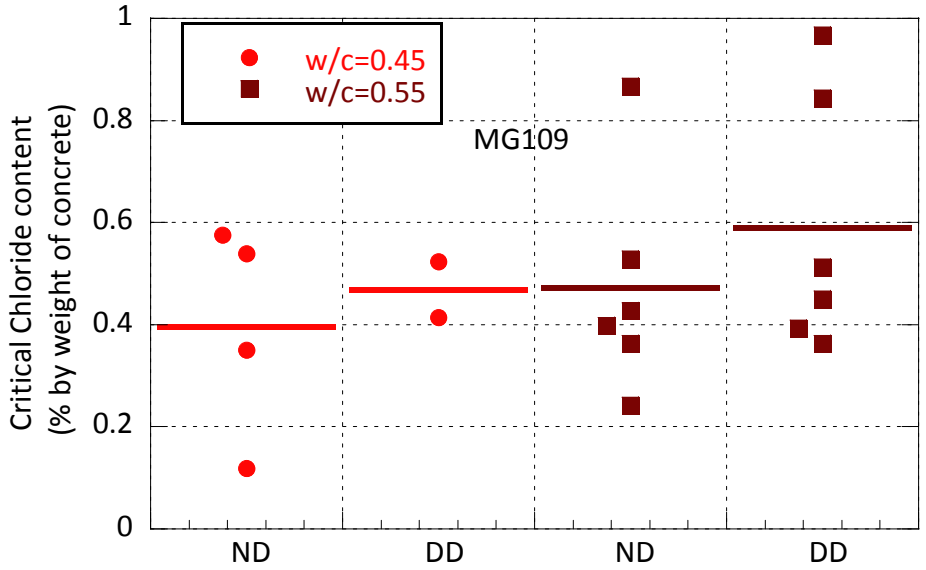


**Figure IV-120 MG 109 Test: Chloride Content of Galvanized Samples.**

## 4.3 SUMMARY

The research test program evaluated several test procedures to determine if these tests were capable of assessing key variables that can impact the corrosion susceptibility and service-life of structures containing steel reinforcement embedded in cementitious materials. It should be noted that as with most research programs not all variables of combination were assessed in this research. However, with the results obtained, the researchers can provide recommendations on possible test methods for assessing different variables that can influence corrosion performance. Table IV-12 shows recommendations for the technical feasibility of the different test methods assessed. These recommendations are based on the results of the research and engineering judgment to assess the potential applicability of the tests; results shown in the table do not consider time requirements, complexity of the tests, or cost considerations to perform the testing. Time requirements, complexity, and costs will be assessed in the following chapter. Engineering judgment is necessary as all ranges, variables, and combinations were not assessed.

**Table IV-12 Technical Feasibility of Various Test Procedures for Assessing Critical Parameters Influencing Corrosion.**

| Test Name | Assessment to Determine the | | | | |
|---|---|---|---|---|---|
| | **Corrosion Resistance of Uncoated Steel Reinforcement** | **Influence of Water-Cement Ratio** | **Influence of Chemical Admixture** | **Influence of Reinforcement Coating Type** | **Influence of Damage to Coated Reinforcement** |
| ASTM G 109 | Possible[2] | Possible | Possible | Possible | Possible |
| MG 109 | Possible[2] | Possible | Possible | Possible | Possible |
| MM[1] | Recommended | Recommended | Possible | Not Recommended | Recommended (ECR Only) |
| CCIA | Possible | Possible | Recommended[3] | Not Recommended | Not Recommended |
| ACT | Possible | Possible | Not recommended | Not Recommended | Not Recommended |

[1]Extreme care must be taken to ensure sample did not crack prior to initiation of test; cracked samples should be discarded.
[2]For higher water-cement ratios and reinforcement with lower critical chloride threshold values;
[3]For lower water-cement ratios as recommended by admixture manufacturer.

# CHAPTER V. ANALYSIS OF TEST PROCEDURES

## 5.1 INTRODUCTION

The previous chapters discussed the repeatability and appropriateness of different accelerated corrosion tests and compared these with long-term, more established corrosion test procedures. If a test procedure is identified that provides a good estimate of key parameters for assessing the corrosion performance of the reinforcement in concrete, the usefulness of the tests would only be considered as value added, if the test can be completed in a relatively short duration, is economical, and is simple to perform. The following sections present results from investigations on the test duration, test cost, and simplicity of the rapid macrocell, ACT, CCIA, G109, and MG109 tests. Tests that are fast, inexpensive, simple to perform, repeatable, and provide realistic results are preferred.

## 5.2 TEST DURATION

The time it takes to complete corrosion testing of a new product is a very important aspect of a test method. The large number of new products being offered by manufacturers and the required evaluation of these products can place a significant burden on State Highway Authorities (SHA) personnel. Although SHA policy should be to identify products that can resist corrosion and extend service-lives of infrastructure, the significant amount of resources required to assess new types of steel or concrete products for improved performance is overwhelming. New assessment methods and procedures are necessary.

The average testing times (average time to activation) of the test methods evaluated in this study are shown in Figure V-1. The rapid macrocell test does not have an activation criteria, and its duration is limited by the standard to a 15-week period. The average time to complete the ACT testing with its current standard is approximately 20 days. However, if the recommended change is implemented and the initial polarization resistance and OCP readings are evaluated without the initial 36 hours of voltage application, the average time to complete the test (for the statistical method to show activation) increases to approximately 50 days. The testing time for the CCIA test varied significantly between samples with different water-cement ratio values. Epoxy coated samples were tested for more than 40 weeks but showed no

activation. Results indicate that the CCIA test may take from 4 to 36 weeks to complete based on the type of steel and concrete mixture if used to evaluate undamaged epoxy coated samples.

The ASTM G 109 test is a long-term test and results indicate that after 49 months of testing samples with a water-cement ratio of 0.45 and samples containing stainless steel did not activate. The test durations shown on Figure V-1 are only valid for conventional reinforcing bars embedded in concrete with a water-cement ratio of 0.55. The modified G 109 test decreases the test duration for all standard reinforcing bar types at water-cement ratio values varying between 0.45 and 0.55 to a period from 17 to 38 months. Epoxy coated samples and stainless steel samples tested using the MG 109 test did not activate as of the writing of this report (48 months of exposure).

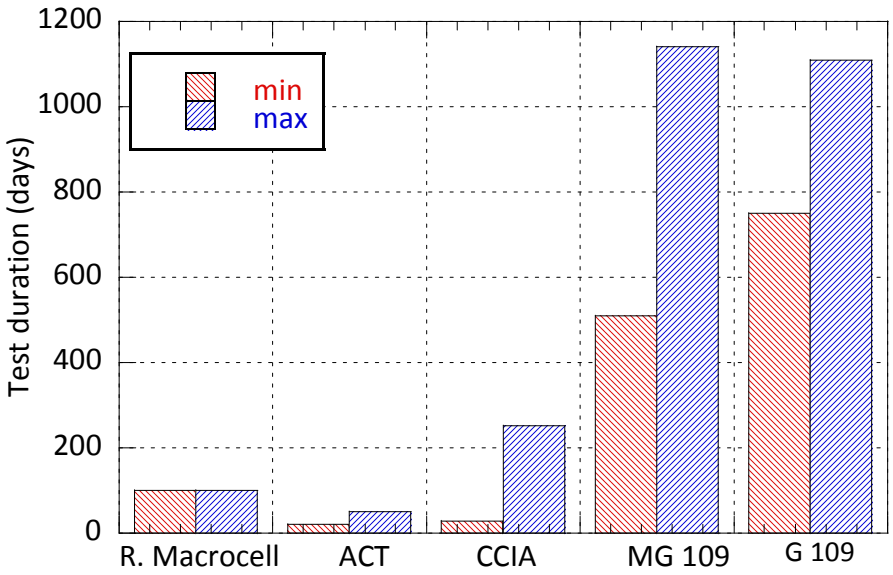


**Figure V-1 Average Durations of Different Test Methods.**

Figure V-1 clearly shows that significant time savings can be achieved by the SHAs by implementing an accelerated corrosion test procedure. It should be noted again that the durations shown in the figure are only for the samples that activated during this test program. It should also be noted that the durations shown in Figure V-1 are only for the duration of actual testing and does not include sample preparation and curing time. Curing time is similar for all

test methods and the sample preparation times are negligible compared to the actual test durations.

## 5.3 COST AND COMPLEXITY

Another important aspect of a test method that needs to be considered when implementing new tests is the cost and complexity of the test. The estimated costs to perform the various test methods were evaluated as part of this research. The cost of each test has two main components: the cost of the test setup (including costs to fabricate components) and the cost of performing the test. Table V-1 through Table V-4 show the costs required to fabricate the test components for each test method. It should be noted that this cost is for 20 samples. This provides a more realistic cost of the specimens as it tends to spread setup time over the cost of more samples. Figure V-2 shows fabrication costs of all test methods. The figure clearly shows that the fabrication cost of the rapid test methods, such as the ACT and rapid macrocell, is much higher compared to the cost of fabricating standard G 109 samples. However, using only fabrication costs to determine which method to use would not be cost effective because the costs required to perform the testing could be significantly higher than the fabrication costs.

**Table V-1 Fabrication Cost of G 109 and M G 109.**

| Description | Quantity | Unit | Unit Cost | Labor (hr) | Cost/hr | Total Cost |
|---|---|---|---|---|---|---|
| Concrete | 0.106 | $yd^3$ | $95 | 3 | $25 | $85 |
| Formwork | 28.4 | $ft^2$ | $0.80 | 24 | $25 | $623 |
| Steel #4 (#13) | 0.027 | ton | $1,200 | 4 | $25 | $132 |
| Steel preparation | | | | 8 | $25 | $200 |
| **Total** | | | | | | $1,040 |

**Table V-2 Fabrication Cost of CCIA.**

| Description | Quantity | Unit | Unit Cost | Labor (hr) | Cost/hr | Total Cost |
|---|---|---|---|---|---|---|
| Concrete | 0.211 | $yd^3$ | $95 | 3 | $25 | $95 |
| Formwork | 20 | cylinder | $1.35 | 1 | $25 | $52 |
| Steel #4 (#13) | 0.027 | ton | $1,200 | 4 | $25 | $132 |
| Steel preparation | | | | 8 | $25 | $200 |
| Cut and epoxy | 1 | can | $100 | 5 | $25 | $225 |
| **Total** | | | | | | $704 |

**Table V-3 Fabrication Cost of ACT.**

| Description | Quantity | Unit | Unit Cost | Labor (hr) | Cost/hr | Total cost |
|---|---|---|---|---|---|---|
| Concrete | 0.042 | $yd^3$ | $95 | 3 | $25 | $79 |
| Formwork | 20 | canister | $100.00 | 1 | $25 | $2,025 |
| Steel #4 (#13) | 0 | ton | $1,200 | 0 | $25 | $0 |
| Steel preparation | | | | 8 | $25 | $200 |
| **Total** | | | | | | $2,304 |

**Table V-4 Fabrication Cost of Rapid Macrocell Test Samples.**

| Description | Quantity | Unit | Unit Cost | Labor (hr) | Cost/hr | Total Cost |
|---|---|---|---|---|---|---|
| Concrete | 0.042 | $yd^3$ | $95 | 3 | $25 | $79 |
| Formwork | 1 | ea | $120.00 | 0 | $25 | $120 |
| Steel #4 (#13) | 0.00675 | ton | $1,200 | 1 | $25 | $33 |
| Steel preparation | | | | 2 | $25 | $50 |
| Cups | 40 | ea | $4 | 2 | $25 | $210 |
| Salt bridge | | | | 10 | $25 | $250 |
| Agar | 1 | can | $65 | 0 | $25 | $65 |
| Tubing | 40 | ft | $0.13 | 0 | $25 | $5 |
| Heating plate | 1 | ea | $700.00 | 0 | $25 | $700 |
| Air scrubber | | | | 3 | $25 | $75 |
| Nalgene container | 1 | ea | $90.00 | 1 | $25 | $115 |
| NaOH | 1 | can | $160.00 | 0 | $25 | $160 |
| Pump | 1 | ea | $650.00 | 0 | $25 | $650 |
| Connections | | | | 3 | $25 | $75 |
| **Total** | | | | | | $2,587 |

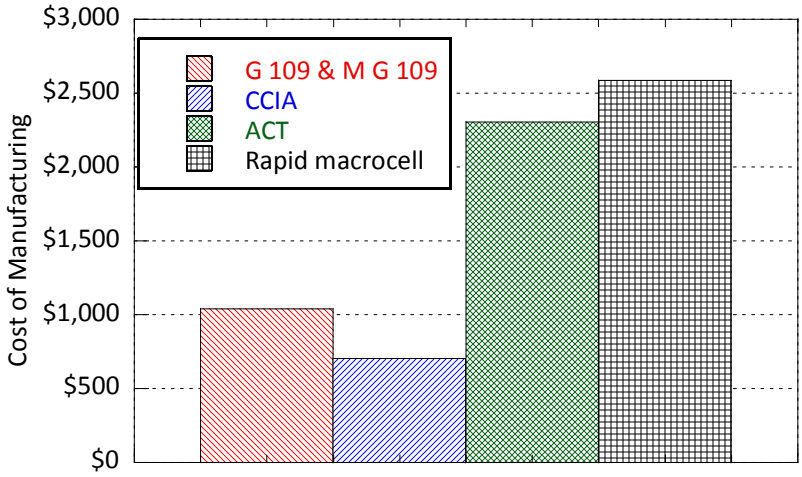


**Figure V-2 Manufacturing Costs of Corrosion Tests.**

Table V-5 to Table V-9 show the operational costs of each test method, i.e., the costs of daily operations to maintain the samples and to collect the data and the cost of necessary equipment for these tests. Each table shows the total operational cost of the corrosion test per month and the minimum and maximum total expected operational costs for a set of 20 samples. The total minimum and maximum costs are calculated based on the minimum and maximum test duration values shown in Figure V-1 for each test method. When calculating the minimum and maximum costs, the cost of necessary operational equipment is not multiplied with duration because these items will only be purchased once at the beginning of the test. Figure V-3 shows the total manufacturing and operational costs for each of the test methods. Figure V-4 shows the total manufacturing and operational costs without the one-time cost of operational equipment (e.g., potentiostat, multimeter) and without the one-time cost of manufacturing equipment (e.g., air scrubber). This allows for the comparison of the pure operational cost for a set of 20 samples after the initial investment for each test. Evaluation of costs shown in Figure V-4 shows that rapid methods can actually save money by decreasing the total manufacturing and operational costs after the initial investment in addition to decreasing the test duration significantly.

**Table V-5 Operational Cost for G 109.**

| Description | Quantity | Unit | Unit Cost | Labor (hr) | Cost/hr | Total Cost |
|---|---|---|---|---|---|---|
| Mix solution | 0 | - | - | 1 | $25 | $25 |
| Pond | 0 | - | - | 0.5 | $25 | $13 |
| Dry | 0 | - | - | 0.5 | $25 | $13 |
| Macrocell reading | 0 | - | - | 0.5 | $25 | $13 |
| Multimeter | 1 | ea | $150 | 0 | $25 | $150 |
| Maintenance | | | | 4 | $25 | $100 |
| Total/month | | | | | | $313 |
| Total min | | | | | | $4,213 |
| Total max | | | | | | $6,163 |

**Table V-6 Operational Cost for MG 109.**

| Description | Quantity | Unit | Unit Cost | Labor (hr) | Cost/hr | Total Cost |
|---|---|---|---|---|---|---|
| Mix solution | 0 | - | - | 1 | $25 | $25 |
| Pond | 0 | - | - | 0.5 | $25 | $13 |
| Dry | 0 | - | - | 0.5 | $25 | $13 |
| Macrocell reading | 0 | - | - | 0.5 | $25 | $13 |
| Maintenance | | | | 4 | $25 | $100 |
| Multimeter | 1 | ea | $150 | 0 | $25 | $150 |
| Environmental chamber | 1 | ea | $7,500 | 0 | $25 | $7,500 |
| Total/month | | | | | | $7,813 |
| Total min | | | | | | $10,413 |
| Total max | | | | | | $13,825 |

**Table V-7 Operational Cost for CCIA.**

| Description | Quantity | Unit | Unit Cost | Labor (hr) | Cost/hr | Total Cost |
|---|---|---|---|---|---|---|
| Mix solution | 0 | - | - | 2 | $25 | $50 |
| Pond | 0 | - | - | 2 | $25 | $50 |
| Dry | 0 | - | - | 2 | $25 | $50 |
| Macrocell reading | 0 | - | - | 2 | $25 | $50 |
| Linear polarization | 0 | - | - | 5 | $25 | $125 |
| Multimeter | 1 | ea | $150 | 0 | $25 | $150 |
| Potentiostat | 1 | ea | $5,000 | 0 | $25 | $5,000 |
| Electrode | 1 | ea | $200 | 0 | $25 | $200 |
| Total/month | | | | | | $5,675 |
| Total min | | | | | | $5,675 |
| Total max | | | | | | $8,080 |

**Table V-8 Operational Cost for ACT.**

| Description | Quantity | Unit | Unit Cost | Labor (hr) | Cost/hr | Total Cost |
|---|---|---|---|---|---|---|
| Mix solution | 0 | - | - | 0.5 | $25 | $13 |
| Pond | 0 | - | - | 0.5 | $25 | $13 |
| Dry | 0 | - | - | 0.5 | $25 | $13 |
| Linear polarization | 0 | - | - | 5 | $25 | $125 |
| Potentiostat | 1 | ea | $5,000 | 0 | $25 | $5,000 |
| Electrode | 1 | ea | $200 | 0 | $25 | $200 |
| Total/month | | | | | | $5,363 |
| Total min | | | | | | $5,308 |
| Total max | | | | | | $5,471 |

**Table V-9 Operational Cost for Rapid Macrocell Test.**

| Description | Quantity | Unit | Unit Cost | Labor (hr) | Cost/hr | Total Cost |
|---|---|---|---|---|---|---|
| Mix solution | 0 | - | - | 0.5 | $25 | $13 |
| Pond | 0 | - | - | 0.5 | $25 | $13 |
| Dry | 0 | - | - | 0.5 | $25 | $13 |
| Macrocell reading | 0 | - | - | 2 | $25 | $50 |
| Maintenance | 0 | - | - | 4 | $25 | $100 |
| Multimeter | 1 | ea | $150 | 0 | $25 | $150 |
| Electrode | 1 | ea | $200 | 0 | $25 | $200 |
| Total/month | | | | | | $538 |
| Total min | | | | | | $975 |
| Total max | | | | | | $975 |

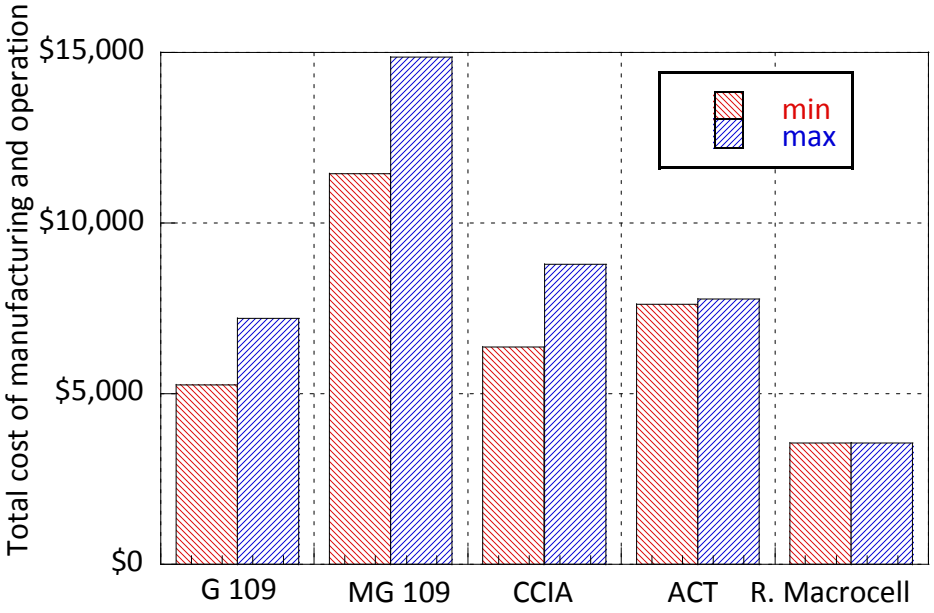


**Figure V-3 Total Manufacturing and Operational Costs.**

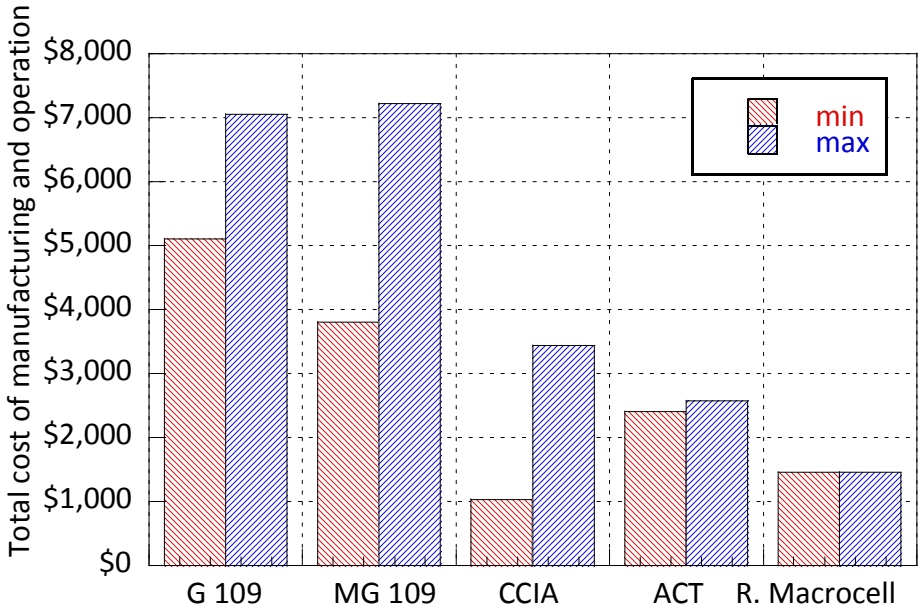


**Figure V-4 Total Manufacturing and Operational Costs without One-Time Cost Items.**

For a corrosion test to be easily implemented by a SHA, the test should be simple and its cost and time required to perform the test should be minimized. Unlike cost and duration, complexity of a corrosion test cannot be quantitatively measured. However, based on the experience of the researchers, test complexity was qualitatively assessed for the different corrosion tests. The assessment was based on a scale of 1 to 5 with 5 being the most complex test method. Details of assembling the test samples, the probability of making mistakes, and the required analysis of the collected raw data were considered in assessing the complexity ranking of corrosion tests. The total average test costs with and without the one-time cost items versus test complexity are shown in Figures V-5 and V-6, respectively. Because the rapid macrocell test has the lowest average total cost with or without the one-time cost items, in Figures V-5 and V-6 the total average cost of all tests are shown as multiples of the cost of the rapid macrocell test. Test methods closer to the origin would be easier to implement and are more cost effective than the other tests. However, the research showed that not all tests are applicable for assessing all materials and conditions. Implementing the simplest and least expensive test should be done only when the test is appropriate for the variable being assessed.

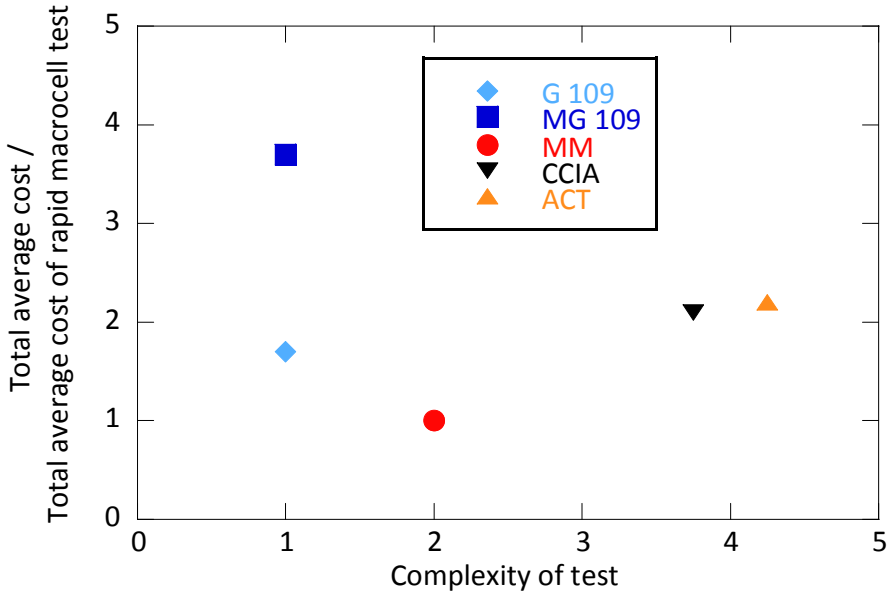


**Figure V-5 Average Total Cost vs. Complexity of Corrosion Tests.**

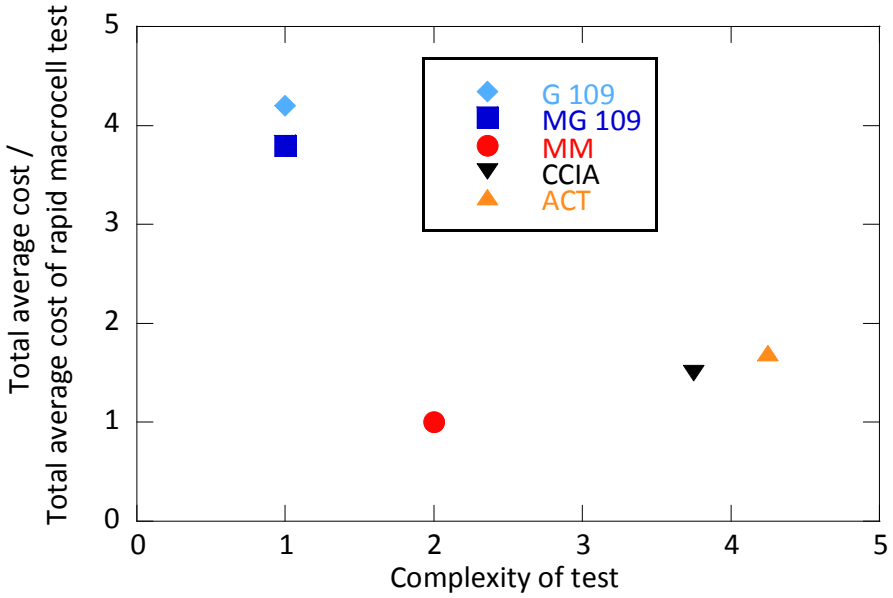


**Figure V-6 Average Total Cost without One-Time Cost Items vs. Complexity of Corrosion Tests.**

## 5.4 SUMMARY

The preceding sections assessed the time requirements, costs, and complexity of the tests evaluated in this research. Table V-10 shows a summary of the assessment with rankings for each test. In the table, a value of 1 is considered to be the best value, and a ranking of 5 is considered to be the worst ranking. In general, a ranking of 5 should require that TxDOT has a specific resource. For the G109 and MG 109 tests this resource would be time; for the ACT test, this resource would be expertise of the personnel performing the tests. Assuming only the cost of the test, the time required to perform the test, and complexity of the test, the tests are ranked in the following order: 1) MM, 2) CCIA, 3) ACT, 4) MG 109, and 5) G 109. Based on the cost, time, and complexity of these tests, the lower ranked tests should be considered before the higher ranked tests. Note that this does not consider applicability of the test, which was discussed earlier.

**Table V-10 Relative Rankings based on Cost, Time, and Complexity of Tests (1 Is Best).**

| Test Name | Ranking based on: | | |
|---|---|---|---|
| | Cost | Time | Complexity |
| ASTM G 109 | 5 | 5 | 1 |
| MG 109 | 4 | 4 | 1 |
| MM | 1 | 2 | 3 |
| CCIA | 2 | 3 | 4 |
| ACT | 3 | 1 | 5 |

# CHAPTER VI. SUMMARY, CONCLUSIONS, AND RECOMMENDATIONS

## 6.1 SUMMARY

The cost of corrosion of infrastructure elements is significant. As new products are developed to address the challenge of reducing corrosion, these products have to be objectively assessed to determine their effectiveness. SHAs do not have the resources to evaluate all products, nor should it be the responsibility of this agency to do this. However, if products can improve the corrosion resistance of infrastructure components and systems, there could be significant value added by implementing the use of these products. A methodology is needed to validate the corrosion performance of new products while at the same time reducing the time and costs necessary to evaluate the performance of these systems.

This research found that the MM test is relatively simple to perform and provides reasonable results for most products in a reasonable time frame with minimal relative cost. The CCIA and ACT tests can provide reasonable results over short periods with relatively low costs but these tests require polarization resistance testing to provide quantitative data. The polarization resistance testing is not commonly performed in SHAs and is considered difficult and complex. The ASTM G 109 and MG 109 tests are simple but can take significant time and effort to determine effectiveness of a product. In most cases the time required to assess the effectiveness of a product is well beyond the time a manufacturer or producer can wait to implement the new product.

## 6.2 CONCLUSIONS

Five different corrosion test methods were evaluated in this report to evaluate their effectiveness in assessing corrosion performance. In addition, comparisons between the results were made with the standard conventional test method, ASTM G 109. Results indicated that SHAs can save considerable time and money by using one of the rapid methods instead of the standard ASTM G 109 method. Although no methods can assess all variables that influence corrosion, the research indicates that information can be gleaned from the rapid tests. Although all tests have benefits and could be considered for evaluating the different variables, the expertise and

time available must be considered before performing the tests. Based on the testing performed in this research, the MM test was identified as providing the most reasonable assessment of different variables for assessing corrosion performance. In addition, this test is relatively economical and can be completed in a relatively short time frame.

## 6.3 RECOMMENDATIONS

The researchers believe the SHAs should not be required to assess new materials for corrosion performance. Realizing that there could be potential value added to the infrastructure and taxpayers, new products should be evaluated. It is recommended that evaluation of products for improved corrosion resistance be performed by independent organizations qualified to assess the product. TxDOT should provide approval of the organization. In addition to the independent assessment, it is recommended that TxDOT perform or contract an agency to perform a limited number of tests to validate the tests from the independent organization. Simple comparison of means tests can be performed to assess the validity of the results performed by the independent organization and TxDOT (or TxDOT's representative). Consistent application of procedures by experienced technicians is very important to obtain reasonable results and to analyze and draw correct conclusions from obtained data. Procedures presented in this program should be used.

Although the researchers believe that the task of testing and evaluating new materials and methods should be contracted to experienced independent research agencies and laboratories, the decisions on which method to use and what kind of experimental program to use should still be made by the SHA. Results of this study showed that different test methods may be more sensitive to different variables, and different test methods may be more appropriate to test different materials.

It is recommended that the MM test be specified to evaluate the corrosion performance instead of the standard ASTM G 109 test. The ASTM G 109 samples take excessive time to activate. Evaluation of results obtained from the MM test were compared with the ASTM G 109 results and were found to be similar for regular steel samples embedded in concrete mixtures with a water-cement ratio of 0.55. Both methods showed that the corrosion exhibited by stainless steel was negligible. For conventional steel samples, the MM method was sensitive to different water-cement ratios and corrosion inhibitor levels. An additional advantage of the

MM test is its fixed duration that would allow the SHAs to know exactly how long it will take to complete the corrosion testing.

Although the MM test is a faster and more feasible alternative to the ASTM G 109 method, results indicate that it cannot be used to test dielectric (epoxy) coated samples. No accelerated test method was identified to quickly evaluate dielectrically coated reinforcement. As such, it is recommended that the MG 109 test be used. However, additional research should be performed to identify alternative reliable and accelerated tests.

If the objective of the SHA is to evaluate the critical chloride threshold of the system being examined, the MM test cannot produce these data. In this case, it is recommended that the CCIA test or ACT test be used. The CCIA test can provide the SHAs with instantaneous corrosion rates as well as total corrosion loss and critical chloride threshold data. Results obtained from the CCIA test were similar to the results of ASTM G 109 testing at a water-cement ratio of 0.55 for conventional steel samples. However, it should be noted that the CCIA method was not found to be an appropriate test to test epoxy coated, galvanized, and stainless steel samples. The ACT test was found to be able to evaluate corrosion resistant reinforcement in earlier studies.

As with any testing, the corrosion test plan will have to determine the number of samples to be tested. Because of the large scatter common with corrosion testing, it is recommended that a minimum of 15 samples of the accelerated test be evaluated by the independent testing agency. Additional samples may be needed. It is also recommended that at least three samples be tested by TxDOT or its representative. Control samples must also be fabricated and tested to compare the performance of the proposed system. It is recommended that 15 control samples be tested by the independent testing agency and 3 control samples be tested by TxDOT or its representative.

# REFERENCES

Al-Amoudi, O. S. B., Maslehuddin, M., Lashari, A. N., and Almusallam, A. A. (2003). "Effectiveness of Corrosion Inhibitors in Contaminated Concrete." *Cement and Concrete Composites*, 25(4-5), 439-449.

Alonso, C., Andrade, C., Novoa, X. R., Izquierdo, D., and Perez, M. C. (1998). "Effect of Protective Oxide Scales in the Macrogalvanic Behaviour of Concrete Reinforcements." *Corrosion Science*, 40(8), 1379-1389.

Alonso, C., Castellote, M., and Andrade, C. (2002). "Chloride Threshold Dependence of Pitting Potential of Reinforcements." *Electrochimica Acta*, 47(21), 3469-3481.

Andrade, C., and Alonso, C. (2001). "On-site Measurements of Corrosion Rate of Reinforcements." *Construction and Building Materials*, 15, 141-145.

Andrade, C., and Alonso, C. (2004). "Test Methods for On-site Corrosion Rate Measurement of Steel Reinforcement in Concrete by Means of Polarization Resistance Method." *Materials and Structures*, 37(9), 623-643.

Andrade, C., and Gonzales, J. A. (1978). "Quantitative Measurements of Corrosion Rate of Reinforcing Steels Embedded in Concrete Using Polarization Resistance Measurements." *Materials and Corrosion*, 29, 515-519.

Andrade, C., Soler, L., and Novoa, X. R. (1995). "Advances in Electrochemical Impedance Measurements in Reinforced Concrete." *Materials Science Forum*, 192-194, 843-56.

Ann, K. Y., Jung, H. S., Kim, H. S., Kim, S. S., and Moon, H. Y. (2006). "Effect of Ccalcium Nitrite-Based Corrosion Inhibitor in Preventing Corrosion of Embedded Steel in Concrete." *Cement and Concrete Research*, 36(3), 530-535.

Arup, H. (1983) "The Mechanisms of the Protection of Steel by Concrete." *Society of Chemical Industry Conference of Reinforcement in Concrete Construction* London, UK, 151.

Balma, J., Darwin, D., Browning, J. P., and Locke, Jr. C. E. (2004). "Evaluation of Corrosion Resistance of Micro-alloyed Reinforcing Steel." *FHWA-KS-02-9*, Kansas Department of Transportation, Topeka.

Balma, J., Darwin, D., Browning, J. P., and Locke, C. E. (2005). "Evaluation of Corrosion Protection Systems and Corrosion Testing Methods for Reinforcing Steel in Concrete." *SM Report No. 76*, The University of Kansas Center for Research, Inc., Lawrence, KS.

Baweja, D., Roper, H., and Sirivivatnanon, V. (2003). "Improved Electrochemical Determinations of Chloride Induced Steel Corrosion in Concrete." *ACI Materials Journal*, 100(3), 228-238.

Berke, N. S. (1998). "Long-Term Corrosion Performance of Epoxy-Coated Steel and Calcium Nitrite." NACE Corrosion 98, NACE, Houston, TX, Paper No. 652.

Berke, N. S., Aldykiewicz, A. J., and Lianfang, L. (2003). "What's New in Corrosion Inhibitors." Structure, NCSEA, CASE, SEI, 10-12.

Berke, N. S., Pfeifer, D. W., and Weil, T. G. (1988). "Protection Against Chloride Induced Corrosion." *Concrete International*, 10(12), 45-55.

Berke, N. S., and Rosenberg, A. (1989). "Technical Review of Calcium Nitrite Corrosion Inhibitor in Concrete." *Transportation Research Record No. 1211*, Transportation Research Board, Washington, D.C.

Berkely, K. G. C., and Pathmanaban, S. (1990). *Cathodic Protection of Reinforcement Steel in Concrete*, Butterworths - Heinemann, London.

Brown, M. C. (1999). "Assessment of Commercial Corrosion Inhibiting Admixtures for Reinforced Concrete," Master of Science, Virginia Polytechnic Institute, Blacksburg, Virginia.

Browne, R. D., Geoghegan, M. P., and Baker, A. F.(1983) "Analysis of Structural Condition from Durability Results." *Corrosion of Reinforcement in Concrete Construction*, London, UK, 193-222.

Burke, D. F. (1994). "Performance of Epoxy-Coated Rebar, Galvanized Rebar, and Plain Rebar with Calcium Nitrite in a Marine Environment." *Concrete Reinforcing Steel Institute, Research Series -2*, CRSI.

Castellote, M., Andrade, C., and Alonso, C. (1999). "Modelling of the Processes During Steady-State Migration Tests: Quantification of transference numbers." *Materials and Structures*, 32, 180-186.

Castellote, M., Andrade, C., and Alonso, C. (2002). "Accelerated Simultaneous Determination of the Chloride Depassivation Threshold and of the Non-Stationary Diffusion Coefficient Values." *Corrosion Science*, 44(11), 2409-2424.

CC-Technologies. (2001). "Corrosion Cost and Preventive Strategies in the United States." *FHWA-RD-01-156*, McLean, VA.

Cella, P. A., and Taylor, S. R. (2000). "Electrical Resistance Changes as an Alternate Method for Monitoring the Corrosion of Steel in Concrete and Mortar." *Corrosion*, 56(9), 951-959.

Chang, Z.-T., Cherry, B., and Marosszeky, M. (2007). "Polarisation Behaviour of Steel Bar Samples in Concrete in Seawater Part 1: Experimental Measurement of Polarisation Curves of Steel in Concrete." *Corrosion Science*, In Press, Corrected Proof.

Chappelow, C. C., McElroy, A. D., Blackburn, R. R., Darwin, D., Noyelles, F. G. d., and Locke, C. E. (1992). "Handbook of Test Methods for Evaluating Chemical Deicers." *SHRP-H-332*, Strategic Highway Research Program, National Research Council, Washington, DC.

Cigna, R., Familiari, G., Gianetti, F., and Proverbio, E. (1994) "Influence of Calcium Nitrite on the Reinforcement Corrosion in Concrete Mixtures Containing Different Cements." *International Conference held at the Univ. of Sheffield*, Sheffield, UK, 878-892.

Clear, K. C. (1992). "Effectiveness of Epoxy-Coated Reinforcing Steel." *Concrete International*, 14(5), 58-64.

Clemena, G. G., and Virmani, Y. P. (2002). "Testing of Selected Metallic Reinforcing Bars for Extending the Service Life of Future Concrete Bridges: Testing in Outdoor Concrete Block." Virginia Department of Transportation, Charlottesville, Virginia.

Cody, R. D., Cody, A. M., Spry, P. G., and Gan, G. (1996). "Experimental Deterioration of Highway Concrete by Chloride Deicing Salts." *Environmental & Engineering Geoscience*, II(4), 575-588.

CRSI. (1995). "Adhesion Loss Mechanisms of Epoxy Coatings on Rebar Surfaces." Surface Science Western, Concrete Reinforcement Steel Institute, Schaumburg, IL.

Daigle, L., Lounis, A., and Cusson, D. (2004) "Numerical Prediction of Early-Age Cracking and Corrosion in High Performance Concrete Bridges - Case Study." *Annual Conference of the Trasnportation Association of Canada*, Quebec City, Quebec, 20.

Darwin, D., Browning, J. P., Ngyuen, T. V., and Locke, C. E. (2002). "Mechanical and Corrosion Properties of a High-Strength, High Chromium Reinforcing Steel for Concrete." *SD2001-05-F*, University of Kansas Center for Research, Inc., Lawrence, Kansas.

El-Jazairi, B., and Berke, N. S. (1990). "The Use of Calcium Nitrite as a Corrosion Inhibiting Admixture to Steel Reinforcement in Concrete." Corrosion of Reinforcement in Concrete, C. L. Page, K. W. J. Treadaway, and P. B. Bamforth, eds., Elsevier Applied Science, London 571-585.

Elsener, B. (2002). "Macrocell Corrosion of Steel in Concrete - Implications for Corrosion Monitoring." *Cement and Concrete Composites*, 24(1), 65-72.

Elsener, B., Andrade, C., Gulikers, J., Polder, R., and Raupach, M. (2003). "Half-cell Potential Measurements - Potential Mapping on Reinforced Concrete Structures." *Materials and Structures*, 36(7), 461-471.

Elsener, B., and Bohni, H. (1992). "Electrochemical Methods for the Inspection of Reinforcement Corrosion in Concrete Structures - Field Experience." *Materials Science Forum*, 111-112, 635-647.

Farzammehr, H. (1985). "Pore Solution Analysis of Sodium Chloride and Calcium Chloride Containing Cement Pastes," University of Oklahoma.

Feliu, S., Gonzalez, J. A., Andrade, M. C., and Feliu, V. (1988). "Determination of Polarization Resistance in Reinforced Concrete Slabs." *Corrosion*, 44(10), 761-765.

Feliu, S., González, J. A., Andrade, M. C., and Feliu, V. (1989). "Determining Polarization Resistance in Reinforced Concrete Slabs." *Corrosion Science*, 29(1), 105-113.

Feliu, S., Gonzalez, J. A., Escudero, M. L., Feliu Jr., S., and Andrade, M. C. (1990). "Possibilities of the Guard Ring for Electrical Signal Confinement in the Polarization Measurements of Reinforcements." *Corrosion*, 46(12), 1015-1020.

Gaidis, J. M., and Rosenberg, A. M. (1987). "The Inhibition of Chloride-Induced Corrosion in Reinforced Concrete by Calcium Nitrite." *Cement, Concrete, and Aggregates*, 9(1), 30-33.

Gamble, W. L. (2003). "Thermex-Processed Reinforcing Bars." *Concrete International*, 25(7), 85-88.

Ge, B., Darwin, D., Locke, C. E., and Browning, J. P. (2004). "Evaluation of Corrosion Protection Systems and Testing Methods for Conventional Steel." *SM Report No. 73*, Lawrence, KS.

Glass, G.K., and Buenfeld, N.R. (2000). "The Participation of Bound Chloride in Passive Film Breakdown on Steel in Concrete." *Corrosion Science*, 42(11), 2013.

Glass, G. K., and Buenfeld, N. R. (1997). "The Presentation of the Chloride Threshold Level for Corrosion of Steel in Concrete." *Corrosion Science*, 39(5), 1001-1013.

Gong, L., Darwin, D., Browning, J. P., and Locke, C. E. (2002). "Evaluation of Mechanical and Corrosion Properties of MMFX Reinforcing Steel for Concrete." *SM Report No. 70*, The University of Kansas Center for Research, Inc., Lawrence, KS.

Gong, L., Darwin, D., Browning, J. P., and Locke, C. E. (2006). "Evaluation of Multiple Corrosion Protection Systems and Stainless Steel Clad Reinforcement for Reinforced Concrete." *SM Report No. 82*, Lawrence, KS.

Guo, G., Darwin, D., Browning, J. P., and Locke, C. E. (2006). "Laboratory and Field Tests of Multiple Corrosion Protection Systems for Reinforced Concrete Bridge Components and 2205 Pickled Stainless Steel." *SM Report No. 85*, Lawrence, KS.

Ha, T.-H., Muralidharan, S., Bae, J.-H., Ha, Y.-C., Lee, H.-G., Park, K.-W., and Kim, D.-K. (2007). "Accelerated Short-Term Techniques to Evaluate the Corrosion Performance of Steel in Fly Ash Blended Concrete." *Building and Environment*, 42(1), 78-85.

Hansson, C. M. (1984). "Comments on Electrochemical Measurements of the Rate of Corrosion of Steel in Concrete." *Cement and Concrete Research*(14), 574-584.

Hansson, C.M., Mammolitu, L., and Hope, B. B. (1998). "Corrosion Inhibitors in Concrete - Part 1: The Principles." *Cement and Concrete Research*, 28(2), 1775-1781.

Herald, S. E., Henry, M., Al Qadi, I. L., Weyers, R. E., Feeney, M. A., Howlum, S. F., and Cady, P. D. (1993). "Condition Evaluation of Concrete Bridges Relative to Reinforcement Corrosion, Volume 6: Method for Field Determination of Total Chloride Content." *SHRP-S-328*, Strategic Highway Research Program (SHRP), National Research Council, Washington, D.C.

Hope, B. B., and Ip, A. K. C. (1989). "Corrosion Inhibitors for Use in Concrete." *ACI Materials Journal*, 86, 602-608.

Izquierdo, D., Alonso, C., Andrade, C., and Castellote, M. (2004). "Potentiostatic determination of chloride threshold values for rebar depassivation: Experimental and statistical study." *Electrochimica Acta*, 49(17-18), 2731-2739.

Jovancicevic, V., Bockris, J. O. M., Carbajal, J. L., Zelenay, P., and Mizuno, T. (1986). "Adsorption and Absorption of Chloride Ions on Passive Iron Systems." *Journal of the Electrochemical Society*, 133(11), 2219-2226.

Kahrs, J. T., Darwin, D., and Locke, C. E. (2001). "Evaluation of Corrosion Resistance of Type 304 Stainless Steel Clad Reinforcing Bars," University of Kansas Center for Research, Inc., Lawrence, Kan.

Liu, Y., and Weyers, R. E. (2003). "Comparison of Guarded and Unguarded Linear Polarization CCD Devices with Weight Loss Measurements." *Cement and Concrete Research*, 33(7), 1093-1101.

Manning, D. G. (1996). "Corrosion Performance of Epoxy-Coated Reinforcing Steel: North American Experience." *Construction and Building Materials*, 10(5), 349-365.

Mansfeld, F. (1981). "Recording and Analysis of AC Impedance Data for Corrosion Studies." *Corrosion*, 37(5), 301-307.

Martinez, S. L., Darwin, D., McCabe, S. L., and Locke, C. E. (1990). "Rapid Test for Corrosion Effects of Deicing Chemicals in Reinforced Concrete." *SL Report 90-4*, University of Kansas Center for Research, Lawrence, KS.

McCrum, L., and Arnold, C. J. (1993). "Evaluation of Simulated Bridge Deck Slabs Using Uncoated, Galvanized, and Epoxy Coated Reinforcing Steel." *No. R-1320*, Michigan Department of Transportation, Lansing, MI.

McCrum, L., Lower, B. R., and Arnold, C. J. (1995). "A Comparison of the Corrosion Performance of Uncoated, Galvanized, and Epoxy Coated Reinforcing Steel in Concrete Bridge Decks." *Research Report No. R-1321*, Michigan Department of Transportation, Lansing, MI.

McDonald, D. B., Pfeifer, D. W., and Sherman, M. R. (1998). "Corrosion Evaluation of Epoxy-Coated, Metallic Clad, and Solid Metallic Reinforcing Bars in Concrete." *FHWA-RD-98-153*, Federal Highway Administration, McLean, VA.

McDonald, D. B., Sherman, M. R., Pfeifer, D. W., and Virmani, Y. P. (1995). "Stainless Steel Reinforcing as Corrosion Protection." *Concrete International*, 17(5), 65-70.

Metha, P. K., and Monteiro, P. J. M. (1993). *Concrete Structure, Properties, and Materials*, Prentice Hall, Inc., Englewood Cliffs, NJ.

Montemor, M. F., Simoes, A. M. P., and Ferreira, M. G. S. (1998). "Analytical Characterization of the Passive Film Formed on Steel in Solutions Simulating the Concrete Interstitial Electrolyte." *Corrosion ; VOL. 54 ; ISSUE: 5 ; PBD: May 1998*, pp. 347-353 ; PL.

Montemor, M. F., Simoes, A. M. P., and Ferreira, M. G. S. (2003). "Chloride-Induced Corrosion on Reinforcing Steel: From the Fundamentals to the Monitoring Techniques." *Cement and Concrete Composites*, 25(4-5), 491-502.

Nmai, C. K., Farrington, S. A., and Bobrowski, G. (1992). "Organic-Based Corrosion Inhibiting Admixture for Reinforced Concrete." *Concrete International*, 14(4), 45-51.

Nurnberger, U., and Beul, W. (1991). "Einfluss einer Feuerverzinki und PVC-Beschichtung von Bewehrungsstahlen und von Irbitoren auf die Korrosion von Stahl in Gerissenem Beton." *Werkst. Korros.*, 42, 537-541.

Nygaard, P., and Geiker, M. (2005). "A Method for Measuring the Chloride Threshold Level Required to Initiate Reinforcement Corrosion in Concrete." *Materials and Structures*, 38(4), 489-494.

Page, C. L. (1975). "Mechanism of Corrosion Protection in Reinforced Concrete Marine Structures." *Nature*, 258(5535), 514-515.

Page, C. L., and Treadaway, K. W. J. (1982). "Aspects of the Electrochemistry of Steel in Concrete." *Nature*, 297(5862), 109-115.

Peabody, A. W. (1967). *Control of Pipeline Corrosion*, National Association of Corrosion Engineers, Houston, TX.

Pfeifer, D. W. (2000). "High Performance Concrete and Reinforcing Steel with 100-Year Service Life." *PCI Journal*, 45(3), 46-54.

Pfeifer, D. W., Landgren, J. R., and Zoob, A. (1987). "Protective Systems for New Prestressed and Substructure Concrete." *FHWA-RD-86-193*, FHWA, McLean, VA.

Pillai, R. G. (2003). "Accelerated Quantification of Critical Parameters for Predicting the Service Life and Life Cycle Costs of Chloride-Laden Reinforced Concrete Structures," M.S. Thesis, Texas A&M University, College Station, TX.

Pyc, W., Weyers, R. E., Sprinkel, M. M., Weyers, R. M., Mokarem, D. W., and Dillard, J. G. (2000). "Performance of Epoxy-Coated Reinforcing Steel." *Concrete International*, 22(2), 57-62.

Qian, S., and Cusson, D.(2007) "Accelerated Laboratory and Field Investigations of Corrosion Inhibiting Systems For Concrete Bridges." *Northern Area Eastern Conference*, Ottawa, Ontario.

Ramachandran, V. S. (1984). *Concrete Admixtures Handbook: Properties, Science, and Technology*, Noyes Publications, Park Ridge, NJ.

Rasheeduzzafar, A., Dakhil, F. H., Bader, M. A., and Khan, M. M. (1992). "Preformance of Corrosion Resisting Steel in Chloride Bearing Concrete." *ACI Materials Journal*, 89(Sept-Oct.), 439-448.

Roberge, P. R. (2000). *Handbook of Corrosion Engineering*, McGraw-Hill, NY, NY.

Rodríquez, P., Ramirez, E., and Bonzales, J. A. (1994). "Method for Studying Corrosion in Reinforced Concrete." *Concrete Research Magazine*, 46(167), 81-90.

Sagues, A. A. (1994). "Corrosion of Epoxy Coated Rebar in Florida Bridges." *WPI No. 0510603*, University of South Florida, Tampa, FL.

Sagues, A. A., Powers, R. G., and Kessler, R. (1994). "Corrosion Processes and Field Performance of Epoxy-Coated Reinforcing Steel in Marine Structures." Corrosion 94, National Association of Corrosion Engineers (NACE), Houston, TX, Paper number 229.

Schiessl, P., and Raupach, M. (1990) "Influence of Concrete Composition and Microclimate on the Critical Chloride Content in Concrete." *Corrosion of Reinforcement in Concrete*, Wishaw, Warwickshire, UK, 49-58.

Schwensen, S. M., Darwin, D., and Locke, C. E. (1995). "Rapid Evaluation of Corrosion-Resistant Concrete Reinforcing Steel in the Presence of Deicers." *SL Report 95-6*, University of Kansas Center for Research, Inc., Lawrence, KS.

Sehgal, A., Kho, Y. T., Osseo-Asare, K., and Pickering, H. W. (1992). "Reproducibility of Polarization Resistance Measurements in Steel-In-Concrete Systems." *Corrosion*, 48, 706-714.

Senecal, M. R., Darwin, D., and Locke, C. E. (1995). "Evaluation of Corrosion-Resistant Steel Reinforcing Bars." *SM Report No. 40*, University of Kansas Center for Research, Inc., Lawrence, KS.

Sherman, M. R., McDonald, D. B., and Pfeifer, D. W. (1996). "Durability Aspects of Precast Prestressed Concrete Part 2: Chloride Permeability Study." *PCI Journal*, 41(4), 76-95.

Smith, F. N., and Tullman, M. (1999). "Using Stainless Steel as Long-Lasting Rebar Material." *Materials Performance*, 38(5), 72-76.

Smith, J. L., Darwin, D., and Locke, C. E. (1995). "Corrosion-Resistant Steel Reinforcing Bars." *SL Report 95-1*, University of Kansas Center for Research, Inc., Lawrence, KS.

Smith, J. L., and Virmani, Y. P. (1996). "Performance of Epoxy-Coated Rebars in Bridge Decks." *FHWA-RD-96-092*, Federal Highway Administration, McLean, VA.

Soleymani, H. R., and Ismail, M. E. (2004). "Comparing Corrosion Measurement Methods to Assess the Corrosion Activity of Laboratory OPC and HPC Concrete Specimens." *Cement & Concrete Research*, 34(11), 2037.

Song, H.-W., and Saraswathy, V. (2007). "Corrosion Monitoring of Reinforced Concrete Structures - A Review." *International Journal of Electrochemical Science*, 2, 1-28.

Stern, M. (1958). "A Method for Determining Corrosion Rates from Linear Polarization Data." *Corrosion*, 14(9), 60-64.

Stern, M., and Geary, A. L. (1957). "A Theoretical Analysis of the Shape of Polarization Curves." *Journal of the Electrochemical Society*, 104(January), 56.

Suryavanshi, A. K., Scantlebury, J. D., and Lyon, S. B. (1996). "Mechanism of Friedel's salt formation in cements rich in tri-calcium aluminate." *Cement and Concrete Research*, 26(5), 717-727.

Torres-Acosta, A. A., and Sagues, A. A. (2004). "Concrete Cracking by Localized Steel Corrosion - Geometric Effects." *ACI Materials Journal*, 101(6), 501-507.

Trejo, D., and Miller, D. R. (2003). "Determination of Chloride Corrosion Threshold for Metals Embedded in Cementitious Material." 11.

Trejo, D., and Pillai, R. G. (2003). "Accelerated Chloride Threshold Testing: Part I - ASTM A 615 and A 706 Reinforcement." *ACI Materials Journal*, 100(6), 519-527.

Trejo, D., and Pillai, R. G. (2004). "Accelerated Chloride Threshold Testing - Part II: Corrosion Resistant Reinforcement." *ACI Materials Journal*, 101(1), 57-64.

Trepanier, S. M., Hope, B. B., and Hansson, C. M. (2001). "Corrosion Inhibitors in Concrete: Part III. Effect on Time to Chloride-Induced Corrosion Initiation and Subsequent Corrosion Rates of Steel in Mortar." *Cement and Concrete Research*, 31(5), 713-718.

Videm, K. (2001). "Phenomena Disturbing Electrochemical Corrosion Rate Measurements for Steel in Alkaline Environments." *Electrochimica Acta*, 46(24-25), 3895-3903.

Viedma, P. G., Castellote, M., and Andrade, C. (2006). "Comparison Between Several Methods for Determining the Depassivation Threshold Value for Corrosion Onset." *Journal of Physique IV*, 136, 79-88.

Virmani, Y. P. (1990). "Effectiveness of Calcium Nitrite Admixtures as a Corrosion Inhibitor." *Public Roads*, 54(1), 171-182.

Virmani, Y. P., Clear, K. C., and Pasko, T. J. (1983). "Time to Corrosion of Reinforcing Steel in Concrete Slabs, Volume 5, Calcium Nitrite Admixture and Epoxy Coated Reinforcing Bars as Corrosion Protection Systems." *FHWA-RD-83-012*, Federal Highway Administration, McLean, VA.

Weyers, R. E., Sprinkel, M. M., Pyc, W., Zemajtis, J., Liu, Y., and Mokarem, D. W. (1998). "Field Investigation of the Corrosion Protection Performance of Bridge Decks and Piles Constructied with Epoxy-Coated Reinforcing Steel in Virginia." *VTRC 98-R4*, Virginia Transportation Research Council, Charlottesville, VA.

Wipf, T. J., Phares, B. M., and Fanous, F. S. (2006). "Evaluation of Corrosion Resistance of Different Steel Reinforcement Types." *CTRE Project 02-103*, Center for Transportation Research and Education, Iowa State University, Ames, IA.

Yeomans, S. R. (1994). "Performance of Black, Galvanized, and Epoxy-Coated Reinforcing Steels in Chloride-Contaminated Concrete." *Corrosion*, 50(1), 72-81.

Yunovich, M., Thompson, N. G., Balvanyos, T., and Lave, L. (2002). "Highway Bridges, Appendix D, Corrosion Cost and Preventive Strategies in the United States," by G.H. Koch, M. H. Broongers, N.G. Thompson, Y.P. Virmani, and J.H. Payer." *FHWA-RD-01-156*, McLean, VA.

Zemajtis, J., Weyers, R. E., and Sprinkel, M. M. (1999). "Performance Evaluation of Corrosion Inhibitors and Galvanized Steel in Concrete Exposure Specimens." *VTRC 99-CR4*, Virginia Transportation Research Council, Charlotte, VA.

# APPENDIX A ACCELERATED CHLORIDE THRESHOLD (ACT) TEST PROCEDURE

Proposed Standard Test Method for THE ACCELERATED DETERMINATION OF THE CRITICAL CHLORIDE THRESHOLD LEVEL OF UNCOATED STEEL REINFORCEMENT EMBEDDED IN MORTAR[1]

1. Scope
   - 1.1 This test method covers the determination of the critical chloride corrosion threshold level for uncoated steel reinforcement in a controlled mortar mix.
   - 1.2 This standard may involve hazardous materials, operations, and equipment. This standard does not purport to address all of the safety problems associated with its use. It is the responsibility of the user to establish appropriate safety and health practices and determine the applicability of regulatory limitations prior to use.
   - 1.3 The top of the mortar surface must be plain, with no liquid-impermeable overlays or coatings in the area of chloride induction.
   - 1.4 The top surface of the reinforcing steel shall not be entirely coated with epoxy, hot-dip zinc (galvanized), or other non-conductive coatings. In this case, the mill scale formed during hot-rolling is not considered to be a coating.
   - 1.5 The ambient temperature during testing shall be between 21°C (70°F) and 27°C (80°F).
   - 1.6 The values stated in SI units are to be regarded as the standard. It is recognized that centimeters are not SI units, but because centimeters are commonly used in electrochemical testing, the units of centimeters will be used. The values in parenthesis are for information only and currently represent only estimates based on no testing.

2. Referenced Documents–ASTM Standards (AASHTO Standards)
   - 2.1 ASTM A615/A615M-00 Standard Specification for Deformed and Plain Billet-Steel Bars for Concrete Reinforcement (AASHTO M 31M)
   - 2.2 ASTM A996/A996M-00 Standard Specification for Rail-Steel and Axle-Steel Deformed Bars for Concrete Reinforcement

[1] After Pillai, R., "Accelerated Quantification of Critical Parameters for Predicting the Service Life and Life Cycle Costs of Chloride-Laden Reinforced Concrete Structures," MS Thesis, August 2003

2.3 ASTM A82 - Standard Specification for Steel Wire, Plain, for Concrete Reinforcement (AASHTO M32)

2.4 ASTM A496 - Standard Specification for Steel Wire, Deformed, for Concrete Reinforcement (AASHTO M225M)

2.5 ASTM G3 - Standard Practice for Conventions Applicable to Electrochemical Measurement in Corrosion Testing

2.6 ASTM G59 - Standard Practice for Conducting Potentiodynamic Polarization Resistance Measurements

2.7 ASTM G102 - Standard Practice for Calculation of Corrosion Rates and Related Information from Electrochemical Measurements

2.8 ASTM C150-97 - Standard Specification for Portland Cement

2.9 ASTM C192/C192M-00 - Standard Practice for Making and Curing Concrete Test Specimens in the Laboratory

2.10 ASTM C778-00 - Standard Specification for Standard Sand

2.11 ASTM C1202-97 - Standard Test Method for Electrical Indication of Concrete's Ability to Resist Chloride Ion Penetration

3. Summary of Test Method

3.1 This method determines a critical chloride corrosion threshold level for steel reinforcement embedded in mortar by accelerating the movement of chlorides from a chloride containing solution ponded on the surface of the mortar toward the reinforcing steel surface. Polarization resistance tests are then performed at defined intervals to determine when corrosion of the reinforcement initiates (in this test, corrosion initiation is defined to occur when a significant increase in the inverse polarization resistance, $1/R_p$, is detected). At this point in time when the reinforcement transfers from a passive to active state, the mortar adjacent to the steel reinforcement is evaluated for chloride concentration. This chloride concentration value is defined in this standard test method as the critical chloride threshold level of the embedded uncoated steel reinforcement. Figure 1 shows the general procedure in a flow diagram.

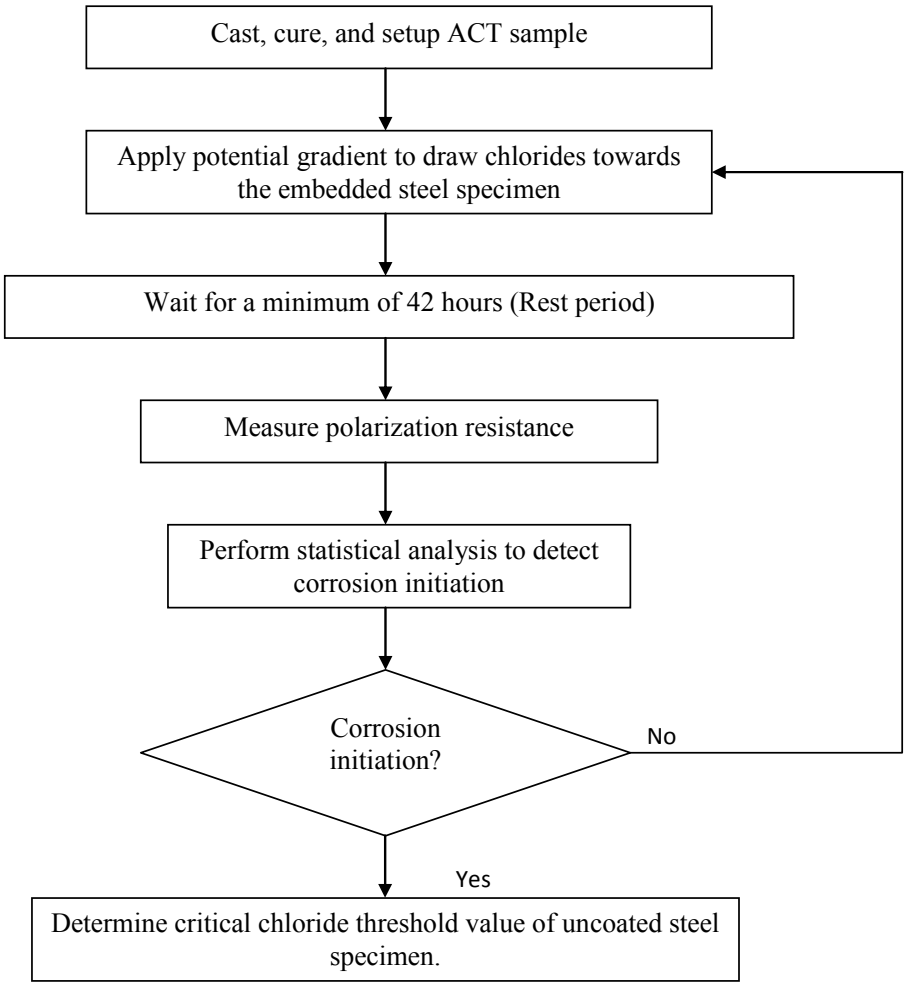


**Figure A-1 Flow Chart for the ACT Test Procedure.**

3.2 For comparison evaluations, the mortar mix and cover above the steel should remain constant for all samples being tested. This method will describe the procedure for casting and testing the specimens. It is assumed that ACT test cylinders have been obtained for casting the specimens. ACT cylinders are commercially available from FastSteel Inc., Anaheim, California, USA, and other agencies. The ACT cylinder design is attached. The instantaneous inverse polarization resistance is determined for a specific area of reinforcing steel, and is expressed in the unit of ( $\frac{1}{k\Omega \cdot cm^2}$ ).

4. Significance and Use

4.1 Critical chloride corrosion threshold levels can be used as a comparative parameter for evaluating new or existing reinforcing products.

4.2 Successive measurements of instantaneous polarization resistances of steel reinforcement embedded in cementitious materials at prescribed time intervals will assist in identifying the time at which the steel begins to actively corrode. At this point when the steel begins to actively corrode, the cementitious material at the steel depth can be evaluated for chloride concentration. This chloride concentration is taken to be the critical chloride threshold, i.e., the chloride level at which the reinforcement becomes active as a result of the presence of chlorides.

5. Interferences

5.1 High electrical resistance of the mortar (as might result from unusually dry conditions, impregnation with dielectric materials, or "internally sealed" mortar) or electrolyte material in the Lugin probe will interfere with obtaining accurate test results.

5.2 Air voids, if any, in the Lugin probe tip will interfere with obtaining results.

5.3 Other external electrical fields (i.e., electric motors in the location near to the ACT test setup) may also cause interferences.

6. Apparatus

6.1 The test equipment consists of the following apparatus:

6.1.1 Potentiostat: For this test, any potentiostat with sufficient compliance voltage should be satisfactory. Original testing in the development of this test method used a Solartron *SI 287 Potentiostat* (20V compliance) in conjunction with an Accumet #13-620-52 Calomel Reference Electrode.

6.1.2 Potential Gradient (Voltage) Source: A device to accelerate the movement of chlorides into the mortar. A floating type voltage source is not sufficient. A potential gradient source, which has a constant ground terminal and a constant -20 Volt terminal, is required. The anode and the cathode should be connected to the ground and the -20 Volt terminals. Original testing in the development of this test method used a DC Power supply system manufactured by Agilent Technologies (Model No. E3611A).

6.1.3 Electrical Timer: An electrical timer can be used to automatically switch the DC Power supply system ON and OFF.

6.1.4 Distribution Box: 10 channel box for distributing potential to each ACT cylinder.

6.1.5 Computer containing software (e.g., CorrWare) for performing polarization resistance tests.

6.2 The testing apparatus consists of the following: a four-piece cylindrical mold (parts A, B, and C), a working electrode (steel reinforcement sample), a working electrode connector, an anode, a counter electrode (and lead wires), a cathode, a Lugin probe, and a chloride solution reservoir (Part D). A drawing and parts list for this ACT kit is shown at the end of this document.

6.2.1 A prefabricated mold, with all electrodes, anode, cathode, and Lugin probe required for casting the test cylinder can be obtained from FastSteel Inc., Anaheim, California, and other agencies.

7. Materials and Reagents

7.1 *Anode* - The anode is a 69 mm (2.8 inch) diameter Nichrome mesh with a 25 x 25 mm (1 x 1 inch) section removed from the center. The anode mesh disk is soldered to two with copper wires such that electrical lead wires can be connected. These copper wires also function as a supporting system for the anode.

7.2 *Cathode* - The cathode is a 44 mm (1.8 inch) diameter Nichrome mesh.

7.3 *Steel Reinforcing Bar (working electrode)* – Any steel reinforcing bar type can be used as a working electrode in this test procedure. The prefabricated ACT kit includes a working electrode made from conventional ASTM A615 steel reinforcement. An additional working electrode is contained in each ACT kit. Figure 2 shows a typical working electrode for the test.

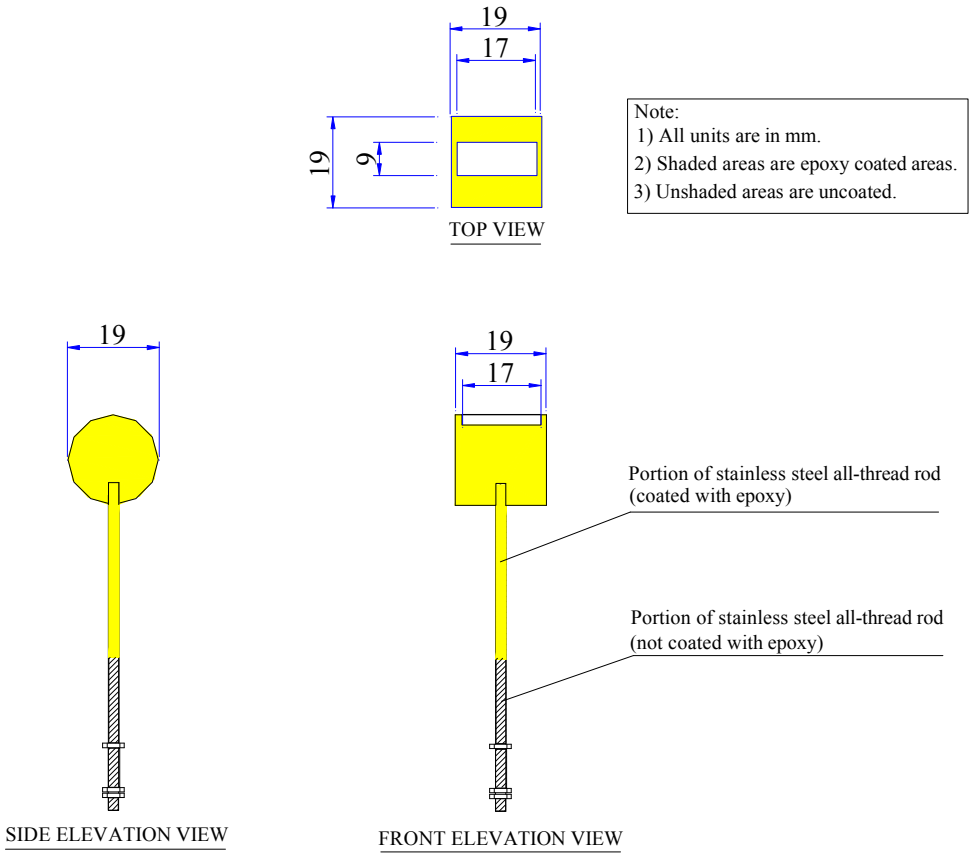


**Figure A-2 Fabrication of Working Electrode for ACT Testing.**

7.4 *Counter Electrode* – The counter electrode is a 25 x 25 mm (1 x 1 inch) square Nichrome mesh. The counter electrode mesh disk is soldered to the copper wires such that electrical lead wires can be connected. These copper wires also function as a supporting system for the counter electrode. The effective surface area of the counter electrode is approximately 3.42 $cm^2$.

7.5 *Mortar* – Cement and clean sand mixed with a constant water-cement (w-c) ratio shall be used. The weight ratio of the constituent materials shall be the same for each sample in each of the tested specimens. For the preliminary testing, a w-c ratio of 0.5 was used, and weight ratios of the materials was 1:2:4.5 (water:cement:sand). Sand meeting ASTM C778 and Type I cement can be used for standardized testing.

7.6 *Test cylinders* – Prefabricated Acrylonitrile-Butilene-Styrene (ABS) cylinders 75 mm (3 inch) in diameter and 115 mm (4.5 inch) in height shall be used for evaluating the critical chloride threshold level. These cylinders can be purchased or made.

7.7 *Reservoir system for chloride solution* – A 50 mm (2 inch) diameter plastic cylinder, open on both ends, will be used to confine the chloride solution on the top of the mortar sample. This reservoir cylinder will be inserted directly onto the top of the ACT specimen during casting. The embedment depth of the reservoir cylinder shall not exceed 6 mm into the mortar. Care shall be taken to ensure that the retaining reservoir is centrally embedded on the top of the specimen.

7.8 *Wire gauze* – A corrosion-resistant, fine mesh gauze will be used as an anode, cathode, and counter electrode for the system. A nickel-chromium (Nichrome) wire mesh with AWG:24 and with 25 meshes/inch has exhibited good performance for these components.

7.9 *Solid Copper Wire (2.2 mm diameter)* – The wire shall be clean and able to support the steel sample without considerable deflection and shall be protected from galvanic corrosion with an epoxy coating.

7.10 *Threading tools* – Required only when evaluating working electrodes not available from ACT kit. Threading tools shall be 5-40 taps and dies for use on the steel and copper wire.

7.11 *Haber-Luggin Probes* – A glass tube with a probe to be used to function as a container for filling the Lugin probe electrolyte, which functions as a conductive bridge between the area near the steel surface and the tip of the reference electrode.

7.12 *Luggin Probe Electrolyte* – Mix 1.651 grams of crystalline NaCl in 1000 mL of distilled for the solution to be placed in Luggin probe. This provides a Luggin probe electrolyte with 0.1 percent chloride solution.

7.13 *Chloride Ponding Solution* – Mix 61.23 grams of crystalline NaCl in 1000 mL of distilled water for the solution to be placed in the reservoir. This provides a 3.5 percent chloride solution or 5.77 percent NaCl solution.

8. Procedure for casting the specimens

8.1 Make sure that the working electrode, the anode, the counter electrode and other parts are properly (i.e., proper dimensional settings) fastened or installed.

8.2 Measure precisely the exposed area of the steel specimen.

8.3 Draw a vertical guideline which will help in aligning different parts of the ACT cylinder while casting.

8.4 Label the ACT cylinder properly.

8.5 Fill the Luggin probe with Luggin probe electrolyte (0.1 percent NaCl solution) as shown in the Figure A.3. Make sure that no air is trapped inside the probe (1.5 mm inner diameter).

8.6 Batch all materials required for making control mortar mixture. Make water content corrections as required for aggregate moisture.

8.7 Mix sand, cement, and water as required by ASTM C192.

8.8 Place lower portion of ACT cylinder (Part A) on a flat surface and ensure that the working electrode is secured in place. The top surface of the working electrode should be even with the level of anode mesh disk.

8.9 Place mortar in cylinder and around the working electrode. The mortar shall be placed in three equal lifts. The side or top of the cylinder shall be tapped 10 times (using a rubber or wooden mallet) to allow entrapped air to escape to the free surface and to ensure proper consolidation.

8.10 Place approximately $5cm^3$ of mortar on top of the steel specimen. This extra mortar should come through the anode mesh disk while placing it as explained next. This will also ensure that no visible air is trapped at the interface between the bottom face of the anode and the mortar.

8.11 Place Part B over Part A, ensuring that the semi-circular cutouts from both parts are aligned (Anode is fastened to the Part B). Part B should fit tightly on top of Part A. If found difficult to place or fit, hammer vertically with a wooden mallet. Care shall be taken, as explained in the previous section, to ensure that no visible air voids are trapped below the anode.

8.12 Recheck if the Luggin probe is properly filled with the Luggin probe electrolyte.

8.13 Cover the top mouth of the Luggin probe with a cap such that contamination of Luggin probe electrolyte with external materials and moisture in the curing room is avoided.

8.14 Insert Luggin probe tip into the hole drilled into the edge of Part B. Place the Luggin probe such that the probe tip is resting on the exposed area of the steel working electrode. The Luggin probe is designed such that the distance between the steel

working electrode and the Luggin probe tip will be equal to the thickness of the shrinking tube, which is less than 1 mm. After the tip has been properly inserted, tape the Luggin probe to the outside edge of Parts A and/or B to secure the Luggin probe to the sample. Care shall be taken as to not break the Luggin probe tip. After the mortar has set (preferably after 1 day), apply silicon to the Luggin probe-cylinder interface to prevent the probe from breaking during testing.

8.15 Place approximately 10 $cm^3$ of mortar on top of the steel specimen-Luggin probe tip region. This extra mortar should come through the counter electrode mesh disk while placing it as explained next. This will also ensure that no visible air is trapped at the interface between the bottom face of the counter electrode and the mortar.

8.16 Place Part C over Part B, ensuring that the semi-circular cutouts from both parts are aligned (Counter electrode is fastened to the Part C). Part C should fit tightly on top of Part B. Care shall be taken to ensure that no visible air voids are trapped below the counter electrode.

8.17 Fill the remaining volume above the counter electrode with mortar. Carefully tap the sides of Part C to ensure proper consolidation of the mortar and removal of big air voids. Strike the surface of the mortar such that it is even with the top of Part C.

8.18 Centrally place chloride solution reservoir (2-inch diameter plastic pipe) on top of mortar surface. Twist the reservoir sample or pipe while pushing into the mortar to a depth of approximately 6 mm. Carefully and gently tap the sides of Part C to reconsolidate the mortar around the reservoir. Hard hitting may cause further settlement of the reservoir pipe.

8.19 Cover sample(s) with moist clothes and plastic sheathing until the cementitious material is hardened. Care should be taken that the clothes or other forms of coverings are not touching the ACT samples until the cementitious material is hardened.

8.20 Cure samples as required. Curing during the initial test program included curing the samples in a 37 ± 1°C and 100 percent relative humidity environment for seven days. Alternative curing conditions (14 days at 21°C and 100 percent relative humidity) can also be used.

9. Procedure for testing the specimens

9.1 After curing the samples for the required time period, the samples shall be placed on a flat surface near the potential source and potentiostat. Connect the system per the manufacturer's recommendations, ensuring that the embedded electrode is the anode, and the electrode in the reservoir is cathode.

9.2 Place the 3.5 percent chloride solution (5.77 percent NaCl) in the reservoir on top of the specimen. The reservoir should be approximately 75 percent filled. New solution shall be placed after every applied potential period and shall not be allowed to dry. In addition, if the sodium chlorides tend to precipitate on the inside of the reservoir, new solution shall be placed after cleaning the reservoir.

9.3 Fasten all the electrical lead wires to the ACT specimen.

9.4 Connect the three electrode system as required by the potentiostat specifications. Determine the open circuit potential (OCP) of the working electrode until stable or for 2 minutes.

9.5 Immediately following the determination of the OCP, hold the sample potentiostatically for another 30 seconds.

9.6 Immediately following the potentiostatic experiment, scan the sample from –0.015 to +0.015 Volts (or minimum allowable range possible) versus the OCP to obtain the polarization resistance ($R_p$). The scan rate shall be 0.1667 mV/sec.

9.7 Immediately after the completion of the OCP, potentiostatic holding, and $R_p$ scans, the data must be downloaded and evaluated. Determine the polarization resistance as follows:

$$R_p = \left[\frac{\Delta E}{\Delta I}\right]_{E\to 0} \qquad \text{(A.5)}$$

where $E$ is the instantaneous overvoltage, and $I$ is the instantaneous applied current.

9.8 Document the inverse polarization resistance and cumulative time of applied voltage.

9.9 Perform statistical analysis with inverse polarization resistance data to determine if there is a significant increase in the corrosion activity. If there is no activation detected, go to step 9.10, otherwise go to step 9.11.

9.10 Connect the ACT specimen to the voltage source and apply potential gradient for 6 hours. (After the first $R_p$ measurement the duration of applied voltage is 3x12 = 36

hours. After the second $R_p$ measurement onward the duration of applied voltage is in an increment of 6 hours). Go to step 9.12.

9.11 If active corrosion is detected, determine critical chloride threshold value as explained in Section 11.

9.12 At a minimum rest period of 42 hours after switching OFF the voltage source, repeat steps 9.4 through 9.9.

9.13 After it has been determined that the working electrode (steel reinforcing sample) is in an active state, the sample shall be disconnected from the potentiostat and voltage source. Separate the Luggin probe and all electrical lead wires from the sample. Cut the plastic chloride reservoir from the top of the sample. Break the sample and remove or peel off the anode mesh disk from the top portion piece of the broken sample as shown in Figure A.3.

**Figure A-3 Top Portion of the ACT Specimen with the Anode Mesh Disk Peeled Off.**

9.14 Obtain ground samples in 2 mm depths for analysis of chloride profile. Figure A.4 shows the broken ACT sample with the center area near the steel reinforcement ground for 2 mm depth. Perform chloride testing following standard total chloride test procedures (acid soluble). A modified version of the *Standard Test Method for Total Chloride Content in Concrete Using the Specific Ion Probe* [SHRP-S/FR-92-110 1992] is available. This modified test procedure is recommended for the chloride analysis of

ACT specimens. The chloride level at the depth of the steel reinforcement is considered the critical chloride threshold value.

**Figure A-4 Broken and Ground ACT Sample.**

10. Estimating Time of Applied Voltage and Test Schedule

10.1 For the conditions outlined in this specification (mortar mixture, 20V of applied potential, 38 mm cover), if an approximate critical chloride threshold value is known, the cumulative time of applied voltage required to obtain the critical chloride threshold level at the steel interface can be estimated from Eq. (A.1) and Eq. (A.2) below. For an estimated critical chloride threshold level less than 1.5;

$$Estimated\ Time\ of\ Applied\ Voltage = \frac{Estimated\ Critical\ Chloride\ Threshold\left(\frac{\#}{cy}\right)}{0.015} \quad (A.1)$$

For an estimated critical chloride threshold level greater than 1.5;

$$Estimated\ Time\ of\ Applied\ Voltage = \frac{Estimated\ Critical\ Chloride\ Threshold\left(\frac{\#}{cy}\right) + 25.5}{0.27} \quad (A.2)$$

10.2 The voltage should be applied in 6-hour increments up until the embedded steel specimen is activated. An example calculation follows.

Assume Type I cement, ASTM C778 sand will be used for the mortar mixture and the water:cement:sand ratio is 1:2:4.5. A 20V potential for applying the potential difference between the anode and the cathode and 38 mm of mortar cover shall be used. Assume that the estimated critical chloride threshold for steel "A" is 1.5 pounds of chloride per cubic yard of mortar. The total time of applied voltage will be:

$$Estimated\ Time\ of\ Applied\ Voltage = \frac{1.5}{0.015} = 100\ \ hours \tag{A.3}$$

To determine the number of 6-hour increments of applied potential, the estimated time of applied voltage shall be multiplied by 0.9 and divided by 6 as follows:

$$Estimated\ \ Number\ of\ \ 6-hour\ Increments\ of\ Applied\ Voltage = \frac{(100 \times 0.9)}{6} = 15 \tag{A.4}$$

Thus, the testing schedule will be as follows:

**Table A-1 Typical Schedule for the Application of Potential Gradient.**

| Cycle Number | Time Increment of Applied Voltage |
|---|---|
| 1 | 6 Hours |
| 2 | 6 Hours |
| 3 | 6 Hours |
| 4,5,6… until corrosion activation | 6 Hours |

Note:
For cycles 1, 2, and 3, a minimum rest period of 12 hours is required between tests.
For cycles 4 and beyond, a minimum rest period of 42 hours is required.

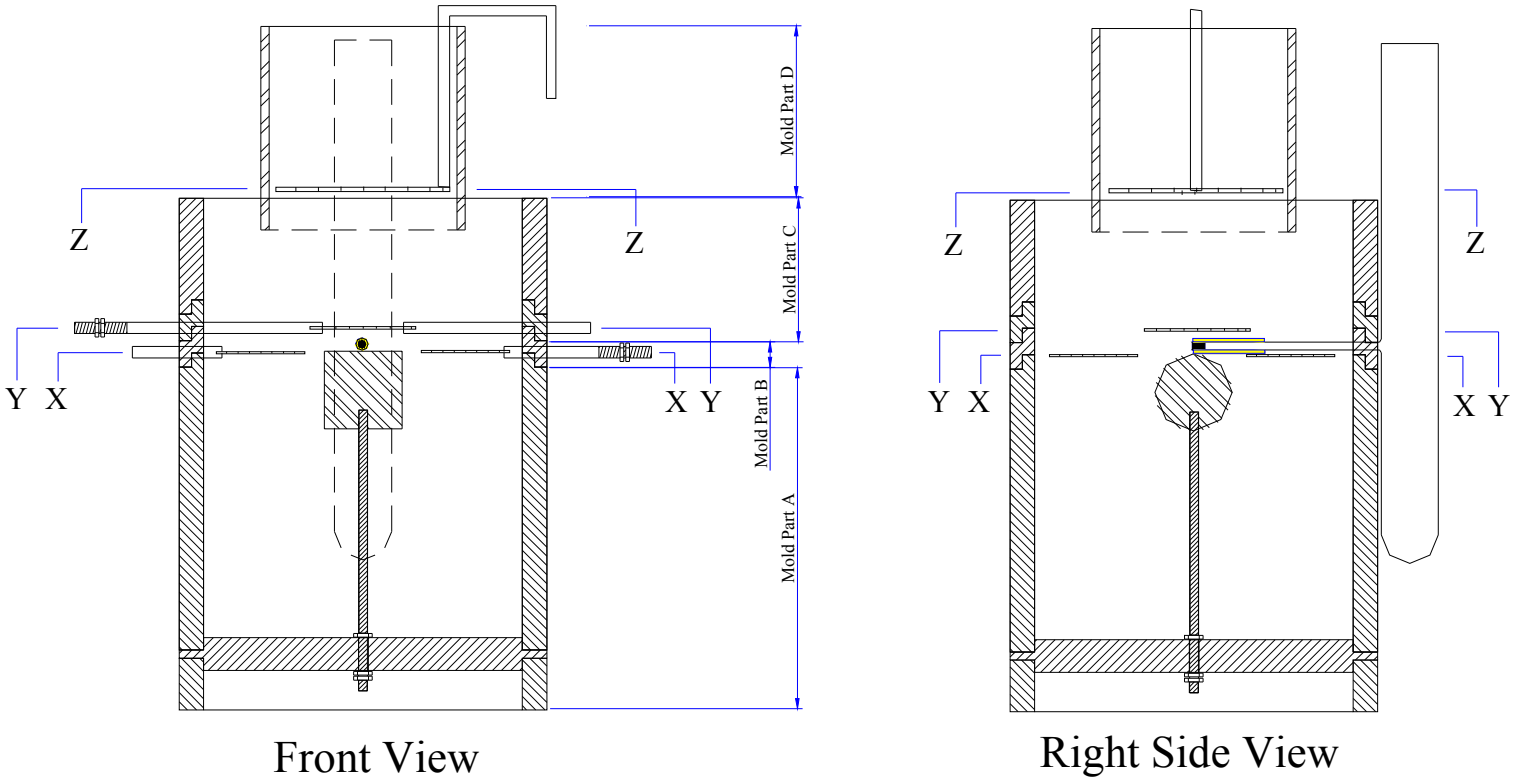


**Figure A-5 Elevation Views of ACT Specimen.**

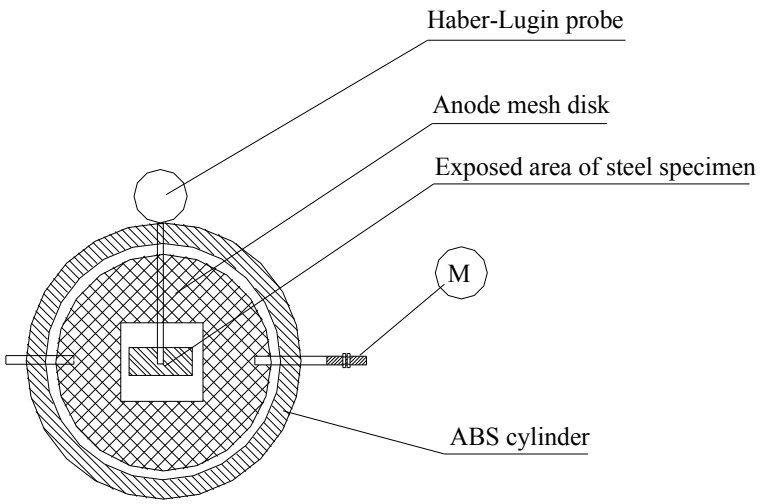


Sectional View (X-X)

Note:
M: Connecting copper wire with threaded (5-40) end

**Figure A-6 X-X Sectional View of ACT Specimen.**

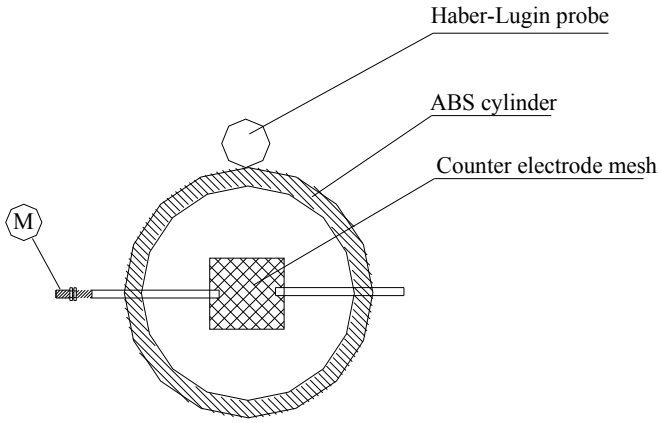


Sectional View (Y-Y)

Note:
M: Connecting copper wire with threaded (5-40) end

**Figure A-7 Y-Y Sectional View of ACT Specimen.**

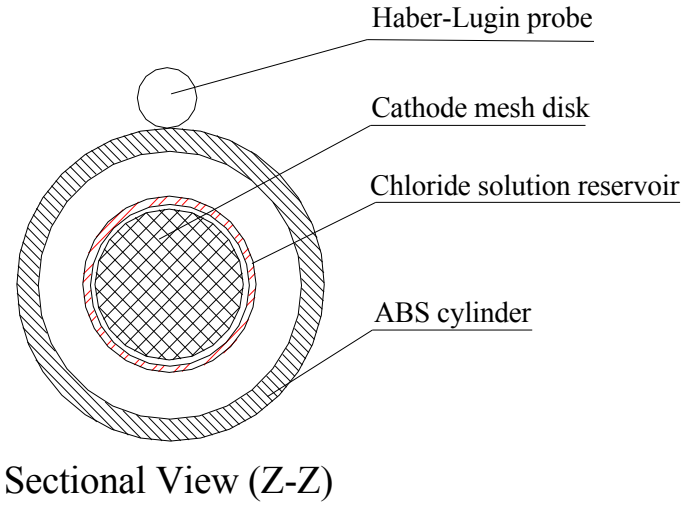


**Figure A-8 Z-Z Sectional View of ACT Specimen.**

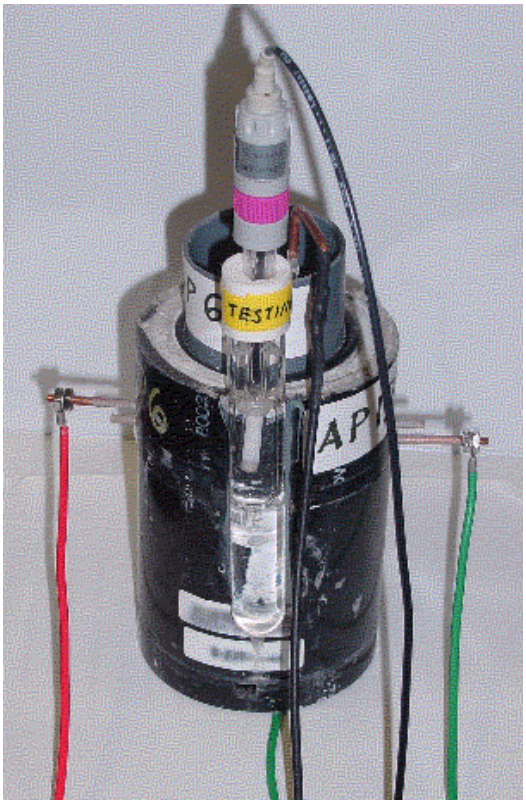

**Figure A-9 Actual ACT Test Specimen Ready for Testing.**


**Figure A-10 Actual ACT Test Specimen Ready for Testing (Side View).**

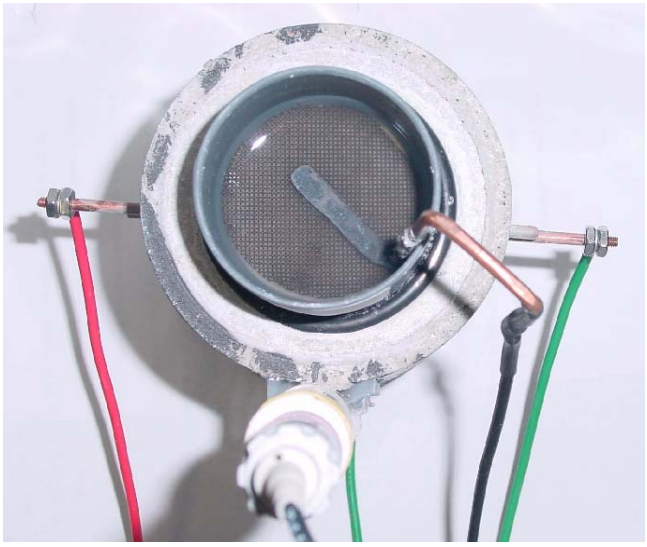

**Figure A-11 Actual ACT Test Specimen Ready for Testing (Top View).**

# APPENDIX B

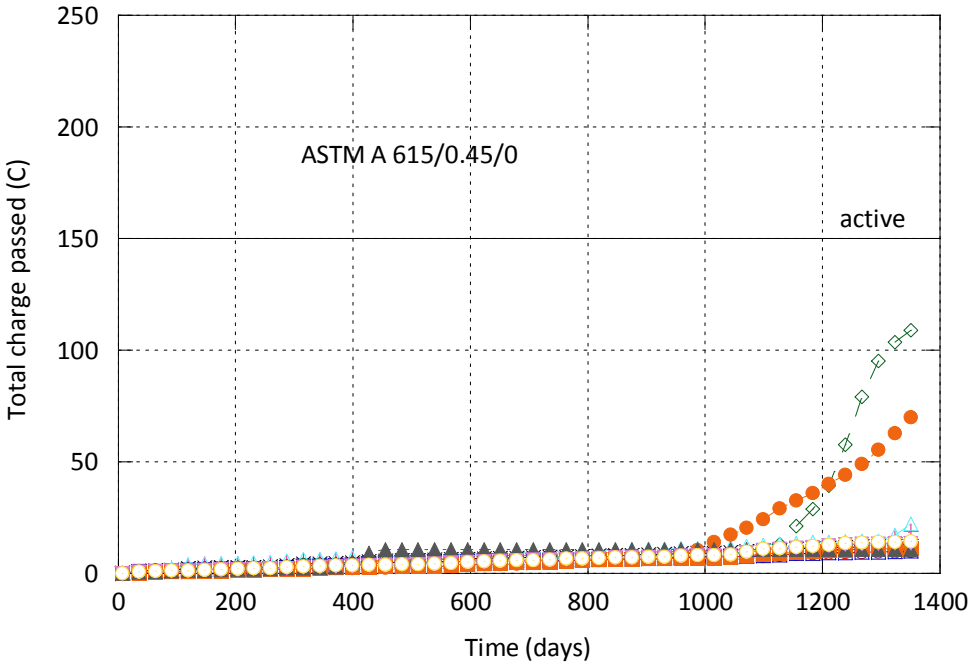


**Figure B-1 ASTM A 615/0.45/0**

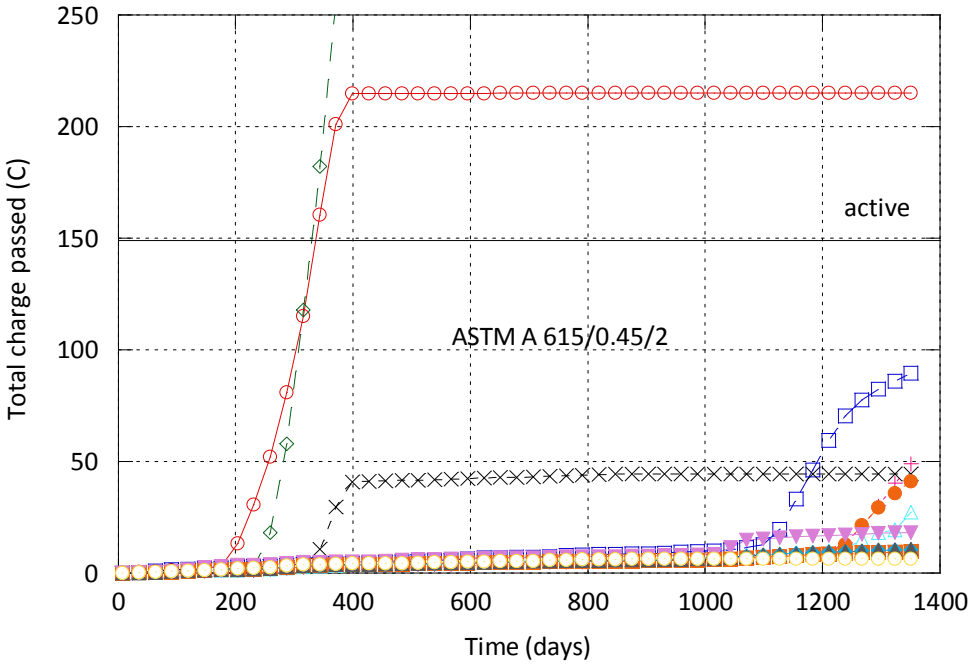


**Figure B-2 ASTM A 615/0.45/2**

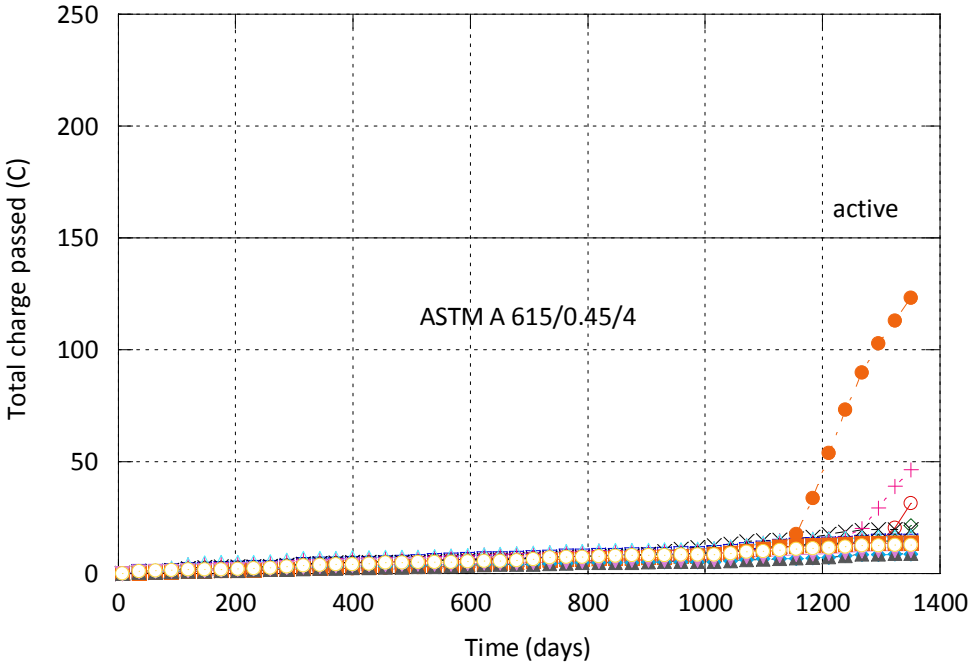


**Figure B-3 ASTM A 615/0.45/4**

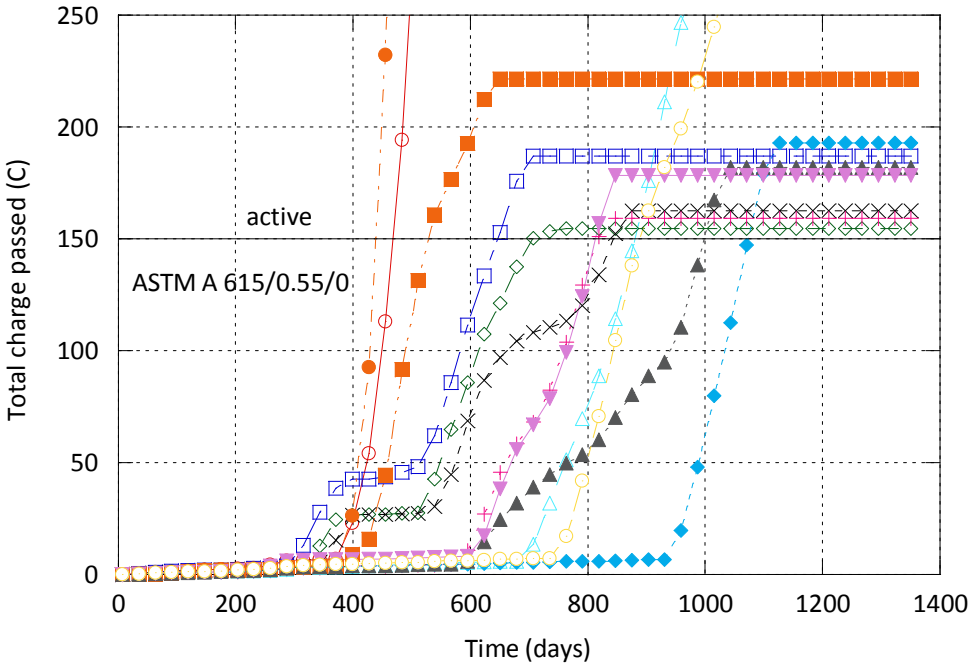


**Figure B-4 ASTM A 615/0.55/0**

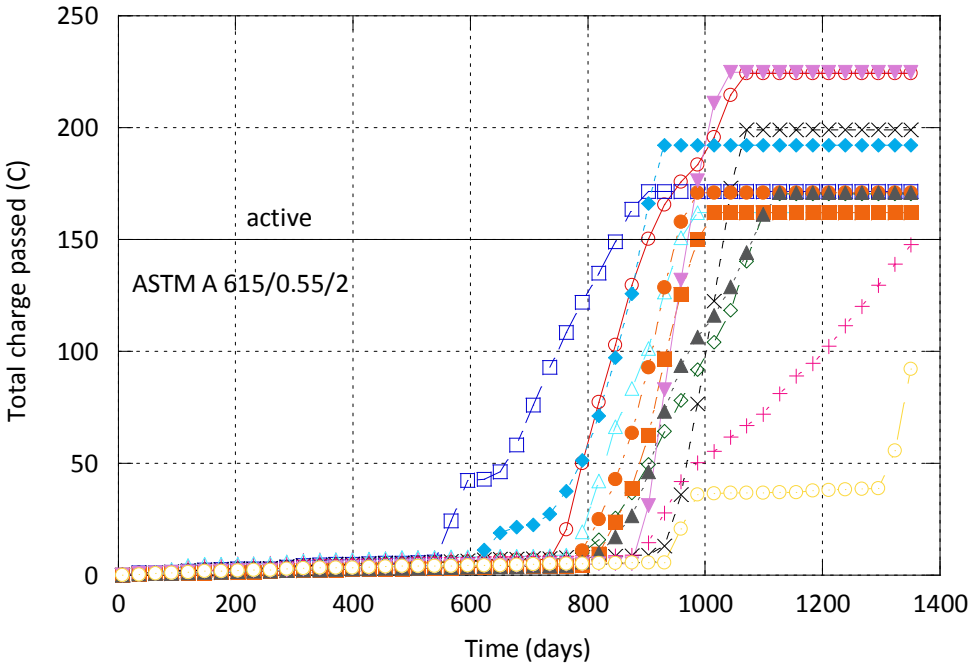


**Figure B-5 ASTM A 615/0.55/2**

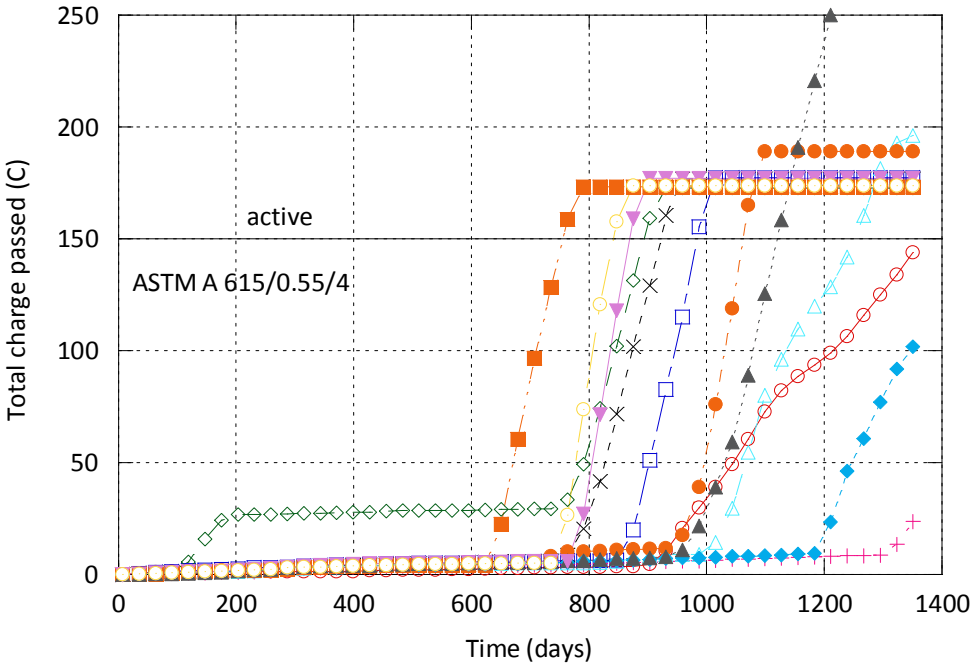


**Figure B-6 ASTM A 615/0.55/4**

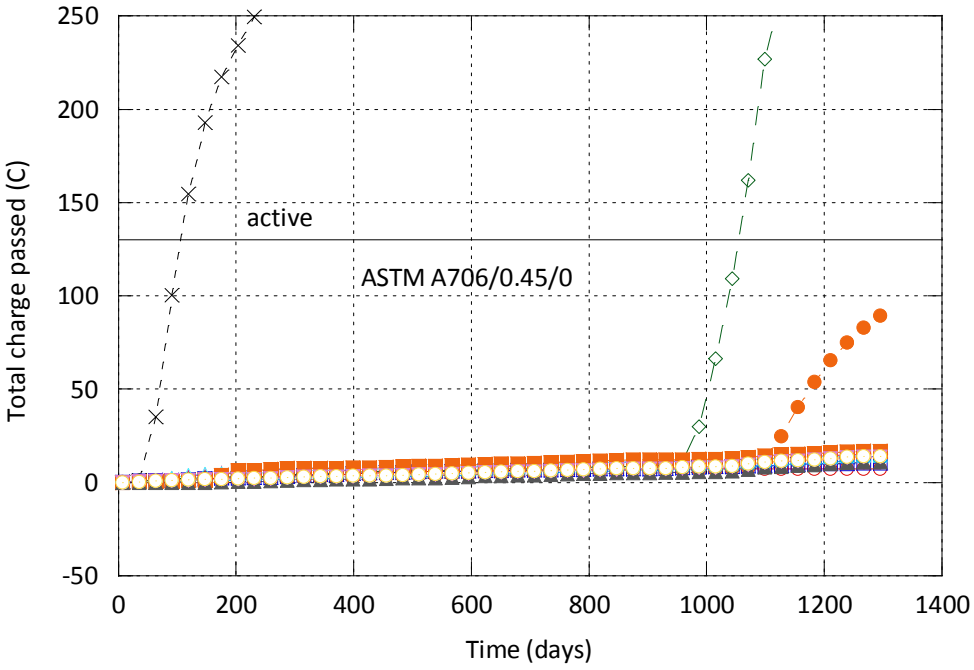


**Figure B-7 ASTM A 706/0.45/0**

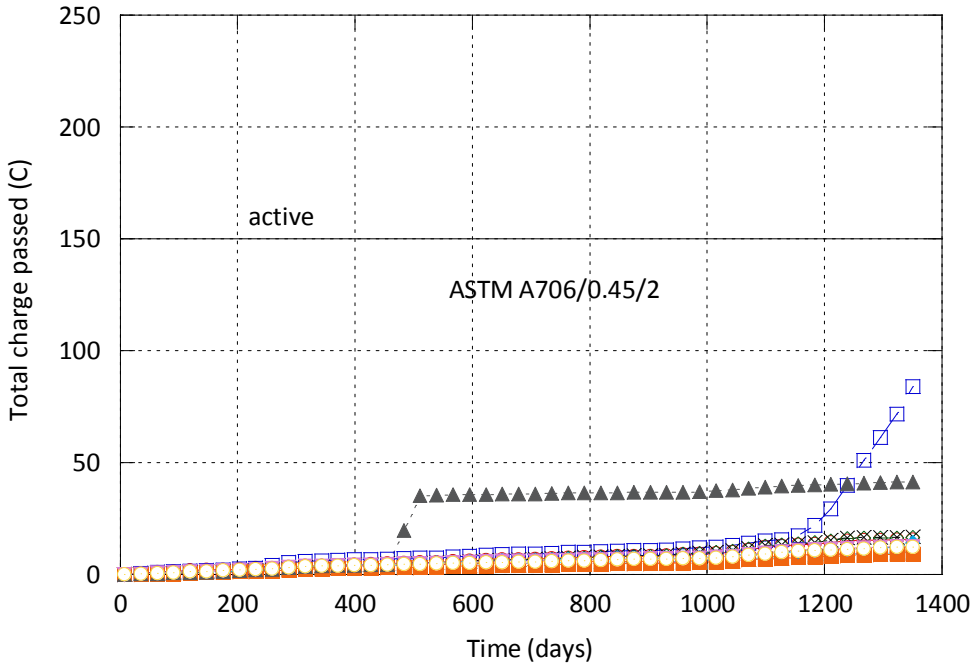


**Figure B-8 ASTM A 706/0.45/2**

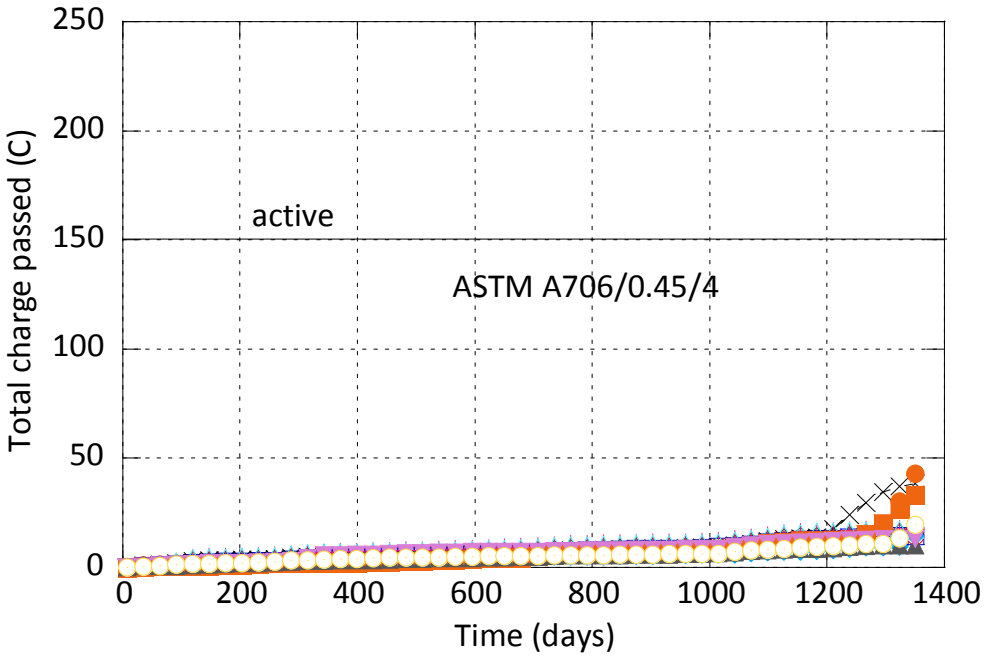


**Figure B-9 ASTM A 706/0.45/4**

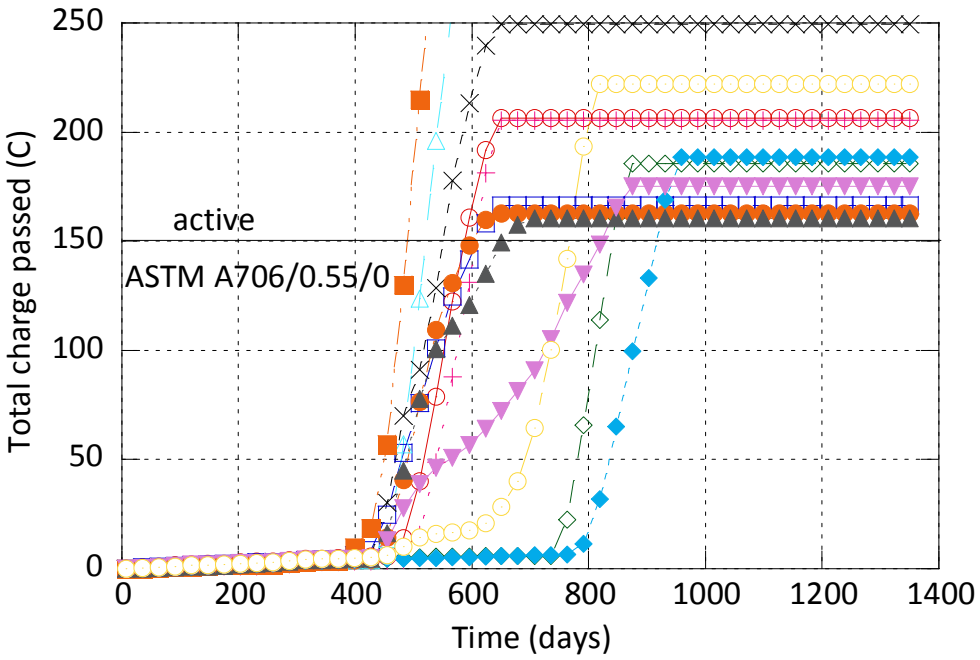


**Figure B-10 ASTM A 706/0.55/0**

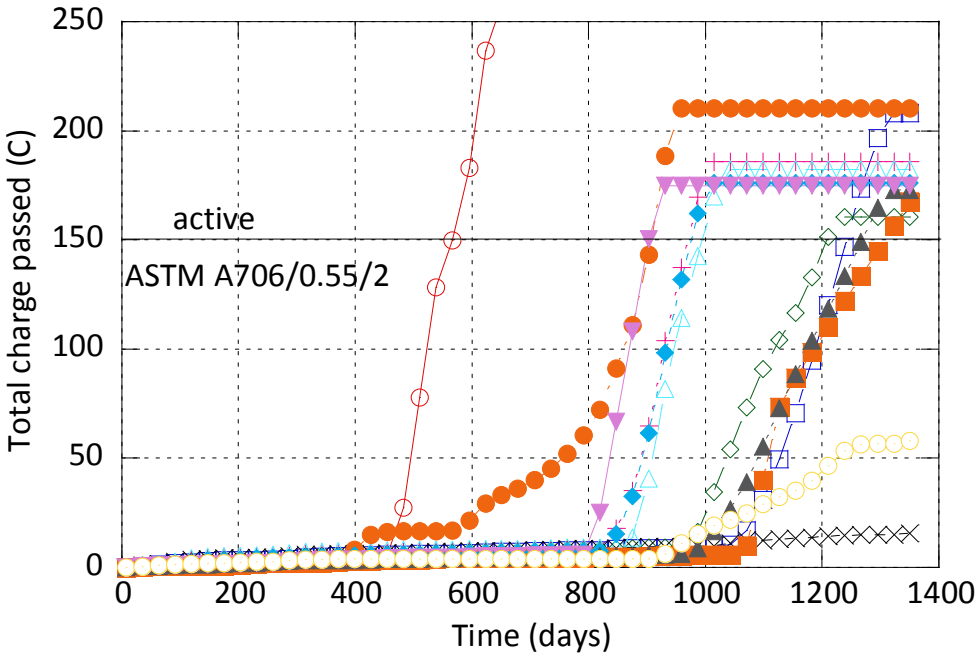


**Figure B-11 ASTM A 706/0.55/2**

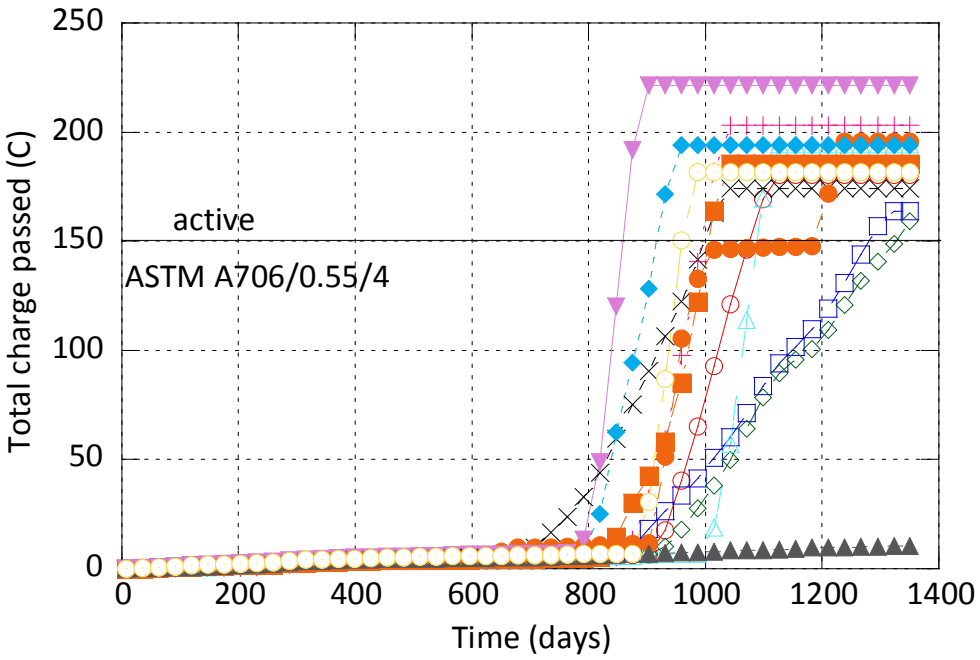


**Figure B-12 ASTM A 706/0.55/4**

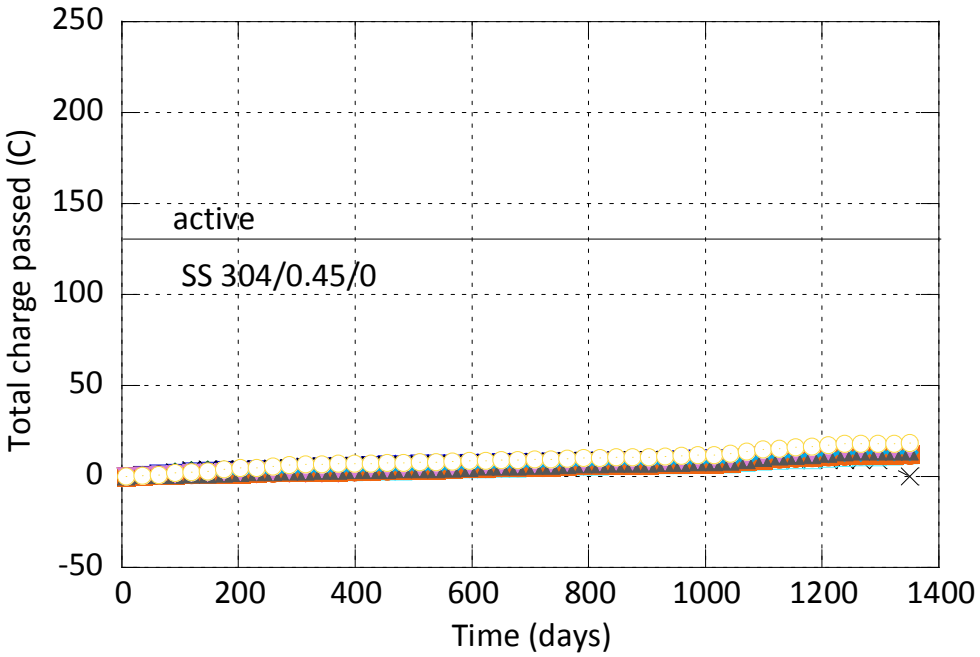


**Figure B-13 ASTM SS304/0.45/0**

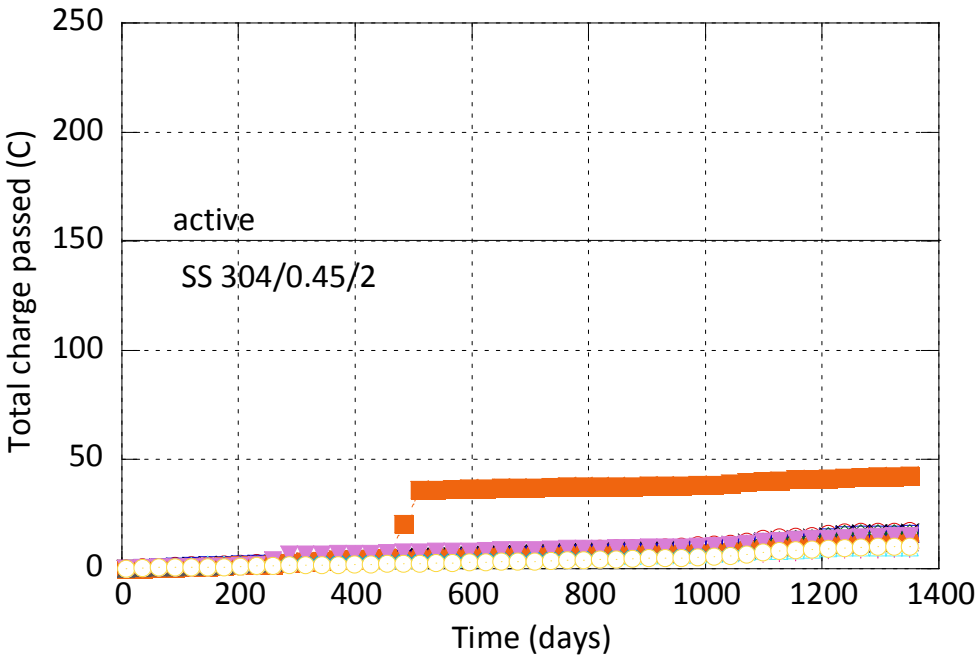


**Figure B-14 ASTM SS304/0.45/2**

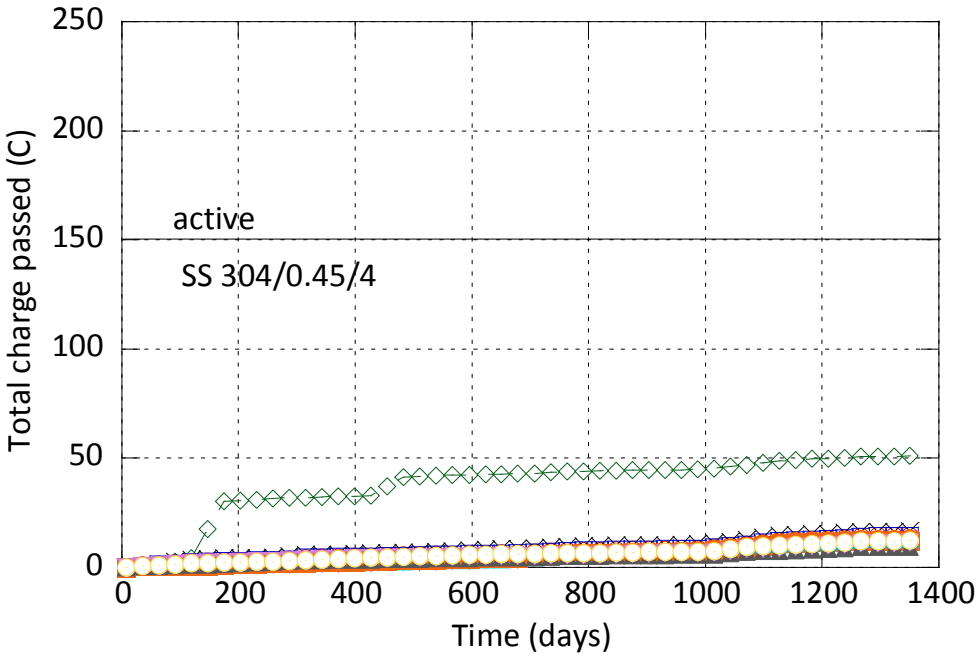


**Figure B-15 ASTM SS304/0.45/4**

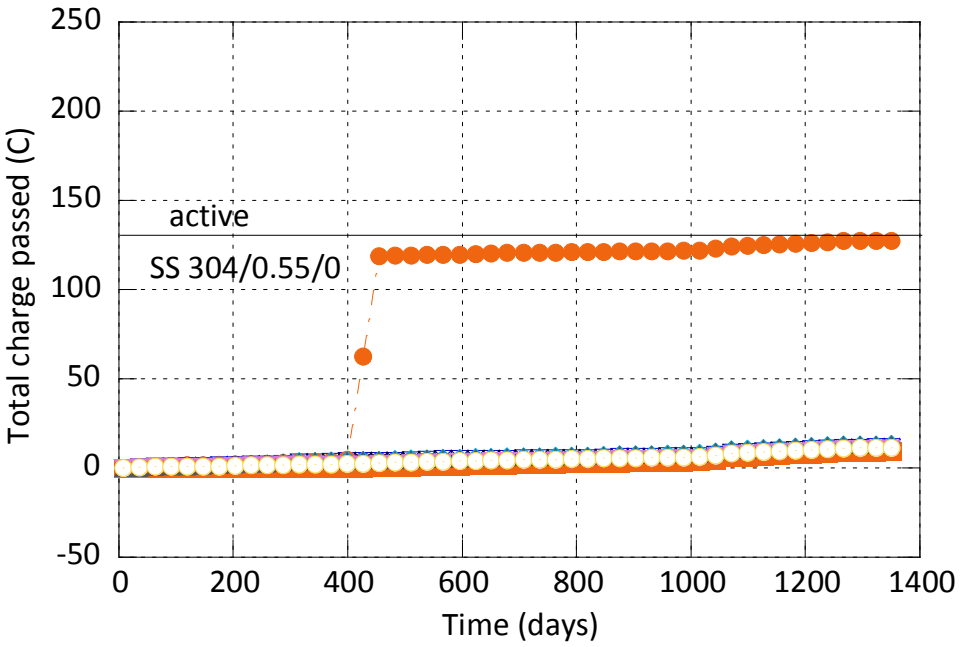


**Figure B-16 ASTM SS304/0.55/0**

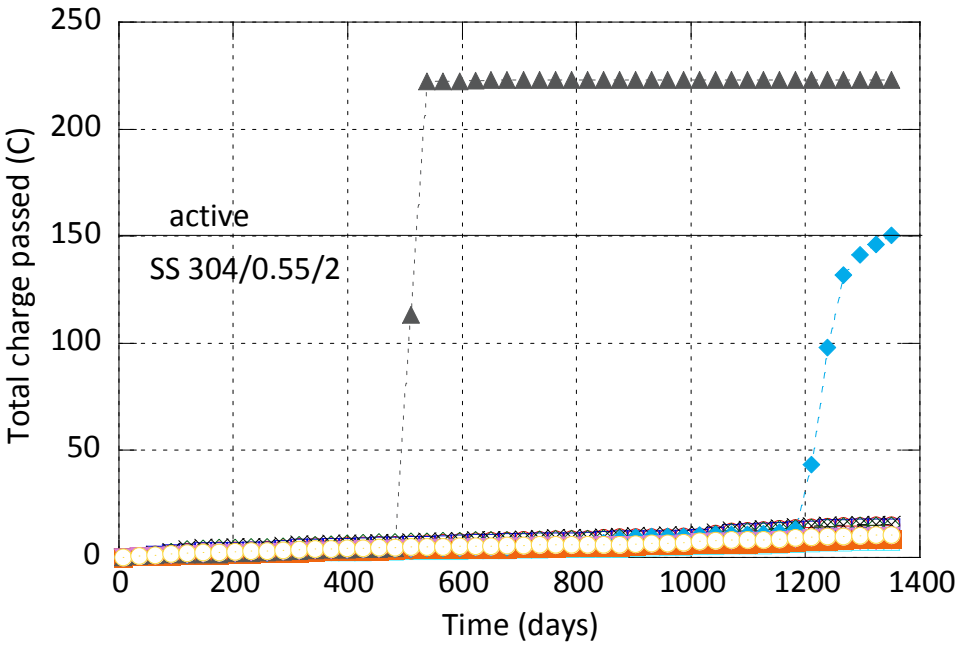


**Figure B-17 ASTM SS304/0.55/2**

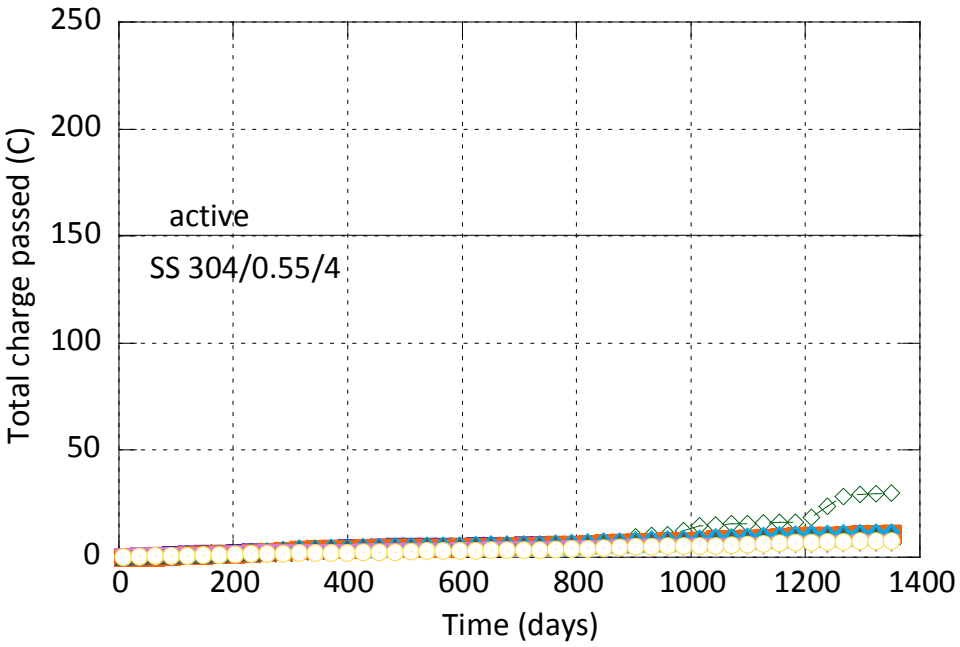


**Figure B-18 ASTM SS304/0.55/4**

MG 109

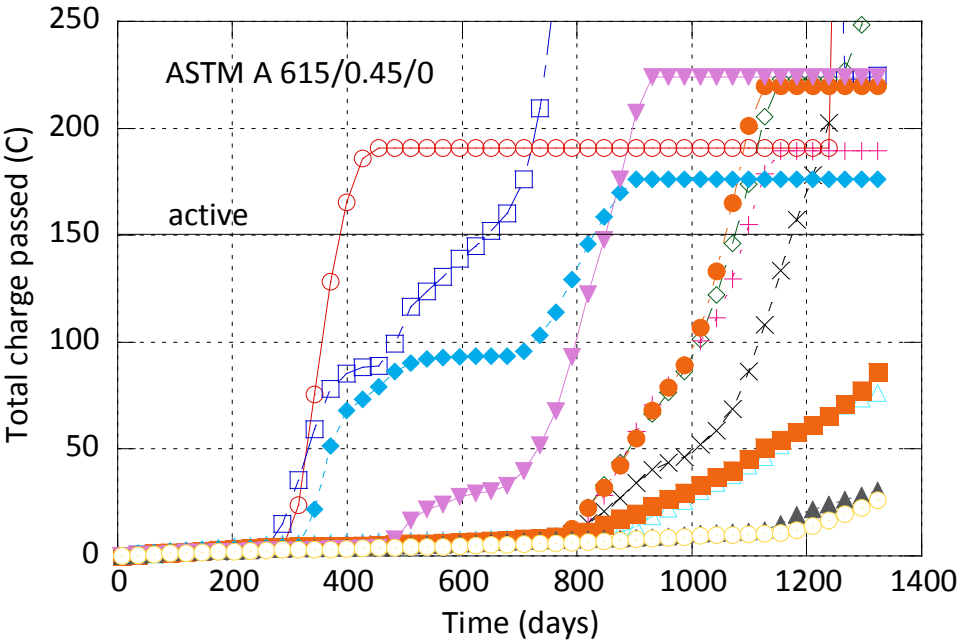


**Figure B-19 ASTM A 615/0.45/0**

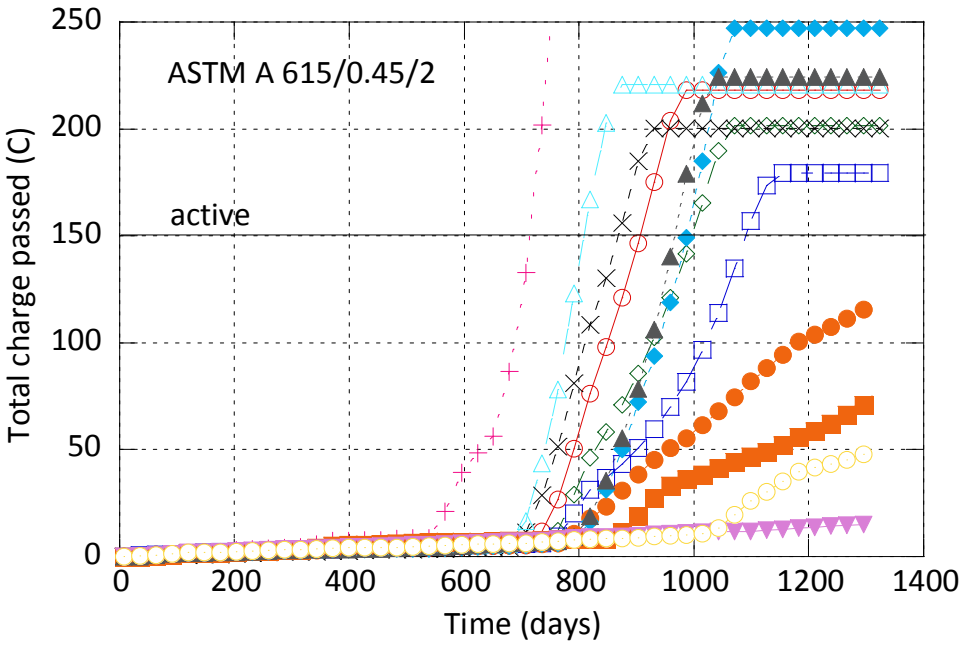


**Figure B-20 ASTM A 615/0.45/2**

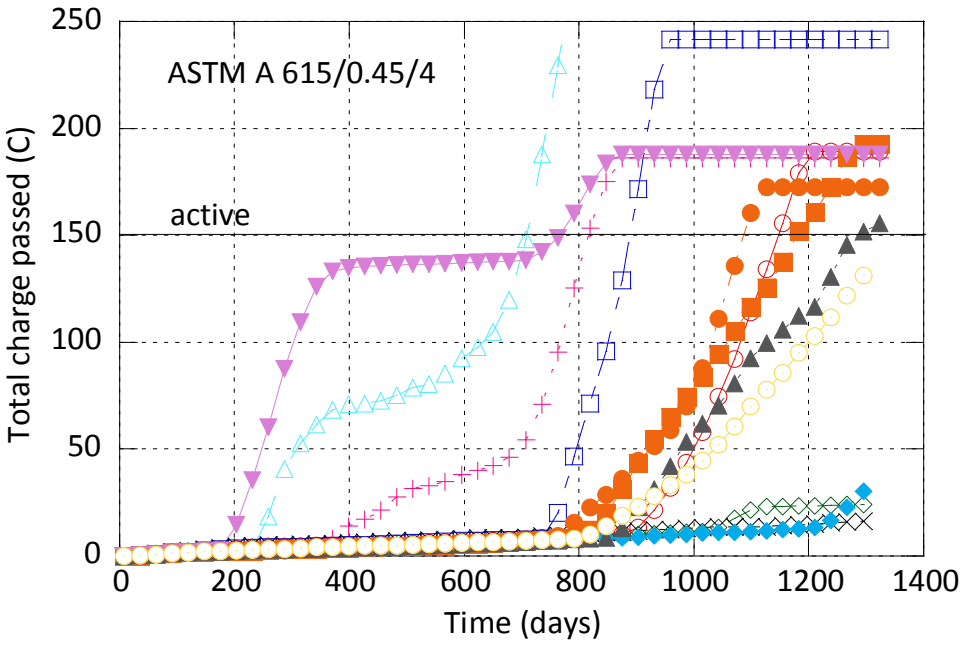


**Figure B-21 ASTM A 615/0.45/4**

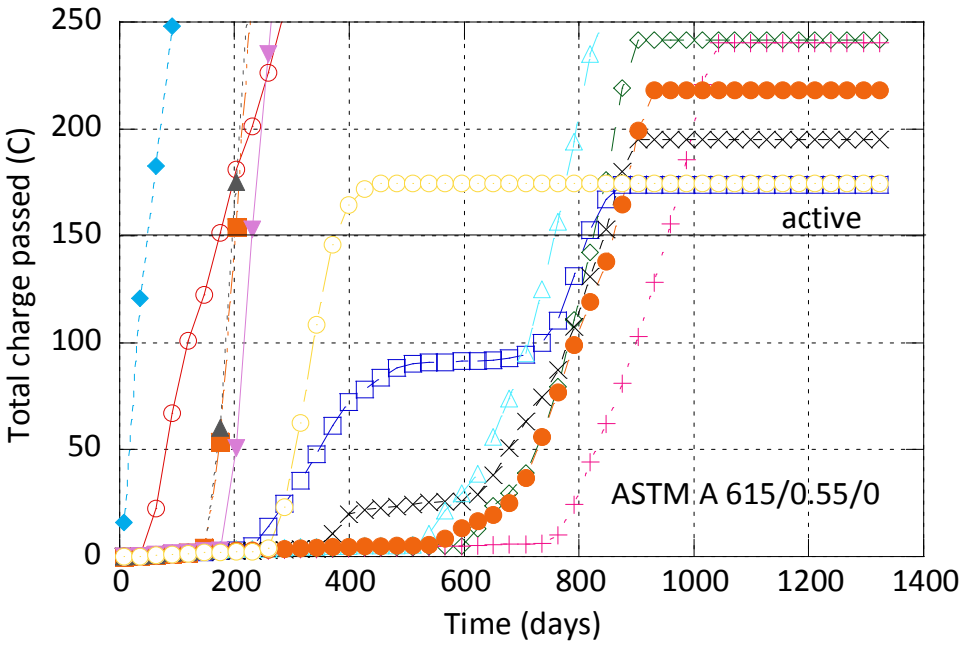


**Figure B-22 ASTM A 615/0.55/0**

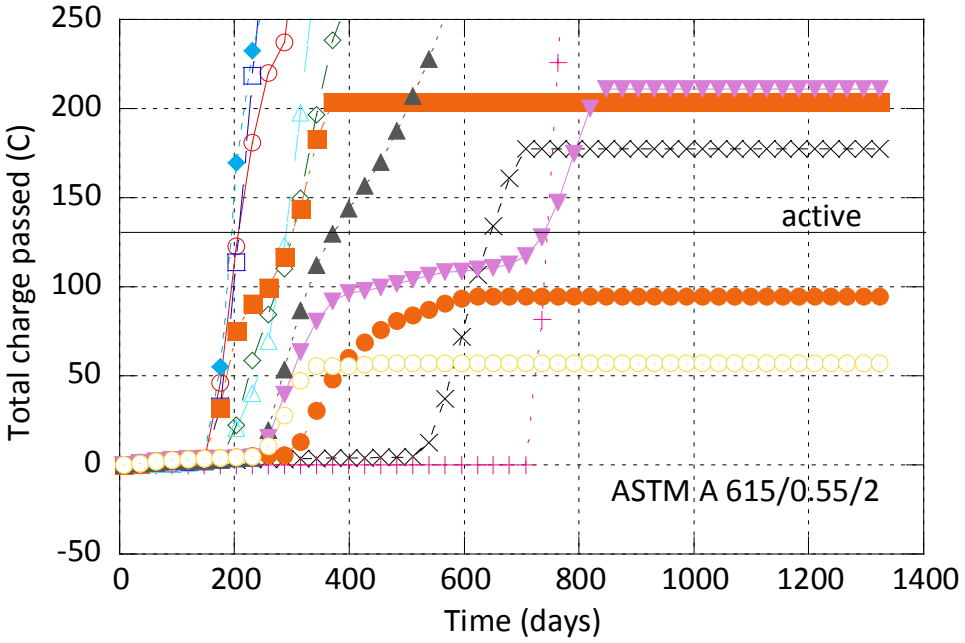


**Figure B-23 ASTM A 615/0.55/2**

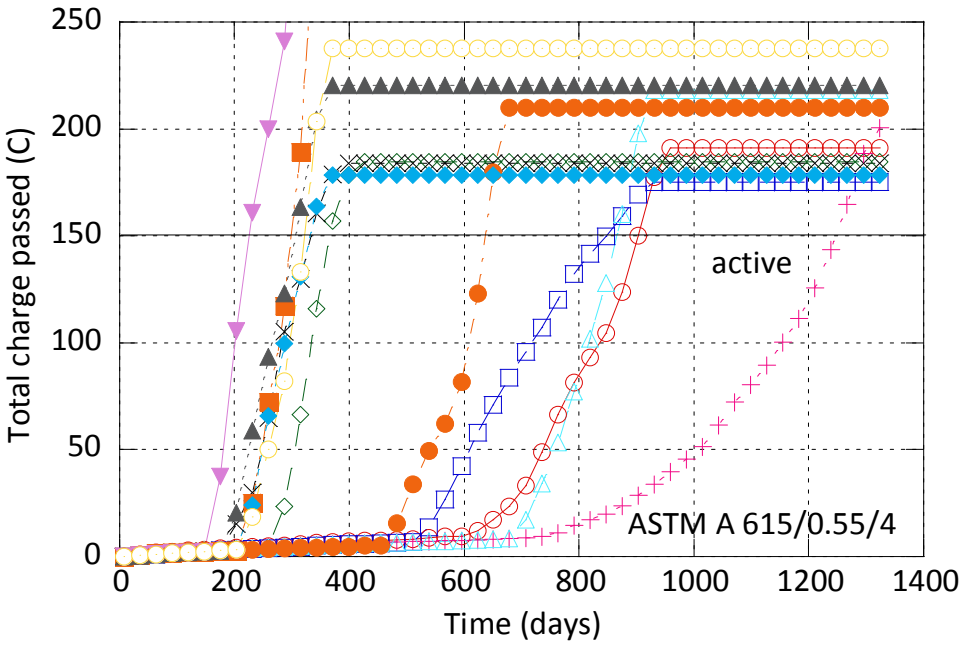


**Figure B-24 ASTM A 615/0.55/4**

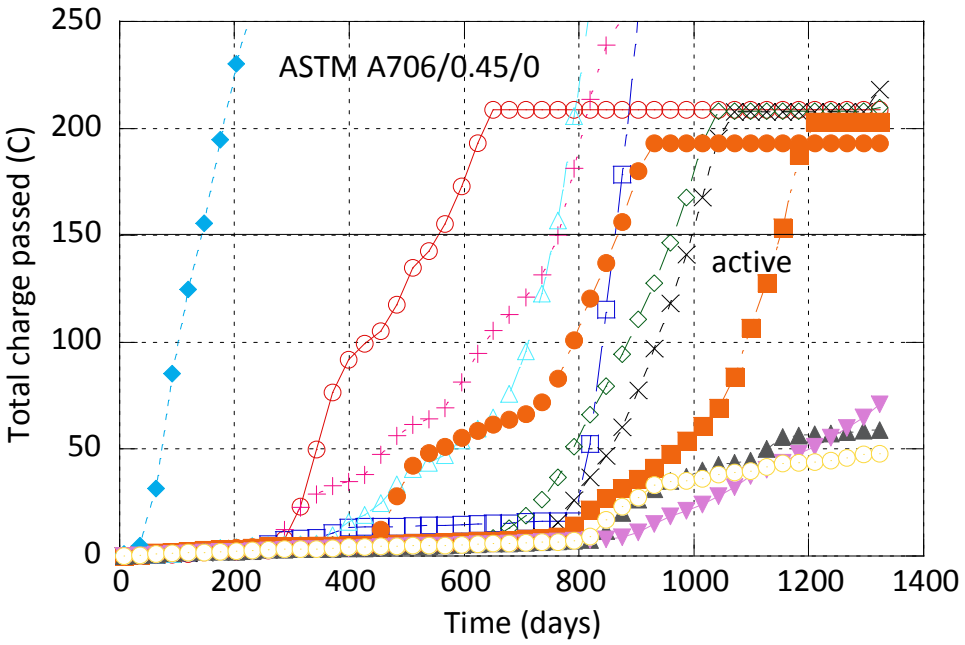


**Figure B-25 ASTM A 706/0.45/0**

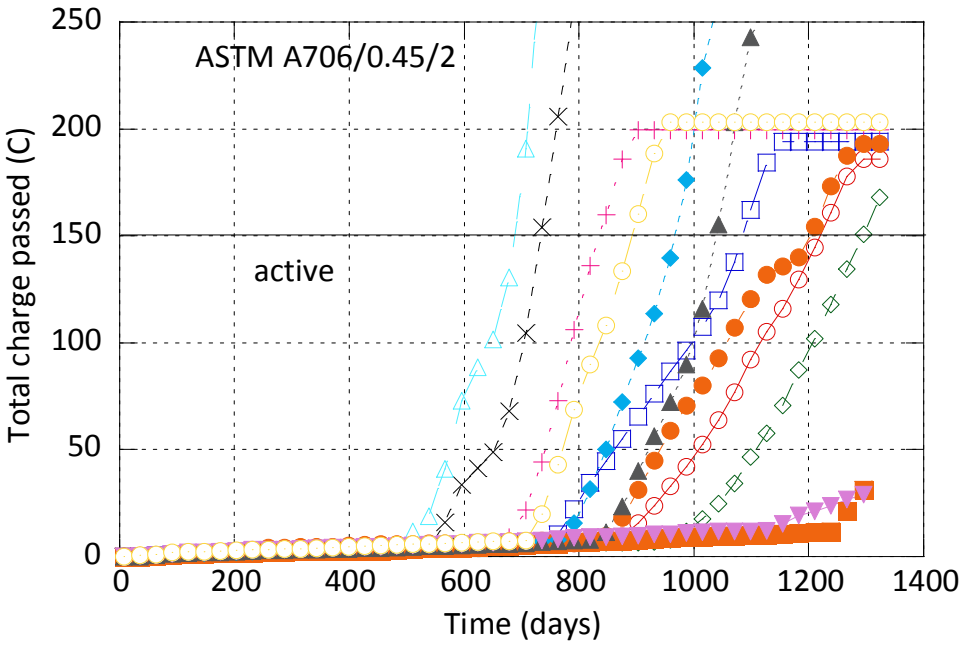


**Figure B-26 ASTM A 706/0.45/2**

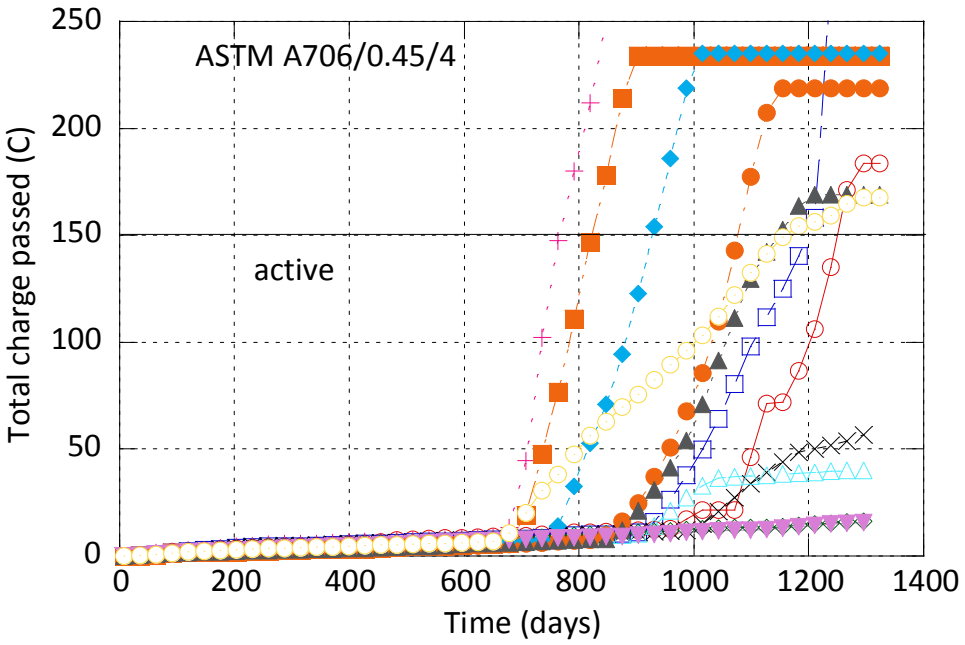


**Figure B-27 ASTM A 706/0.45/4**

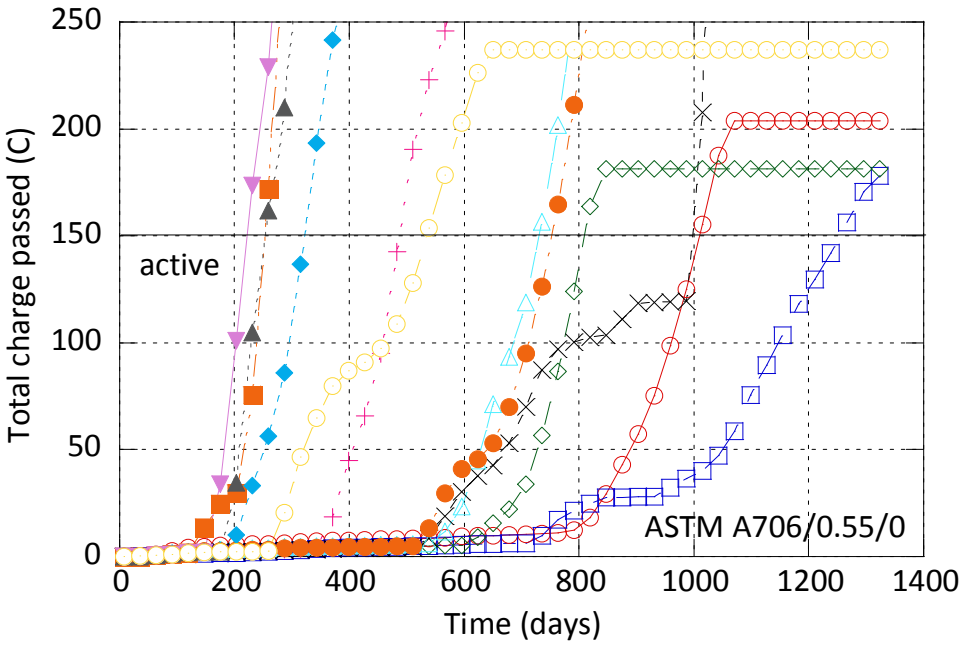


**Figure B-28 ASTM A 706/0.55/0**

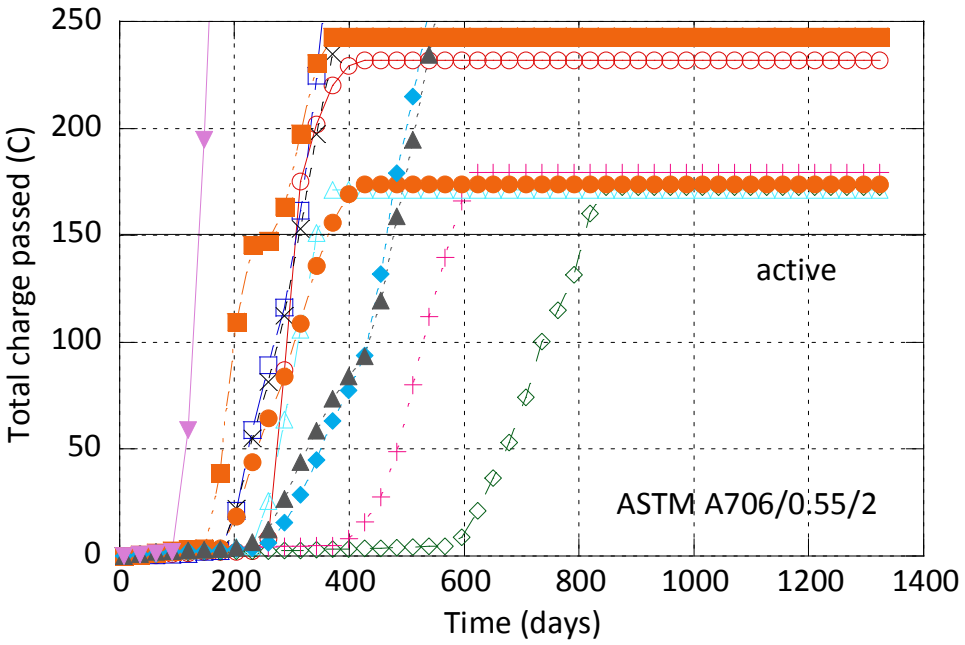


**Figure B-29 ASTM A 706/0.55/2**

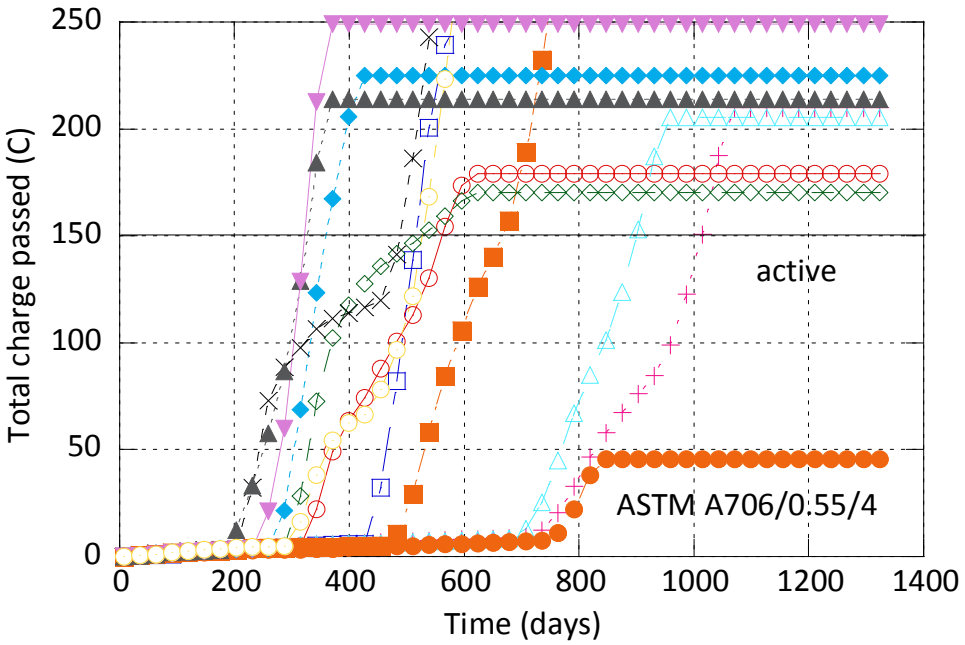


**Figure B-30 ASTM A 706/0.55/4**

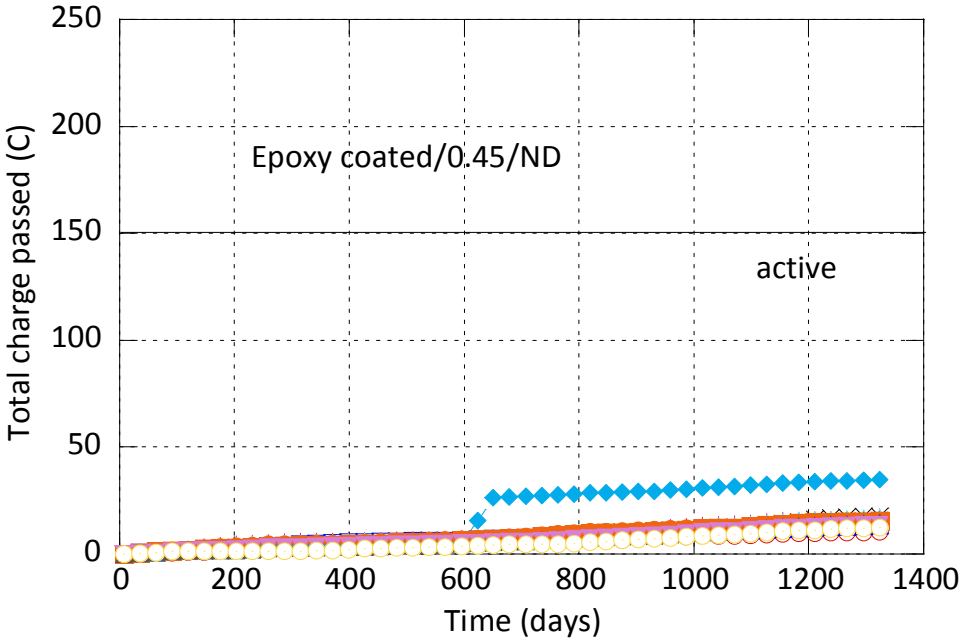


**Figure B-31 ECR/0.45/ND**

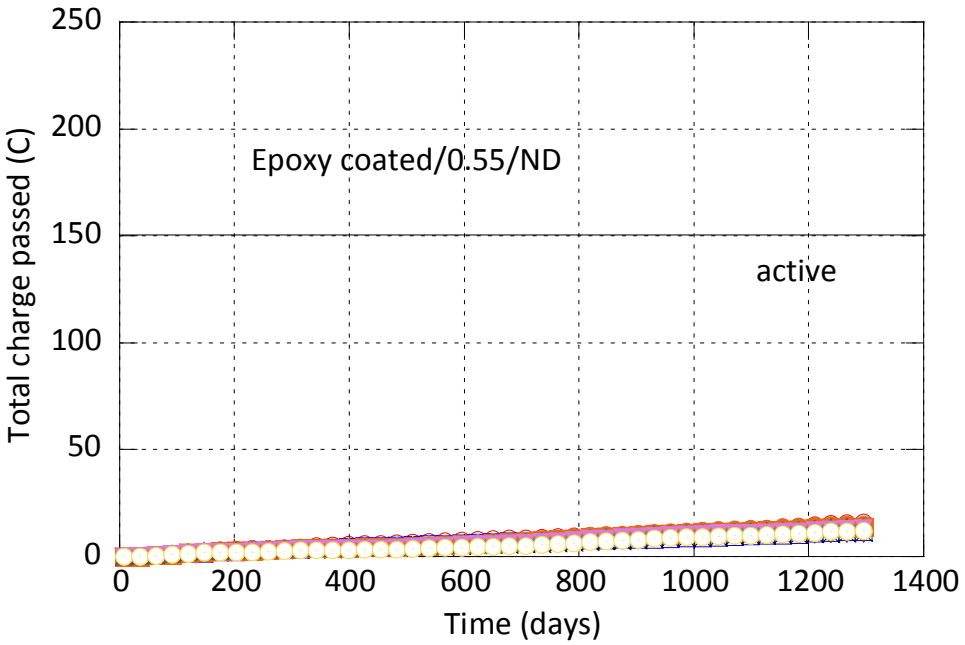


**Figure B-32 ECR/0.55/ND**

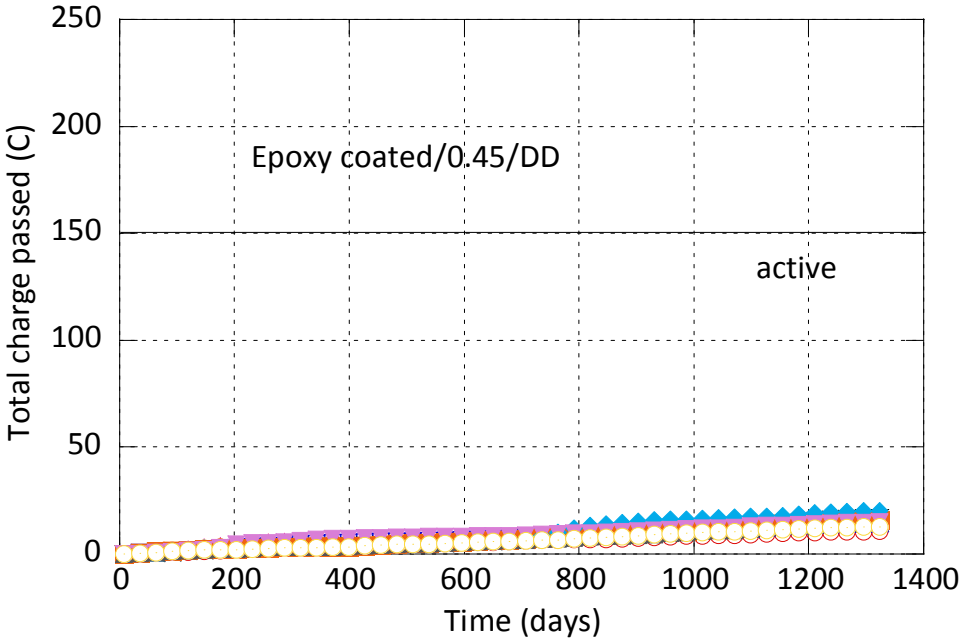


**Figure B-33 ECR/0.45/DD**

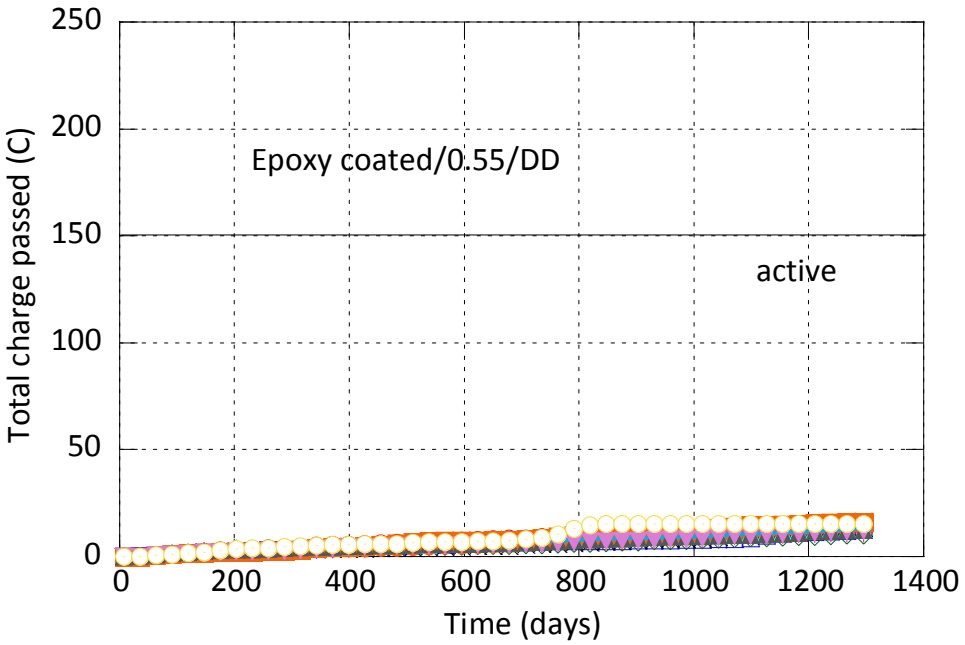


**Figure B-34 ECR/0.55/DD**

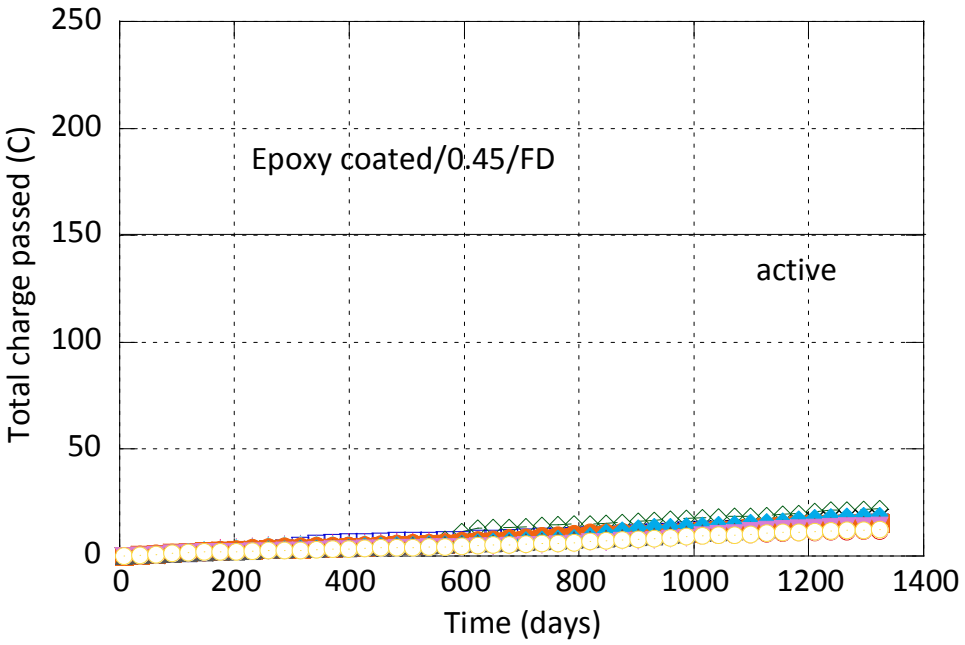


**Figure B-35 ECR/0.45/FD**

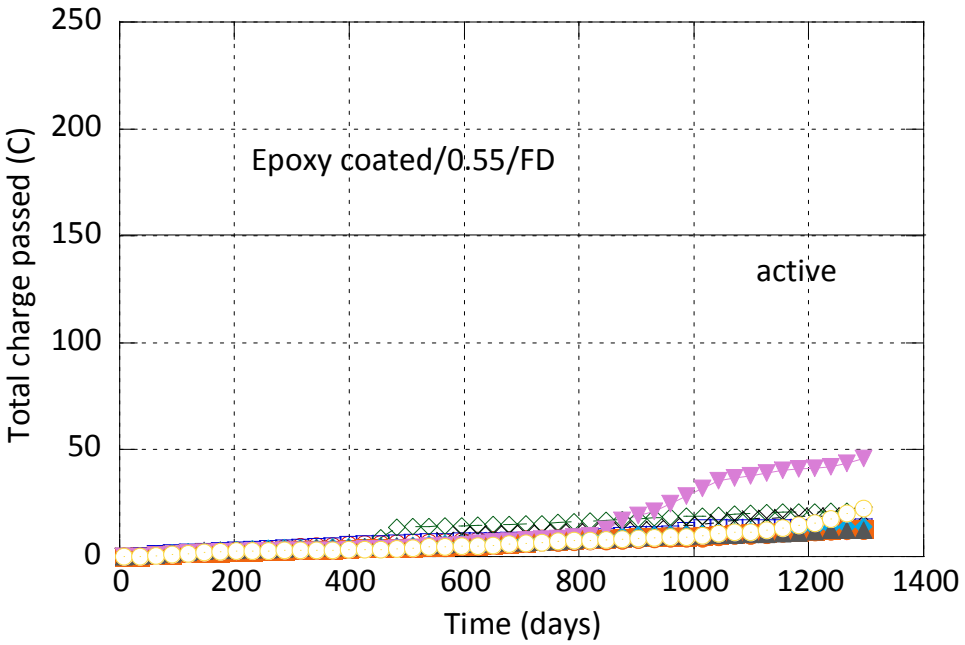


**Figure B-36 ECR/0.55/FD**

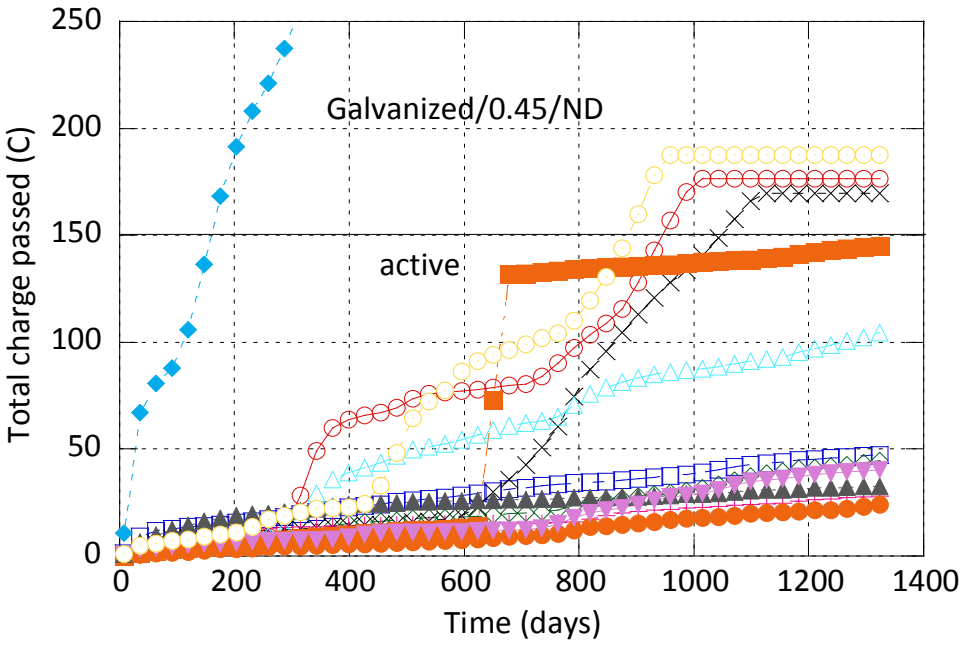


**Figure B-37 GR/0.45/ND**

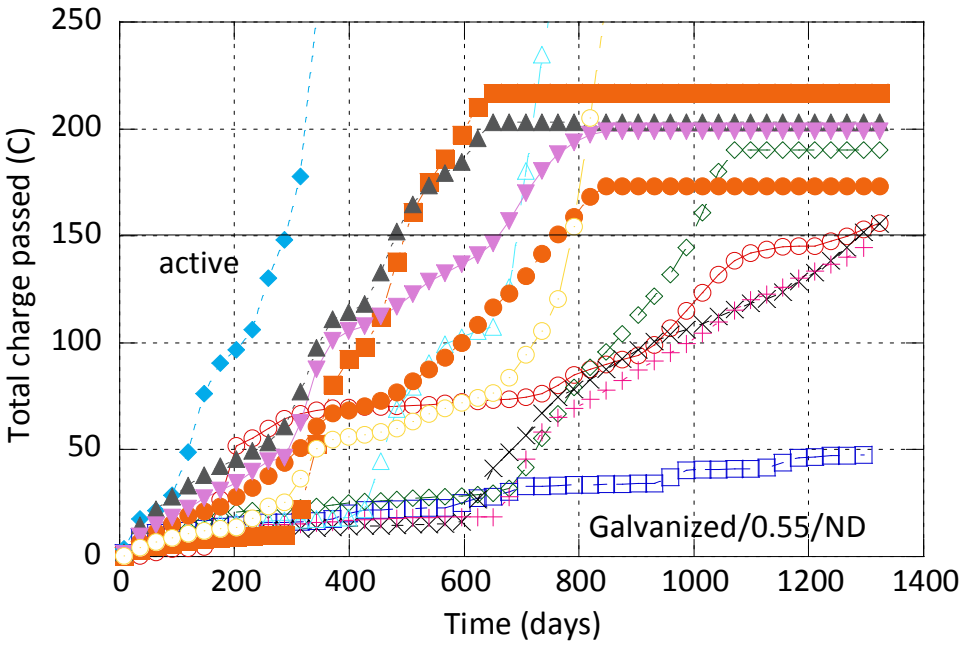


**Figure B-38 GR/0.55/ND**

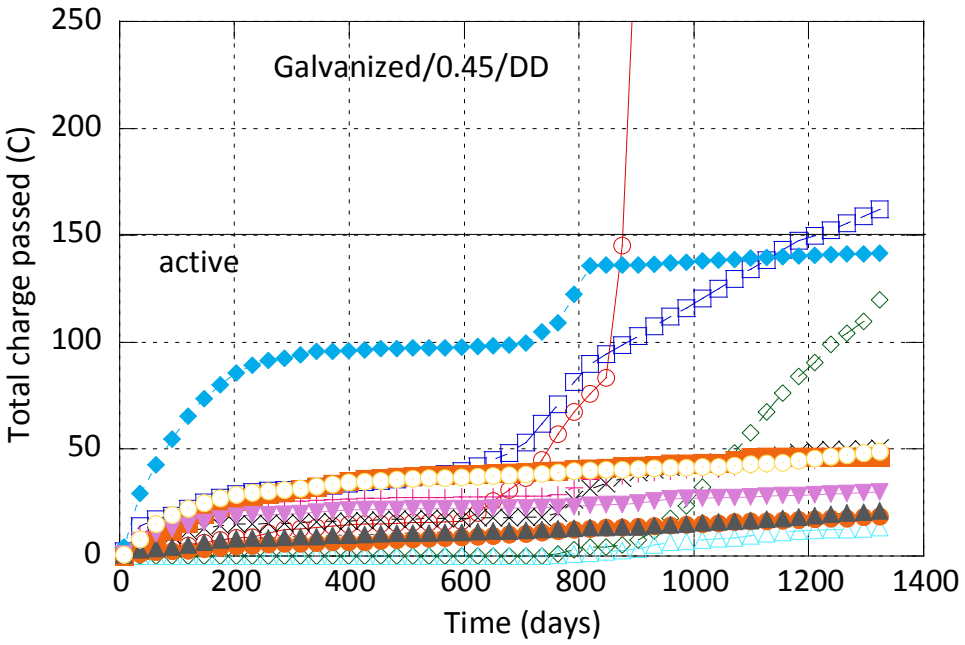


**Figure B-39 GR/0.45/DD**

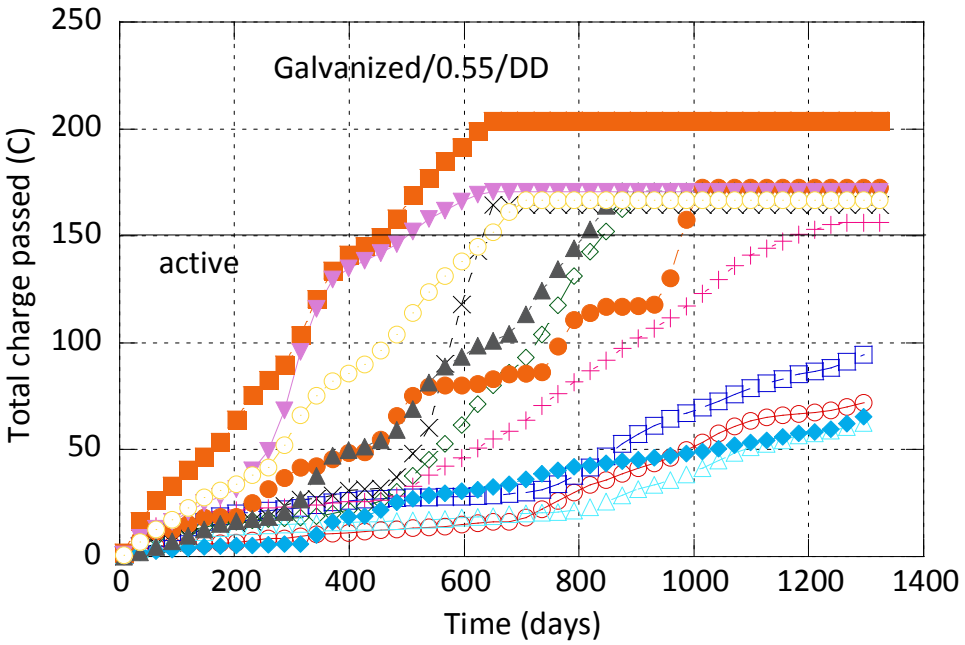


**Figure B-40 GR/0.55/DD**

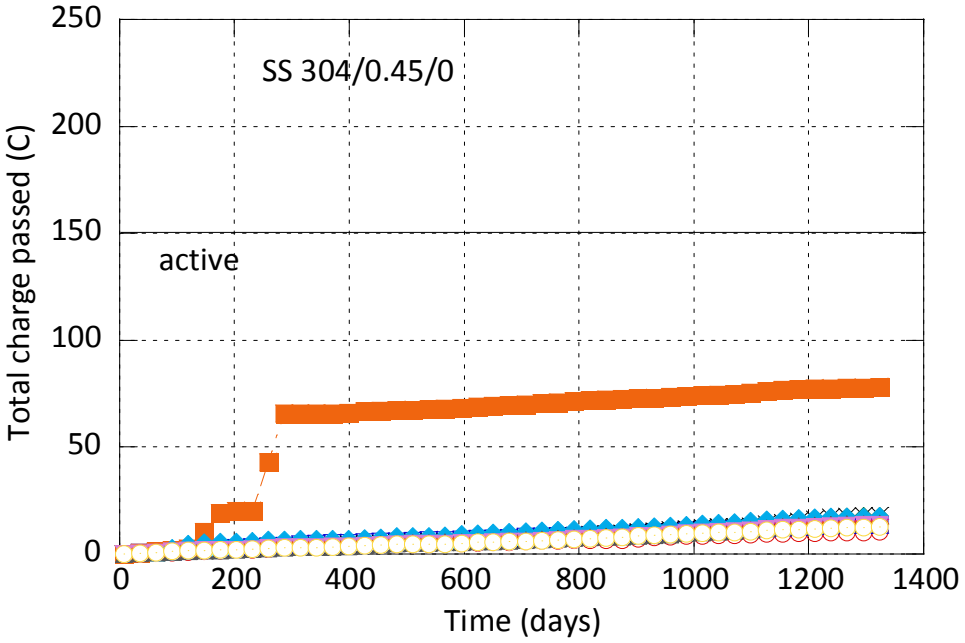


**Figure B-41 SS304/0.45/0**

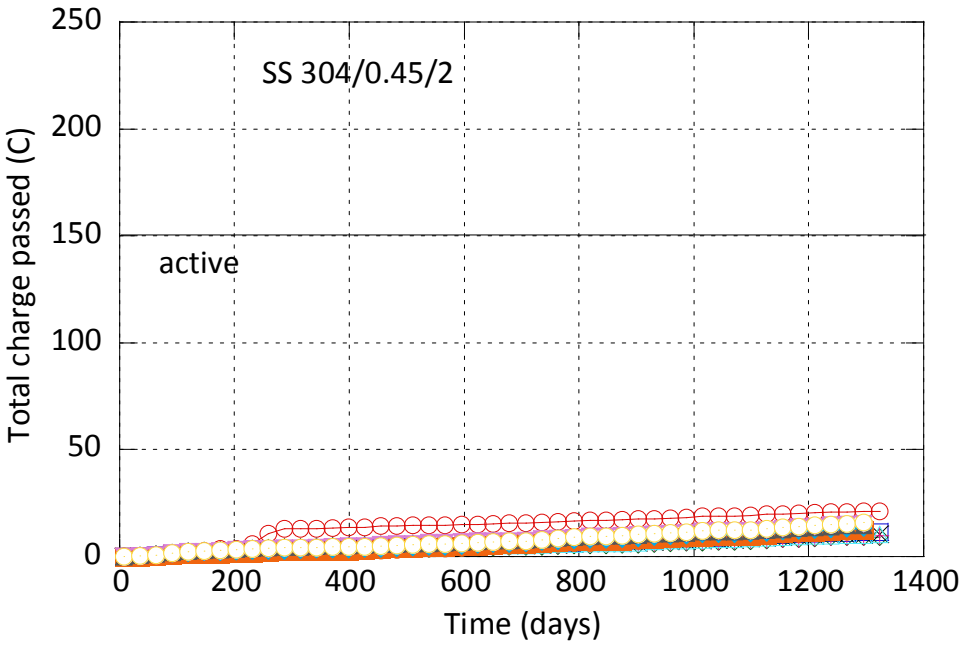


**Figure B-42 SS304/0.45/2**

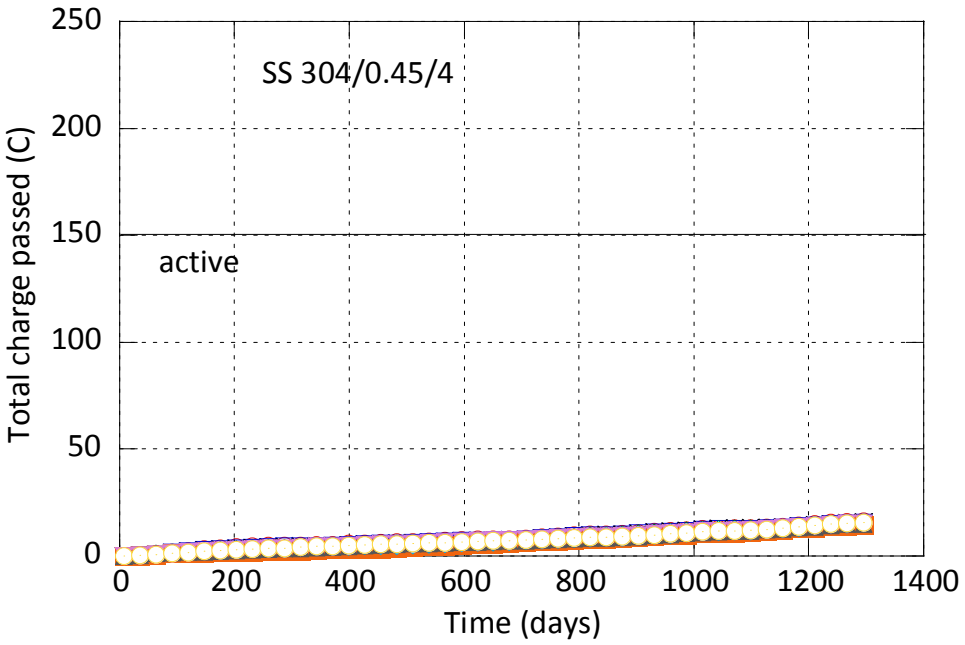


**Figure B-43 SS304/0.45/4**

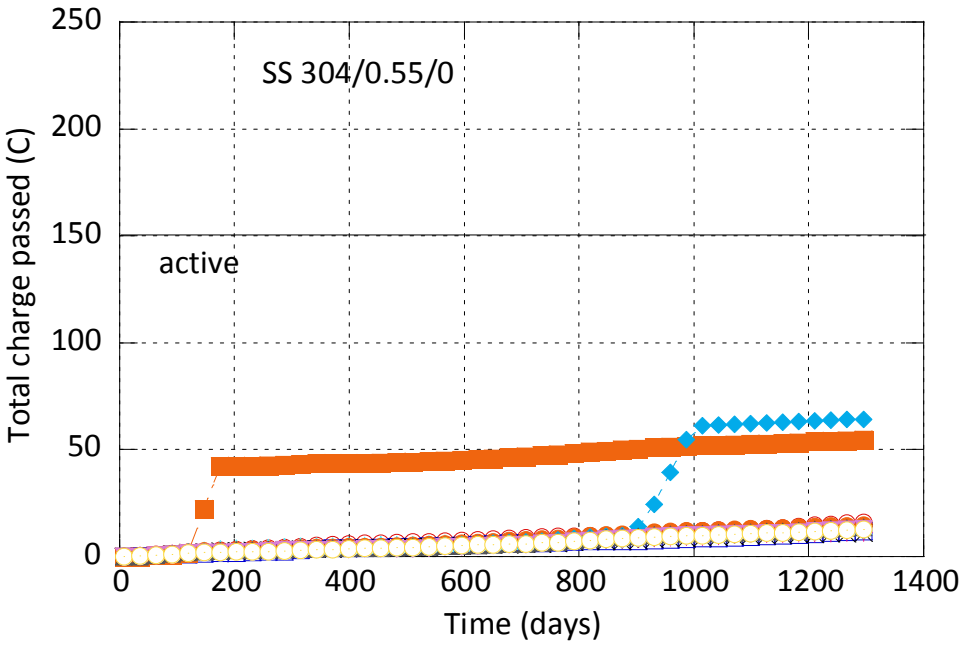


**Figure B-44 SS304/0.55/0**

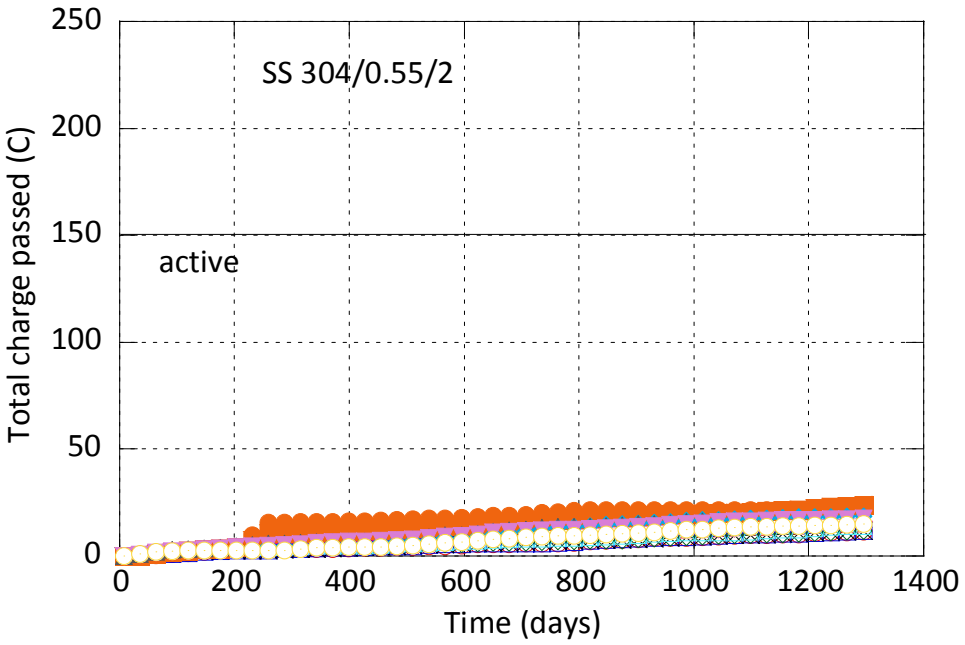


**Figure B-45 SS304/0.55/2**

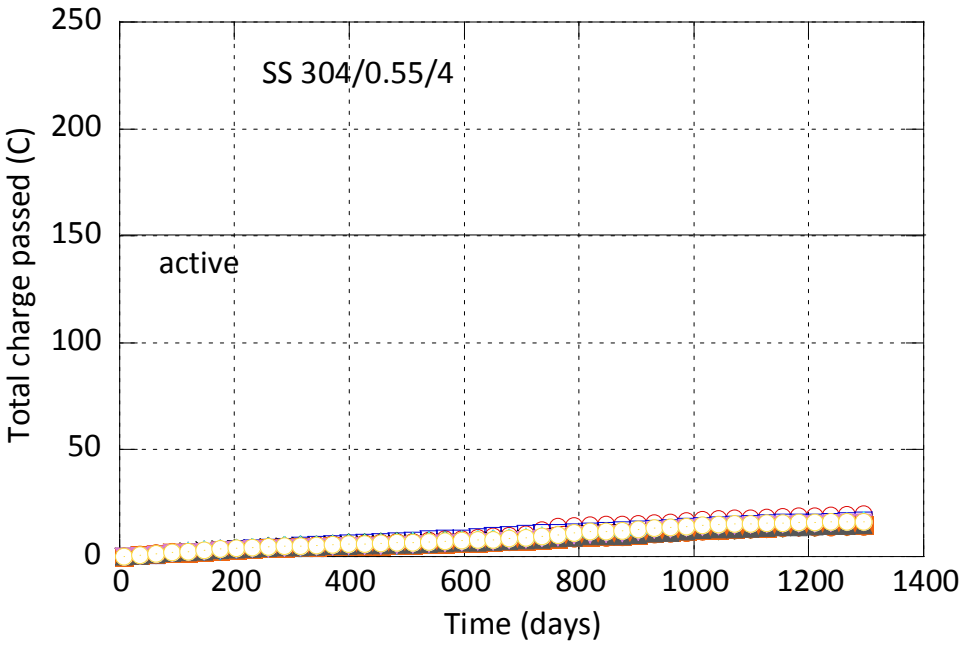


**Figure B-46 SS304/0.55/4**